Effects of high carrier concentrations on some optical properties of semiconductors

G.N. Childs

I confirm that this thesis or any part of the work herein has not previously been submitted for a degree at any university or college.

EFFECTS OF HIGH CARRIER CONCENTRATIONS ON SOME OPTICAL PROPERTIES OF SEMICONDUCTORS

by

G.N. Childs, B.Sc. (UEA)

A thesis submitted for the degree of Doctor of Philosophy at the University of Durham.

1987.

Acknowledgements

During the course of this work I have received support and encouragement from many colleagues and friends and I gratefully acknowledge their help. In particular I wish to thank my supervisor Dr. R. Abram for his tireless direction and patience. I also wish to thank Dr. S. Brand for loan of computer programs and many helpful discussions, Dr. R. Jones for his diversionary expertise, and the staff of the computing centre for their helpful advice and de-bugging abilities.

I gratefully acknowledge financial support from the SERC and Plessey Research (Caswell) Ltd., and the helpful suggestions provided by my industrial supervisors, Dr. D. Robbins and Dr. G. Rees.

Thanks are also due to Mrs. J. Cox for typing this manuscript and to Miss K. Cummins for producing the diagrams.

Finally, I wish to thank my wife Hilary for her endless support and patience at all times, and my daugther Kathryn and baby Christopher for keeping me in touch with the real world.

EFFECTS OF HIGH CARRIER CONCENTRATIONS ON SOME OPTICAL PROPERTIES OF SEMICONDUCTORS

by

G. Childs

ABSTRACT

Many semiconductor devices, such as heterostructure lasers and silicon bipolar transistors, require large concentrations of free carriers in the conduction and/or valence band of an active region. Under these conditions the band gap of the material is reduced by the many-body interactions of the carrier gas. The band gap narrowing results from a lowering of the conduction and raising of the valence band edge energies and is evaluated for a range of carrier concentrations (10^{17} - 10^{22} cm^{-3}) in p-type Si and p- and n-type GaAs, $Ga_{0.47}In_{0.53}As$ and $Ga_{0.28}In_{0.72}As_{0.6}P_{0.4}$ at T = OK. A plasmon-pole approximation for the carrier gas dielectric function is used in the calculations. For all these materials, the largest energy shift occurs in the band containing the free carriers.

For comparison the band edge shifts in all four materials are evaluated at finite temperature (300 K). The band gap narrowing at finite and zero temperatures differ notably only for low carrier concentrations (e.g. $p < 5 \times 10^{19}$ cm^{-3} in p-type Si) where the thermal excitation of the carriers reduces their screening effect so producing smaller band gap reduction.

High hole concentrations also lead to increased optical losses in semiconductor lasers due to intervalence band absorption (IVBA) transitions. These losses, which are considered to be partially responsible for the temperature dependence of threshold current densities in some semiconductor lasers, are evaluated in bulk laser materials using a pseudopotential bandstructure model. The temperature dependencies of the IVBA coefficients in GaAs, $Ga_{0.47}In_{0.53}As$ and $Ga_{0.28}In_{0.72}As_{0.6}P_{0.4}$ are shown to be either small or the coefficients themselves are negligible.

Intervalence band absorption is also calculated for a 100/200 A^{o} $GaAs/Ga_{0.7}Al_{0.3}As$ quantum well laser structure for which the electronic bandstructure is determined using a variational $\underline{k \cdot p}$ approach. The wavelength dependence of the IVBA coefficients differs notably from corresponding results derived using simpler effective mass and pseudopotential models. In particular the $\underline{k \cdot p}$ model gives significant contributions to the total loss, from certain 'forbidden' transitions.

LIST OF CONTENTS

		Page
CHAPTER 1:	INTRODUCTION	1
1.0.	Preliminary discussion.	1
1.1.	Band gap narrowing.	2
1.2.	Intervalence band absorption.	3
CHAPTER 2:	ELECTRON-ELECTRON SELF ENERGY	5
2.0.	Introduction.	5
2.1.	Semiconductors considered and their electronic bandstructure.	5
2.2.	Introduction to the theory of heavy doping in semiconductors.	7
2.3.	Self energy - a physical description.	11
2.4.	Self energy - a diagrammatic interpretation.	13
2.5.	Self energy in a semiconductor.	17
2.5.1.	Evaluation of Bloch function overlap integrals.	20
2.6.	Evaluation of the dynamically screened Coulomb interaction.	22
2.6.1.	Derivation of the carrier gas dielectric function.	23
2.6.2.	The plasmon pole approximation.	25
2.7.	Summary.	31
CHAPTER 3:	BAND GAP NARROWING DUE TO MANY BODY INTERACTIONS AT T = OK	32
3.0.	Introduction.	32
3.1.	Derivation of the screened exchange and Coulomb-hole terms.	34
3.2.	Band edge shifts in p-type material.	36
3.2.1.	Valence band energy shift - introduction .	36
3.2.2.	Derivation of general terms.	37

		Page
3.2.3.	Definition of energy parameters and discussion of difficulties in evaluation of general terms.	41
3.2.4.	Evaluation of $\Delta E_{HH}^{\Sigma SXA}$ and $\Delta E_{HH}^{\Sigma CH}$ terms.	42
3.2.5.	Evaluation of $\Delta E_{HH}^{\Sigma SXU}$ and ΔE_{HH}^{Σ} terms.	44
3.2.6.	Comparision with the use of the Thomas-Fermi approximation for the dielectric function.	46
3.2.7.	Conduction band shift - screened exchange term.	47
3.2.8.	Conduction band shift - Coulomb-hole term.	48
3.2.9.	Conduction band shift in the Thomas-Fermi approximation.	50
3.2.10.	Results for p-type materials.	50
3.3.	Band gap narrowing in n-type material.	51
3.3.1.	Introduction.	51
3.3.2.	Basic formulae - conduction band shift.	52
3.3.3.	Basic formulae - valence band shift.	53
3.3.4.	Results for n-type material.	54
3.4.	Band gap narrowing due to electron-hole plasmas.	55
3.4.1.	Introduction and general discussion.	55
3.4.2.	Results for materials containing electron-hole plasmas.	56
3.5.	The effects of hole occupation of the spin split-off band in p-type silicon.	56
3.5.1.	Introduction.	56
3.5.2.	Effects on parameters and band edge shifts.	56
3.6.	Summary.	57
CHAPTER 4:	BAND GAP NARROWING DUE TO MANY BODY INTERACTIONS AT FINITE (T = 300 K) TEMPERATURE	59
4.0.	Introduction.	59
4.1.	Self-energy due to electron-electron interactions.	61

Page

4.1.1. Finite temperature Green's function. 61

4.1.2. Finite temperature inverse dielectric function. 63

4.1.3. Finite temperature Thomas-Fermi screening wavevector and Fermi energy. 65

4.1.4. Finite temperature plasmon dispersion relation. 67

4.2. Derivation of the generalised screened exchange and Coulomb hole terms. 68

4.3. Band edge shifts in p-type material. 71

4.3.1. Introduction. 71

4.3.2. Conduction band shift. 71

4.3.3. Conduction band shift using the Thomas-Fermi approximation for the dielectric function. 74

4.3.4. Valence band shift. 74

4.3.5. Derivation of valence band CH term. 75

4.3.6. Derivation of valence band SX term. 76

4.3.7. Evaluation of $\Delta E_{HH}^{\Sigma SXA}$ and $\Delta E_{HH}^{\Sigma CH}$ terms. 78

4.3.8. Evaluation of $\Delta E_{HH}^{\Sigma SXU}$ and ΔE_{HH}^{Σ} terms. 79

4.3.9. Valence band shift in the Thomas-Fermi approximation. 81

4.3.10. Results and discussion. 82

4.4. Finite temperature band gap narrowing in n-type material. 83

4.4.1. Introduction. 83

4.4.2. Valence band shift. 83

4.4.3. Conduction band shift. 84

4.4.4. Results and discussion. 85

4.5. Summary. 86

CHAPTER 5: INTERVALENCE BAND ABSORPTION AS A LOSS MECHANISM IN HETERO-STRUCTURE LASERS 87

5.0. Introduction. 87

Page

5.1. The IVBA mechanism. 88

5.2. Theory of photon absorption and the IVBA transition. 89

5.3. Choice of directions. 95

5.4. Evaluation of the hole quasi-Fermi level. 96

5.5. Bandstructure - discussion and comparison of models used. 97

5.6. Results and discussion. 100

5.6.1. Energy dependence of the absorption coefficients. 100

5.6.2. Temperature dependence. 101

5.6.3. Concentration dependence. 102

5.7. Summary. 102

CHAPTER 6: SUPERLATTICE AND QUANTUM WELL STRUCTURES 103

6.0. Introduction. 103

6.1. Superlattices and quantum wells - basic theory. 103

6.2. Derivation of superlattice bandstructure. 107

6.2.1. Introduction. 107

6.2.2. The variational technique. 108

6.2.3. Choice of trial wave function. 110

6.2.4. Evaluation of the interface integrals in equation (6.6). 112

6.2.5. The normalisation term. 114

6.2.6. The envelope function expansion. 115

6.2.7. Solution of the variational expression. 115

6.3. Results and discussion. 118

6.3.1. Introduction. 118

6.3.2. Bandstructure. 118

6.3.3. Wavefunctions and momentum matrix elements. 121

a) Preliminary discussion. 121

b) Transitions between the spin split-off and heavy/ light hole sub-bands at $\underline{k}_{11} = 0$. 123

Page

c) Transitions between the spin split-off and heavy/ light hole sub-bands at $\underline{k}_{11} \neq 0$. 126

6.4. Summary. 128

CHAPTER 7: INTERVALENCE BAND ABSORPTION IN QUANTUM WELL LASERS 130

7.0. Introduction. 130

7.1. Intervalence band absorption transitions. 130

7.2. Bandstructure models. 132

7.3. Determination of sub-band edges. 133

7.4. Determination of hole quasi-Fermi level. 135

7.5. Distribution of holes between sub-bands. 139

7.6. Evaluation of the IVBA coefficients. 141

7.7. Results and discussion. 145

7.7.1. Introduction. 145

7.7.2. SEMA and pseudopotential models. 145

a) Wavelength dependence. 145

b) Temperature dependence. 146

c) Concentration dependence. 147

d) Well width dependence. 147

7.7.3. The $\underline{k}\cdot\underline{p}$ model. 147

7.8. Summary. 149

CHAPTER 8: CONCLUSIONS AND SUGGESTIONS FOR FUTURE WORK 150

8.0. Conclusion. 150

8.1. Suggestions for future work. 152

APPENDICES

1. Parameter values.

2. Evaluation of integral expression (2.36).

3. Classical derivation of plasma frequency.

4. Derivation of averaged momentum matrix elements of a bulk semiconductor.

5. Derivation of the variational expression (6.6).

6. Proof of reality of eigenvalues in variational expression (6.6).

7. Evaluation of integral terms from the matching conditions.

8. Normalisation factor for the quantum well wavefunctions and evaluation of normalisation integral (6.20).

9. Derivation of momentum matrix elements for quantum well states.

CHAPTER 1

INTRODUCTION

1.0. Preliminary Discussion

The operation of many semiconductor devices is based on large concentrations of carriers in the conduction and/or valence bands of an active region in the device. These high carrier concentrations can be produced by processes such as current injection (used in semiconductor lasers (Casey and Panish (1978)), and by heavy doping which is used in bipolar transistors (Sze (1981)).

The presence of these large carrier concentrations, greatly in excess of that found in an intrinsic semiconductor, affects some of the fundamental optical and electrical properties of the material. Two such effects of particular importance are the narrowing of the fundamental semiconductor band gap produced by electrons and/or holes and the increase in optical absorption over a range of wavelengths due to the inter-valence band transitions occuring when large hole concentrations are present.

In view of the possible influence of these effects on device performance, the dependence of band gap narrowing and intervalence band absorption IVBA) on carrier concentration (and other parameters) has been studied. The various models used and results derived from the calculations form the basis of the work in this thesis.

As the two effects are concerned with separate physical processes the thesis is essentially divided into two parts. Chapters 2-4 are concerned with the band gap narrowing effects while Chapter 5-7 consider inter-valence band absoprtion and different bandstructure models in which it is calculated.

1.1. Band Gap Narrowing

In this thesis particular emphasis is given to the changes in the energies of the band edges produced by p-type doping. However, the band gap narrowing for several n-type materials is also evaluated and is designed to complement the similar work by Saunderson (1983) on n-type Si. The analysis is also extended to the evaluation of the band gap narrowing produced by the introduction of an electron-hole plasma (which could be achieved for example by current injection or optical excitation).

For the purposes of the present work a heavily doped semiconductor is defined as one in which the concentration of dopant atoms is sufficiently high that the impurity band and adjacent host band have merged to produce a single band similar to the original host band with a large concentration of free carriers.

A heavily doped uncompensated semiconductor contains a large concentration of free carriers and an equal concentration of impurity ions both of which perturb the energy states of the carriers in such a way as to cause a reduction in the fundamental band gap. The Coulombic interaction between free carriers and the ionised dopant atoms provides significant perturbations of carrier wavefunctions and energies and has been discussed in some detail by several authors (see for example Halperin and Lax (1966), Serre and Ghazali (1983)). However, these impurity effects are not considered in the present work, the emphasis instead being placed on the changes induced by the many-body electron-electron interactions. It should be noted that the model is also applicable to semiconductors containing carriers introduced by means other than heavy doping, such as electrical injection or optical excitation.

As the free carrier concentration is increased two effects act to alter the energies of the electronic states in the semiconductor; (a) an

electron's interactions with the other electrons in the semiconductor is screened by the free carrier gas(es), (b) the number of electrons with which an electron interacts is changed by the introduction of free carriers. Both of these effects act to shift the energies of states in the conduction and valence bands and the nett shifts generally produce a narrowing of the fundamental band gap. The evaluation of the concentration dependence of these shifts for states at the band edge at temperatures T = OK and 300K forms the basis of the work in Chapters 3 and 4. The relevant expressions used in these calculations together with a discussion of the basic concepts is given in Chapter 2.

The materials for which the energy shifts are derived are chosen on the basis of their use in devices operating under conditions of high carrier concentrations. The band gap narrowing is therefore evaluated in silicon which is used in heavily doped bipolar transistors and in the 3-5 compound and alloy materials GaAs, $Ga_{0.47}In_{0.53}As$ and $Ga_{0.28}In_{0.72}As_{0.6}P_{0.4}$ used in heterostructure lasers.

1.2. Intervalence Band Absorption

Intervalence band absorption (IVBA) is an optical loss mechanism in which photons are absorbed by excitation of electrons from low energy valence band states to states occupied by holes higher in the valence band. Absorption due to these transitions becomes more significant as the valence band hole population is increased. Several workers have suggested that IVBA is partly or largely responsible for the exponential temperature dependence of the threshold current density ($J_{th} \propto \exp(T/T_o)$) in long wavelength double heterostructure (DH) lasers (see for example Adams et al (1980)). The concentration, wavelength and temperature dependence of the IVBA coefficients are therefore evaluated in the materials GaAs, $Ga_{0.47}In_{0.53}As$ and $Ga_{0.28}In_{0.72}As_{0.6}P_{0.4}$ commonly used in these laser structures. The physical model used and the results of the calculations are given in Chapter 5.

Quantum well lasers also exhibit an exponential temperature dependence of the threshold current density (Chin (1980). However a larger T_o value makes this dependence less pronounced than that found in bulk DH lasers. This temperature dependence is largely attributed to loss mechanisms such as Auger recombination (Dutta (1983)) with IVBA providing only a small contribution. However IVBA can still be an important intrinsic loss mechanism in these structures and a model for the evaluation of these absorption coefficients is presented in Chapter 7.

In a quantum well structure the restriction of carrier motion perpendicular to the well creates new energy states (sub-bands) for the carriers. The energy-wavevector dispersion relations for these sub-bands are of crucial importance in any realistic derivation of IVBA losses. A model (based on a modified k.p approach) for the derivation of the sub-band structure and relevant momentum matrix elements is presented in Chapter 6 together with the corresponding results derived for a $GaAs/Ga_{0.7}Al_{0.3}As$, 100/200 Å quantum well structure. The bandstructure derived in this model was however limited by computer time and complexities in the calculation to regions close to the sub-band edges. IVBA coefficients for transitions at lasing wavelengths therefore could not be determined for GaAs. However, the model could be extended for use in alloy materials in which these transitions occur near the band edge and provide more important contributions to the optical loss.

The wavelength dependence of absorption coefficients derived in the k.p model is given in Chapter 7 and compared with the corresponding results derived using simple effective mass and pseudopotential sub-bandstructures. These latter models are easily extended to the derivation of IVBA losses at shorter wavelengths (higher energy transtions) and are therefore used to evaluate the concentration and temperature dependence of the absorption coefficients at several different wavelengths.

CHAPTER 2

ELECTRON-ELECTRON SELF ENERGY

2.0. Introduction

A brief discussion was given in Chapter 1 of the band gap narrowing effects produced by the introduction of large concentrations of carriers into the conduction and/or valence bands of a semiconductor. The shifts in the host band edges which produce the band gap narrowing, can be explained in terms of changes in the many-body (electron-electron) interactions of a band edge electron. This chapter introduces the concept of the self energy of an electron due to its many-body interactions and provides the background material for the detailed calculations in the next two chapters. A Feynman diagrammatic approach is used initially to derive an expression for the self energy of a state $\underline{k}$ in a metal. The modifications required to make the theory appropriate to a semiconductor are then considered, with particular emphasis on the form of the hole gas dielectric function occurring in a heavily doped p-type semiconductor (comparison can then be made with the corresponding work on n-type Si by Saunderson (1983)). Two possible theoretical expressions for this dielectric response are compared and their ease of use in analytic calculations is considered. However, before examining the self energy concept, the materials for which the band edge shifts are to be evaluated and some basic parameters based on their band structure are discussed.

2.1. Semiconductors Considered and Their Electronic Bandstructure

The introduction of high carrier concentrations into the conduction or valence bands of a semiconductor causes a narrowing of the fundamental band gap E_g. This change in band gap correspondingly causes changes

in the optical emission and absorption spectra of the material, which in a lasing material may modify its operational wavelength. With this consideration in mind the band gap narrowing in two alloy materials used in semiconductor lasers for optical fibre communcation $Ga_{0.47}In_{0.53}As$ (λ = 1.6 μm) and $Ga_{0.28}In_{0.72}As_{0.6}P_{0.4}$ (λ = 1.3 μm) is evaluated. Band gap narrowing in the important prototype material GaAs (λ = 0.87 μm) is also determined.

In addition, band gap changes affect the current gain in silicon bipolar transistors. The band gap narrowing in p-type silicon is thus evaluated and compared with the results of Saunderson (1983) for n-type Si.

All four chosen materials have a similar valence band structure which for simplicity is taken to consist of parabolic, isotropic, heavy (HH) and light hole (LH) bands (of masses m_H and m_L respectively), degenerate at the Brillouin zone centre (Γ-point) with a similarly parabolic, isotropic, spin split off (SS) band (mass m_S) separated from these bands by the spin splitting energy Δ. A valence band density of states effective mass is defined in the usual way by

$$m_{Dv} = (m_H^{3/2} + m_L^{3/2})^{2/3} \qquad (2.1) \quad .$$

The three gallium based materials all have a direct energy gap at $\underline{k} = 0$ and a single lowest conduction band minimum which is taken to be isotropic with a density of states effective mass m_{De}. In contrast the band gap of silicon is indirect, the lower part of the conduction band consisting of six valleys formed some 85% of the way from the Brillouin zone centre (Γ) to the zone edges (X) along each of the six [100] directions. The constant energy surfaces of these valleys are not isotropic but near to the band edge may be approximated by ellipsoids characterized by a longitudinal (parallel to the appropriate

[100] direction) mass $m_\ell (= 0.98\ m_o)$ and two transverse masses m_t $(= 0.18\ m_o)$. For each valley i we can define a new set of axes $(\underline{k}'_x, \underline{k}'_y, \underline{k}'_z)$ with origin at the ellipsoid centre $\underline{k}_i$ and with the k'_x axis orientated longitudinally. The energy of a state $\underline{k} = (k_x, k_y, k_z)$ in that valley is then given by

$$E = E_c + \frac{\hbar^2}{2}\left[\frac{k'^2_x}{m_\ell} + \frac{(k'^2_y + k'^2_z)}{m_t}\right] \qquad (2.2)$$

where $\underline{k}'_x = \underline{k}_x - \underline{k}_{ix}$ etc.

The ellipsoidal form of equation (2.2) would present many difficulties in the self energy analysis and hence for each valley the energy-wavevector relation is approximated by

$$E = E_c + \frac{\hbar^2 k^2}{2m_{De}} \qquad (2.3)$$

where m_{De} is the density of states effective mass given by $m_{De} = (m_\ell m_t^2)^{1/3}$. The values of effective masses and the other parameters used in the present calculation are given in Appendix 1.

2.2. Introduction to the Theory of Heavy Doping in Semiconductors

This section contains a preliminary discussion of the effects of adding large concentrations of dopants to otherwise pure semiconductors, a process often used to reduce the size of the depletion region in p-n junction devices.

The dopants of interest in the present work are shallow donors or acceptors - that is they produce energy levels close to the band edges of the host material, e.g. phosphorous in Si. For a single shallow impurity state with a loosely bound electron or hole the carrier wave function is assumed to be of the hydrogenic form

$$\phi(r) = \frac{\exp(-r/a_f)}{(\pi a_f^3)^{1/2}} \qquad (2.4)$$

where a_f is the effective Bohr radius given by,

$$a_f = \frac{\hbar^2 4\pi\varepsilon_o\varepsilon_r}{m_D e^2} = \frac{\hbar^2 4\pi\varepsilon_o\varepsilon_r}{m_D^* m_o e^2} = \frac{\varepsilon_r a_o}{m_D^*} \qquad (2.5)$$

i.e. the normal hydrogenic Bohr radius a_o is modified by the static relative permittivity of the host material ε_r and the density of states effective mass m_D ($m_D = m_D^* m_o$) of the relevant host band.

The corresponding binding energy is given by

$$E_B = \frac{m_D e^4}{2\hbar^2 (4\pi\varepsilon_o\varepsilon_r)^2} \qquad (2.6)$$

The impurity concentration N is often expressed in the form of the dimensionless parameter $N^{1/3}a_f$ (≈ Bohr radius/impurity separation) because this is a convenient way of comparing doping levels in materials with different effective masses and relative permittivities. A related parameter r_s much used in many body theory is defined as the ratio of the carrier spacing to the effective Bohr radius

$$r_s = \left(\frac{3}{4\pi}\right)^{1/3} \frac{1}{N^{1/3}a_f} = \frac{0.62}{N^{1/3}a_f} \qquad (2.7)$$

The approximations implicit in the above expressions are that the host band has a single isotropic valley with a simple effective mass and a Coulombic impurity potential with an absence of chemical effects; that is independent of the type of dopant used.

At low dopant concentrations the impurities are well separated in the host semiconductor and the hydrogencnic like states are well localised around the impurity cores. As the dopant concentration increases the

random distribution of impurities and the decreasing impurity-impurity separation results in a significant overlap of wave functions from two or more impurities. The resulting coupling of the impurity states leads to wave functions that extend over larger and larger regions of space. In uncompensated materials at higher concentrations, e.g. $N^{1/3}a_f \approx 0.25 - 0.33$ ($r_s = 2.5 - 1.88$) (Mott (1974)) states have finite amplitude throughout the system, i.e. are completely delocalised, and metallic like conduction occurs in the impurity states. The concentration at which this transition from insulator to 'metal' occurs is called the Mott critical density N_c.

It has generally been accepted that as the dopant concentration increases the splitting of the impurity levels forms an impurity band which is initially separate from the host band edge but merges with it on increasing the concentration. However, recent work by Mott and Kaveh (1983) and others, indicates that there is no real evidence for the existence of a separate impurity band and there is a discontinuous transition between the existence of localised states close to the host band edge and metallic conduction occurring in the host bands. These arguments however do not affect the present work for which the Mott critical density represents a lower bound to the range of concentrations of interest. The calculations in this thesis are concerned with the high density regime where the delocalised states are in the host band and $r_s \lesssim 2.5$ ($N^{1/3}a_f \gtrsim 0.25$). In this case the large density of carriers occupying the host band fill states up to the Fermi level (at T = OK) and the carrier gas is degenerate. The interaction between electrons is then represented by a screened Coulomb potential of the form

$$V(r) = \frac{e^2 e^{-K|\underline{r}-\underline{r}'|}}{4\pi\varepsilon_o\varepsilon_r|\underline{r}-\underline{r}'|} \qquad (2.9)$$

where K is the Thomas Fermi (T.F.) wavevector defined for electrons in n-type material as;

$$K^2 = \frac{M^{2/3} m_{De} e^2 (3\pi^2 n)^{1/3}}{\pi^2 \hbar^2 \varepsilon_r \varepsilon_o} \tag{2.10}$$

(n being the elctron concentration and M the number of conduction band valleys) and in p-type material as

$$K^2 = \frac{m_{Dv} e^2 (3\pi^2 p)^{1/3}}{\pi^2 \hbar^2 \varepsilon_r \varepsilon_o} \tag{2.10a}$$

where p is the hole concentration.

If both conduction and valence bands are occupied by an electron-hole plasma the T.F. wavevector is defined as:

$$K^2 = K^2 \text{ (electrons)} + K^2 \text{ (holes)} . \tag{2.11}$$

The Fermi level E_f in the conduction and valence bands can be described in terms of another useful parameter, the Fermi wavevector k_f. For electrons this is defined as

$$k_{fe} = \left(\frac{3\pi^2 n}{M}\right)^{1/3} \tag{2.12}$$

and $$E_{fe} = \frac{\hbar^2 k_{fe}^2}{2m_{De}} \tag{2.12a}$$

where if $M > 1$, k_{fe} represents the Fermi wavevector in one valley. The corresponding expressions for holes are

$$k_{fv} = (3\pi^2 p)^{1/3} \tag{2.13}$$

and $E_{fv} = \frac{\hbar^2 k_{fv}^2}{2m_{Dv}}$ (2.13a) .

The concentration dependence of the inverse Fermi wavevector, T.F. screening length $\lambda (= 1/K)$ and the effective Bohr radius for p-type silicon are shown in Figure (2.1)

Having described the important features of the electronic band-structure and defined some basic parameters a brief physical explanation of the self energy concept is now given.

2.3. Self Energy - A Physical Description

In many areas of semiconductor physics carrier-carrier interactions are tacitly ignored. However, in a semiconductor with a high concentration of free carriers the carrier-carrier interactions have been shown to have an important influence on the electronic bandstructure. A simple explanation of these interactions and their effects on the physical properties of the material can be given in terms of the quasi particle concept described below.

For definiteness consider an electron gas in the conduction band of a semiconductor with uniform neutralizing, positive jellium type background. Choosing any one electron as a test particle, examination of its motion through the 'gas' would show that it repels other electrons in its vicinity producing a 'hole' around it in which the positive background charge is exposed. This 'hole' tends to neutralise the charge of the test electron so effectively screening its interaction with other electrons, resulting in a much weakened Coulombic repulsion. The repulsion of electrons to create the initial 'hole' is clearly a dynamic situation as electrons are continually scattered in and out of the region of space near the test electron, and in addition the test particle must be scattered in and out of the 'holes' of other particles. The test particle with its surrounding hole is called a quasi particle and it

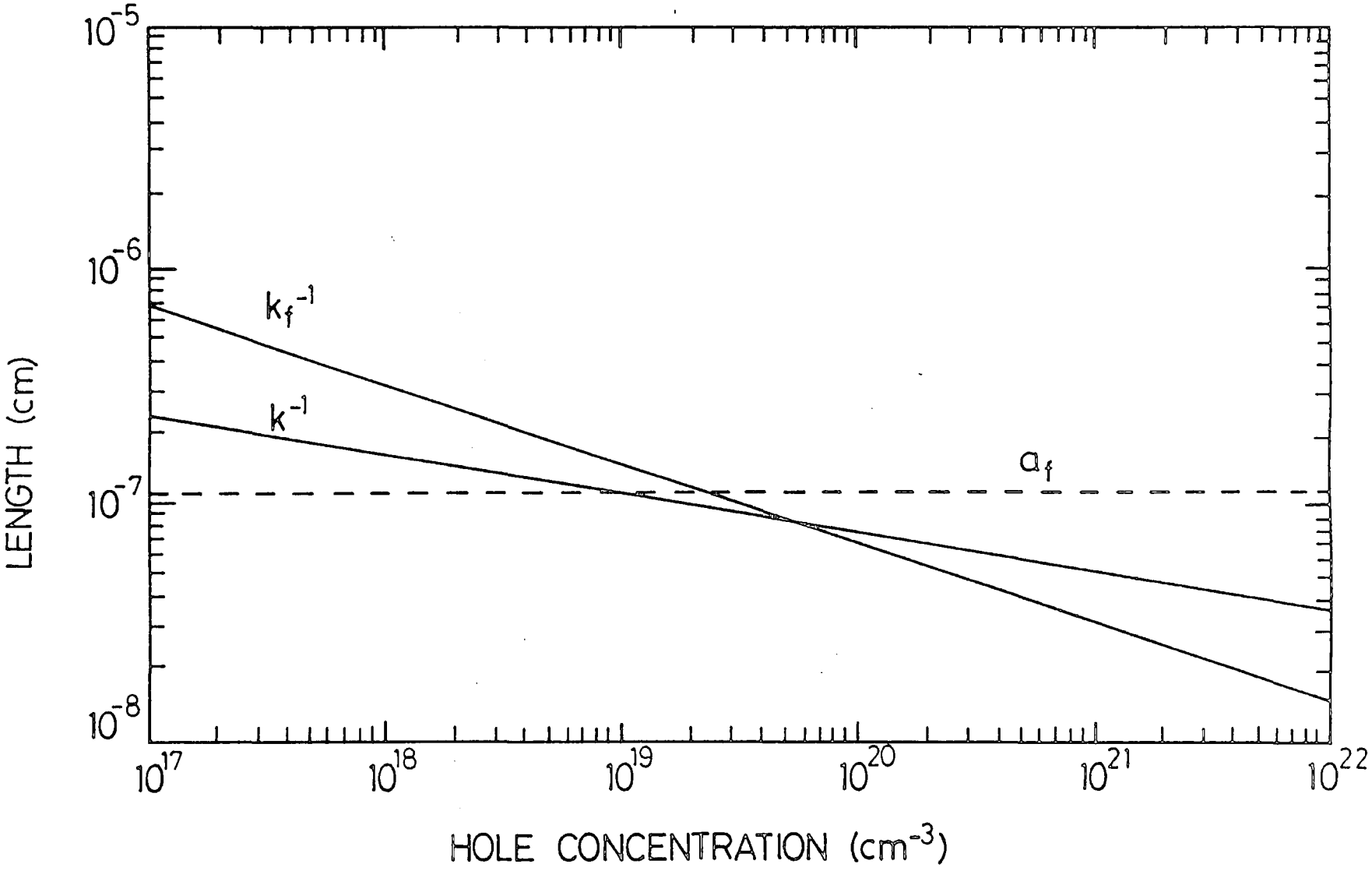

Figure 2.1: The concentration dependence of the inverse Fermi wavevector k_f^{-1} Thomas-Fermi screening length K^{-1} and the effective Bohr radius in p-type Silicon at T = OK.

is a useful concept when its interaction with other quasi particles is weak.

The interaction of the test particle on the surrounding carrier gas which in turn reacts on the test particle causes a contribution to the energy of the quasi particle, which is called the self energy. It is changes in the real part of this self energy brought about through heavy doping, carrier injection or optical excitation which produce energy shifts in the bands and changes in the semiconductor band gap, the carrier concentration dependence of which is evaluated in Chapter 3.

As the quasi particles interact with each other and their environment they have a finite lifetime which is defined by the imaginary part of the self energy. This imaginary part is manifested by a broadening of the quasi particle energy levels and is normally much smaller than the real part. The work in this thesis is concerned only with the real part of the self energy and the energy broadening effects are not considered.

Although all calculations in the present work are for band edge states, energy shifts for other states away from the band edge have been shown in various simplified models (Abram et al 1978 (using the T.F. screening approximation), Rice (1974) and Inkson (1984) for metals) to be approximately the same. The recent work of Sernelius (1986) indicates the difference in energy shift between states at the band edge and the Fermi level is larger than that derived in the simple models. However, for electron-electron interactions these changes are still small. The shift variation with state that does occur causes a distortion of the $E - \underline{k}$ dispersion relation and modifies the quasi particle effective mass. However, for the present work these changes are ignored and the host bands are considered to shift rigidly for $\underline{k}$-values close to the band edge.

2.4. Self Energy Expression - A Diagrammatic Interpretation

The derivation of the self energy of a state in the conduction or valence band of a semiconductor, closely follows that for a high density electron gas in a metal. Hence the well documented procedure (see for example Mattuck 1976) for obtaining the self energy of an electron in a metal using a Feynman (1949) diagrammatic analysis is reviewed first. The changes required to derive the appropriate expression for a semiconductor are discussed in section 2.5.

The single particle propagator or Green's function for a quasi particle in a high density electron gas can be expressed as a sum over all repetitions of all irreducible self-energy parts, which for diagrams in $(\underline{k},\omega)$ space is:

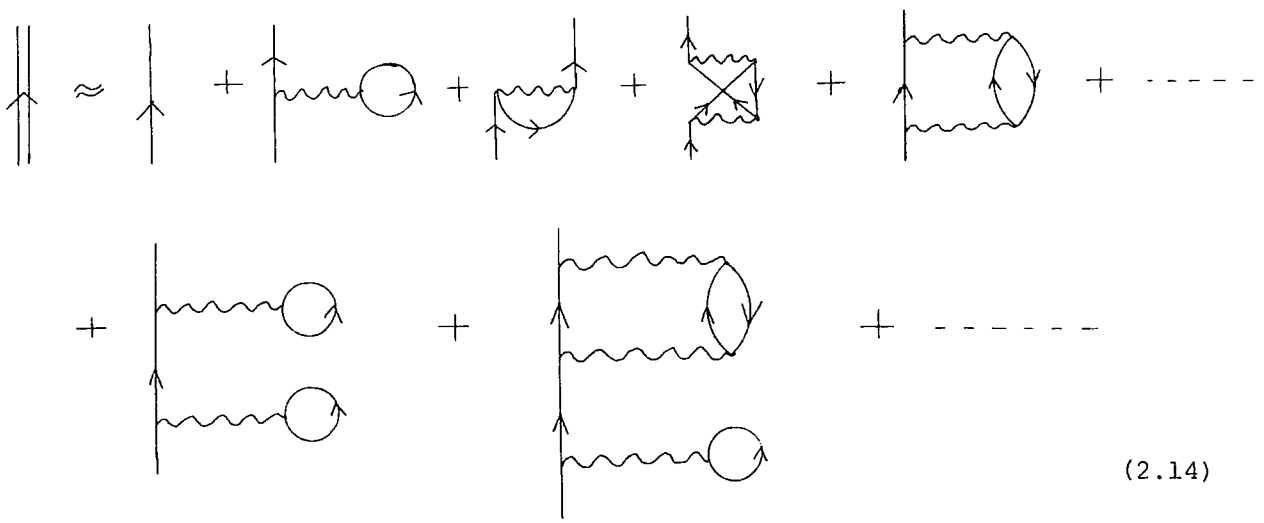

(2.14)

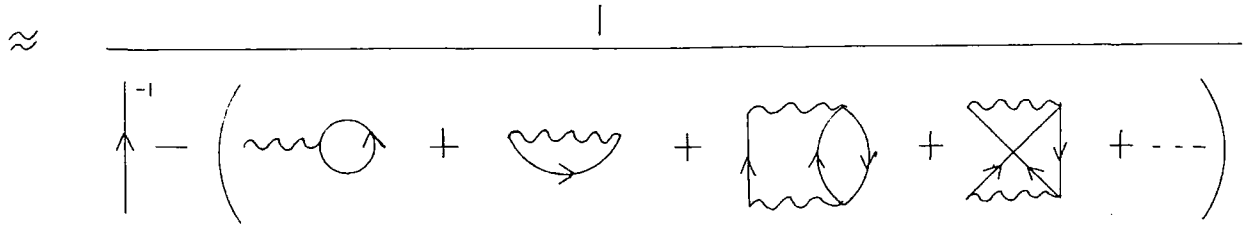

(2.15)

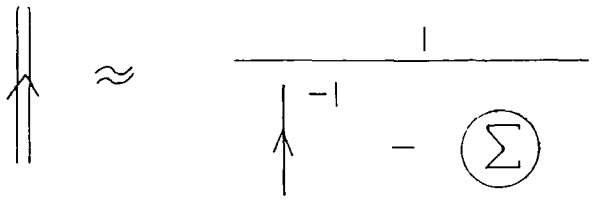

(2.16)

where single lines represent the single free particle propagator or Green's function, double lines represent the quasi particle propagator, and wiggly lines represent the unscreened interaction $(-iV_{og})$ between two particles. The self energy (Σ) is then given by:

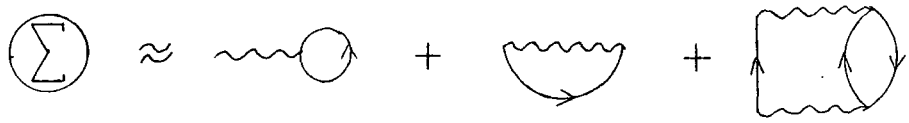

(2.17) .

The above expressions for the self energy and propagator are indicated as being approximate due to the omission of factors such as vertex corrections (see Chapter 11, Mattuck 1976).

The Dyson equation (2.16) can be expressed algebraically as:

$$G(\underline{k},\omega) = \frac{1}{[G^{o}(\underline{k},\omega)]^{-1} - \Sigma(k,\omega)/\hbar} \tag{2.18}$$

where $G^{o}(\underline{k},\omega)$ is the free particle propagator or Green's function for an electron in state $\underline{k}$, $G(\underline{k},\omega)$ is the quasi particle propagator or total Green's function and $\Sigma(\underline{k},\omega)$ is the self energy of state $\underline{k}$. The free particle propagator is defined as:

$$G^{o}(\underline{k},\omega) = \frac{1}{\omega-\omega_{\underline{k}}+i\delta\,\mathrm{sgn}(\hbar\omega_{\underline{k}}-\hbar\omega_{f})} \tag{2.19}$$

where $\hbar\omega_{k}$ is the energy of state $\underline{k}$ the value of which with respect to the Fermi energy $\hbar\omega_{f}$ determines the sign of the complex infinitesimal $i\delta$.

The quasi particle propagator thus has the same form as the free particle Green's function but with a modified energy $\hbar\omega_{\underline{k}} + \Sigma(\underline{k},\omega)$

rather than $\hbar\omega_k$. In general the self energy is a complex term where the imaginary part defines the quasi particle lifetime τ or energy broadening $\Delta E = \hbar/\tau$ of the state $\underline{k}$, and the real part defines the quasi particle energy, i.e.

$$E_{\underline{k}} = \hbar\omega_{\underline{k}} + \mathrm{Re}[\Sigma(\underline{k},\omega)] \qquad (2.20)$$

The Dyson equation (2.16) can also be expressed in its more general form through algebraic manipulation as:

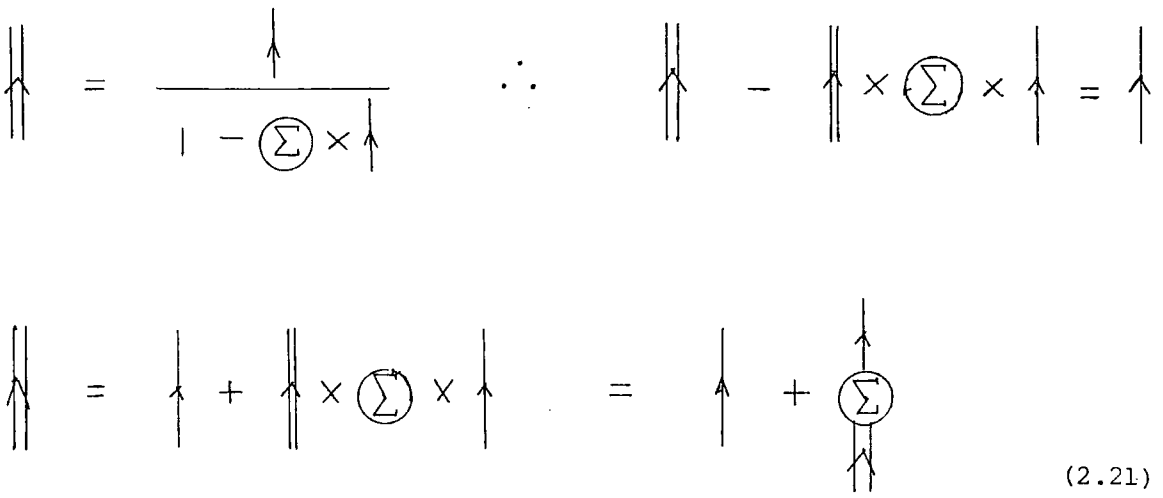

(2.21)

The first term in expression , (2.17) the bubble diagram, represents the average electron-electron interaction which cancels with the positive jellium background and therefore can be removed from the diagram sum. Of the remaining terms only the most divergent of the irreducible polarisation parts in (2.17) are considered to be important. These dominant terms in the self energy series then give

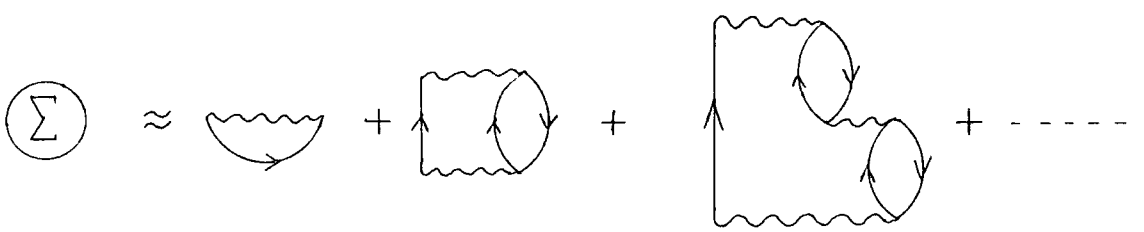

(2.22)

That is, the only remaining diagrams are the first order exchange diagram and the infinite series of pair-bubble diagrams. The partial sum (so called because many terms are now omitted) over repeated pair-bubble diagrams, is the Random Phase Approximation (RPA) for the self energy. Factoring out a free propagator from each diagram in equation (2.22) gives:

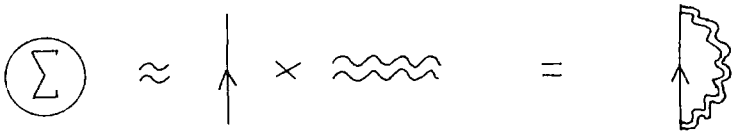

(2.23)

where

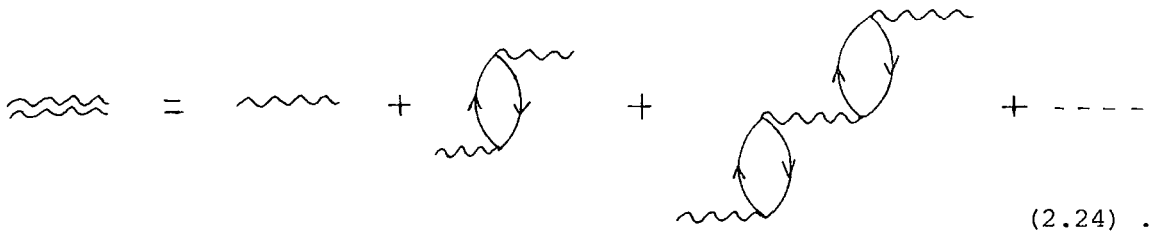

(2.24) .

The double wiggle in equations (2.23) and (2.24) is the effective interaction calculated in the RPA and is essentially the screened interaction ($-iV_{eff}$(RPA)) between two particles.

Expression (2.24) can be factorised as:

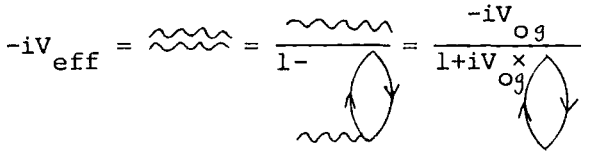

(2.25) .

As will be seen in more detail in section 2.6 the denominator in equation (2.25) represents the dielectric function of the electron gas.

Using expression (2.23) and the diagrammatic rules given by Mattuck (1976) the general self energy expression in the random phase approximation is written as:

$$-i\Sigma(\underline{k},\omega) = \frac{1}{(2\pi)^4}\int [iG_o(\underline{k}-\underline{q},\omega-\nu)][-iV_{eff}(\underline{q},\nu)]e^{-i\nu\delta}\, d^3\underline{q}\, d\nu \quad (2.26)$$

where a sum over spin states is included, δ is a positive infinitesimal and the exponential factor conserves causality. This final expression can now be used as a basis for the derivation of the self energy of a conduction or valence band state in a semiconductor.

2.5. Self Energy in a Semiconductor

The analysis in the previous section related to a high density electron gas and can be applied directly to a simple free electron model of a metal. However, in a semiconductor we must take account of the fact that electrons exist in several bands, and holes can occupy overlapping valence bands. To be able to incorporate these factors into the self energy calculation we revert to the spatially dependent form of expression (2.26) in which the semiconductor bandstructure is included through the appropriate Bloch wave functions and effective masses, in the Green's function and effective interaction V_{eff}.

Fourier transformation of both sides of equation (2.26) gives the spatially dependent self energy operator:

$$\Sigma(\underline{r},\underline{r}',\omega) = \frac{i}{2\pi}\int G^o(\underline{r},\underline{r}',\omega-\nu)V_{eff}(\underline{r},\underline{r}',\nu)e^{-i\nu\delta}\, d\nu \quad (2.27)$$

To determine the energy shifts induced by adding carriers to the conduction or valence bands we need to evaluate the expectation value of the real part of the self energy operator $\Sigma(\underline{r},\underline{r}',\omega)$ for these bands, for both doped and intrinsic material. The following derivation of appropriate expressions for these energy shifts and the subsequent determination of the dielectric function is essentially the same as the analysis used in the paper by Abram et al (1984).

If the expectation value of $\Sigma(\underline{r},\underline{r}',\omega)$ for band n at wavevector $\underline{k}$ is $E_n^{\Sigma}(\underline{k})$ then the shift of the state $n,\underline{k}$ upon doping is given by:

$$\Delta E_n^{\Sigma}(\underline{k}) = \mathrm{Re}[E_n^{\Sigma}(\underline{k})]\Big|_{\text{doped}} - \mathrm{Re}[E_n^{\Sigma}(\underline{k})]\Big|_{\text{intrinsic}} \tag{2.28}$$

and the resulting band gap narrowing is determined by shifts in the conduction and valence band edges:

$$\Delta E_g = \Delta E_c^{\Sigma}(\underline{k}_{co}) - \Delta E_v^{\Sigma}(\underline{k}_{vo}) \tag{2.29}$$

where $\underline{k}_{co}$ and $\underline{k}_{vo}$ represent the appropriate band edge states. $E_n^{\Sigma}(\underline{k})$ is evaluated using the expression (Hedin and Lundqvist, 1969).

$$E_n^{\Sigma}(\underline{k}) = \int \phi^*_{n\underline{k}}(\underline{r})\Sigma(\underline{r},\underline{r}',\omega_{n\underline{k}})\phi_{n\underline{k}}(\underline{r}')d^3\underline{r}\, d^3\underline{r}' \tag{2.30}$$

where the $\phi_{n\underline{k}}(\underline{r})$ are the semiconductor Bloch functions for state $\underline{k}$ in band n, and we have assumed the Bloch functions do not change with doping. The self energy operator is given by expression (2.27) in which the spatially dependent Green's function is derived from the wavevector dependent free particle propagator as:

$$G^{o}(\underline{r},\underline{r}',\omega-\nu) = \sum_{n''\underline{k}''} \frac{\phi_{n''\underline{k}''}(\underline{r})\phi^*_{n''\underline{k}''}(\underline{r}')}{\omega-\nu-\omega_{n''\underline{k}''}+i\delta\,\mathrm{sgn}(\hbar\omega_{n''\underline{k}''}-\hbar\omega_f)} \tag{2.31}$$

and the dynamically screened Coulomb interaction is given by the Fourier transform of the wavevector dependent expression (2.25) i.e.

$$V_{\text{eff}}(\underline{r},\underline{r}',\nu) = \frac{1}{(2\pi)^3}\int V_{\text{eff}}(\underline{q},\nu)\exp[i\underline{q}\cdot(\underline{r}-\underline{r}')]d^3\underline{q} \tag{2.32}$$

The explicit derivation of $V_{eff}(\underline{q},\nu)$ is given in section 2.6.

Substitution of expressions (2.31), (2.32) and (2.27) into (2.30) gives:

$$E_n^{\Sigma}(\underline{k}) = \frac{i}{(2\pi)^4}\int\int\int\int\int \sum_{n''\underline{k}''} \frac{\phi^*_{n\underline{k}}(\underline{r})\phi_{n\underline{k}}(\underline{r}')\phi_{n''\underline{k}''}(\underline{r})\phi^*_{n''\underline{k}''}(\underline{r}')e^{i\underline{q}\cdot(\underline{r}-\underline{r}')}}{\omega_{n\underline{k}}-\nu-\omega_{n''\underline{k}''}+i\delta\,\mathrm{sgn}(\hbar\omega_{n''\underline{k}''}-\hbar\omega_f)} \cdot$$

$$V_{eff}(\underline{q},\nu)e^{-i\delta\nu}\, d\nu d^3\underline{q} d^3\underline{r} d^3\underline{r}' \qquad (2.33)$$

which can be reduced to

$$E_n^{\Sigma}(\underline{k}) = \frac{i}{(2\pi)^4}\iint \sum_{n''\underline{k}''} \left|\int \phi^*_{n\underline{k}}(\underline{r})\phi_{n''\underline{k}''}(\underline{r})e^{i\underline{q}\cdot\underline{r}}\, d^3\underline{r}\right|^2 V_{eff}(\underline{q},\nu) \cdot$$

$$\frac{e^{-i\delta\nu}}{\omega_{n\underline{k}}-\nu-\omega_{n''\underline{k}''}+i\delta\,\mathrm{sgn}(\hbar\omega_{n''\underline{k}''}-\hbar\omega_f)}\, d^3\underline{q}\, d\nu \qquad (2.34) \cdot$$

The squared factor involving Bloch functions can also be simplified as follows. For states normalised to the crystal volume Ω and Bloch periodic parts normalised to the unit cell volume Ω_{cell} the Bloch functions are given by:

$$\phi_{n\underline{k}}(\underline{r}) = \left\{\frac{\Omega_{cell}}{\Omega}\right\}^{1/2} u_{n\underline{k}}(\underline{r})e^{i\underline{k}\cdot\underline{r}} \qquad (2.35)$$

which gives

$$\int \phi^*_{n\underline{k}}(\underline{r})\phi_{n''\underline{k}''}(\underline{r})e^{i\underline{q}\cdot\underline{r}}\, d^3\underline{r} = \frac{\Omega_{cell}}{\Omega}\int u^*_{n\underline{k}}(\underline{r})u_{n''\underline{k}''}(\underline{r})e^{i(\underline{k}''+\underline{q}-\underline{k})\cdot\underline{r}}\, d^3\underline{r} \qquad (2.36) \cdot$$

This expression is evaluated in Appendix 2 by expanding the Bloch product in terms of reciprocal lattice vectors $\underline{g}$ and then retaining only terms for which $\underline{g} = 0$ on the assumption that contributions from

terms with finite $\underline{q}$ values are very small. Expression (2.36) then reduces to:

$$\int \phi^*_{n\underline{k}}(\underline{r})\phi_{n''\underline{k}''}(\underline{r})e^{i\underline{q}\cdot\underline{r}}d^3r = \delta_{o,\underline{k}-\underline{k}''-\underline{q}}\, I_{n\underline{k},n''\underline{k}''} \qquad (2.37)$$

where $I_{n\underline{k},n''\underline{k}''}$ is the overlap integral between the Bloch function periodic parts:

$$I_{n\underline{k},n''\underline{k}''} = \int_{\Omega_{cell}} u^*_{n\underline{k}}(\underline{r})u_{n''\underline{k}''}(\underline{r})d^3\underline{r} \qquad (2.38)\ .$$

Substitution of equation (2.37) into (2.34) and performing the sum over $\underline{k}''$ gives:

$$E^{\Sigma}_{n}(\underline{k}) = \frac{i}{(2\pi)^4}\int \sum_{n''} \left|I_{n\underline{k},n''\underline{k}-\underline{q}}\right|^2 \frac{V_{eff}(\underline{q},\nu)e^{-i\nu\delta}d^3\underline{q}\,d\nu}{\omega_{n\underline{k}}-\nu-\omega_{n''\underline{k}-\underline{q}}+i\delta\,sgn(\hbar\omega_{n''\underline{k}-\underline{q}}-\hbar\omega_f)} \qquad (2.39)\ .$$

The explicit determination of the squared moduli of the overlap integrals is now considered.

2.5.1. Evaluation of Bloch Function Overlap Integrals

The inter- and intraband overlap integrals between states $\underline{k}$ and $\underline{k}'$ for the heavy and light hole valence bands have been derived for a range of semiconductor materials by Wiley (1971), using wave functions derived from Kane's (1957) four band $\underline{k}\cdot\underline{p}$ model. In this model the conduction band states at the band edge have purely s-like symmetry and the valence band states have p-like symmetry. For states away from the band edge the $\underline{k}\cdot\underline{p}$ perturbation mixes s and p like orbitals in both conduction and valence bands and the overlap integrals are determined by the coefficients of the different orbital symmetries at the relevant values of $\underline{k}$ and $\underline{k}'$.

In the present analysis the evaluation of equation (2.39) for the band edges requires $\underline{k} = 0$ (corresponding to the band edge) and $\underline{k}' = \underline{k} - \underline{q}$ with small $\underline{q}$ (as only small $\underline{q}$ values provide a significant contribution to the integral in equation (2.39)). Under these circumstances the expressions derived by Wiley and used in the present analysis for the squared moduli of the valence band overlap integrals are given by

$$\left|I_{n\underline{k},n''\underline{k}-\underline{q}}\right|^2 \approx \frac{3}{4}\sin^2\theta \qquad n \neq n'' \text{ where } n,n'' \equiv \text{HH or LH bands}$$

$$\left|I_{n\underline{k},n''\underline{k}-\underline{q}}\right|^2 \approx \frac{1}{4}(1 + 3\cos^2\theta) \qquad n = n'' \text{ where } n,n'' \equiv \text{HH or LH bands}$$

$$\left|I_{n\underline{k},n''\underline{k}-\underline{q}}\right|^2 \approx 0 \qquad n \neq n'' \text{ where } n \equiv \text{HH or LH and } n'' \text{ is SS band or vice-versa} \tag{2.40a}$$

where θ is the angle between $\underline{k}$ and $\underline{k} - \underline{q}$, HH, LH and SS are the heavy hole, light hole and spin split-off bands respectively. The angular dependence of these terms arises from the predominantly p-like nature of the Bloch function period parts.

The corresponding overlap term for state $\underline{k}$ near the conduction band edge is determined by the predominant s-like character of the conduction band Bloch periodic part and its orthogonality to the Bloch function period parts of other bands at the same $\underline{k}$, thus

$$\left|I_{c\underline{k},n''\underline{k}-\underline{q}}\right|^2 \approx \begin{cases} 1 & n'' \text{ same conduction band minimum} \\ 0 & n'' \text{ all other bands} \end{cases} \tag{2.40b}$$

These results from a simplified $\underline{k}\cdot\underline{p}$ calculation are in excellent agreement with pseudopotential bandstructure calculations of the same quantities carried out by Brand (1984). The overlap integrals between the spin split-off and the heavy and light hole valence bands in the materials considered is only relevant in the case of silicon for which the spin splitting energy Δ is relatively small ($\Delta \simeq 0.045$ eV) resulting in occupancy of the spin split-off band for high hole densities. The spin splitting energy of the other materials considered, is too large for hole occupancy of this band (at $T = 0K$) to occur.

To evaluate the integral equation (2.39) we must now derive an explicit expression for the screened Coulomb term $V_{eff}(\underline{q},\nu)$ applicable to electron, hole or plasma screening gases.

2.6. Evaluation of the Dynamically Screened Coulomb Interaction

The Coulomb interaction between two electrons is given by

$$V_{og}(r) = \frac{e^2}{4\pi\varepsilon_o r} \qquad (2.41)$$

In a semiconductor with an intrinsic dielectric constant ε_r the interaction becomes

$$V_o(r) = \frac{e^2}{4\pi\varepsilon_r\varepsilon_o r} \qquad (2.42)$$

Expressed in wavevector space this interaction is

$$V_o(\underline{q}) = \frac{e^2}{\varepsilon_o\varepsilon_r q^2} \qquad (2.43)$$

where ε_r is taken to be independent of wavevector and frequency.

In a heavily doped semiconductor with an electron or hole gas in the relevant band, the Coulomb interaction is screened by the carrier gas. The susceptibility of the carrier gas must therefore be added to the intrinsic dielectric constant of the semiconductor to give a wavevector and frequency dependent dielectric function $\varepsilon(\underline{q},\nu)$ which converts the bare Coulomb interaction into the screened interaction

$$V_{eff}(\underline{q},\nu) = \frac{V_o}{\varepsilon(\underline{q},\nu)} \qquad (2.44) \ .$$

We thus need to determine the dielectric function $\varepsilon(\underline{q},\nu)$ for the doped semiconductor.

2.6.1. Derivation of the Carrier Gas Dielectric Function

The form of equation (2.44) for a free electron gas has already been introduced in equation (2.25) which was obtained by a diagrammatic derivation. In equation (2.25) the effective interaction is given as:

$$V_{eff}(\underline{q},\nu) = \frac{V_{og}}{1+V_{og}\, i\times \text{(bubble)}} = \frac{V_{og}}{1+V_{og}\pi^{o}(\underline{q},\nu)} \qquad (2.45)$$

or

$$V_{eff}(\underline{q},\nu) = \frac{V_{og}}{\varepsilon_g(\underline{q},\nu)} \qquad (2.46)$$

where $\varepsilon_g(\underline{q},\nu) = 1 + V_{og}\pi^{o}(\underline{q},\nu)$ is the dielectric function for a free electron gas.

The pair-bubble diagram represents the polarisability $-i\pi^{o}(\underline{q},\nu)$ of the electron gas to zeroth order, that is it represents the simplest process showing the effects of correlation on the motion of a particle. The pair-bubble term can be evaluated using the dictionary interpretation of the free particle propagator (Mattuck 1976, Fetter and Walecka 1971).

The resulting expression for $\varepsilon_g(\underline{q},\nu)$ is the Lindhard dielectric function for an electron gas, which can also be derived in the Random Phase Approximation by perturbation theory (Wooten 1972, Ziman 1972). The modifications necessary to convert the Lindhard expression for a free electron gas to that appropriate for electrons in the conduction band of a semiconductor amount to the replacement of the free electron mass with the conduction band density of states effective mass m_{De}, and the inclusion of the static dielectric constant ε_r in the bare interaction term. The corresponding expression for p-type materials is however complicated by hole occupation of two (heavy and light hole) and possible three (spin split-off) valence bands and also by the resulting increase in the polarisability due to interband transitions. The complexity of the resulting expression is increased further by the angular dependence of the overlap integrals $(I_{n\underline{k},n''\underline{k}''})$ between the Bloch function periodic parts of the heavy and light hole states as shown in section 2.5.

A full derivation of the hole gas dielectric function incorporating the above modifications is given by Bardyszewski (1986). However, it has a very complicated algebraic form which makes its use in the energy expression (2.39) prohibitive. An obvious simplification of the Bardyszweski expression can be made by approximating the valence band to a single isotropic band with a density of states effective mass m_{Dv} and an overlap between the Bloch periodic parts of unity. The resulting Lindhard expression for the dielectric function (equation (2.47)) then has the same form as that derived for the conduction band electron gas.

$$\varepsilon(\underline{q},\nu) = 1 + \frac{K^2}{2q^2}\left[1 + \frac{k_{fv}}{2q}\left[f\left(\frac{k_{fv}(E_q - \hbar(\nu+i\delta))}{E_{fv}q}\right) + f\left(\frac{k_{fv}(E_q + \hbar(\nu+i\delta))}{E_{fv}q}\right)\right]\right] \quad (2.47)$$

where E_{fv} is the Fermi energy, k_{fv} is defined as

$$E_{fv} = \frac{\hbar^2 k_{fv}^2}{2m_{Dv}} \qquad \text{and} \qquad f(x) = \left(\frac{1-x^2}{4}\right) \ln\left|\frac{(x+2)}{(x-2)}\right| \tag{2.48}$$

It is possible to use dielectric function expressions of the form of equation (2.47) in the self energy calculation (see for example Berggren and Sernelius (1981)) but the Lindhard form leads to a cumbersome analysis. However, a useful and accurate approximation to the inverse dielectric function of an electron gas has been used by several authors (Lundqvist (1967 a,b), and Inkson (1984)) and it is this plasmon pole approximation for both electron and hole gases in a semiconductor which is described in the next section and used for the evaluation of equation (2.39) in the present work.

2.6.2. The Plasmon Pole Approximation

The detailed derivation for the plasmon pole expression in n-type silicon has been given by Saunderson (1983), but for clarity the basic concepts (omitting much of the algebra) are given below.

Examination of expression (2.46) indicates that as $\varepsilon(\underline{q},\nu) \rightarrow 0$ the effective interaction $V_{eff}(\underline{q},\nu) \rightarrow \infty$ that is the zeros in the Lindhard dielectric function correspond to a self-exciting system in which the mode of excitation is a plasma oscillation, that is a collective oscillation of the carrier gas. In the plasmon pole approximation it is assumed that the dominant response of the carrier gas to the field of another carrier can be described in terms of plasmons (the quanta of plasma oscillations). On this assumption the resulting expression for the inverse dielectric function in the plasmon pole approximation for a carrier gas in a single isotropic parabolic band is given by (Hedin and Lundqvist (1969)).

$$(\varepsilon(\underline{q},\nu))^{-1} = 1 + \frac{\omega_p^2}{2\omega_1(\underline{q})}\left(\frac{1}{\nu-\omega_1(\underline{q})+i\delta} - \frac{1}{\nu+\omega_1(\underline{q})-i\delta}\right) \qquad (2.49)$$

where

$$\omega_1^2(q) = \omega_p^2 + aq^2 + bq^4 \qquad (2.50)$$

$\omega_1(\underline{q})$ is the plasmon angular frequency expressed as a function of wavevector $\underline{q}$, and ω_p is the $\underline{q} = 0$ plasmon angular frequency. In fact the constants a and b in the second and third terms of the plasmon dispersion relation $\omega_1(\underline{q})$ are normally chosen to get the correct screening behaviour in certain limits. In the present calculation the constant a is chosen to give the value of $\varepsilon(\underline{q},\nu)$ predicted by the Thomas-Fermi (T.F) theory for $\nu = 0$ and $\underline{q} \to 0$. That is, $a = \omega_p^2/K^2$ where K takes the appropriate form of equations (2.10) and (2.10a) for electrons and holes. Then

$$\omega_1^2(q) \simeq \omega_p^2\left(1 + \frac{q^2}{K^2}\right) \quad \text{as} \quad \underline{q} \to 0 \qquad (2.51)$$

and substitution into (2.49) gives the T.F. approximation to the inverse dielectric function

$$\frac{1}{\varepsilon(\underline{q},0)} = 1 - \frac{\omega_p^2}{\omega_1^2(q)} = \frac{q^2}{q^2+K^2} \qquad (2.52)$$

The third term in the plasmon dispersion relation is quartic in q and gives an approximate representation of the effects of particle-hole transitions - that is the single particle excitations that have hitherto been ignored in the plasmon pole approximation. It is important for obtaining the right sort of behaviour for $\varepsilon(\underline{q},\nu)^{-1}$ at large values of $\underline{q}$ where the Thomas-Fermi theory becomes inadequate. The constant b is thus chosen to make the quartic term have the form of a carrier dispersion relation $\left(\omega_{nq} = \frac{\hbar q^2}{2m_n}\right)$ relevant to band n. Hence $b = \frac{\hbar^2}{4m_n^2}$

where m_n is the density of states effective mass for a carrier in band n. The plasmon dispersion relation is then given by:

$$\omega_l^2(q) = \omega_p^2\left(1 + \frac{q^2}{K^2}\right) + \omega_{nq}^2 \qquad (2.53)$$

The above discussion and expressions (2.49) and (2.53) are based on carriers in a single isotropic parabolic band. For electrons in the single valley conduction band of the gallium based materials discussed in section 2.1 this represents a good approximation and expressions (2.49) and (2.53) can be applied without modification using:

$$\omega_{cq} = \frac{\hbar q^2}{2m_{De}} \quad \text{and} \quad \omega_p^2 = \frac{ne^2}{\varepsilon_o \varepsilon_r m_{De}} \qquad (2.54)$$

and expressions (2.10/2.10a) for the T.F. screening wavevector with the number of conduction band valleys M = 1.

In n-type Si however the electrons occupy six anisotropic conduction band valleys and a single parabolic conduction band model is clearly inadequate. The simplest way to account for this difference in bandstructure is to incorporate the band parameters into the plasmon dispersion relation $\omega_l(\underline{q})$ and then use this relation in expression (2.49) as before. The appropriate expressions for K and the density of states effective mass have already been given in section 2.2. The expression for the $\underline{q} = 0$ plasmon angular frequency ω_p is derived in Appendix 3 using a classical model based on equal populations of electrons in each valley, and is given by:

$$\omega_p^2 = \frac{ne^2}{\varepsilon_o \varepsilon_r m_{ope}} \qquad (2.55)$$

where n is the electron concentration, and m_{ope} is the electron optical mass defined as:

$$\frac{1}{m_{ope}} = \frac{1}{3}\left(\frac{2}{m_t} + \frac{1}{m_\ell}\right) \qquad (2.56)$$.

Allowing for the somewhat indefinite nature of the prefactor b for the quartic q term the density of states (rather than the optical) effective mass is retained, i.e. $b = \frac{\hbar^2}{4m_{De}^2}$.

As already discussed for p-type materials the holes occupy two (heavy and light hole) and possibly three (spin split off band in the case of Si) valence bands. The T.F. wavevector is given by expression (2.10a) with the density of states effective mass defined as equation (2.1). Note, the hole occupancy of the silicon spin split off band will be discussed in the next chapter and for the remainder of the present discussion is ignored.

The plasma frequency ω_p is modified to account for occupancy of light and heavy hole bands by the expression

$$\omega_p^2 = \frac{pe^2}{\varepsilon_o \varepsilon_r m_{ov}} \qquad (2.57)$$

where

$$\frac{1}{m_{ov}} = \frac{m_H^{1/2}}{m_H^{3/2} + m_L^{3/2}} + \frac{m_L^{1/2}}{m_H^{3/2} + m_L^{3/2}} \qquad (2.57a)$$.

The above expression is derived in Appendix 3 using a classical calculation, with the resulting mass term differing slightly from the hole optical mass $\frac{1}{m_{oH}} = \frac{1}{2}\left(\frac{1}{m_H} + \frac{1}{m_L}\right)$. An equivalent expression is

$$\omega_p^2 = \frac{e^2}{\varepsilon_o \varepsilon_r}\left(\frac{p_H}{m_H} + \frac{p_L}{m_L}\right) \qquad (2.58)$$

where p_H and p_L are the concentrations of heavy and light holes respectively. For the quartic term in the plasmon dispersion relation the density of states effective mass is again used, i.e. $b = \hbar^2/4m_{Dv}^2$.

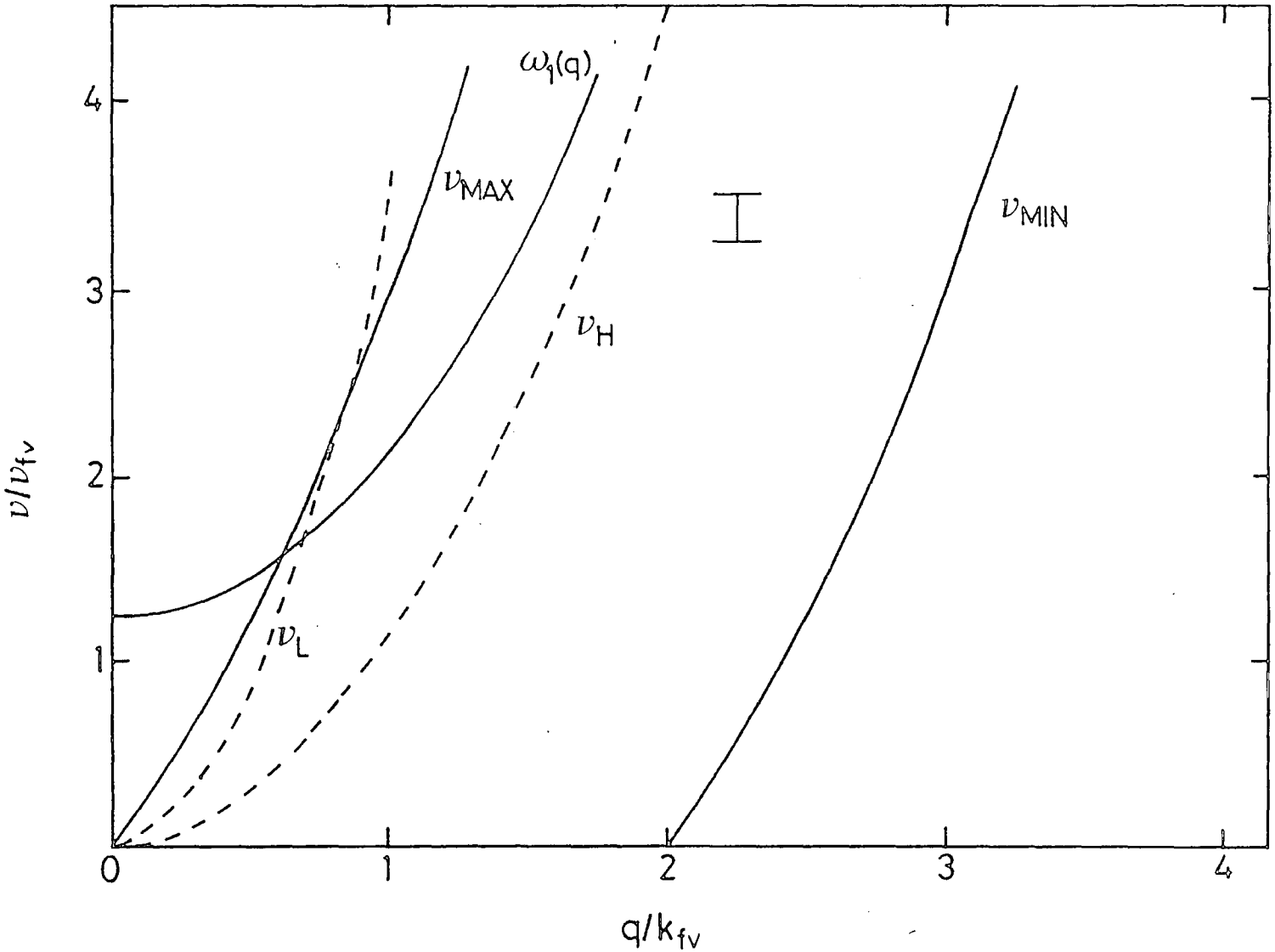

Figure 2.2: The plasmon dispersion curve for a hole concentration in Silicon of 10^{20} cm^{-3}. Region I indicates the region of allowed single particle excitations between ν_{max} and ν_{min}. The heavy and light hole dispersions $\nu_{H,L} = \hbar q^2/2m_{H,L}$ are also shown.

For materials containing an electron-hole plasma, expression (2.11) is used for the T.F. wavevector and a natural extension of the above arguments gives (Appendix 3).

$$\omega_p^2 = \omega_p^2(\text{electrons}) + \omega_p^2(\text{holes}) \qquad (2.59) \ .$$

An average mass $m_{AV} = (m_H + m_L + m_{De})/3$ is used in the quartic term.

Using the approximations described above, the plasmon dispersion relation $\omega_l(\underline{q})$ for a hole gas in the silicon valence band (for $p = 10^{20} cm^{-3}$) is drawn in Figure 2.2 together with the light and heavy hole dispersion relations $\nu = \hbar q^2/2m_{H,L}$. The region (I) of q and ν for which single particle excitations are possible (that is the region in which plasmon oscillations are damped) is also shown, with the maximum ν_{max} and minimum ν_{min} energy values for these transitions indicated.

$$\frac{\nu_{max}}{\nu_{fv}} = \frac{q^2}{k_{fv}^2} + \frac{2q}{k_{fv}}$$

$$\frac{\nu_{min}}{\nu_{fv}} = \frac{q^2}{k_{fv}^2} - \frac{2q}{k_{fv}} \qquad (2.60) \ .$$

A comparison of the real parts of the inverse dielectric functions $\mathrm{Re}(\varepsilon(\underline{q},\nu)^{-1})$ for n-type Si in the Lindhard and plasmon pole approximations has been given by Saunderson (1983), Figures 2.3a and b, and agreement between the two models is seen to be good. A corresponding comparison for p-type silicon would involve a derivation of the Lindhard function using the full complexity of the valence band structure and incorporating the light-heavy hole interband transitions (Bardyszewski 1986). This derivation however is somewhat lengthy and a simpler comparison can be made using the single band approximation to the Lindhard function

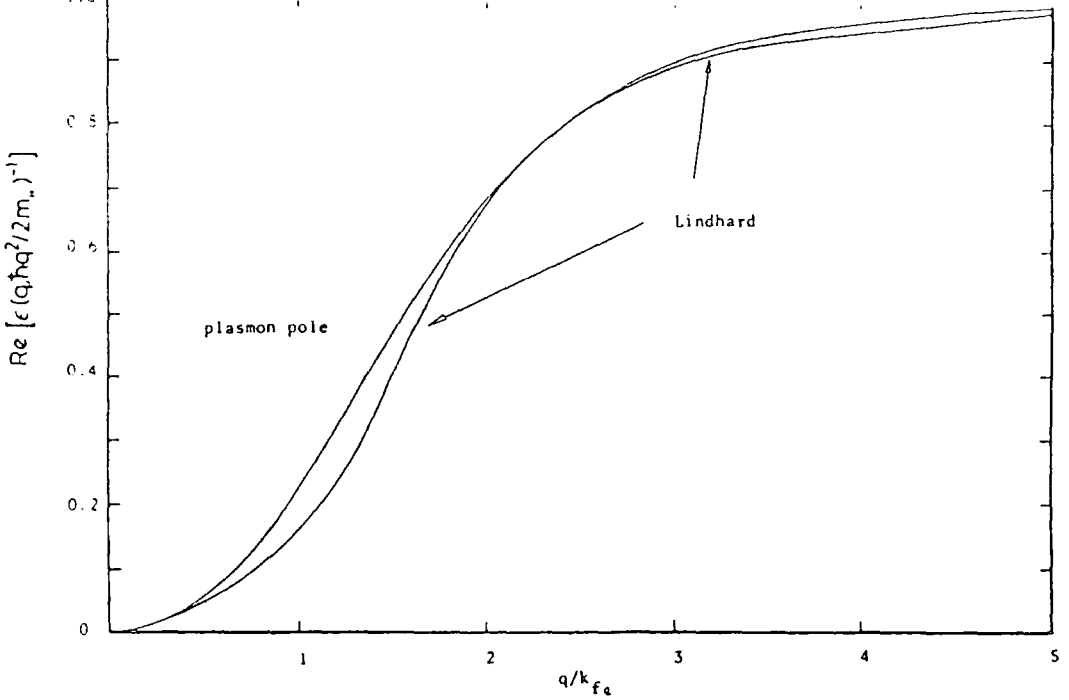

Figure 2.3a: The real part of the inverse Lindhard and plasmon pole dielectric functions for $\nu = \hbar q^2/2m_H$ for an electron concentration of 10^{20} cm^{-3} in Si.

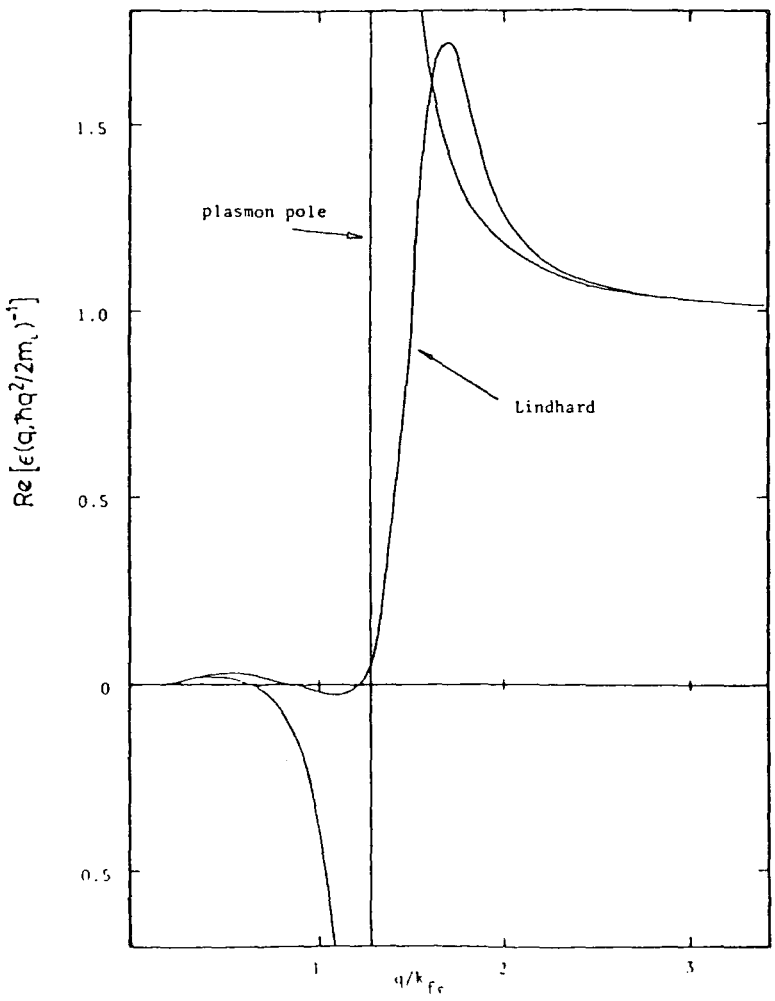

Figure 2.3b: The real part of the inverse Lindhard and plasmon pole dielectric functions for $\nu = \hbar q^2/2m_L$ for an electron concentration of 10^{20} cm^{-3} in Si.

given in expression (2.47). As the plasmon pole equation (2.49) is derived from a single band Lindhard expression, comparison of these two models is more relevant to the present calculation, than use of the full Lindhard expression. This comparison of the real parts of the inverse dielectric functions is made in Figures 2.4 and 2.5 for a range of $\underline{q}$ and corresponding ν coupled by the heavy hole (Figure 2.4) and light hole (Figure 2.5) band dispersion relation (i.e. $\nu = \hbar\underline{q}^2/2m_{H,L}$). In Figure 2.4 the inverse dielectric function in the plasmon pole approximation diverges at $\underline{q} \approx 3\underline{k}_{fv}$ where the heavy hole dispersion $\nu = \hbar\underline{q}^2/2m_H$ coincides with the plasmon. However, the real part of the inverse Lindhard dielectric function exhibits no divergence as the values of $\underline{q}$ and ν at which the plasmon and heavy hole dispersions are equal occurs well into the spectrum of single particle excitations shown in Figure 2.2. These single particle transitions which are included in the Lindhard function, damp the plasmon modes and the dielectric response of the hole gas at large $\underline{q}$ becomes dominated by these transitions. In Figure 2.5 the inverse dielectric function for both models is seen to diverge for $\underline{q} \approx 0.6\ \underline{k}_{fv}$. In this case, the damping effect of the single particle excitations in the Lindhard function is small as the values of $\underline{q},\nu$ at which the inverse Lindhard and light hole dispersion relations coincide, only just falls into the single particle excitation spectrum. The comparison between the plasmon pole and inverse Lindhard dielectric functions for a hole gas in Si is similar to that for n-type Si and shows good agreement over the low $\underline{q}$ range dominant in the present calculation.

All the relevant terms of expression (2.39) have now been explicitly derived and the energy shifts of the band edge states can now be determined. The evaluation of the band edge shifts for the four materials under consideration is given in the next chapter.

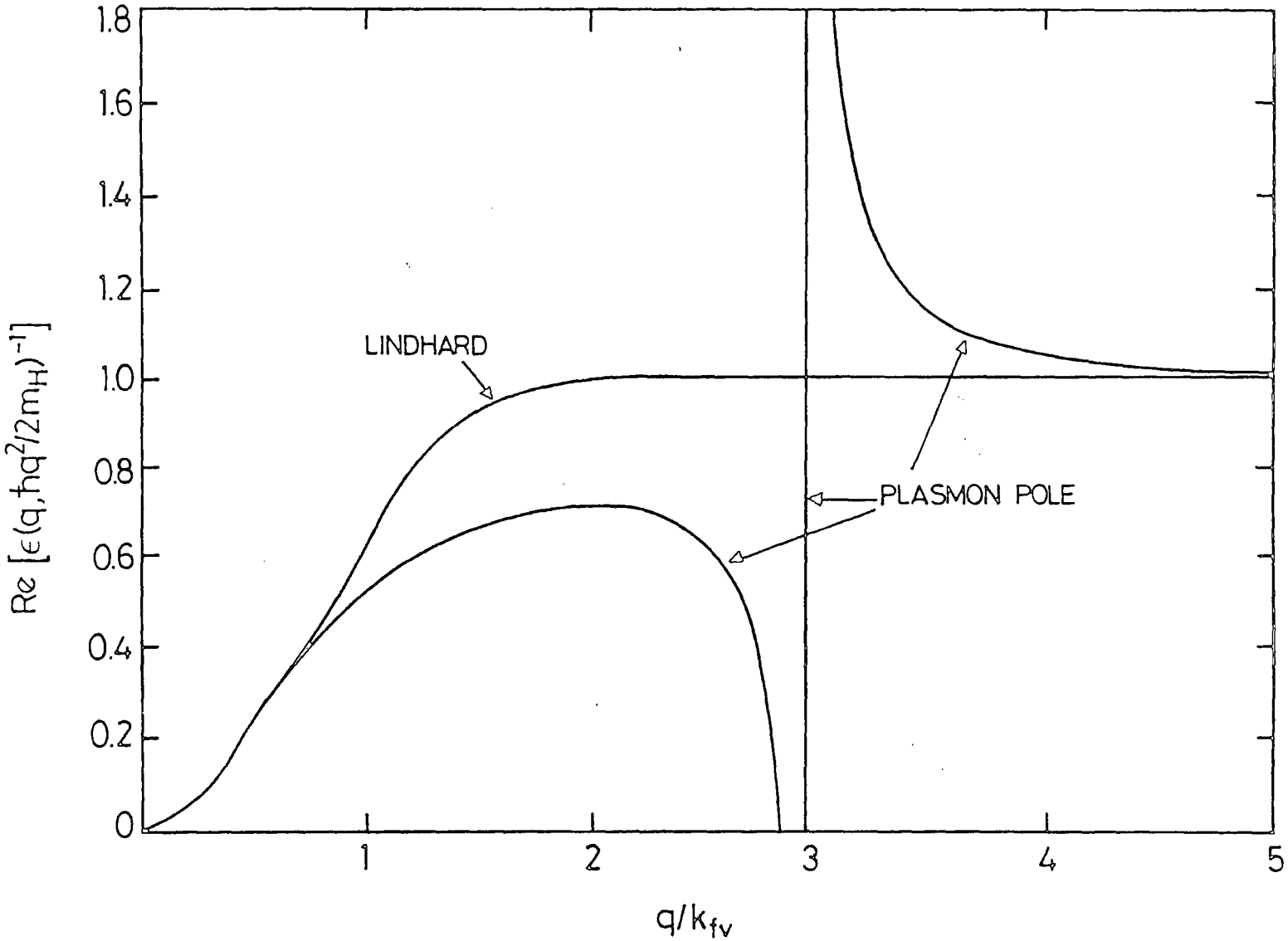

Figure 2.4: The real part of the inverse Lindhard and plasmon pole dielectric functions for $\nu = \hbar q^2/2m_H$ for a hole concentration of 1.0^{20} cm^{-3} in Si.

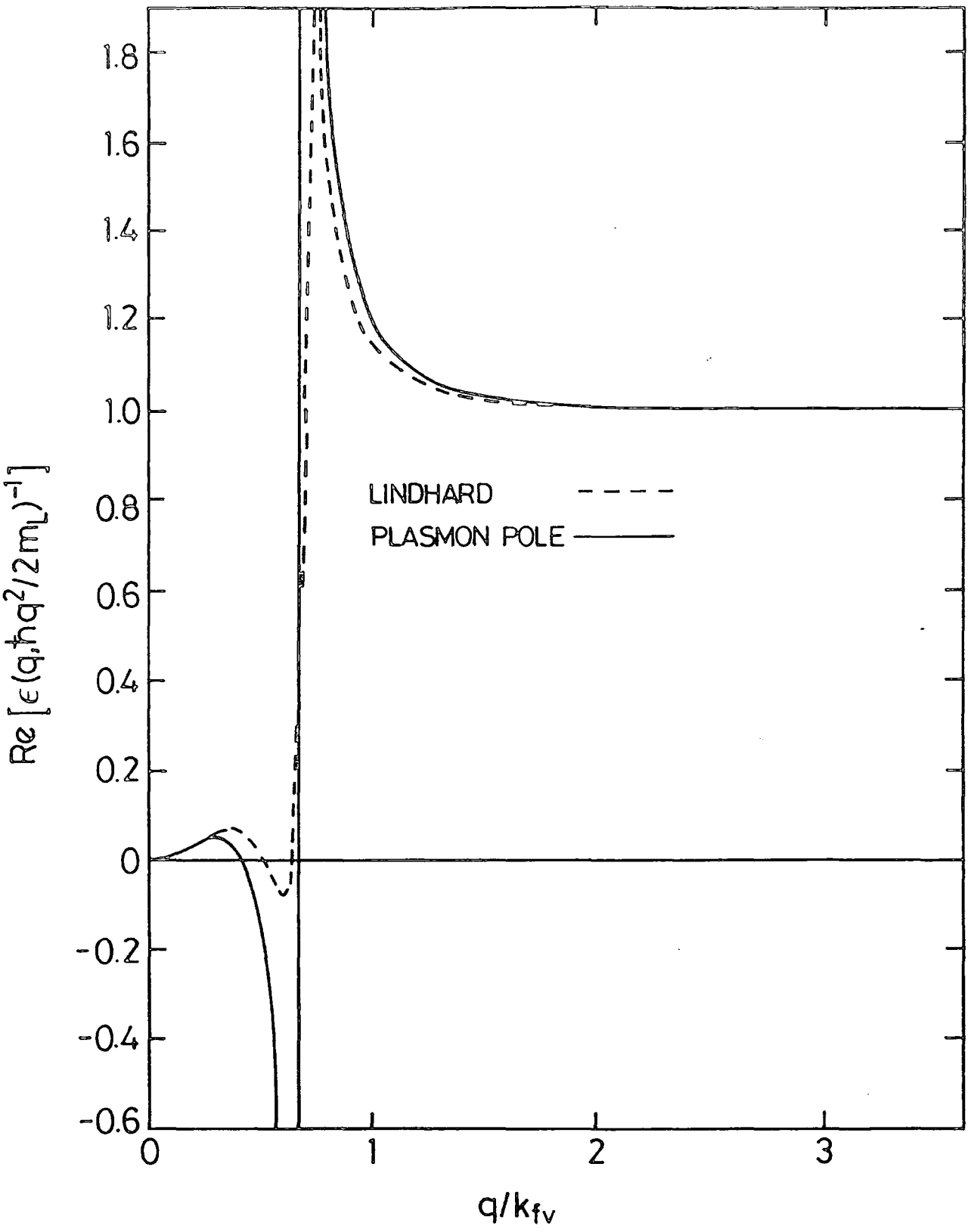

Figure 2.5: The real part of the inverse Lindhard and plasmon pole dielectric functions for $\nu = \hbar q^2/2m_L$ for a hole concentration of 10^{20} cm^{-3} in Si.

2.7. Summary

A heavily doped or optically excited semiconductor can contain large concentrations of carriers in the conduction and/or valence band. The energy of a state $\underline{k}$ in band n of the intrinsic material is then modified by screening of the carrier-carrier interaction and by carrier-carrier exchange energy. This change in energy of state $\underline{k}$ can be determined by evaluating the difference between the self energies of the state for doped and intrinsic material. An expression for the self energy of state $n,\underline{k}$ has been derived using a Feynman diagrammatic analysis for a state in a free electron gas and the necessary modifications to make the expression appropriate to a semiconductor have been made. The principle modification of the expression occurs in the screened Coulomb potential in which a plasmon pole approximation for the frequencey dependent dielectric function is used.

CHAPTER 3

BAND GAP NARROWING DUE MANY BODY INTERACTIONS AT T = OK

3.0. Introduction

The analysis and results presented in this chapter, closely follows the publication by Abram, Childs and Saunderson (1984). The present work provides more extensive information on individual terms contributing to the band edge shifts, and a comparison with the band gap narrowing derived using the Thomas-Fermi approximation to the dielectric response is made. The band gap narrowing in two more materials ($Ga_{0.47}In_{0.53}As$ and $Ga_{0.28}In_{0.72}As_{0.6}P_{0.4}$) is also evaluated.

An expression (2.39) for the self-energy at T = OK of a state $\underline{k}$ in band n has been derived for a model semiconductor with large carrier concentrations in the conduction and/or valence band. These carriers are assumed derived from the merging of an impurity band (induced by heavy doping) into the host semiconductor band or are derived from some form of excitation such as by light. As the calculations in this chapter refer to the absolute zero of temperature, the electrons in n-type material occupy the host conduction band up to the Fermi level E_{fe} and in p-type material the valence states are occupied by holes (or unoccupied by electrons) down to the Fermi level E_{fv}.

To determine the shift in each band edge energy resulting from changes in the elctron-electron interactions due to the presence of these carriers, we must evaluate the difference in the real part of the self energy at the band edge between the doped and intrinsic material. That is, the shift of band n at its edge, located at wavevector $\underline{k}_o$ is

$$\Delta E_n^{\Sigma}(\underline{k}_o) = \mathrm{Re}[E_n^{\Sigma}(\underline{k}_o)]\Big|_{\text{doped}} - \mathrm{Re}[E_n^{\Sigma}(\underline{k}_o)]\Big|_{\text{intrinsic}} \qquad (3.1)\ .$$

The calculation of $\Delta E_n^{\Sigma}(\underline{k}_o)$ requires consideration of the changes in electron-electron interaction energies due to the changed electron occupancy and the screening effect of the introduced free carriers.

Before explicitly evaluating the terms in $\Delta E_n^{\Sigma}(\underline{k}_o)$ it is instructive to examine in a simple diagrammatic form the effects of introducing carriers into the host bands. In figure 3.1 some of the possible interactions between test electrons at the band edges and the other electrons, are compared with those in the intrinsic material using the simplest model of an n-type semiconductor. The unscreened interactions between the test electron and the valence band electrons are marked as full lines in the intrinsic material. On introduction of the electron gas to the conduction band, these interactions are screened (dashed lines). In addition a test electron at the conduction band edge now has a screened interaction with the new electrons in this band. In the empty conduction band of the intrinsic material no electron-electron interactions were possible. (Note this simplified picture includes no interactions between electrons in different bands, but does provide a useful visual introduction to some of the important changes in electron-electron interactions).

The corresponding case for p-type material is shown in Figure 3.2 where the interactions in the intrinsic material take the same form as those illustrated in figure 3.1. The introduction of a hole gas into the valence band removes electrons from states near the band edge thus lowering the electron-electron interactions available to the test electron. In addition the remaining interactions are screened (dashed lines) by the hole gas. The host conduction band remains empty of carriers but the energy of a band edge test electron is altered by the Coulombic response of the hole gas, which is not shown.

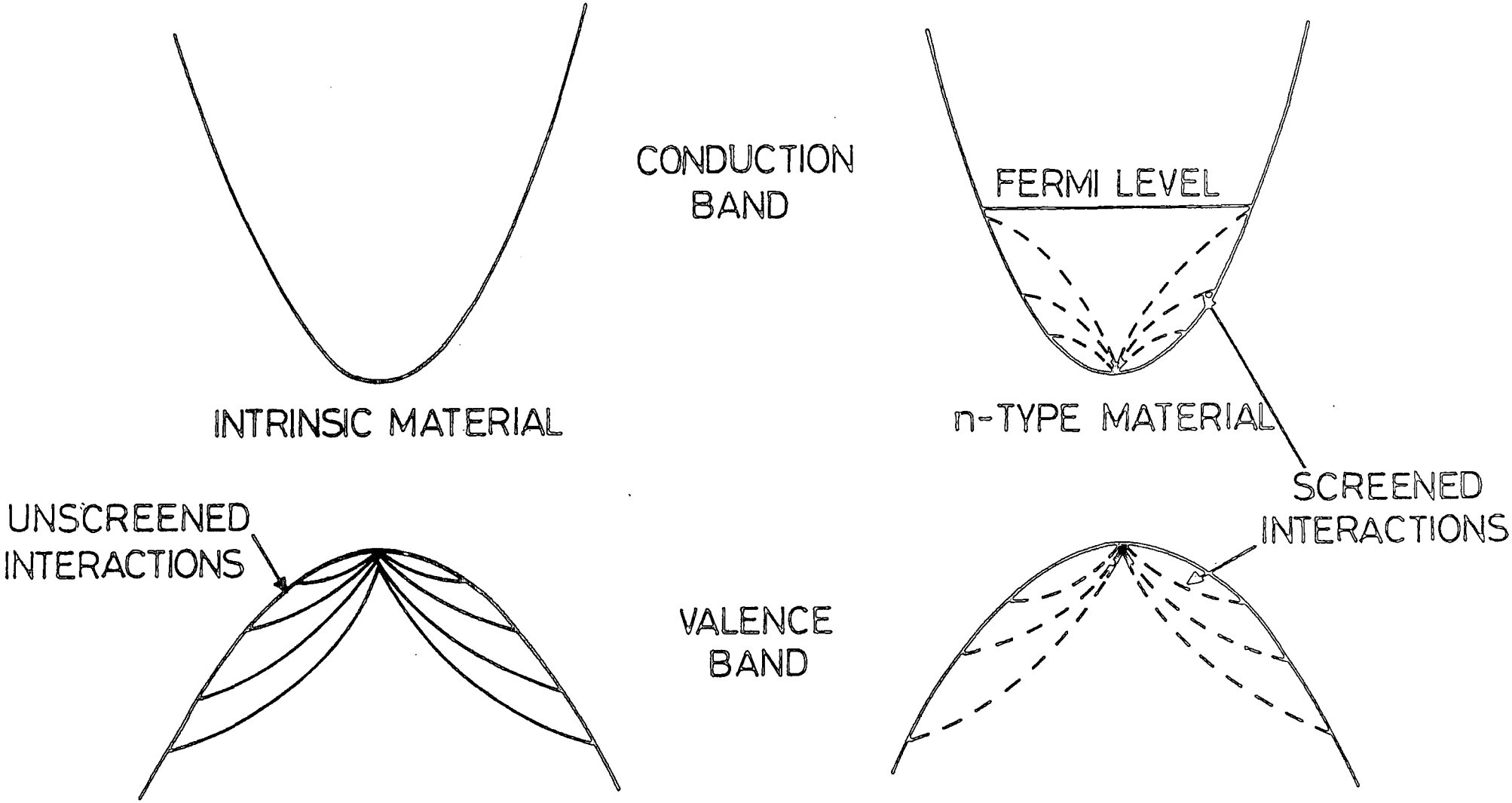

Figure 3.1: The screened (dashed lines) and unscreened (full lines) interactions in a model (single valence and conduction bands) intrinsic and n-type semiconductor at T = OK.

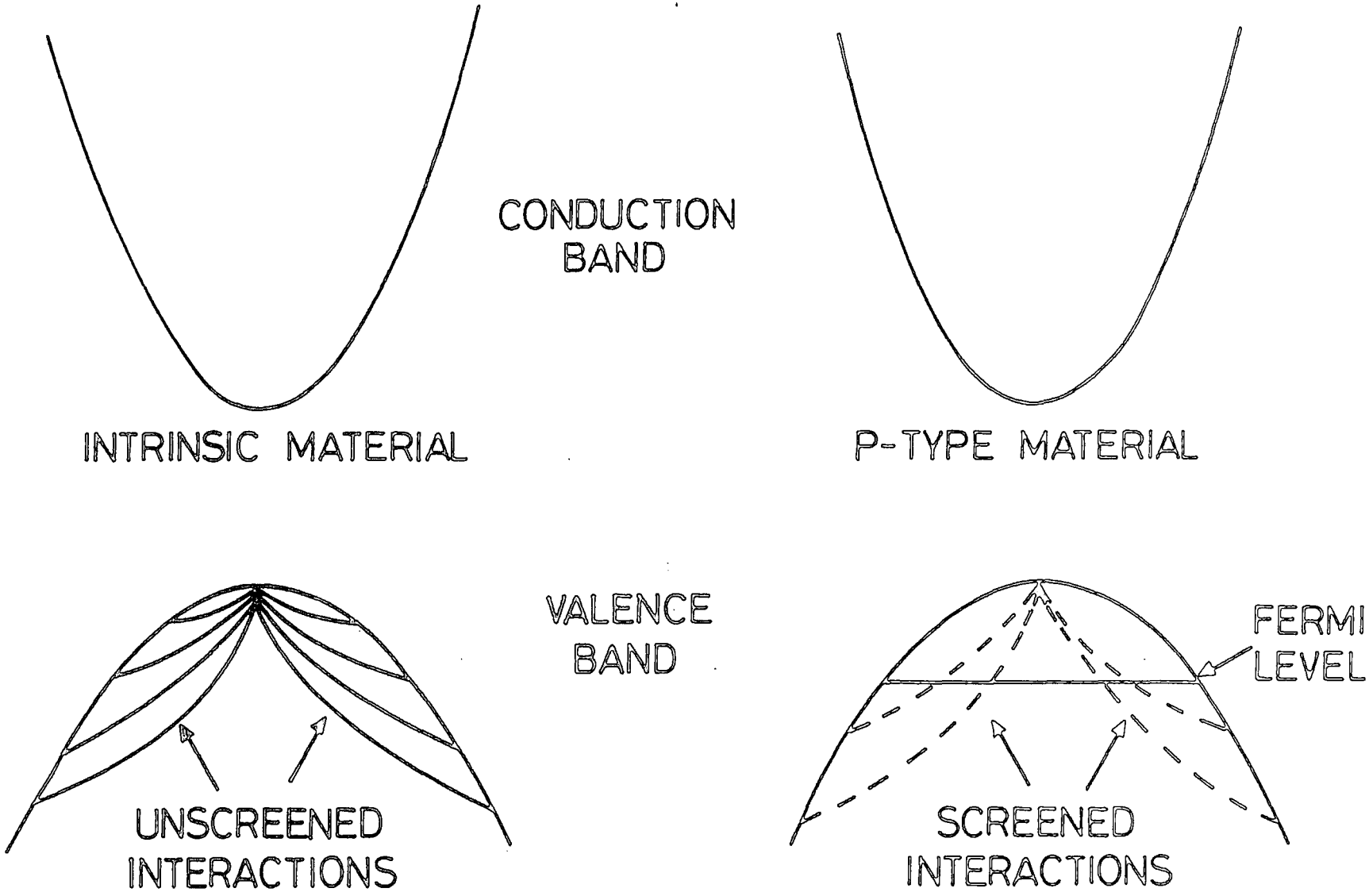

Figure 3.2: The screened (dashed lines) and unscreened (full lines) interactions in a model (single valence and conduction bands) intrinsic and p-type semiconductor at T = OK.

3.1. Derivation of Screened Exchange and Coulomb Hole Terms

The self energy expression (2.39) for the doped material can be written as

$$E_n^{\Sigma d}(\underline{k}) = \frac{i}{(2\pi)^4}\int \sum_{n''} \left|I_{n\underline{k},n''\underline{k}-\underline{q}}\right|^2 \frac{e^2}{\varepsilon_o \varepsilon_r q^2} \cdot \tag{3.2}$$

$$\left[1 + \frac{\omega_p^2}{2\omega_l(\underline{q})}\left(\frac{1}{\nu-\omega_l(\underline{q})+i\delta} - \frac{1}{\nu+\omega_l(\underline{q})-i\delta}\right)\right] \frac{e^{-i\nu\delta}\, d\nu d^3\underline{q}}{(\omega_{n\underline{k}}-\nu-\omega_{n''\underline{k}-\underline{q}}+i\delta\,\mathrm{sgn}(\hbar\omega_{n''\underline{k}-\underline{q}}-\hbar\omega_f)}$$

The frequency integral ν in the above expression can be evaluated analytically by contour integration. The causality factor $e^{-i\delta\nu}$ dictates that the contour be completed by a semicircle at infinity in the lower half of the complex ν plane. Hence only those poles in the Green's function and the effective interaction lying in the lower half plane can contribute to the integral. That is contributions arise from poles at

$$\nu = \omega_{n\underline{k}} - \omega_{n''\underline{k}-\underline{q}} - i\delta \qquad (\hbar\omega_{n''\underline{k}-\underline{q}} < \hbar\omega_f) \tag{3.3}$$

in the Green's function and

$$\nu = \omega_l(\underline{q}) - i\delta \tag{3.3a}$$

in the effective interaction.

The condition $\omega_{n''\underline{k}-\underline{q}} < \omega_f$ derived from the sgn term in the Green's function implies that the resulting wavevector $\underline{q}$ integral is over occupied states only. The two contributions to the self energy in the doped semiconductor derived from the frequency integral around the above poles are:

a) The screened exchange (SX) term from poles in the Green's function:

$$E_n^{\Sigma dSX}(\underline{k}) = -\frac{1}{(2\pi)^3} \int_{\substack{\text{states} \\ n'',\underline{k}-\underline{q} \\ \text{occupied} \\ \text{by electrons}}} \sum_{n''} \left| I_{n\underline{k},n''\underline{k}-\underline{q}} \right|^2 \frac{e^2}{\varepsilon_o \varepsilon_r q^2} \frac{d^3\underline{q}}{\varepsilon(\underline{q},\omega_{n\underline{k}}-\omega_{n''\underline{k}-\underline{q}})} \qquad (3.4) .$$

For static screening, i.e. $\varepsilon(\underline{q},\omega_{n\underline{k}} - \omega_{n''\underline{k}-\underline{q}}) = 1$ this expression has the same form as the Hartree-Fock (H-F) exchange energy for an electron gas, hence the origin of the terminology "screened exchange".

b) The Coulomb-hole (CH) term resulting from poles in the effective interaction

$$E_n^{\Sigma dCH}(\underline{k}) = \frac{1}{(2\pi)^3} \int_{\substack{\text{all } n'' \\ \text{and } \underline{q}}} \sum_{n''} \left| I_{n\underline{k},n''\underline{k}-\underline{q}} \right|^2 \frac{e^2}{\varepsilon_o \varepsilon_r q^2} \frac{\omega_p^2}{2\omega_l(\underline{q})} \cdot$$

$$\frac{d^3\underline{q}}{\omega_{n\underline{k}}-\omega_l(\underline{q})-\omega_{n''\underline{k}-\underline{q}}+i\delta\,\mathrm{sgn}(\hbar\omega_{n''\underline{k}-\underline{q}}-\hbar\omega_f)} \qquad (3.5) .$$

This Coulomb-hole term corresponds to the self energy resulting from the region around the test particle being denuded of other electrons by Coulomb repulsion (see Section 2.3).

The self energy of the intrinsic semiconductor is given by:

$$E_n^{\Sigma i}(\underline{k}) = \frac{i}{(2\pi)^4} \int \sum_{n''} \left| I_{n\underline{k},n''\underline{k}-\underline{q}} \right|^2 \frac{e^2}{\varepsilon_o \varepsilon_r q^2}$$

$$\frac{e^{-i\delta\nu}\, d^3\underline{q}\, d\nu}{\omega_{n\underline{k}}-\nu-\omega_{n''\underline{k}-\underline{q}}+i\delta\,\mathrm{sgn}(\hbar\omega_{n''\underline{k}-\underline{q}}-\hbar\omega_f)} \qquad (3.6) .$$

Where the screening effect of the carrier gas has vanished and the Coulomb interaction is simply modified by the static dielectric constant

of the semiconductor. The frequency integral can again be carried out by contour integration with contributions coming from poles in the Green's function giving:

$$E_n^{\Sigma i}(\underline{k}) = -\frac{1}{(2\pi)^3} \int_{\substack{\text{all } n'' \text{ and} \\ \underline{q} \equiv \text{valence} \\ \text{bands}}} \sum_{n''} \left| I_{n\underline{k},n''\underline{k}-\underline{q}} \right|^2 \frac{e^2}{\varepsilon_o \varepsilon_r q^2} d^3\underline{q} \qquad (3.7)$$

which is again of the form of a H-F exchange energy.

Having derived the general self energy expressions (3.4) - (3.7) for the state $\underline{k}$ in band n we now proceed to evaluate these terms for the particular case of a p-type material.

A brief presentation of the equivalent expressions and results for n-type materials is then made subsequently in Section 3.6.

3.2. Band Edge Shifts in p-type Material

3.2.1. Valence Band Energy Shift - Introduction

The valence band of each of the four materials discussed in the present work is considered to consist of isotropic, parabolic heavy and light hole bands degenerate at the Brillouin zone centre, with an isotropic, parabolic spin split off band separated from these at $\underline{k} = 0$ by the spin splitting energy Δ(eV). In the gallium based compounds the spin splitting parameter is relatively large (Δ = 0.34 eV in GaAs) and the band is unoccupied by free carriers (holes) for the range of hole concentration of interest in the present work. For silicon however the spin splitting parameter is quite small (Δ = 0.044 eV) and the spin split off band is occupied with holes for concentrations $\gtrsim 1.7 \times 10^{19}$ cm^{-3}. The effect of hole occupancy of the SS band is shown in section 3.8 to be small and for the present, occupancy of the heavy and light hole bands only is considered.

3.2.2. Derivation of General Terms

For the present the energy shift at $\underline{k} = 0$ of the heavy hole (HH) band is considered but it is shown later that an equal shift of the light hole (LH) band edge also occurs.

As indicated in figure 3.2 the energy shift of this band edge state is evaluated by determining the self energy of a test electron at the top of the heavy hole valence band due to its screened interactions with the electrons in the electron occupied part of the valence band and subtracting from this the unscreened exchange interaction with the electrons in the valence band full of electrons. In algebraic terms the band edge shift is given by evaluation of the real parts of expressions (3.4) - (3.7) using the relevant occupancies of the heavy and light hole bands. Thus

$$\Delta E^{\Sigma}_{HH}(\underline{0}) = \left(\mathrm{Re}\left[E^{\Sigma CH}_{HH}(\underline{0}) \right] + \mathrm{Re}\left[E^{\Sigma SX}_{HH}(\underline{0}) \right] \right)\Big|_{DOPED} - \mathrm{Re}\left[E^{\Sigma i}_{HH}(\underline{0}) \right]\Big|_{INTRINSIC} \qquad (3.8) .$$

The real parts of these expressions are derived by taking the Cauchy principal part of each expression which in the present case amounts to ignoring the complex infinitesimals in equations (3.4) - (3.6). For the remainder of this chapter the real part of each expression is taken and this is not written explicitly.

The last two terms in the above expression both take the form of the Hartree-Fock exchange interaction and can be combined to give the change in the heavy hole band screened exchange term $\Delta E^{\Sigma SX}_{HH}(\underline{0})$ as;

$$\Delta E_{HH}^{\Sigma SX}(\underline{0}) = \frac{-e^2}{8\pi^3\varepsilon_o\varepsilon_r} \int_{\substack{\text{states} \\ -\underline{q},n" \\ \text{occupied} \\ \text{by electrons}}} \sum_{n"} \left| I_{HH\underline{0},n"-\underline{q}} \right|^2 \frac{d^3\underline{q}}{q^2\varepsilon(\underline{q},\omega_{HH\underline{0}}-\omega_{n"-\underline{q}})}$$

$$+ \frac{e^2}{8\pi^3\varepsilon_o\varepsilon_r} \int_{\text{all } n" \text{ and } \underline{q}} \sum_{n"} \left| I_{HH\underline{0},n"-\underline{q}} \right|^2 \frac{d^3\underline{q}}{q^2} \qquad (3.9) .$$

There is no Coulomb hole term in the intrinsic material so the change in this term is given by:

$$\Delta E_{HH}^{\Sigma CH}(\underline{0}) = E_{HH}^{\Sigma CH}(\underline{0}) = \frac{e^2}{8\pi^3\varepsilon_o\varepsilon_r} \int_{\text{all } n" \text{ and } \underline{q}} \sum_{n"} \left| I_{HH\underline{0},n"-\underline{q}} \right|^2$$

$$\frac{\omega_p^2}{2q^2\omega_1(\underline{q})} \frac{d^3\underline{q}}{((\omega_{HH\,\underline{0}}-\omega_{n"-\underline{q}})-\omega_1(\underline{q}))} \qquad (3.10) .$$

The first term in expression (3.9) can alternatively be expressed as the difference between the screened exchange of the full valence band and the screened exchange of the states occupied down to the Fermi level, i.e.

$$\Delta E_{HH}^{\Sigma SX}(\underline{0}) = \frac{-e^2}{8\pi^3\varepsilon_o\varepsilon_r} \int_{\text{all } n" \text{ and } \underline{q}} \sum_{n"} \left| I_{HH\underline{0},n"-\underline{q}} \right|^2 \frac{d^3\underline{q}}{q^2\varepsilon(\underline{q},\omega_{HH\underline{0}}-\omega_{n"-\underline{q}})}$$

$$+ \frac{e^2}{8\pi^3\varepsilon_o\varepsilon_r} \int_{\substack{\text{all valence} \\ \text{band} \\ \text{unoccupied} \\ \text{states}}} \sum_{n"} \left| I_{HH\underline{0},n"-\underline{q}} \right|^2 \frac{d^3\underline{q}}{q^2\varepsilon(\underline{q},\omega_{HH\underline{0}}-\omega_{n"-\underline{q}})}$$

$$+ \frac{e^2}{8\pi^3\varepsilon_o\varepsilon_r} \int_{\text{all } n" \text{ and } \underline{q}} \sum_{n"} \left| I_{HH\underline{0},n"-\underline{q}} \right|^2 \frac{d^3\underline{q}}{q^2} \qquad (3.11) .$$

The first and third terms in this expression can now be combined to give:

$$\Delta E^{\Sigma SX}_{HH}(\underline{0}) = \frac{e^2}{8\pi^3 \varepsilon_o \varepsilon_r} \int_{\text{all } n'' \text{ and } -\underline{q}} \sum_{n''} \left| I_{HH\underline{0},n''-\underline{q}} \right|^2 \left(1 - \frac{1}{\varepsilon(\underline{q}, \omega_{HH\underline{0}} - \omega_{n''-\underline{q}})} \right) \frac{d^3\underline{q}}{q^2}$$

$$+ \frac{e^2}{8\pi^3 \varepsilon_o \varepsilon_r} \int_{\substack{\text{unoccupied} \\ \text{valence band} \\ \text{states}}} \sum_{n''} \left| I_{HH\underline{0},n''-\underline{q}} \right|^2 \frac{d^3\underline{q}}{q^2 \, \varepsilon(\underline{q}, \omega_{HH\underline{0}} - \omega_{n''} - \underline{q})} \qquad (3.14).$$

The form of the overlap integrals given by equation (2.40) can now be substituted into equation (3.14) and (3.10). As indicated in section 2.5.1, for a test electron in the HH band the only overlap integrals of significant magnitude are with states in the heavy and light hole bands. These are:

$$\text{for } n'' \equiv HH \quad \left| I_{HH\underline{k},HH\underline{k}'} \right|^2 \simeq \frac{1}{4}(1 + 3\cos^2\theta)$$

$$\text{for } n'' \equiv LH \quad \left| I_{HH\underline{k},LH\underline{k}'} \right|^2 \simeq \frac{3}{4}\sin^2\theta \qquad (3.14a).$$

The sum over bands n'' therefore reduces to a sum over HH and LH bands only. For a state at the band edge $\underline{k} = 0$ the angle θ between states $\underline{k}$ and $\underline{k} - \underline{q}$ has little meaning. To define θ therefore a $\underline{k}$ of infinitesimal size but definite direction (e.g. z-direction) is taken, the angular part of the wavevector integrals of equation (3.14) then have the form:

$$\int_0^{2\pi} \int_0^{\pi} \frac{1}{4}(1 + 3\cos^2\theta) \sin\theta \, d\theta \, d\phi = 2\pi \,, \quad \text{for } n'' \equiv HH$$

$$\int_0^{2\pi} \int_0^{\pi} \frac{3}{4}\sin^2\theta \sin\theta \, d\theta \, d\phi = 2\pi, \quad \text{for } n'' \equiv LH \qquad (3.15).$$

Substitution of these terms into expressions (3.10) and (3.14) give the remaining parts of the wavevector integrals as

$$\Delta E_{HH}^{\Sigma SX}(\underline{O}) = \Delta E_{HH}^{\Sigma SXA}(\underline{O}) + \Delta E_{HH}^{\Sigma SXU}(\underline{O}) \tag{3.16}$$

where

$$\Delta E_{HH}^{\Sigma SXA} = \frac{-e^2}{\varepsilon_o \varepsilon_r 4\pi^2} \int_{\substack{\text{all } -q \\ n''\equiv HH,LH}} \sum_{n''} \frac{\omega_p^2 \, dq}{(\omega_{HHO}-\omega_{n''}-q)^2-\omega_1^2(q)} \tag{3.17}$$

$$\Delta E_{HH}^{\Sigma SXU} = \frac{e^2}{\varepsilon_o \varepsilon_r 4\pi^2} \int_{\substack{\text{unoccupied} \\ HH \text{ and } LH \\ \text{states}}} \sum_{n''} \left[1 + \frac{\omega_p^2}{(\omega_{HHO}-\omega_{n''}-q)^2-\omega_1^2(q)} \right] dq \tag{3.18}$$

and the superscripts A and U on ΔE imply integration over all states, and unoccupied states respectively. The CH term is given as:

$$\Delta E_{HH}^{\Sigma CH} = \frac{e^2}{4\pi^2 \varepsilon_o \varepsilon_r} \int_{\text{all } q} \sum_{n''} \frac{\omega_p^2}{2\omega_1(q)} \frac{dq}{[(\omega_{HHO}-\omega_{n''}-q)-\omega_1(q)]} \; . \tag{3.19}$$

To simplify the notation the wavevector ($\underline{k} = 0$) at which the ΔE of equation (3.16 - 19) are evaluated is dropped and will be omitted for the remainder of this section.

The total energy shift of the heavy-hole band edge ΔE_{HH}^{Σ} is thus given by the sum of equations (3.16 - 19) as

$$\Delta E_{HH}^{\Sigma} = \Delta E_{HH}^{\Sigma CH} + \Delta E_{HH}^{\Sigma SXA} + \Delta E_{HH}^{\Sigma SXU} \tag{3.19a} \; .$$

The evaluation of these individual terms is performed in the next three sections.

3.2.3. Definition of Energy Parameters and Discussion of Difficulties in Evaluation of General Terms.

To evaluate these terms explicitly we define the energy difference between the two eigenvalues $\hbar\omega_{HHO}$ and $\hbar\omega_{n''-q}$ for parabolic, isotropic valence bands as

$$\hbar\omega_{HHO} - \hbar\omega_{n''-q} = \frac{\hbar^2 q^2}{2m_{n''}} \quad \text{where} \quad n'' \equiv H \text{ or } L \qquad (3.20).$$

Note this energy difference is positive as the band edge state $\underline{k} = 0$ is higher in energy than any valence band state at $\underline{q}$.

As discussed in section 2.3 the effective masses $m_{n''}$ are assumed to have the same value as in the undoped material. This implies the assumption of a rigid shift of all bands due to many body effects. This assumption was recently validated by Sernelius (1986) for the band shifts in n-type GaAs.

For a state at the light hole band edge (which is degenerate with the heavy hole band edge) an expression

$$\hbar\omega_{LHO} - \hbar\omega_{n''-q} = \frac{\hbar^2 q^2}{2m_{n''}} \qquad n'' = H \text{ or } L \qquad (3.21)$$

also applies.

Now by changing the HH subscripts in expressions (3.17 - 3.18) to LH it can be seen that $\Delta E^{\Sigma}_{HH} = \Delta E^{\Sigma}_{LH}$ so the band shifts of the heavy and light hole valence band edges are in fact equal.

Considering now the evaluation of the integrals over wavevector magnitude q in the equations (3.17) and (3.19), it can be seen from figure 2.2 for p-type Silicon with a hole concentration of $10^{20}\,cm^{-3}$ that the plasmon dispersion curve crosses the frequency-wavevector curve for the light hole band $(\nu = \hbar q^2/2m_L)$ at $q \approx 0.6\, k_{fv}$ and for the heavy hole band at $q \simeq 3\, k_{fv}$. This results in a singularity in the integrals over q, the magnitude of q at which this occurs being

dependent on the carrier concentration. The evaluation of the Coulomb-hole term then becomes particularly difficult by either analytical or numerical methods. To overcome this problem the SXA and CH terms (3.17) and (3.19) are added together giving:

$$\Delta E_{HH}^{\Sigma SXA+CH} = \frac{e^2}{4\pi^2\varepsilon_o\varepsilon_r} \int_{\text{all } q} \sum_{n''} \frac{\omega_p^2}{2\omega_l(q)} \frac{dq}{\left(\frac{\hbar q^2}{2m_{n''}} + \omega_l(q)\right)} \qquad (3.22) .$$

This term contains no poles and can be evaluated numerically. To determine the individual contributions to the above integral the screened exchange term is evaluated analytically and the CH term can then be derived by subtraction.

3.2.4. Evaluation of $\Delta E_{HH}^{\Sigma SXA}$ and $\Delta E_{HH}^{\Sigma CH}$ Terms

Substitution of the plasmon dispersion relation

$$\omega_l^2(q) = \omega_p^2 \left(1 + \frac{q^2}{K^2}\right) + \frac{\hbar^2 q^4}{4m_{Dv}^2} \qquad (3.23)$$

into expression (3.22) yields

$$\Delta E_{HH}^{\Sigma SXA+CH} = \frac{e^2}{4\pi^2\varepsilon_o\varepsilon_r} \sum_{n''} \int_0^{\infty} \frac{dq}{2\left(1 + \frac{q^2}{K^2} + \frac{\beta q^4}{K^2 k_{fv}^2}\right) + \frac{\hbar q^2}{m_{n''}\omega_p}\left(1 + \frac{q^2}{K^2} + \frac{\beta q^4}{K^2 k_{fv}^2}\right)^{1/2}} \qquad (3.24)$$

where $\beta = \frac{3}{4}\frac{m_{ov}}{m_{Dv}}$ (3.24) .

This integral was evaluated numerically using the NAG quadrature routine Dϕ1 APF for a range of hole concentrations 10^{17} - 10^{22} cm^{-3}; the results for p-type Si are shown in figure 3.3.

The evaluation of the screened exchange term for the full valence band can now be performed as follows. Substitution of the plasmon dispersion relation into equation (3.17) gives:

$$\Delta E_{HH}^{\Sigma SXA} = \frac{e^2K^2}{4\pi^2\varepsilon_o\varepsilon_r k_{fv}} \int_0^{\infty} \sum_{n''} \frac{dx}{\left(\frac{K}{k_{fv}}\right)^2 + x^2 + \alpha_{n''}x^4} \qquad (3.25)$$

where $x = q/k_{fv}$ and $\alpha_{n''} = \frac{3}{4}\frac{m_{ov}}{m_{Dv}}\left(1 - \left(\frac{m_{Dv}}{m_{n''}}\right)^2\right)$.

This integral is evaluated analytically using formulae from Gradshteyn and Ryzhik (1980) (2.161, 2.141/2 and 2.143/2) and the resulting expression has the form

$$\Delta E_{HH}^{\Sigma SXA} = \frac{e^2K^2}{8\pi\varepsilon_o\varepsilon_r} \sum_{n''} \left[\frac{-2\alpha_{n''}k_{fv}}{(k_{fv}^2 - 4\alpha_{n''}K^2)\left[(k_{fv}^2 - 4\alpha_{n''}K^2)^{1/2} - k_{fv}\right]} \right]^{1/2} \qquad (3.26) .$$

The results derived from this expression for a range of hole concentrations in p-type silicon are illustrated in Figure 3.3 together with the Coulomb hole term derived from:

$$\Delta E_{HH}^{\Sigma CH} = \Delta E_{HH}^{\Sigma SXA+CH} - \Delta E_{HH}^{\Sigma SXA} \qquad (3.27) .$$

It should be noted that the SX and CH terms make opposing contributions to the band edge shift. The CH contribution lowers the band edge energy, but the dominant contribution comes from the change in the screened exchange term which is positive. This latter contribution can be regarded as the lowering of the magnitude of the exchange energy (the exchange energy is negative) of the full valence band due to the screening effect of the hole gas that has been introduced.

Another effect of the introduction of holes is that the magnitude of the exchange energy is further reduced by the removal of the valence band

electrons down to the Fermi level and the term representing this, $\Delta E_{HH}^{\Sigma SXU}$, is now evaluated.

3.2.5. Evaluation of $\Delta E_{HH}^{\Sigma SXU}$ and ΔE_{HH}^{Σ} Terms

Expression (3.18) gives

$$\Delta E_{HH}^{\Sigma SXU} = \frac{e^2}{4\pi^2\varepsilon_o\varepsilon_r} \int_{\substack{\text{unoccupied} \\ \text{states}}} \sum_{n''} \left[1 - \frac{\omega_p^2}{\omega_1^2(q) - \left(\frac{\hbar q^2}{2m_{n''}}\right)^2} \right] dq \qquad (3.28) .$$

In this case the range of integration covers values of q down to the Fermi level $E_{fv} = \frac{\hbar^2 k_{fv}^2}{2m_{Dv}}$. For each valence sub-band the wave-vector limit of the unoccupied states is now defined as:

$$E_{fv} = \frac{\hbar^2 k_{fn''}^2}{2m_{n''}}, \quad \text{hence} \quad k_{fn''}^2 = k_{fv}^2 \frac{m_{n''}}{m_{Dv}} . \qquad (3.29) .$$

The integral over the first term in the brackets is now straightforward and represents the Hartree-Fock exchange energy in a coupled valence band. Expression (3.28) now reduces to

$$\Delta E_{HH}^{\Sigma SXU} = \sum_{n''} \frac{e^2 k_{fn''}}{4\pi^2\varepsilon_o\varepsilon_r} - \frac{e^2}{4\pi^2\varepsilon_o\varepsilon_r} \sum_{n''} \int_0^{k_{fn''}} \frac{\omega_p^2 \, dq}{\left(\omega_1^2(q) - \frac{\hbar^2 q^4}{4m_{n''}^2}\right)} \qquad (3.30) .$$

The remaining integral has the same form as expression (3.25) for the screened exchange over the full valence band but the range of integration is now finite. Once again the expression has poles where the band energy $\hbar\omega_{n''}$ corresponds to the plasmon energy. This pole falls outside the range of integration for the heavy hole band for reasonable hole concentrations but may fall within the range for the light hole band. If no pole exists within the range of integration the integral is performed

using the NAG quadrature routine Dϕ1 AHF. When a pole falls within the range of integration the integral reduces to

$$\Delta E_{HH}^{\Sigma SXU} = \sum_{n''} \frac{e^2 k_{fn''}}{4\pi^2 \varepsilon_o \varepsilon_r} - \sum_{n''} \frac{e^2 K^2}{4\pi^2 \varepsilon_o \varepsilon_r k_{fn''}} \left[\frac{c_{n''}}{h_{n''}} \sqrt{\frac{1}{cf_{n''}}} \operatorname{arctg} \sqrt{\frac{c_{n''}}{f_{n''}}} + \frac{1}{2a_1 h_{n''}} \ell n \left(\frac{1+a_1}{1-a_1} \right) \right]$$

where $c_{n''} = \frac{3}{4} \frac{m_{ov} m_{n''}}{m_{Dv}^2} \left(1 - \frac{m_{Dv}^2}{m_{n''}^2} \right)$

$$h_{n''} = \left\{ 1 - 4c_{n''} \frac{K^2}{k_{fn''}^2} \right\}^{1/2} \qquad f_{n''} = \frac{1}{2} - \frac{h_{n''}}{2}$$

and $$a_1 = \left[- \frac{(1 + h_{n''})}{2c_{n''}} \right]^{1/2} \qquad (3.31) .$$

This term must now be added to the valence band shift determined from $\Delta E_{HH}^{\Sigma SXA+CH}$ to give the total shift of the band edge state ΔE_{HH}^{Σ}. The contribution of $\Delta E_{HH}^{\Sigma SXU}$ is seen from figure 3.3 for p-type silicon to be very small compared to $\Delta E_{HH}^{\Sigma SXA}$.

It should be noted however that for GaAs in particular the integration over the pole in equation (3.30) is badly behaved giving a large increase in the contribution due to this term over a small range of carrier concentration. This large increase leads to a rapid pole like decrease in the band gap narrowing, for a hole concentration $p \approx 7.5 \times 10^{20}$ cm^{-3}. As this effect has its origin in the numerical difficulties encountered in the integration over the pole the somewhat unphysical behaviour of a pole like drop in the band gap narrowing has been ignored. The results shown for the band gap narrowing in GaAs thus represent an extrapolation over the region of high carrier concentration in which the fine structure occurs.

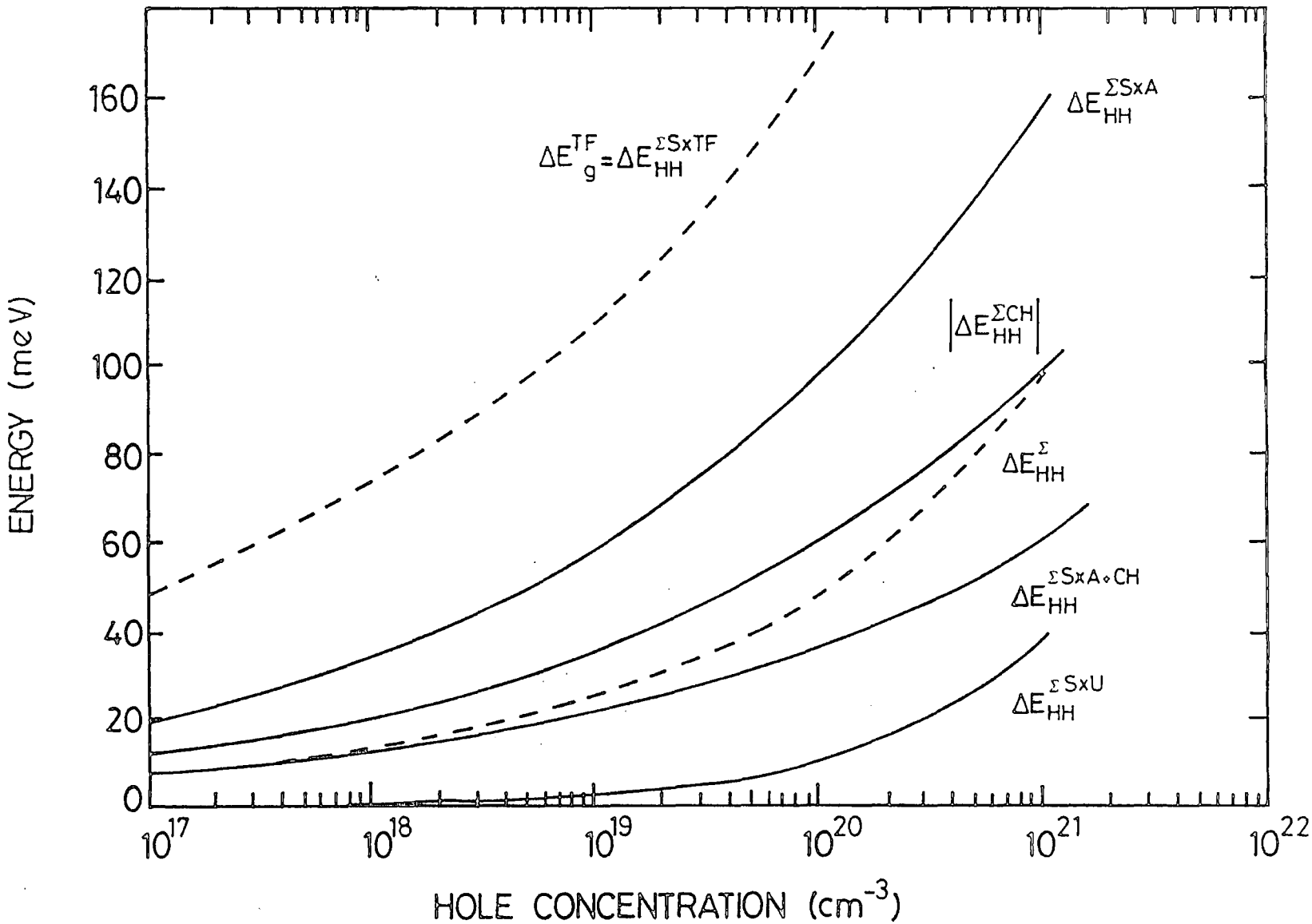

Figure 3.3: The hole concentration dependence of all terms contributing to the energy shift of the valence band edge in p-type Si at T = OK.

3.2.6. Comparison with the Use of the Thomas-Fermi Approximation for the Dielectric Function.

If the frequency independent Thomas-Fermi approximation to the hole gas dielectric function is used in expressions (3.17) and (3.18) for the valence band screened exchange terms, the resulting integrals can all be performed analytically. Using:

$$\frac{1}{\varepsilon(\underline{q},0)} = \frac{q^2}{q^2+K^2} \qquad (3.32)$$

gives

$$\Delta E_{HH}^{\Sigma SXTF} = \frac{e^2 K}{4\pi\varepsilon_o\varepsilon_r} + \sum_{n''} \frac{e^2 k_{fn''}}{4\pi^2\varepsilon_o\varepsilon_r}\left[1 - \frac{K}{k_{fn''}}\,\text{arctg}\left(\frac{k_{fn''}}{K}\right)\right] \qquad (3.33)\ .$$

As with the frequency dependent model the dominant term in the T.F. approximation arises from the screened exchange of the full valence band which corresponds to the first term in the above expression. The hole concentration dependence of $\Delta E_{HH}^{\Sigma SXTF}$ for p-type Si is compared with the frequency dependent model in figure 3.3, from which it can be seen that the resulting band shifts are exaggerated by the TF approximation due to the overestimation of carrier screening.

The TF approximation to the valence band CH term can also be derived analytically and provides a downward shift of the valence band given by:

$$\Delta E_{HH}^{\Sigma CHTF} = -\frac{e^2 K}{8\pi\varepsilon_o\varepsilon_r}\ . \qquad (3.34)\ .$$

As figure 3.4 shows this contribution is also larger for p-type Si than the corresponding frequency dependent term.

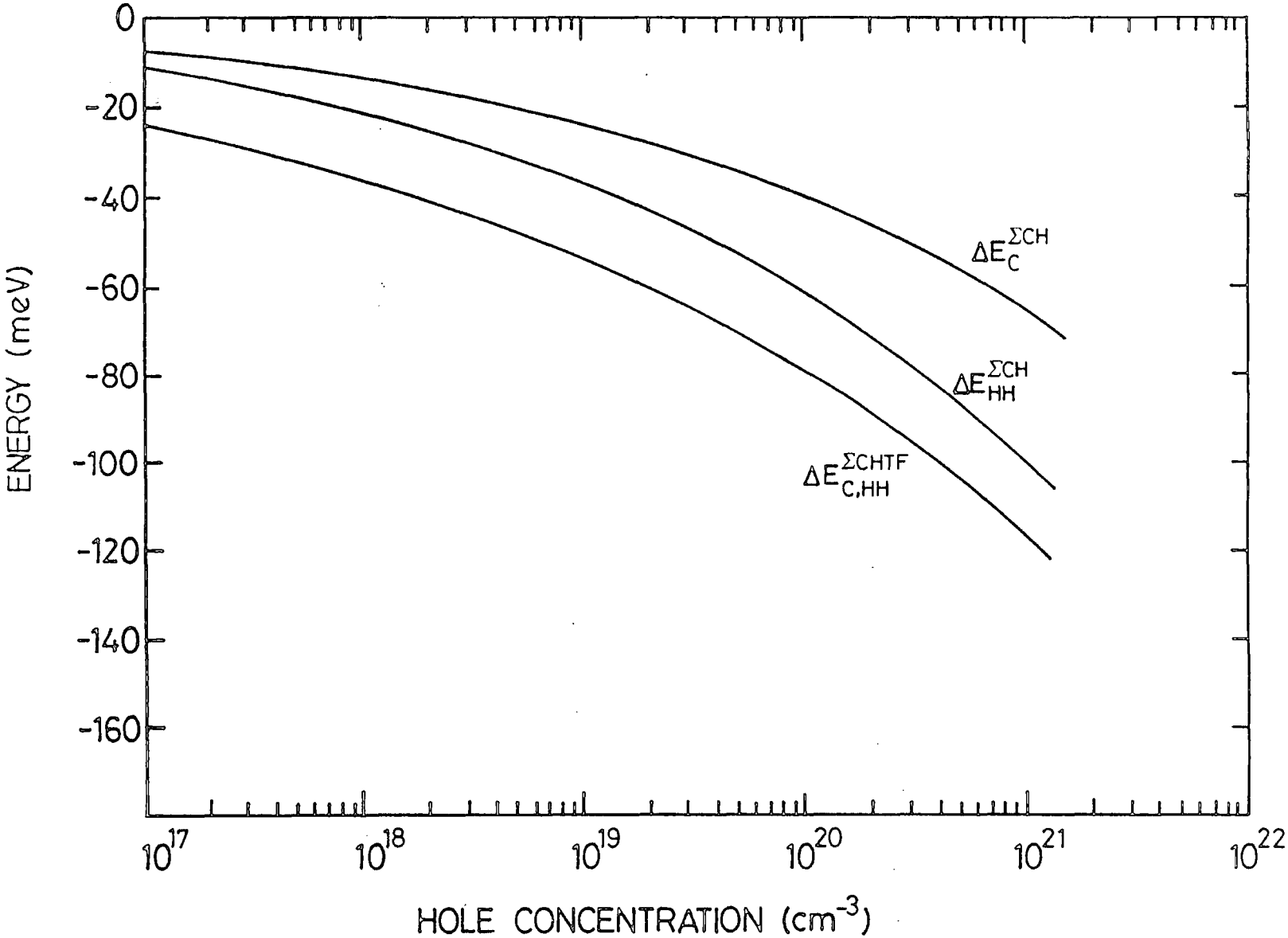

Figure 3.4: The hole concentration dependence of the Coulomb-hole energy shifts in the conduction $\Delta E_C^{\Sigma CH}$ and valence $\Delta E_{HH}^{\Sigma CH}$ band edges of p-type Si at T = OK. $\Delta E_{C,HH}^{\Sigma CHTF}$ is the Coulomb-hole energy shift in the conduction and valence bands, derived in T.F. approximation.

3.2.7. Conduction Band Shift - Screened Exchange Term

In equation (2.40) the overlap integral $(I_{n\underline{k},n''\underline{k}-\underline{q}})$ between conduction and valence band states is taken as zero and consequently, no energy contribution to the SX terms in the doped (equation (3.4)) and intrinsic (equation (3.6)) material arises from interactions between these bands. From these same expressions it is also seen that the SX energy is dependent on state occupancy. As the conduction band is unoccupied in both doped and intrinsic material no contribution to the band edge energy shift arises from the SX term, i.e.

$$\Delta E_c^{SX} = 0 \qquad (3.35).$$

The Coulomb-hole term is, however, non zero and provides the band edge shift which is now evaluated. This shift can be considered to arise from correlation effects of the hole gas.

3.2.8. Conduction Band Shift - Coulomb-Hole Term

Taking the real part of expression (3.5) the energy shift of a state at the band edge $\underline{k}_o$ is given by:

$$\Delta E_C^{\Sigma CH}(\underline{k}_o) = \frac{e^2}{8\pi^3 \varepsilon_o \varepsilon_r} \int_{\substack{\text{all } n'' \\ \text{and } \underline{q}}} \sum_{n''} \left| I_{c\underline{k}_o, n''\underline{k}_o - \underline{q}} \right|^2 \frac{\omega_p^2}{2q^2 \omega_l(\underline{q})} \frac{d^3\underline{q}}{((\omega_{c\underline{k}_o} - \omega_{n''\underline{k}_o - \underline{q}}) - \omega_l(\underline{q}))} \quad (3.36) .$$

In section 2.5.1 the overlap integral between the conduction band states and states in band n" was shown to be unity for n" corresponding to the same conduction band minimum and zero otherwise. Applying this prescription to the above formula gives

$$\Delta E_C^{\Sigma CH}(\underline{k}_o) = \frac{e^2}{8\pi^3 \varepsilon_o \varepsilon_r} \int_{\text{all } \underline{q}} \frac{\omega_p^2}{2\omega_l(\underline{q}) q^2 ((\omega_{c\underline{k}_o} - \omega_{c\underline{k}_o - \underline{q}}) - \omega_l(\underline{q}))} d^3\underline{q} \quad (3.37) .$$

Note in silicon the appropriate band edge state is $\underline{k}_o = \underline{k}_i$ where $\underline{k}_i$ is the minimum of one of the six valleys, and the above expression therefore gives the shift of that minimum.

Using spherical polar co-ordinates, the angular integrals in equation (3.37) are straightforward:

$$\int_0^{2\pi} \int_0^{\pi} \sin\theta \, d\theta \, d\phi = 4\pi \quad (3.38) .$$

Then,

$$\Delta E_C^{\Sigma CH}(k_o) = \frac{e^2}{2\pi^2 \varepsilon_o \varepsilon_r} \int_0^\infty \frac{\omega_p^2}{2\omega_1(q)} \frac{dq}{((\omega_{ck_o} - \omega_{ck_o - q}) - \omega_1(q))} \qquad (3.39) .$$

Following the prescription of equation (3.20) we now define the energy difference between the eigenvalues $\hbar\omega_{ck_o}$ and $\hbar\omega_{ck_o - q}$ as follows. For the gallium based materials $\underline{k}_o = 0$ and the parabolic, isotropic conduction band gives:

$$\hbar\omega_{co} - \hbar\omega_{c-q} = -\frac{\hbar^2 q^2}{2m_{De}} \qquad (3.40) .$$

For silicon each of six valleys can be considered separately and for valley i the equivalent of equation (3.40) is:

$$\hbar\omega_{ck_i} - \hbar\omega_{ck_i - \underline{q}} = -\frac{\hbar^2 q^2}{2m_{De}} \qquad (3.41) .$$

Note this energy difference is a negative quantity as the conduction band edge is lower in energy than state $-\underline{q}$. Substitution of these equations into (3.39) gives:

$$\Delta E_C^{\Sigma CH}(k_o) = -\frac{e^2}{2\pi^2 \varepsilon_o \varepsilon_r} \int_0^\infty \frac{\omega_p^2}{2\omega_1(q)} \frac{dq}{\left(\omega_1(q) + \frac{\hbar q^2}{2m_{De}}\right)} \qquad (3.42) .$$

This expression has the same form as equation (3.22) for the sum of the full valence band SX and CH terms and is evaluated in a similar manner using the NAG library routine Dϕ1 APF.

As with the valence band, the contribution of the CH term lowers the energy of the band edge state, and as the magnitudes of the shifts in both bands do not differ considerably the resulting contribution from CH terms to the band gap change is small. The carrier concentration dependence of the conduction and valence band CH terms in p-type Si is shown in figure 3.4.

3.2.9. Conduction Band Shift in the Thomas-Fermi Approximation

If the TF approximation to the dielectric function is used the conduction band CH term is the same as that derived for the valence band CH term. The Coulomb-hole contribution to the band gap narrowing is therefore zero in the TF approximation, as pointed out by Inkson (1976). The carrier concentration dependence of the TF, CH term, given by

$$\Delta E_{C,HH}^{\Sigma CHTF} = - \frac{e^2 K}{8\pi\epsilon_o\epsilon_r} , \tag{3.43}$$

is shown in Figure 3.4 for p-type Si. The resulting band shifts are larger than those produced in the frequency dependent plasmon pole approximation, which again is a result of the overestimation of the carrier screening effects in the TF approximation.

3.2.10. Results for p-type Materials

The hole concentration dependence of the upward valence band and downward conduction band shifts with the resulting band gap narrowing, for p-type Si, GaAs, $Ga_{0.47}In_{0.53}As$, and $Ga_{0.28}In_{0.72}As_{0.6}P_{0.4}$ are illustrated in figures 3.5 to 3.8 respectively. For comparison the band gap narrowing derived in the T.F. approximation (which equals the shift due to the valence band SX term) for p-type Si is also shown in figure 3.5. The band shifts in all four materials follow a similar pattern with the greatest shift occurring in the valence band.

The narrowing of the band gap causes a shift towards lower frequencies in the fundamental optical emission spectrum of the material. However, the corresponding shift in the absorption spectrum is compensated to a greater or lesser extent by the Moss-Burstein (1954) shift arising from

the removal of electrons from valence band states down to the Fermi level. The fundamental absorption frequency ω_A is then given by:

$$\hbar\omega_A = E_{fv} + E_g - \Delta E_g^{\Sigma} \qquad (3.44) .$$

The concentration dependence of the Fermi level in Si and GaAs is shown in figures 3.5 and 3.6, from which it can be seen that $|E_{fv}| > |\Delta E_g^{\Sigma}|$ for $p \simeq 10^{19}$ cm^{-3} in GaAs and $p \simeq 3 \times 10^{19}$ cm^{-3} in Si. The fundamental absorption frequency therefore increases for hole concentrations in excess of these values.

Several authors including Casey (1976) and Vol'fson (1967) have deduced from optical measurements a $p^{1/3}$ power law for the carrier concentration dependence of the band gap reduction in semiconductors. This power law provides an approximate relationship for the results derived in the present model. For example the relationship $|\Delta E_g| = 16 \times 10^{-8} p^{1/3}$ provides a reasonable fit to the band gap narrowing for p-type GaAs in figure 3.6.

3.3. Band Gap Narrowing in n-type Material

3.3.1. Introduction

A detailed analysis of the band edge shifts due to many body effects in n-type Si has been performed by Saunderson (1983) and the results repeated in the work of Abram et al (1984). However, to illustrate the similarities between the derivations of the band shifts in n and p-type material a brief comparison of the fundamental expressions is given below. Saunderson's work is then extended to derive the band gap narrowing in the n-type gallium based materials. This comparison also serves to

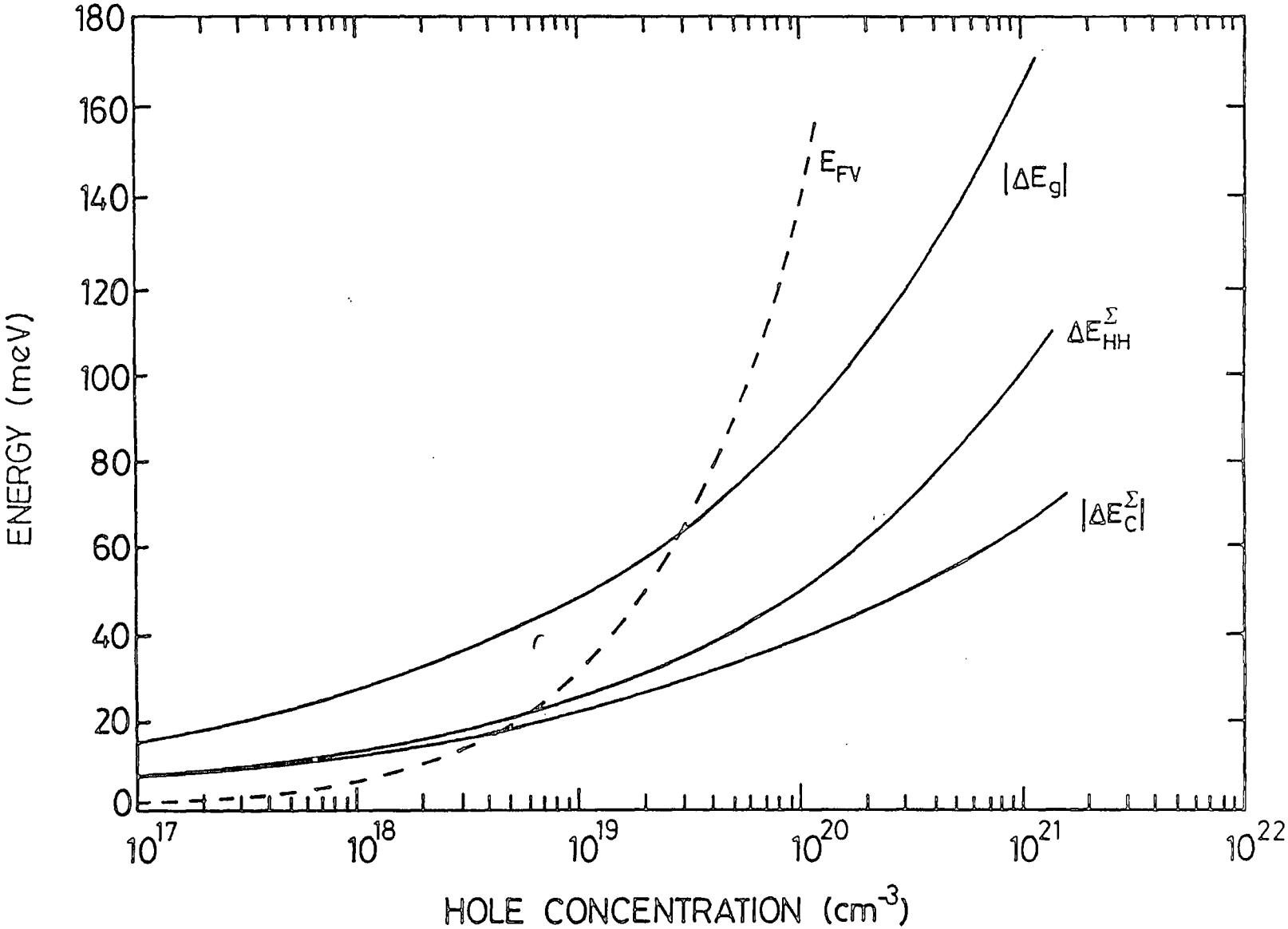

Figure 3.5: The hole concentration dependence of the energy shifts in the conduction $|\Delta E_C^{\Sigma}|$ and valence ΔE_{HH}^{Σ} band edges, and the corresponding band gap narrowing $|\Delta Eg|$, in p-type Si at T = OK. The position of the Fermi level E_{FV} is also shown.

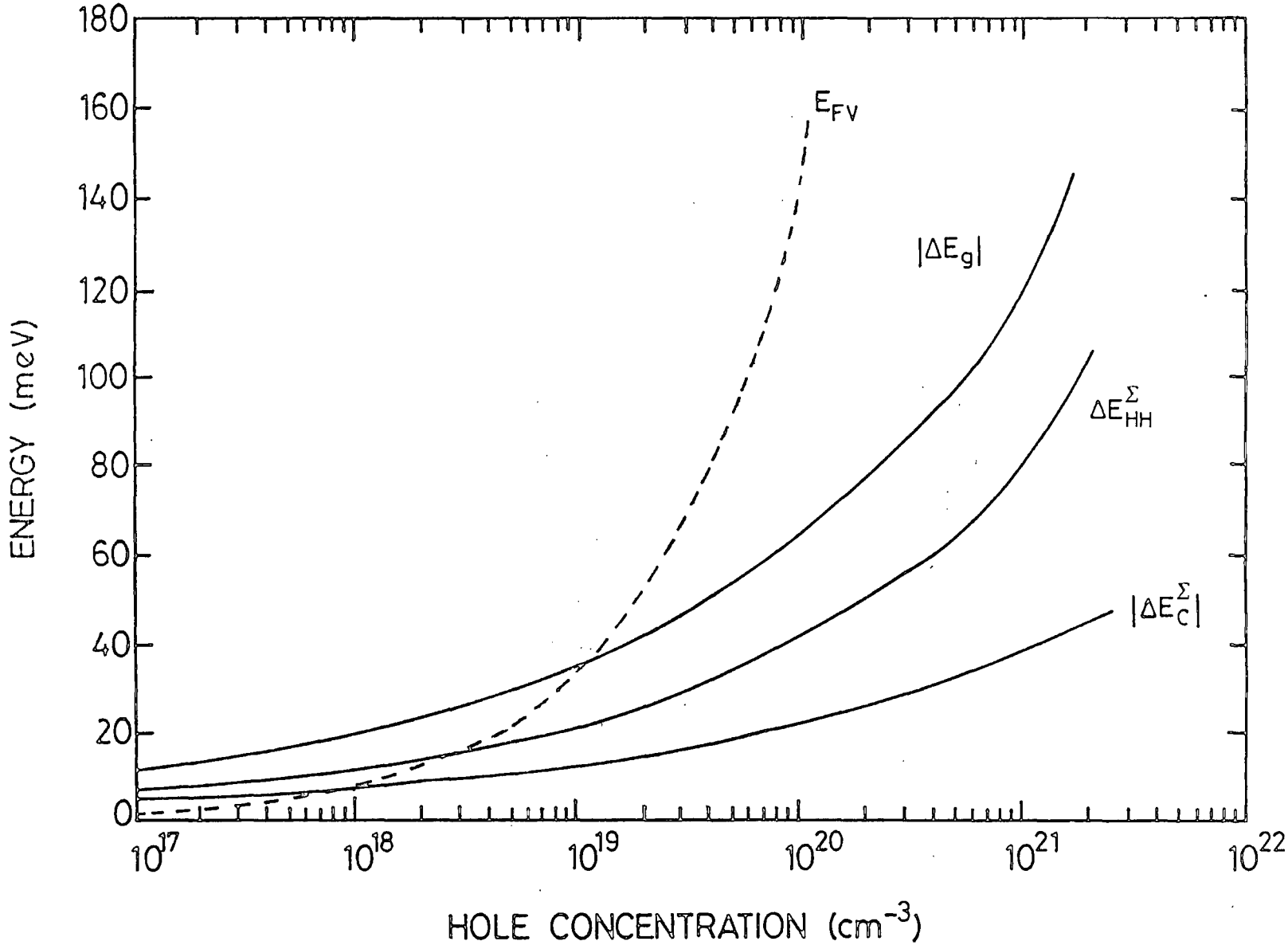

Figure 3.6: The hole concentration dependence of the energy shifts in the conduction $|\Delta E_C^{\Sigma}|$ and valence ΔE_{HH}^{Σ} band edges, and the corresponding band gap narrowing $|\Delta Eg|$, in p-type GaAs at T = OK. The position of the Fermi level E_{FV} is also shown.

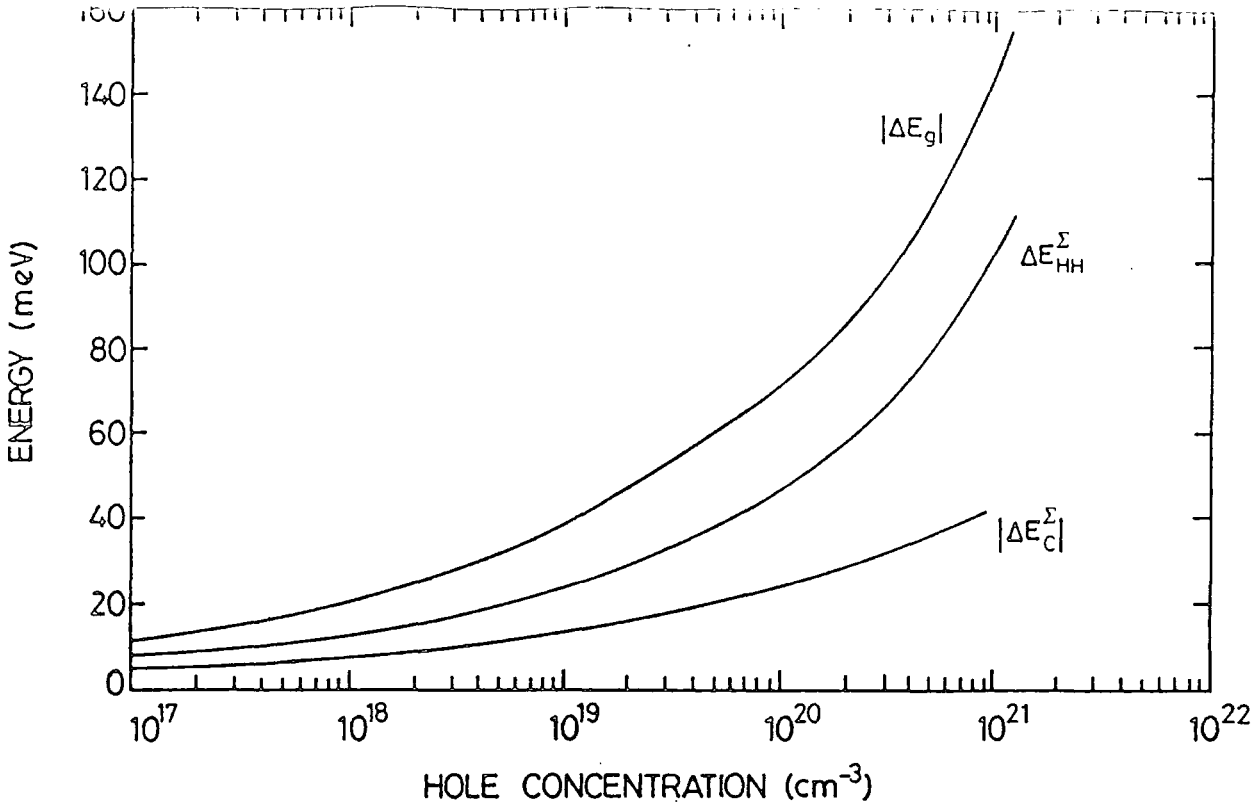

Figure 3.7: The hole concentration dependence of the energy shifts in the conduction and valence band edges and the corresponding band gap narrowing $|\Delta Eg|$ in p-type $Ga_{0.47}\ In_{0.53}\ As$ at T = OK.

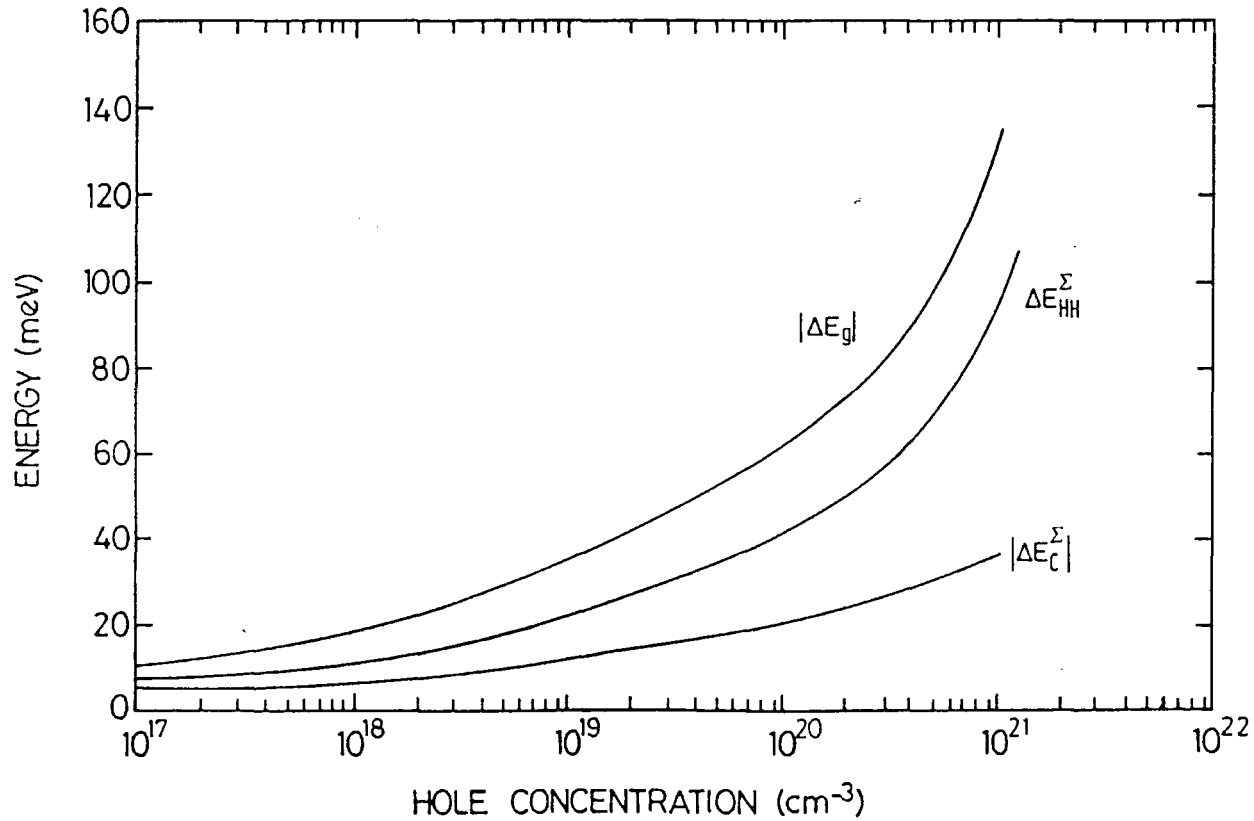

Figure 3.8: The hole concentration dependence of the energy shifts in the conduction and valence band edges and the corresponding band gap narrowing $|\Delta Eg|$ in p-type $Ga_{0.28}\ In_{0.72}\ As_{0.6}\ P_{0.4}$ at T = OK.

outline the procedure for deriving the band gap narrowing in electron-hole plasmas.

As shown in figure 3.1 the conduction band in n-type material is occupied by electrons up to the Fermi level and the response of the electron gas to test electrons at the band edges provides Coulomb-hole terms contributing to the shifts in both band edges. The terms are similar to the corresponding terms in p-type material. Unlike p-type material however the test electron in the conduction band now has a screened exchange interaction with the carriers of the electron gas in the conduction band which then contributes to the downward shift in the conduction band. In addition the electron gas screens carrier interactions in the full valence band.

3.3.2. Basic Formulae - Conduction Band Shift

Substituting the relevant overlap integral (2.40) into the Coulomb-hole term (3.5) and performing the angular integration in wavevector space gives:

$$\Delta E_C^{\Sigma CH}(k_o) = \frac{e^2}{2\pi^2 \varepsilon_o \varepsilon_r} \int_{\text{all } q} \frac{\omega_p^2}{2\omega_1(q)} \frac{dq}{[(\omega_{ck_o} - \omega_{ck_o - q}) - \omega_1(q)]} \qquad (3.45)$$

which is identical to equation (3.39) for the conduction band CH term in p-type material, except ω_p and $\omega_1(q)$ now refer to the electron gas. It is also interesting to note that this term has the same form as that for the sum $\Delta E_{HH}^{\Sigma SXA} + \Delta E_{HH}^{\Sigma CH}$ (see equations (3.17) + (3.19)) in p-type material.

The screened exchange interaction for the states occupied up to the Fermi level is expressed as:

$$\Delta E_C^{SX} = -\frac{e^2}{2\pi^2\varepsilon_o\varepsilon_r}\int_{\substack{\text{occupied}\\ \text{states}}}\frac{dq}{\varepsilon(\underline{q},\omega_{c\underline{k}_o}-\omega_{c\underline{k}_o}-\underline{q})} \qquad (3.46)$$

which has the same form as expression (3.18) for the valence band shift $\Delta E_{HH}^{\Sigma SXU}$ in p-type material. However, the comparison is somewhat obscured due to the coupling of the heavy and light hole valence bands in $\Delta E_{HH}^{\Sigma SXU}$. Nevertheless it is now possible to see a physically sensible correspondence between the contributions to the conduction band shift in n-type material and the valence band shift in p-type material.

3.3.3. Basic Formulae- Valence Band Shift

The shifts of the heavy hole band edge are again considered and a similar argument to that used in section 3.2.3 can be used to show $\Delta E_{HH}^{\Sigma} = \Delta E_{LH}^{\Sigma}$ i.e. the shifts in the heavy and light hole band edges are equal.

The valence band CH term takes the same form as that derived for the valence band in p-type material (expression 2.19) apart from the relevant changes to ω_p and $\omega_1(\underline{q})$, and is given by

$$\Delta E_{HH}^{\Sigma CH}(\underline{O}) = \frac{e^2}{8\pi^3\varepsilon_o\varepsilon_r}\int_{\substack{\text{all } -\underline{q}\\ \text{and } n''}}\sum_{n''}\left|I_{HH\underline{O},n''-\underline{q}}\right|^2\frac{\omega_p^2}{2\omega_1(\underline{q})}\frac{d^3\underline{q}}{[(\omega_{HH\underline{O}}-\omega_{HH-\underline{q}})-\omega_1(\underline{q})]} \qquad (3.47)\ .$$

The screened exchange term for the full valence band is expressed as:

$$\Delta E_{HH}^{\Sigma SXA}(\underline{O}) = \frac{e^2}{8\pi^3\varepsilon_o\varepsilon_r}\int_{\substack{\text{all } n''\\ \text{and } -\underline{q}}}\sum_{n''}\left|I_{HH\underline{O},n''-\underline{q}}\right|^2\left[1-\frac{1}{\varepsilon(\underline{q},\omega_{HH\underline{O}}-\omega_{n''-\underline{q}})}\right]d^3\underline{q} \qquad (3.48)\ .$$

If $\Delta E_{HH}^{\Sigma CH}$ and $\Delta E_{HH}^{\Sigma SXA}$ are added the resulting expression takes the same form as the conduction band CH term in p-type material. Hence there is

a direct correspondence between the valence band shift in n-type material and conduction band shift in p-type material.

3.3.4. Results for n-type Materials

The carrier concentraion dependence of the conduction and valence band shifts together with the corresponding band gap narrowing for n-type Si, GaAs, $Ga_{0.47}In_{0.53}As$, and $Ga_{0.28}In_{0.72}As_{0.6}P_{0.4}$ is illustrated in figures 3.9 to 3.12 respectively. The relatively light effective masses of the single valley conduction bands of the gallium compounds (e.g. $m_{De} = 0.067\ m_o$ in GaAs) makes the free electron screening quite weak. In any of these materials the resulting changes in the interactions in the full valence band are therefore small giving only a small shift in the valence band edge. However, in the conduction band the weak screening of the interaction with the newly introduced electrons ensures a large contribution from the screened exchange term and a correspondingly large conduction band shift. The relatively heavy density of states effective mass of each conduction band valley of silicon and the fact that there are six valleys to be occupied ensures good carrier screening and results in a large shift in the valence band edge and small shift in the conduction band edge compared to those found in the gallium compounds.

The light conduction band effective mass in the gallium compounds causes the Fermi level to increase rapidly with increasing concentration as shown in figure 3.10 for GaAs. The Moss-Burstein shift is therefore quite significant in these compounds and $|E_{fe}| > |\Delta E_g|$ giving a large increase in the fundamental absorption frequency. The Moss-Burstein shift in n-type Si is however considerably smaller than in the gallium compounds due to the heavy conduction band density of states effective mass and 6 valleys. As shown in figure 3.9 the Fermi energy is less than the band gap narrowing for electron concentrations $\lesssim 10^{20}\ cm^{-3}$.

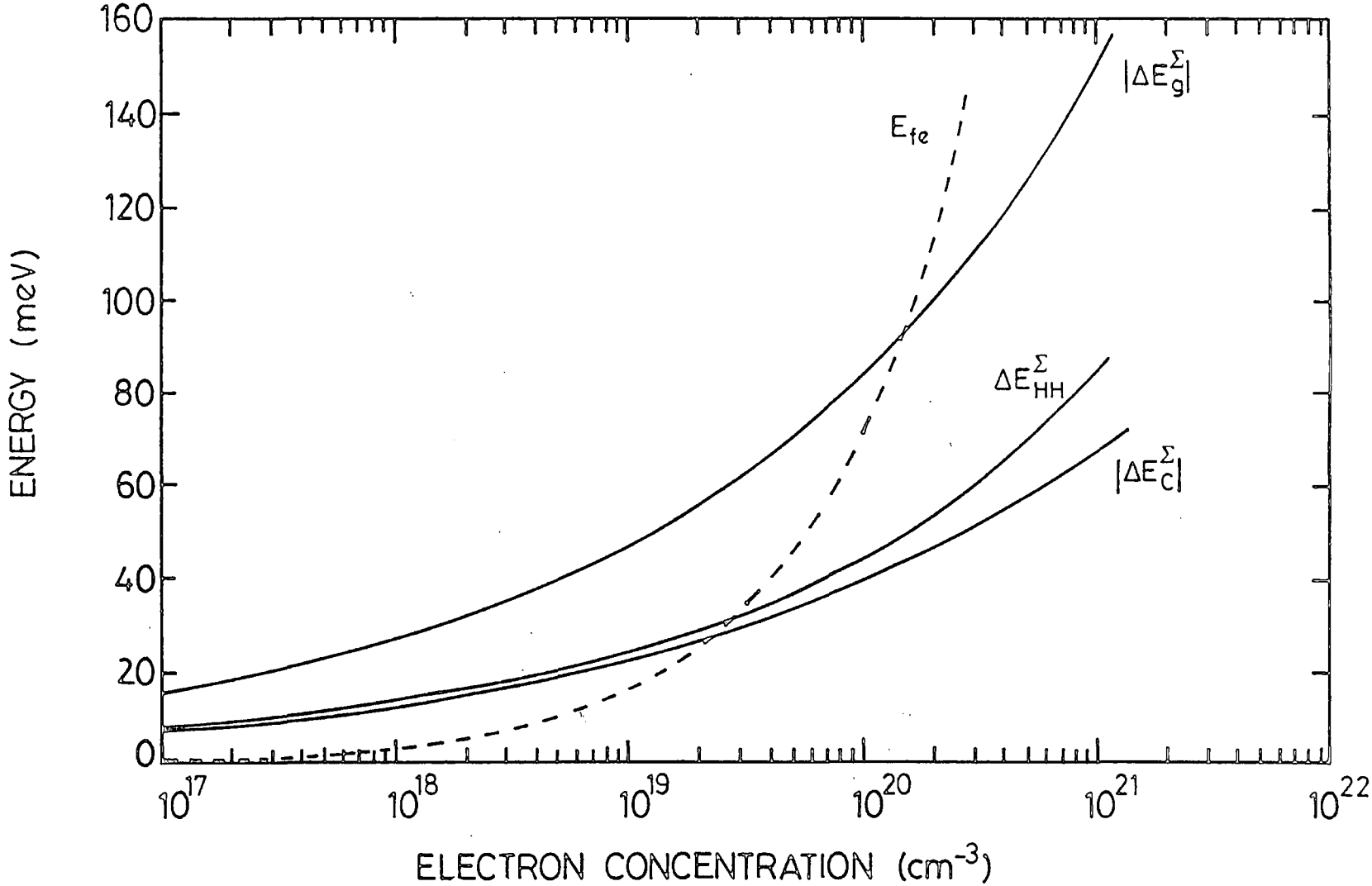

Figure 3.9: The electron concentration dependence of the energy shifts in the conduction and valence band edges and the corresponding band gap narrowing $|\Delta Eg|$ in n-type Si at T = OK. The position of the Fermi level E_{fe} is also shown.

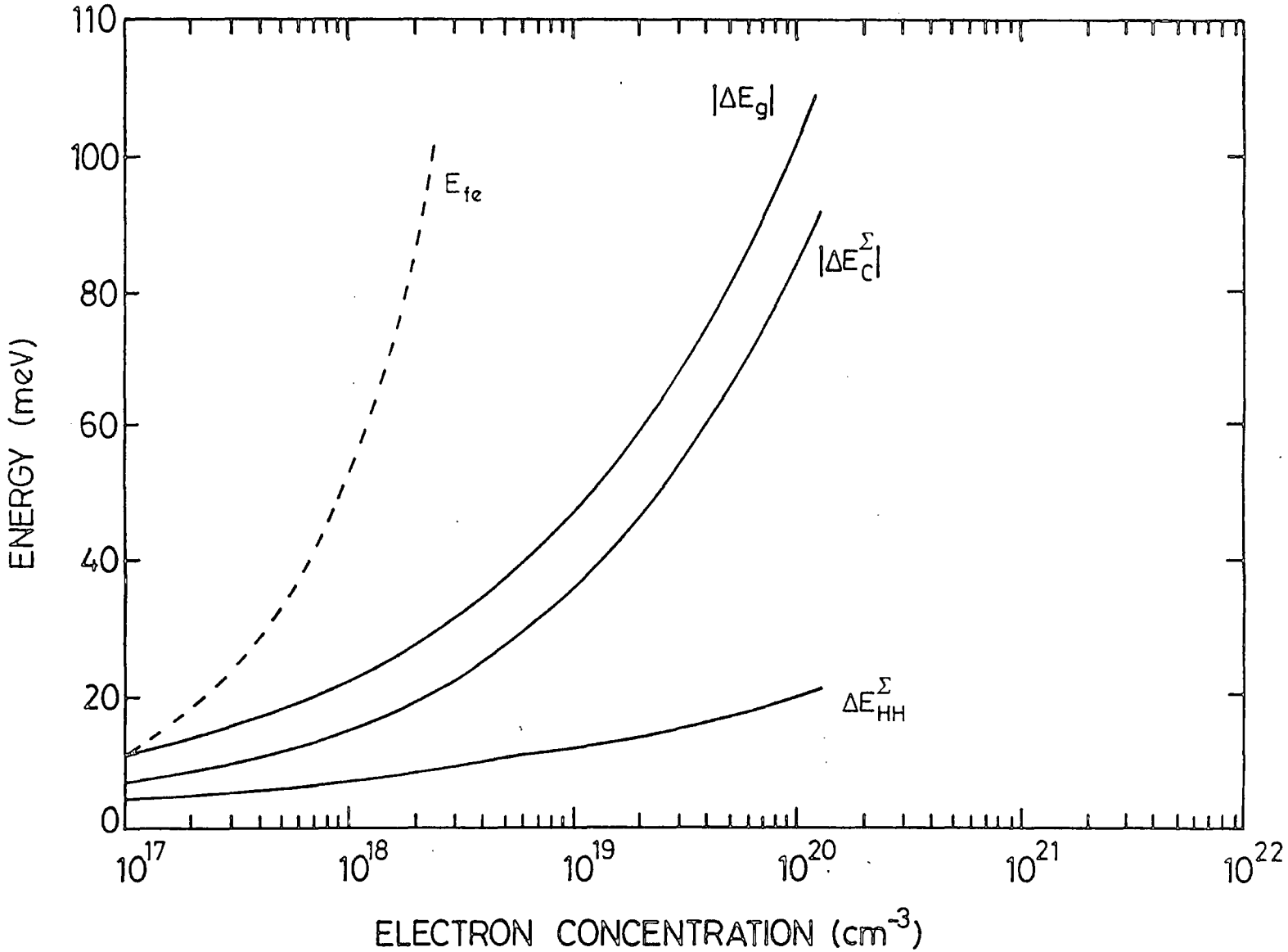

Figure 3.10: The electron concentration dependence of the energy shifts in the conduction and valence band edges and the corresponding band gap narrowing $|\Delta Eg|$ in n-type GaAs at T = OK. The position of the Fermi level E_{fe} is also shown.

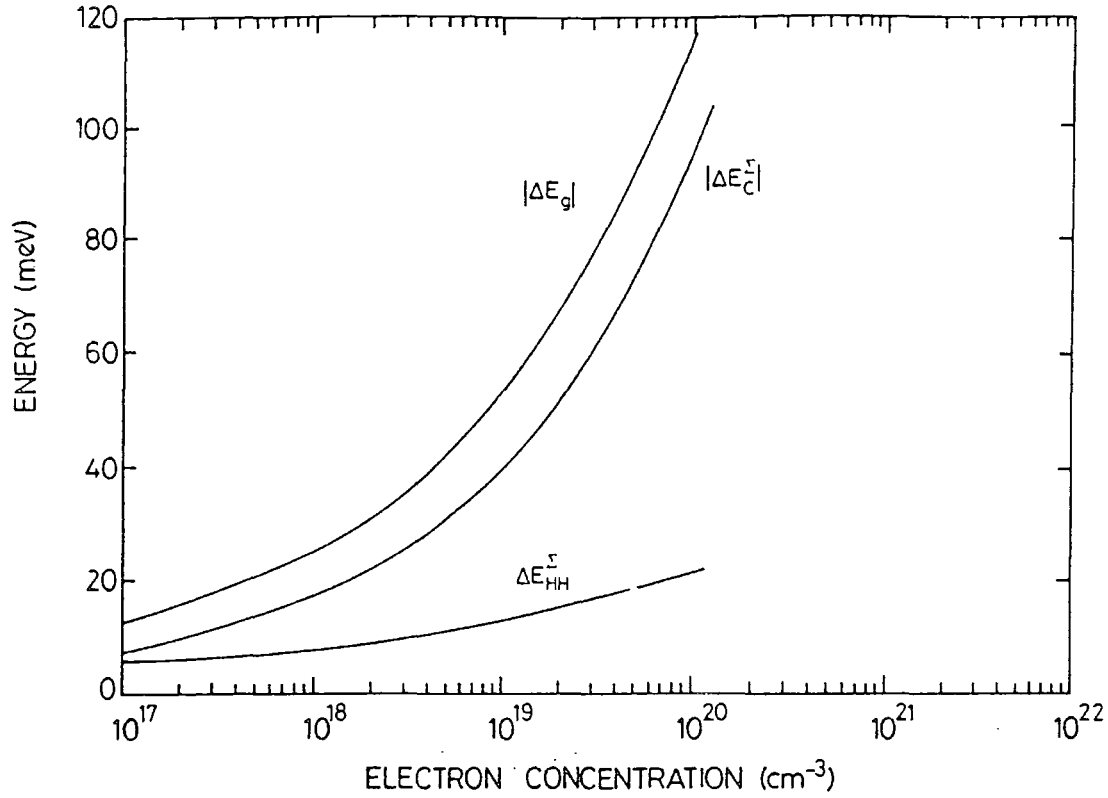

Figure 3.11: The electron concentration dependence of the energy shifts in the conduction and valence band edges and the corresponding band gap narrowing $|\Delta Eg|$ in n-type $Ga_{0.47}\ In_{0.53}\ As$ at T = OK.

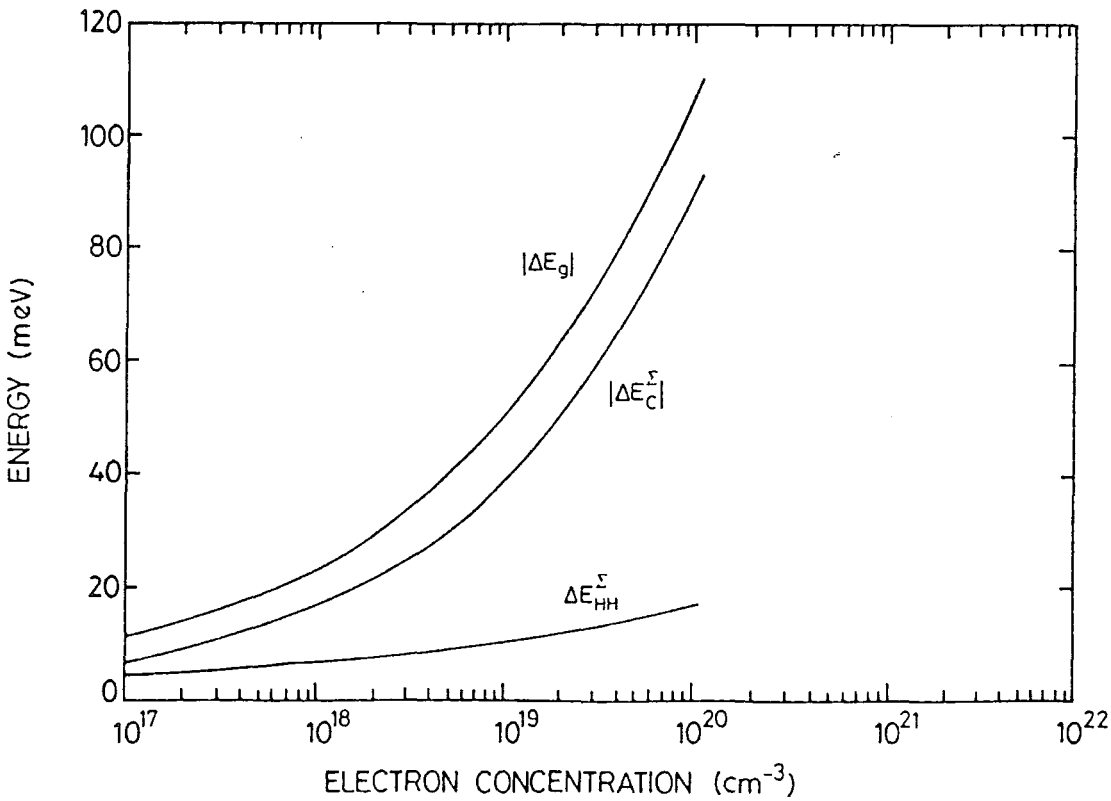

Figure 3.12: The electron concentration dependence of the energy shifts in the conduction and valence band edges and the corresponding band gap narrowing $|\Delta Eg|$ in n-type $Ga_{0.28}\ In_{0.72}\ As_{0.6}\ P_{0.4}$ at T = OK.

The band gap narrowing derived for the n-type gallium compounds is in excellent agreement with the power law $|\Delta E_g| = Bn^{1/3}$. For example $B = 22.1 \times 10^{-8}$ provides a very good fit to results shown in figure 3.10 for n-type GaAs. A similar power law relationship for the band gap narrowing in n-type Si can be deduced, however the fit to the calculated result is less accurate than in the gallium compounds.

3.4. Band Gap Narrowing due to Electron-Hole Plasmas

3.4.1. Introduction and General Discussion

The calculations described so far have related to heavily doped material with a single species carrier gas in the host conduction or valence band.

However, if the semiconductor material is pumped by say optical excitation, large and equal concentrations of electrons and holes are produced in the relevant bands. This electron-hole (e-h) plasma acts to screen interactions in the same manner as a single species gas but with a T.F. screening wavevector K and plasma frequency ω_p, modified as discussed in sections 2.2 and 2.6.2 respectively.

The conduction band contains newly occupied states and the band edge shift is evaluated using the procedure derived for n-type material with the expressions ω_p, $\omega_1(\underline{q})$ and $\varepsilon(\underline{q},\nu)$ modified accordingly. Similarly the valence band states are unoccupied by electrons down to the Fermi level and the valence band shift is derived in the same manner as that in p-type material. A similar calculation for the band shifts due to an electron-hole plasma in germanium has been performed by Rice (1974) using the plasmon pole approximation to the dielectric function, with a modified damping factor to account for interband transitions.

3.4.2. Results for Materials Containing Electron-Hole Plasmas

The concentration dependence of the band edge shifts and band gap narrowing for e-h plasmas in Si and GaAs are shown in figures 3.13 and 3.14. The increased screening effect of the plasma results in greater band gap narrowing for a given electron or hole concentration than is produced in materials with a single species carrier. The results for GaAs compare well with those derived by Tanaka et al (1980) from measurement of the luminescence spectra. However, the range of carrier concentrations over which their results were measured was less than 5×10^{18} cm^{-3} which represents the lowest range of validity of the present calculation.

3.5. The Effects of Hole Occupation of the Spin Split Off Band in p-type Silicon

3.5.1. Introduction

The spin split off band edge lies some 44 mev below the degenerate HH and LH band edge at $\underline{k} = 0$. The SS band becomes occupied with holes at T = OK when the Fermi level passes below -44 mev which occurs for carrier concentrations $\gtrsim 1.7 \times 10^{19}$ cm^{-3}. This occupancy alters some of the basic parameters used in the present calculations. These changes and the effects they have on the band edge shifts are discussed below.

3.5.2. Effects on Parameters and Band Edge Shifts

From section 2.5.1 it is seen that the overlap integral between states in the spin split-off and the other three relevant bands (HH, LH and C) can be taken as zero. Thus no changes in the forms of the derived expressions for the band edge shifts are required due to the hole occupancy of the SS band although some of the parameters in these expressions are

affected. A larger density of states exists at a given energy E ($E < E_v - \Delta$) than for the two band case. At the Fermi level this density of states is given by:

$$\rho(E_{fv}) = \frac{2^{1/2} E_{fv}^{1/2}}{\pi^2 \hbar^3} (m_H^{3/2} + m_L^{3/2}) + \frac{2^{1/2} (E_{fv} - \Delta)^{1/2}}{\pi^2 \hbar^3} m_S^{3/2} \qquad (3.49)$$

where m_S is the density of states effective mass in the SS band. This increase in the density of states causes a raising in the Fermi energy so that it is closer to the valence band edge than in the two band model. The change becomes significant (>10 mev) for carrier concentrations $\gtrsim 10^{20}$ cm^{-3}. The main effect of the raised Fermi level is that, for a given carrier concentration, more heavy and light hole states remain occupied with electrons. Hence, in the evaluation of $\Delta E_{HH}^{\Sigma SXU}$ for the HH and LH bands, there are fewer unoccupied states to integrate over. The increase in the density of states at the Fermi level additionally affects the T.F. screening wavevector defined as

$$K^2 = \frac{e^2}{\varepsilon_o \varepsilon_r} \sum_i \int \rho(E) \left[\frac{-\partial f(E)}{\partial E} \right] dE \qquad (3.50)$$

(ref. Abram et al 1978) where i represents all bands occupied with holes, and f(E) is the occupation factor which at T = OK is a step function at E_{fv}. Hence

$$K^2 = \frac{e^2}{\varepsilon_o \varepsilon_r} \sum_i \int \rho(E) \delta(E - E_{fv}) \, dE = \frac{e^2}{\varepsilon_o \varepsilon_r} \sum_i \rho(E_{fv}) \qquad (3.51)$$

$$\text{i.e. } K^2 = \frac{e^2}{\varepsilon_o \varepsilon_r} \frac{2^{1/2}}{\pi^2 \hbar^3} [E_{fv}^{1/2} (m_L^{3/2} + m_H^{3/2}) + (E_{fv} - \Delta)^{1/2} m_S^{3/2}] \qquad (3.52)$$

This expression is approximately equal to:

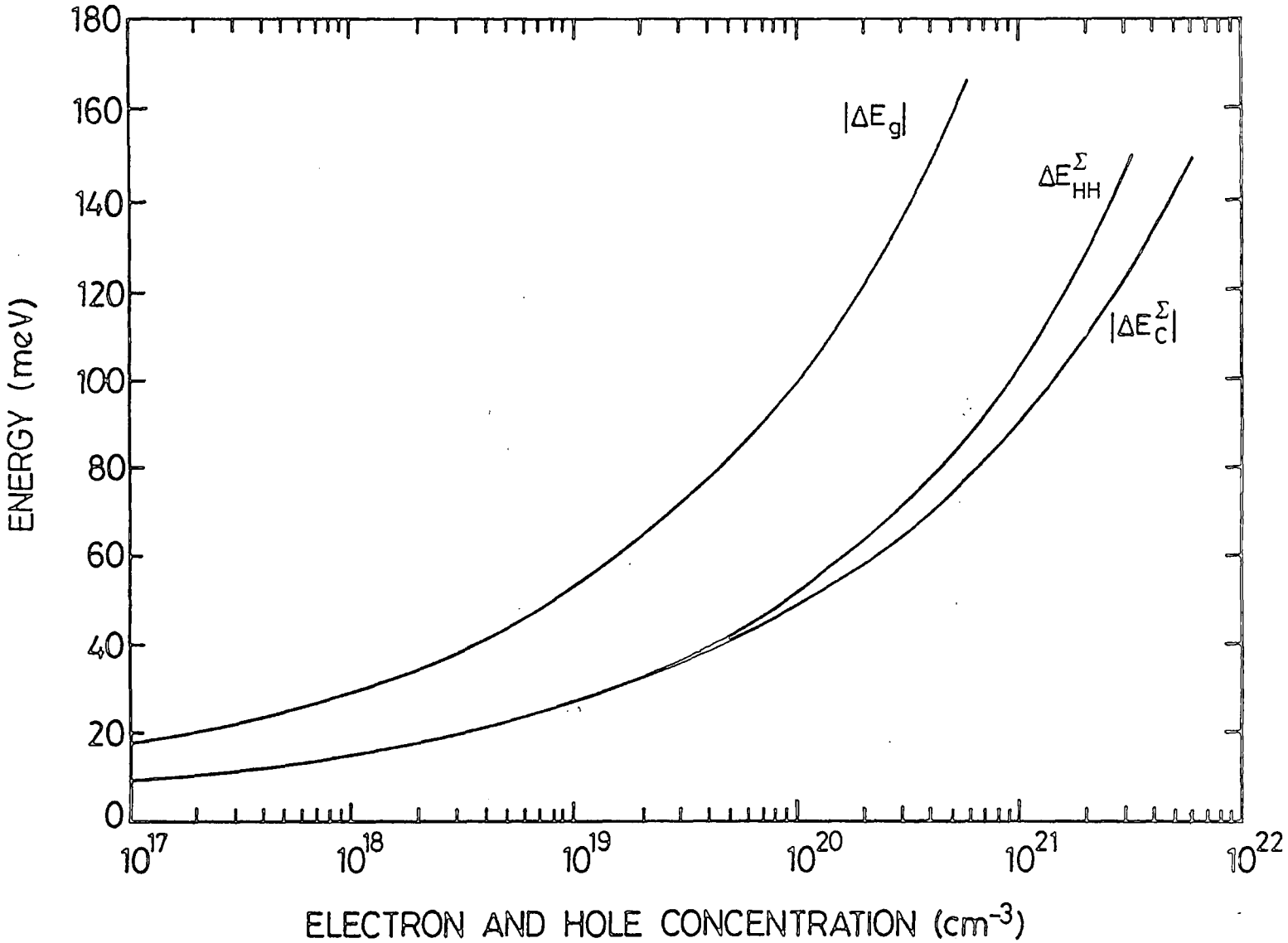

Figure 3.13: The hole concentration dependence of the energy shifts in the conduction and valence band edges and the corresponding band gap narrowing $|\Delta Eg|$ in Si under electron-hole plasma conditions at T = OK.

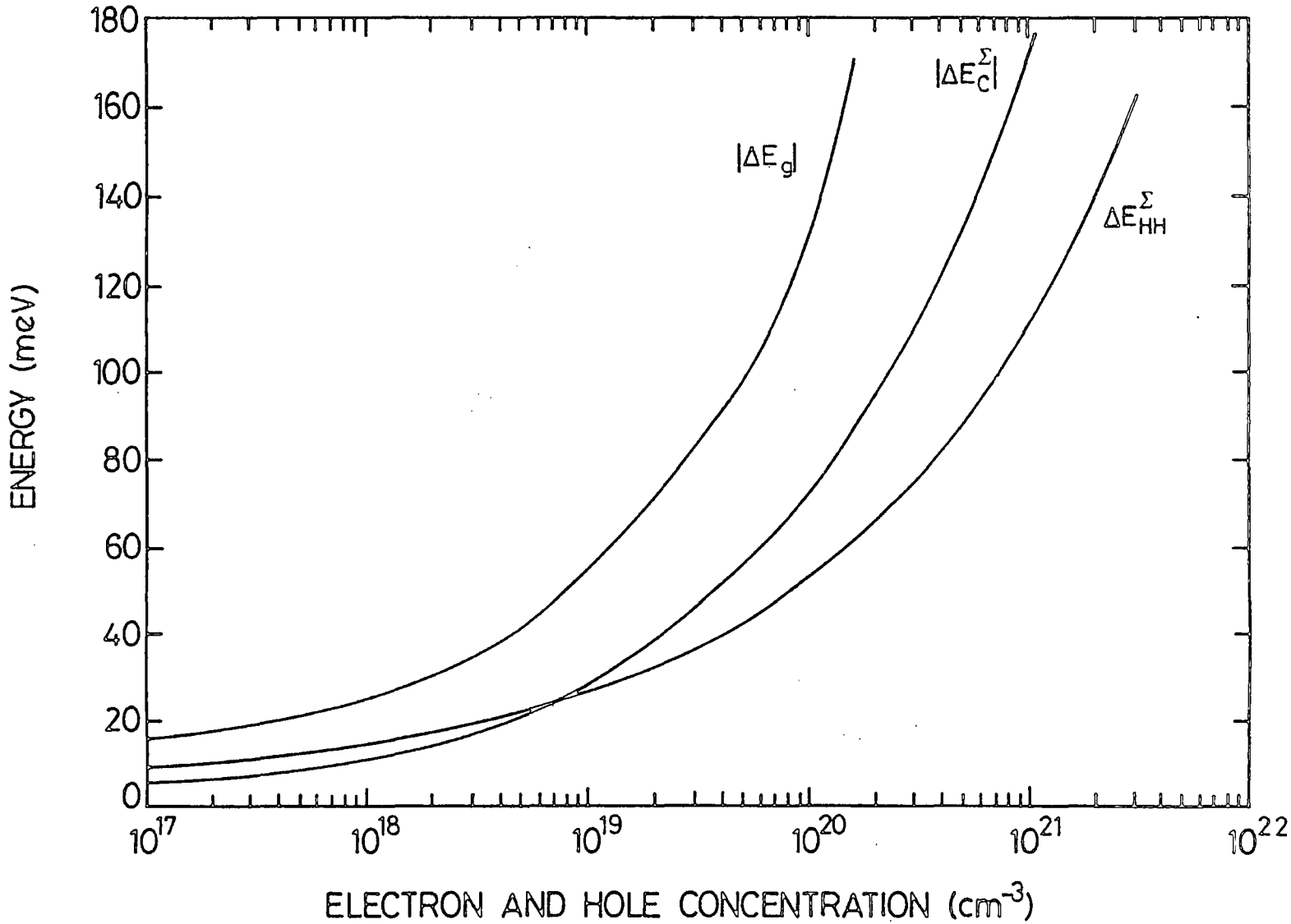

Figure 3.14: The hole concentration dependence of the energy shifts in the conduction and valence band edges and the corresponding band gap narrowing $|\Delta Eg|$ in GaAs under electron-hole plasma conditions at T = OK.

$$K^2 = \frac{e^2 m_{Dvs} (3\pi^2 p)^{1/3}}{\varepsilon_o \varepsilon_r \pi^2 \hbar^2} \tag{3.53}$$

where m_{Dvs} is the density of states effective mass

$$m_{Dvs} = (m_L^{3/2} + m_H^{3/2} + m_S^{3/2})^{2/3} \tag{3.54}$$.

The zero wavevector plasmon frequency ω_ρ contains the mass m_{ovs} which on following a similar derivation to that in appendix 3 for three valence bands becomes:

$$\frac{1}{m_{ovs}} = \frac{\lambda_H}{m_H} + \frac{\lambda_L}{m_L} + \frac{\lambda_S}{m_S} \tag{3.55}$$

where λ_x is the fraction of the total hole concentration in band x.

Finally the prefactor of the q^4 term in the plasmon dispersion relation is altered to the new value of $\hbar^2/4m_{Dvs}^2$.

The nett effect of making the above changes in the various parameters is only a small increase in the band edge shifts (6 meV for the heavy hole band and 3 meV for the conduction band at $p = 10^{20}$ cm^{-3}, giving an increased band gap narrowing of 9 meV). These changes represent only a small percentage of the band edge shift and justify the use of the two band approximation in Si.

3.6. Summary

The frequency integral part of the fundamental self energy expression (2.39) has been performed, reducing this expression to the form of two wavevector integrals known as the screened exchange and Coulomb hole terms. The sum of the real parts of these terms evaluated under the relevant occupancy conditions gives the self energy of a state $\underline{k}$ in band n.

The difference between this self energy evaluated for the doped and intrinsic material provides the energy shift of the state. The band gap narrowing has thus been derived by evaluation of this shift for states at the conduction and valence band edges. Comparison between expressions derived for these shifts in n and p-type material indicate a correspondence between the valence band shift in p-type material and the conduction band shift in n-type material and vice versa.

The band gap narrowing has been calculated for p and n-type Si, GaAs, $Ga_{0.47}In_{0.53}As$ and $Ga_{0.28}In_{0.72}As_{0.6}P_{0.4}$ and for Si and GaAs containing an electron-hole plasma. The carrier concentration dependence of the band edge shifts follow a similar pattern in all four materials with the largest shift occurring in the band containing the carriers. The band edge shifts are also seen to reflect the effective mass and screening properties of the carrier gas.

The results derived for the band edge shifts using the Thomas-Fermi approximation to dielectric response are seen to be much larger than those derived in the plasmon pole approximation, but the model provides a rough guide to the energy shifts of the band edges.

CHAPTER 4

BAND GAP NARROWING DUE TO MANY BODY INTERACTIONS AT FINITE (T = 300 K) TEMPERATURE

4.0. Introduction

The work in this chapter provides a direct extension to finite temperatures of the band edge energy shifts derived at T = OK in the electron-electron self energy model of Chapters 2 and 3. The main emphasis will again be on deriving band edge shifts in p-type material with a brief comparison of the corresponding shifts in n-type material given in section 4.4. The work thus complements the analysis of Saunderson (1983) who evaluated the band gap narrowing in n-type silicon at T = 300 K.

The effect of the hole occupancy of the spin split-off band in p-type silicon at T = OK was shown to be small and this occupancy is therefore ignored in the finite temperature (T = 300 K) calculations.

At large carrier concentrations ($\gtrsim 10^{20}$ cm^{-3}) the band edge shifts at room temperature in n and p-type material are found to differ little from those at zero temperature. A similar effect will be seen for semiconductors with conduction and valence bands occupied by an electron-hole plasma. The extension to finite temperatures of the calculations in section 3.4 for the band gap narrowing induced by e-h plasmas is therefore not given, the band shifts at the high carrier concentrations found in for example operational lasers can be assumed to be approximately equal to the zero temperature shifts.

A direct extension from zero to finite temperatures is possible in the description of the electron-electron interactions through the use of

the finite temperature plasmon pole approximation to the dielectric function derived in section 2.6.2. This removes the complexities involved in using the full finite temperature Lindhard dielectric function.

At finite temperatures (T = 300 K) the host bands of a doped semiconductor will be occupied by carriers thermally excited from shallow donor or acceptor centres. However, as with the zero temperature model the present analysis is valid in uncompensated material for the range of impurity concentration for which the impurity band has merged with the host semiconductor band and each impurity has donated a single carrier to the host band. The dopant concentration at which this occurs (the Mott critical density N_c) is, however, different from that at T = OK. The thermal energy of the carriers now acts to reduce their screening response to a perturbation. This weaker screening (larger screening length λ) increases the impurity concentration required to produce a screening length λ smaller than the effective Bohr radius a_f; the approximate condition for which the carriers are no longer bound to the impurity ions. The dopant concentration at which $\lambda = a_f$ for p-type Si at room temperature (T = 300 K) can be estimated from the carrier concentration dependence curves of these two parameters given in figure 4.1. This dopant concentration ($p \simeq 2.5 \times 10^{19}$ cm^{-3}) represents a lower bound for the validity of the present work.

The reduction in screening with decreasing carrier concentration can be attributed to the change in the carrier distribution function. At low dopant concentrations the Fermi level lies in the band gap (particularly for p-type material with large valence band effective masses and a large density of states near the band edge) and the carrier

distribution is Boltzmann like. However, at high dopant concentrations the carrier distribution is little different from that at $T = 0K$, and the band edge shifts are correspondingly similar to those at zero temperature.

The detailed evaluations of the Thomas-Fermi (T.F.) screening wavevector and Fermi energy upon which the self energy calculations are dependent is dealt with in section 4.1.3. In the next section the finite temperature versions of the Green's functions and effective potential are derived, and the resulting expression for the self energy of state $\underline{k}$ due to electron-electron interactions is given.

4.1. Self Energy due to Electron-Electron Interactions

In chapter 2 the basic expression for the self energy of state $\underline{k}$ in band n due to electron-electron interactions was derived using a Feynman diagrammatic approach. The same expression (2.39)

$$E_n^{\Sigma}(\underline{k}) = \frac{i}{(2\pi)^4} \int \sum_{n''} |I_{n\underline{k},n''\underline{k}-\underline{q}}|^2 V_{eff}(q,\nu) G^o_{n''}(\underline{k}-\underline{q},\omega_{n\underline{k}}-\nu) e^{-i\nu\delta} d^3\underline{q} d\nu \qquad (4.1)$$

is used for the evaluation of self energies at finite temperature but the Green's function and effective interaction V_{eff} now take their modified finite temperature form. The host band Bloch functions are assumed to be unaltered by the temperature changes and the squared overlap integrals $|I_{n\underline{q},n''\underline{k}-\underline{q}}|^2$ are accordingly unaltered and take the forms given in equation (2.40).

4.1.1. Finite Temperature Green's Function

The Green's function or free particle propagator given in equation (4.1) has been defined at zero temperature as:

$$G^{o}_{n''}(\underline{k}-\underline{q},\omega_{n\underline{k}}-\nu) = \frac{1}{\omega_{n\underline{k}}-\nu-\omega_{n''\underline{k}-\underline{q}}+i\delta\,\mathrm{sgn}(\hbar\omega_{n''\underline{k}-\underline{q}}-\hbar\omega_{f})} \qquad (4.2)$$

This is simply a reduced form of the full expression:

$$G^{o}_{n''}(\underline{k}-\underline{q},\omega_{n\underline{k}}-\nu) = \frac{\theta(\hbar\omega_{f}-\hbar\omega_{n''\underline{k}-\underline{q}})}{\omega_{n\underline{k}}-\nu-\omega_{n''\underline{k}-\underline{q}}-i\delta} + \frac{\theta(\hbar\omega_{n''\underline{k}-\underline{q}}-\hbar\omega_{f})}{\omega_{n\underline{k}}-\nu-\omega_{n''\underline{k}-\underline{q}}+i\delta} \qquad (4.3)$$

where the first term represents propagation of a hole below the Fermi surface and the second term propagation of an electron above it. The θ terms are unit step functions. At finite temperatures however the step function distribution is smeared out by the thermal motion of the carriers and the carrier distribution is then described by the Fermi-Dirac functions $f_{n''\underline{k}-\underline{q}}$. The finite temperature Green's function is then defined as

$$G^{o}_{n''}(\underline{k}-\underline{q},\omega_{n\underline{k}}-\nu) = \frac{f_{n''\underline{k}-\underline{q}}}{\omega_{n\underline{k}}-\nu-\omega_{n''\underline{k}-\underline{q}}-i\delta} + \frac{1-f_{n''\underline{k}-\underline{q}}}{\omega_{n\underline{k}}-\nu-\omega_{n''\underline{k}-\underline{q}}+i\delta} \qquad (4.4)$$

where $f_{n''\underline{k}-\underline{q}}$ is the electron occupancy factor for state $\underline{k}-\underline{q}$ in band n'' given by

$$f_{n''\underline{k}-\underline{q}} = \frac{1}{1+\exp[(\hbar\omega_{n''\underline{k}-\underline{q}}-E_{f})/kT]} \qquad (4.5)$$

(E_{f} is the appropriate Fermi energy) and $(1 - f_{n''\underline{k}-\underline{q}})$ is the corresponding hole occupation factor.

In p-type material the Fermi energy is several kT below the conduction band which is therefore unoccupied. Similarly in n-type material the Fermi energy is several kT above the valence band which is therefore fully occupied and $f_{n''\underline{k}-\underline{q}} = 1$.

4.1.2. Finite Temperature Inverse Dielectric Function

The limitations of the plasmon pole approximation to the carrier gas dielectric function for p-type material were discussed in section 2.6 where a comparison with a simplified Lindhard dielectric function was made. The results of this comparison indicated a fair agreement of the two models over the range of $\underline{q}$ of interest in the present work. The plasmon pole approximation at finite temperature could in prinicple be derived from the zeros of the full finite temperature Lindhard expression involving sub-band coupling and Fermi factors. However, the complexity of this procedure is removed by directly extending the zero temperature plasmon pole approximation to finite temperatures, on the basis of its good agreement with the Lindhard function at zero temperature. This extension is made by interpretation of the inverse dielectric function in terms of a Bose (plasmon) propagator and a coupling constant (for a full discussion see Lundqvist (1967)).

At zero temperature the effective interaction is defined as

$$V_{eff}(\underline{q},\nu) = \frac{V(\underline{q})}{\varepsilon(\underline{q},\nu)} = \frac{e^2}{\varepsilon_o \varepsilon_r \, q^2 \, \varepsilon(\underline{q},\nu)} \tag{4.6}$$

where from equation (2.49)

$$\frac{1}{\varepsilon(\underline{q},\nu)} = 1 + \frac{\omega_p^2}{\nu^2 - (\omega_1(\underline{q}) - i\delta)^2} \tag{4.7}$$

Now the zero temperature plasmon propagator $D(\underline{q},\nu)$ is defined as

$$D(\underline{q},\nu) = \frac{2\omega_1(\underline{q})}{\nu^2 - (\omega_1(\underline{q}) - i\delta)^2} \tag{4.8}$$

Relating expression (4.8) to (4.7) gives

$$\frac{1}{\varepsilon(\underline{q},\nu)} = 1 + \frac{\omega_p^2}{2\omega_1(\underline{q})} D(\underline{q},\nu) \tag{4.9}$$

or $$\frac{1}{\varepsilon(\underline{q},\nu)} = 1 + (\text{coupling constant}) \times (\text{Bose propagator}) \tag{4.10}$$

where:

$$\text{coupling constant} = \frac{\omega_p^2}{2\omega_1(\underline{q})} . \tag{4.11}$$

The finite temperature plasmon-pole approximation to the dielectric function can then be defined by a straightforward extension of equation (4.9) using the finite temperature Bose propagator defined as (Mahan 1981)

$$D(\underline{q},\nu) = 2\omega_1(\underline{q})\left[\frac{1+N_q}{\nu^2-(\omega_1(\underline{q})-i\delta)^2} - \frac{N_q}{\nu^2-(\omega_1(\underline{q})+i\delta)^2}\right] \tag{4.12}$$

where $\omega_1(\underline{q})$ is the finite temperature plasmon dispersion relation discussed in section 4.1.4 and N_q is the Bose-Einstein distribution function for plasmons defined by

$$N_q = \frac{1}{\exp[\hbar\omega_1(\underline{q})/kT]-1} \tag{4.13} .$$

The inverse dielectric function in the plasmon pole approximation is therefore given by

$$\frac{1}{\varepsilon(\underline{q},\nu)} = 1 + \omega_p^2\left[\frac{1+N_q}{\nu^2-(\omega_1(\underline{q})-i\delta)^2} - \frac{N_q}{\nu^2-(\omega_1(\underline{q})+i\delta)^2}\right] \tag{4.14} .$$

Substitution of equations (4.4) and (4.14) into (4.1) gives the expression for the finite temperature self energy of state $\underline{k}$ due to e - e interactions as

$$E_n^{\Sigma}(\underline{k}) = \frac{i}{(2\pi)^4}\int \sum_{n''} \left| I_{n\underline{k},\, n''\underline{k}-\underline{q}} \right|^2 \left[\frac{f_{n''\underline{k}-\underline{q}}}{\omega_{n\underline{k}} - \nu - \omega_{n''\underline{k}-\underline{q}} - i\delta} + \frac{1-f_{n''\underline{k}-\underline{q}}}{\omega_{n\underline{k}} - \nu - \omega_{n''\underline{k}-\underline{q}} + i\delta} \right] \frac{e^2}{\varepsilon_r \varepsilon_o q^2} \cdot$$

$$\left[1 + \omega_p^2 \left(\frac{1+N_{\underline{q}}}{\nu^2 - (\omega_1(\underline{q}) - i\delta)^2} - \frac{N_{\underline{q}}}{\nu^2 - (\omega_1(q) + i\delta)^2} \right) \right] e^{-i\delta\nu} d^3\underline{q}\, d\nu \qquad (4.15) \cdot$$

Expression (4.15) can be evaluated through substitution of the appropriate finite temperature forms of the T.F. screening wavevector, Fermi energy and plasmon dispersion relation derived in the next section.

4.1.3. Finite Temperature Thomas-Fermi Screening Wavevector and Fermi Energy

a) Fermi Energy

Using the same basic assumptions applied in the zero temeprature calculations, of isotropic, parabolic heavy and light hole valence bands degenerate at the Brillouin zone centre and ignoring the spin split off band, the Fermi energy E_{fv} for a hole gas in the valence band is given by

$$p = \frac{1}{2\pi^2}\left[\left(\frac{2m_H}{\hbar^2} \right)^{3/2} + \left(\frac{2m_L}{\hbar^2} \right)^{3/2} \right] \int_{-\infty}^{E_v} \frac{(E_v - E)^{1/2} dE}{1+\exp[(E_{fv} - E)/kT]} \qquad (4.16)$$

where E_v is the energy of the valence band edges. This expression reduces to

$$p = \frac{1}{2\pi^2} \left(\frac{2m_{Dv}}{\hbar^2} \right)^{3/2} (kT)^{3/2} \int_0^{\infty} \frac{E^{1/2} dE}{1+\exp(E+F)} \qquad (4.17)$$

where $F = \dfrac{E_{Fv} - E_v}{kT}$.

A similar expression is derived for the Fermi level E_{fe} due to an electron gas in the conduction band. The Fermi level for a given hole or electron concentration can then be found from the above expression using the NAG root finding routine CØ5ADF combined with the integral routine DØ1AJF.

The carrier concentration dependence of the Fermi level for p-type Si at T = 0 and 300 K is shown in figure 4.2. For low carrier concentrations the finite temperature Fermi level is found to be well into the band gap due to the large density of states near the band edge. At high carrier concentrations the hole gas becomes strongly degenerate and the Fermi energy approaches its zero temperature value. A similar behaviour is exhibited for the Fermi level in the p-type gallium compounds. For gallium compounds doped n-type the single valley conduction band and very light effective mass give a small density of states near the band edge and the Fermi level enters the conduction band for quite low carrier concentrations, ($n \approx 3 \times 10^{17}$ cm^{-3} in GaAs). However in silicon the six conduction band valleys and relatively heavy density of states effective mass produce a large density of states and the Fermi level only enters the conduction band for a dopant concentration $n \approx 2.5 \times 10^{19}$ cm^{-3}.

b) T.F. Screening Wavevector

The definition of the T.F. wavevector for holes in the valence band was given in equation (3.50) as

$$K^2 = \frac{e^2}{\varepsilon_o \varepsilon_r} \sum_i \int \rho_i(E) \left(\frac{-\partial f(E)}{\partial E} \right) dE \qquad (4.18)$$

where the sum i is over all occupied valence bands. On substitution of the differentiated Fermi factor this above expression reduces to

$$K^2 = \frac{e^2}{\epsilon_o \epsilon_r} \frac{1}{2\pi^2}\left(\frac{2m_{Dv}}{\hbar^2}\right)^{3/2} (kT)^{1/2} \int_0^\infty \frac{E^{1/2}\exp(F+E)dE}{[1+\exp(F+E)]^2} \qquad (4.19)$$

A similar expression exists for the electron gas.

The above expression can again be evaluated using the NAG integral routine DϕlAJF. As either $T \rightarrow 0K$ or the carrier concentration increases and the hole gas becomes more degenerate the value of the finite temperature K tends towards the zero temperature value. This is clearly seen in figure 4.1 which illustrates the hole concentration dependence of $\lambda(=1/K)$ for p-type Si at T = 0 and 300 K.

4.1.4. Finite Temperature Plasmon Dispersion Relation

The finite temperature plasmon dispersion relation can be defined in a manner similar to the zero temperature relationship (2.53) i.e.

$$\omega_l^2(q) = \omega_p^2\left(1 + \frac{q^2}{K^2}\right) + \omega_{nq}^2 \qquad (4.20)$$

where K now takes its finite temperature form. If we now define a normalising parameter k_{fT} by

$$\frac{1}{k_{fT}^2} = \frac{1}{(3\pi^2 p)}\left(\frac{2m_{Dv}}{\hbar^2}\right)^{1/2} (kT)^{1/2} \int_0^\infty \frac{E^{1/2}\exp(F+E)dE}{[1+\exp(F+E)]^2} \qquad (4.21)$$

so that

$$K^2 k_{fT}^2 = \frac{\omega_p^2 3 m_{ov} m_{Dv}}{\hbar^2} \qquad (4.22)$$

then equation (4.20) gives

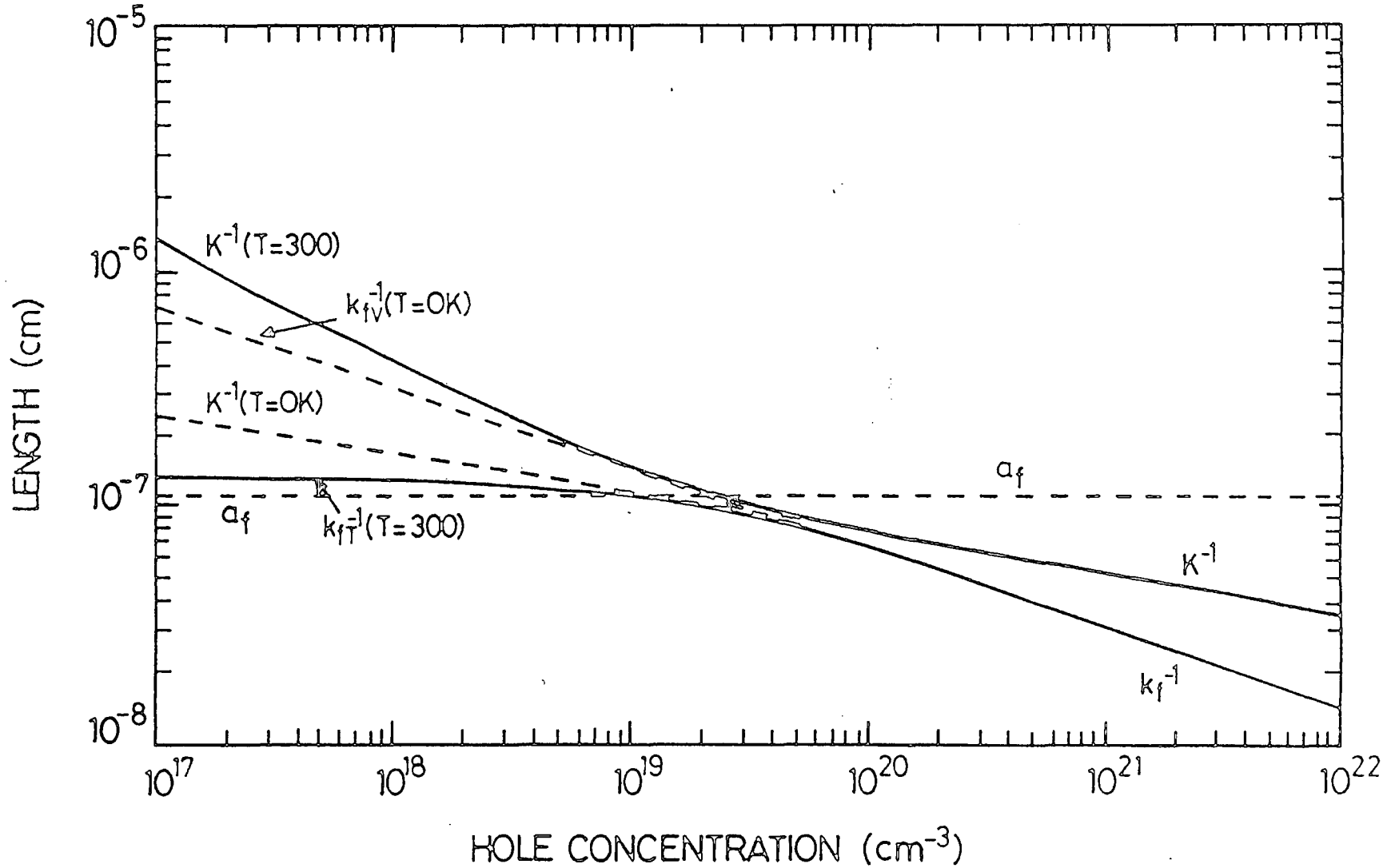

Figure 4.1: The hole concentration dependence of the Thomas-Fermi screening length K^{-1}, effective Bohr radius a_f and normalisation term k_{fT}^{-1} for p-type Si at T = 300 K.

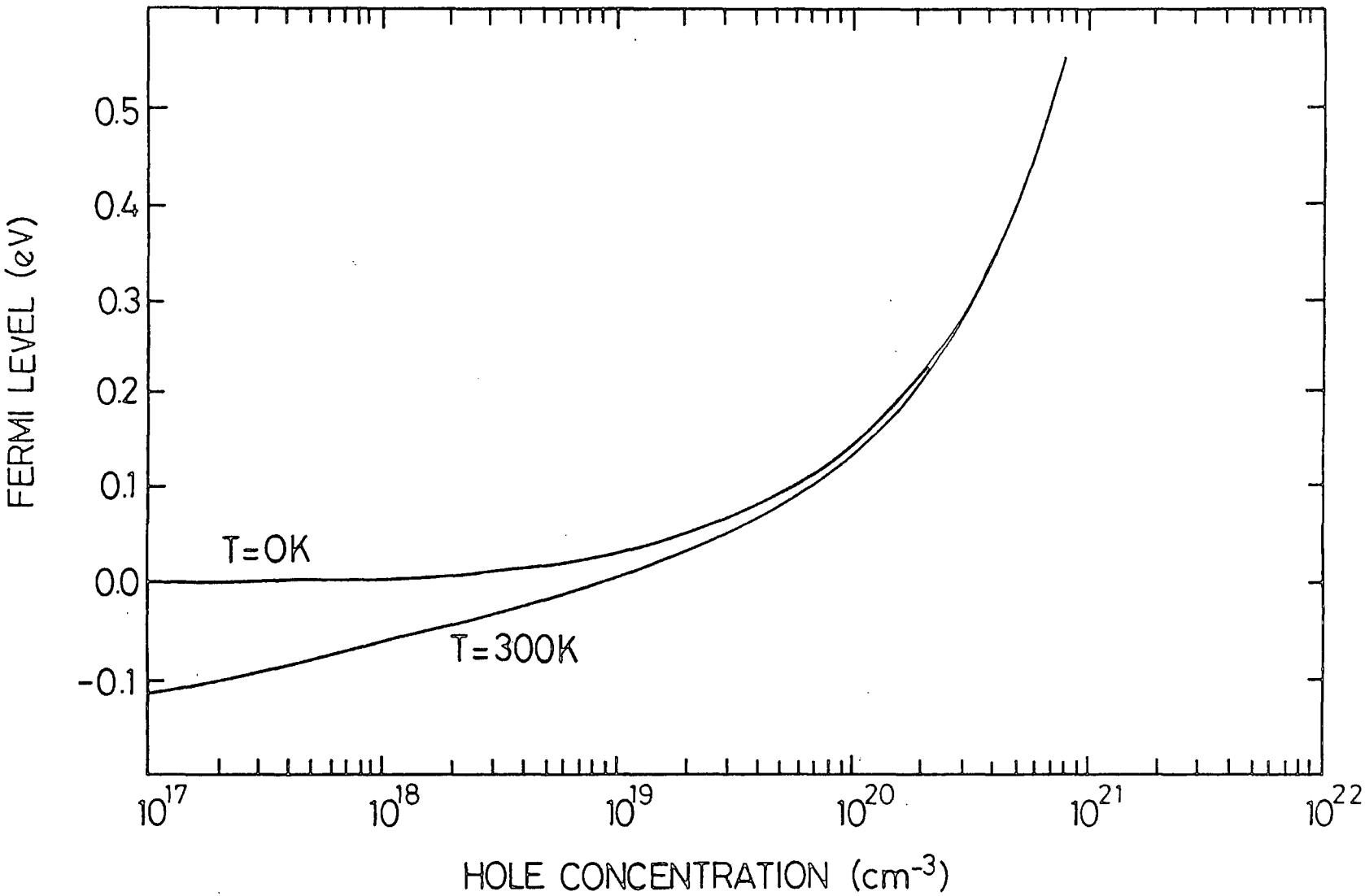

Figure 4.2: The hole concentration dependence of the Fermi level in p-type Si at T = OK and 300 K.

$$\omega_l^2(q) = \omega_p^2\left[1 + \frac{q^2}{K^2} + \frac{3m_{ov}}{4m_{Dv}}\frac{q^4}{K^2 k_{fT}^2}\right] \qquad (4.23)\ .$$

The above form of the plasmon dispersion relation is used in the subsequent derivatives of the band edge shifts and makes comparision with the zero temperature model more straightforward. The carrier concentration dependence of the inverse normalising parameter k_{fT}^{-1} is given in figure 4.1 where it is seen to tend to the zero temperature value k_{fV}^{-1} at higher concentrations.

Having derived expressions for all the terms relevant to the self energy expression (4.15) this can now be evaluated by division into the screened exchange and Coulomb hole terms through contour integration.

4.2. Derivation of the Generalised Screened Exchange and Coulomb Hole Terms

The expressions for the self energy of state $\underline{k}$ in band n and the various finite temperature parameters have been defined in the previous sections. To determine the band edge shifts due to the introduction of the carrier gas into the host band, the difference in the real part of the self energy between doped and intrinsic material must be evaluated.

We first evaluate the self energy for the doped material by separating expression (4.15) into two terms as

$$E_n^{\Sigma d}(\underline{k}) = E_{n1}^{\Sigma d}(\underline{k}) + E_{n2}^{\Sigma d}(\underline{k}) \qquad (4.24)$$

where

$$E_{n1}^{\Sigma d}(\underline{k}) = \frac{i}{(2\pi)^4}\frac{e^2}{\varepsilon_o \varepsilon_r}\sum_{n''}\int_{\substack{\text{all } n'' \\ \text{and } -\underline{q}}} \left|I_{n\underline{k},n''\underline{k}-\underline{q}}\right|^2 \frac{e^{-i\delta\nu}}{q^2}\cdot$$

$$\left[\frac{f_{n''\underline{k}-\underline{q}}}{\omega_{n\underline{k}}-\nu-\omega_{n''\underline{k}-\underline{q}}-i\delta} + \frac{1-f_{n''\underline{k}-\underline{q}}}{\omega_{n\underline{k}}-\nu-\omega_{n''\underline{k}-\underline{q}}+i\delta}\right] d^3\underline{q}\, d\nu \qquad (4.25)$$

and

$$E_{n2}^{\Sigma d}(\underline{k}) = \frac{i}{(2\pi)^4}\frac{e^2}{\varepsilon_o\varepsilon_r}\sum_{n''}\int_{\substack{\text{all } n''\\ \text{and } -\underline{q}}}\left|I_{n\underline{k},n''\underline{k}-\underline{q}}\right|^2\frac{\omega_p^2}{q^2}e^{-i\delta\nu}\cdot$$

$$\left[\frac{f_{n''\underline{k}-\underline{q}}}{\omega_{n\underline{k}}-\nu-\omega_{n''\underline{k}-\underline{q}}-i\delta}+\frac{1-f_{n''\underline{k}-\underline{q}}}{\omega_{n\underline{k}}-\nu-\omega_{n''\underline{k}-\underline{q}}+i\delta}\right]\cdot$$

$$\left[\frac{1+N_{\underline{q}}}{\nu^2-(\omega_1(\underline{q})-i\delta)^2}-\frac{N_{\underline{q}}}{\nu^2-(\omega_1(\underline{q})+i\delta)^2}\right]d^2\underline{q}\,d\nu \qquad (4.26)\ .$$

The frequency integrals in equations (4.25) and (4.26) can now be performed by contour integration completing the contour in the lower half of the complex ν plane as required by the causality factor $e^{-i\delta\nu}$.

In expression (4.25) only the pole in the Green's function at $\nu = \omega_{n\underline{k}} - \omega_{n''\underline{k}-\underline{q}} - i\delta$ contributes to the integral giving

$$E_{n1}^{\Sigma d}(\underline{k}) = \frac{-e^2}{8\pi^3\varepsilon_o\varepsilon_r}\sum_{n''}\int_{\substack{\text{all } n''\\ \text{and } -\underline{q}}}\left|I_{n\underline{k},n''\underline{k}-\underline{q}}\right|^2\frac{f_{n''\underline{k}-\underline{q}}}{q^2}\,d^3\underline{q} \qquad (4.27)\ .$$

The same Green's function pole also provides a contribution to the contour integration of equation (4.26) as

$$E_{n2}^{\Sigma d}(\underline{k})\ \text{(Green's function pole)} = \frac{-e^2}{8\pi^3\varepsilon_o\varepsilon_r}\omega_p^2\sum_{n''}\int_{\substack{\text{all } n''\\ \text{and } -\underline{q}}}\left|I_{n\underline{k},n''\underline{k}-\underline{q}}\right|^2\frac{f_{n''\underline{k}-\underline{q}}}{q^2}$$

$$\left[\frac{1+N_{\underline{q}}}{(\omega_{n\underline{k}}-\omega_{n''\underline{k}-\underline{q}}-i\delta)^2-(\omega_1(\underline{q})-i\delta)^2}-\frac{N_{\underline{q}}}{(\omega_{n\underline{k}}-\omega_{n''\underline{k}-\underline{q}}-i\delta)^2-(\omega_1(\underline{q})+i\delta)^2}\right]d^3\underline{q} \qquad (4.28)\ .$$

Combining equations (4.28) and (4.27) as contributions from poles in the Green's function gives the screened exchange term defined in terms of equations (4.6) and (4.14) as

$$E_n^{\Sigma dSX}(\underline{k}) = -\frac{1}{8\pi^3}\sum_{n''}\int_{\substack{\text{all } n'' \\ \text{and } -q}} \left|I_{n\underline{k},n''\underline{k}-\underline{q}}\right|^2 f_{n''\underline{k}-\underline{q}}\, V_{eff}(\underline{q},\omega_{n\underline{k}}-\omega_{n''\underline{k}-\underline{q}}-i\delta)\,d^3\underline{q} \quad (4.29)\ .$$

This expression differs from the zero temperature SX term in that the wavevector integral is now over all states defined by $-\underline{q}$ and n'', and is limited for carrier occupancy by the Fermi distribution function.

Of the poles in the effective interaction of equation (4.26) only the poles at

$$\nu = \omega_l(\underline{q}) - i\delta \qquad \text{and} \qquad \nu = -\omega_l(\underline{q}) - i\delta$$

contribute to the contour integration. Performing this integral and expressing the result in terms of equation (4.4) for the Green's function gives the Coulomb hole term:

$$E_n^{\Sigma dCH}(\underline{k}) = \frac{e^2}{8\pi^3\varepsilon_o\varepsilon_r}\sum_{n''}\int_{\substack{\text{all } n'' \\ \text{and } -\underline{q}}} \left|I_{n\underline{k},n''\underline{k}-\underline{q}}\right|^2 \frac{\omega_p^2}{2\omega_l(\underline{q})q^2}$$

$$\left[(1+N_q)G^o_{n''}(\underline{k}-\underline{q},\omega_{n\underline{k}}-\omega_l(\underline{q})) + N_q G^o_{n''}(\underline{k}-\underline{q},\omega_{n\underline{k}}+\omega_l(\underline{q}))\right]d^3\underline{q} \quad (4.30)\ .$$

The self energy for state $\underline{k}$ in band n in the intrinsic material takes the same form as equation (4.27) which is the unscreened Hartree-Fock exchange energy between an electron in state $\underline{k}$ in band n and the electrons in the full valence band of the intrinsic material:

$$E_n^{\Sigma i}(\underline{k}) = \frac{-e^2}{8\pi^3\varepsilon_o\varepsilon_r}\sum_{n''}\int_{\text{all } n'',-\underline{q}} \left|I_{n\underline{k},n''\underline{k}-\underline{q}}\right|^2 \frac{f_{n''\ \underline{k}-\underline{q}}}{q^2}\,d^3\underline{q} \quad (4.31)\ .$$

As the Fermi factor $f_{n''\underline{k}-\underline{q}}$ equals unity for the fully occupied valence band (ignoring the small number of electrons thermally excited to the conduction band) this expression is the same as the zero temperature equation (3.7).

4.3. Band Edge Shifts in p-type Material

4.3.1. Introduction

The basic concepts used in deriving the band gap narrowing at finite temperature are the same as those discussed for T = OK. The hole gas introduced into the semiconductor valence band screens the exchange interaction of the test electron at the band edge with the remaining electrons in the valence band. Both the screening of the carrier gas and the removal of electrons from the valence band states then contribute to the change in self energy of the band edge test electron. The self energy of state $\underline{k}$ in the valence band of the intrinsic material is simply the Hartree-Fock exchange energy, which must be subtracted from the screened exchange energy of the doped material. A shift in the conduction band edge is again produced by the correlation of the hole gas in response to the test electron.

4.3.2. Conduction Band Shift

The intrinsic semiconductor at T = OK has no occupied states in the conduction band and this situation prevails on doping the material p-type. The Fermi factors in the real parts of equations (4.29) and (4.31) are therefore zero for the conduction band states. As the squared overlap integral between states in the conduction band and the valence band is also taken as zero (the sums in expressions (4.29) and (4.31) thus reducing to n" ≡ conduction band), the change in screened exchange energy for the conduction band is zero, i.e.

$$\Delta E_C^{\Sigma SX}(\underline{k}_o) = 0 \qquad (4.32)$$

where $\underline{k}_o$ again represents the wavevector of a conduction band minimum.

However, the response of the hole gas in the doped material to the presence of a test electron affects the band edge energy through the

the Coulomb hole (CH) term. In the intrinsic material the Coulomb term is zero. The change in self energy of the conduction band edge is then given by the real part (the Cauchy principal part) of equation (4.30) as:

$$\Delta E_C^{\Sigma CH}(\underline{k}_o) = \frac{e^2}{8\pi^3 \varepsilon_o \varepsilon_r} \sum_{n''} \int_{\substack{\text{all } n'' \\ \text{and } -\underline{q}}} \left| I_{c\underline{k}_o, n''\underline{k}_o - \underline{q}} \right|^2 \frac{\omega_p^2}{2\omega_l(\underline{q}) q^2}$$

$$\left[\frac{1+N_{\underline{q}}}{\omega_{c\underline{k}_o} - \omega_l(\underline{q}) - \omega_{n''\underline{k}_o - \underline{q}}} + \frac{N_{\underline{q}}}{\omega_{c\underline{k}_o} + \omega_l(\underline{q}) - \omega_{n''\underline{k}_o - \underline{q}}} \right] d^3\underline{q} \qquad (4.33) .$$

Using expression (2.40) for the conduction band overlap integrals (which is unity for states in the same conduction band minima and zero otherwise) and performing the angular part of the polar co-ordinate wavevector integral (equation 3.38) this expression reduces to

$$\Delta E_C^{\Sigma CH}(\underline{k}_o) = \frac{e^2}{4\pi^2 \varepsilon_o \varepsilon_r} \int_0^\infty \frac{\omega_p^2}{\omega_l(q)} \left[\frac{2\omega_{cq} N_q}{\omega_l^2(q) - \omega_{cq}^2} - \frac{1}{\omega_l(\underline{q}) + \omega_{cq}} \right] dq \qquad (4.34)$$

where the substitution

$$\omega_{c\underline{k}_o} - \omega_{c\underline{k}_o - \underline{q}} = -\omega_{c\underline{q}} = -\frac{\hbar q^2}{2m_{De}} \qquad (4.35)$$

has been made.

The second term in the square brackets gives an integral expression ($\Delta E_C^{\Sigma CH2}$) identical to the zero temperature CH term (3.42) but the finite temperature parameters for $\omega_l(\underline{q})$ apply in the present case. This term is therefore evaluated in a similar manner to equation (3.42) using the NAG integral routine Dϕ1 APF.

The first term in the square brackets provides an integral not previously encountered which on substitution of the various parameters takes the form

$$\Delta E_C^{\Sigma CH1}(\underline{k}_o) = \frac{e^2K^2}{k_{fT}^2 2\pi \varepsilon_o \varepsilon_r} \beta^{1/2} \frac{m_{Dv}}{m_{De}} \cdot$$

$$\int_0^\infty \frac{x^2 \, dx}{(k'^2+x^2+\beta x^4)^{1/2}(k'^2+x^2+\alpha_e x^4)\left[\exp\left[\frac{\hbar\omega_p}{k'kT}(k'^2+x^2+\beta x^4)^{1/2}\right]-1\right]} \qquad (4.36)$$

where

$$k' = \frac{K}{k_{fT}} \qquad x = \frac{q}{k_{fT}} \qquad \beta = \frac{3}{4}\frac{m_{Dv}}{m_{Dv}} \qquad \text{and} \qquad \alpha_e = \beta\left(1 - \frac{m_{Dv}^2}{m_{De}^2}\right) .$$

This expression contains a singularity where the plasmon energy $\hbar\omega_1$ equals the conduction band energy ω_{cq} and is therefore evaluated using the NAG Cauchy principal part routine Dϕ1 AQF. The energy values obtained from this expression are very small (< 0.5 mev) for the range of concentrations above the Mott critical density and its contribution to the band edge shift at high carrier concentrations can be ignored without significant loss of accuracy.

The carrier concentration dependence of the terms $\Delta E_C^{\Sigma CH1}$ and $\Delta E_C^{\Sigma CH2}$ for p-type Si at T = 300 K is shown in figure 4.3 and compared with the zero temperature conduction band CH term. In general the CH contribution lowers the band edge but at finite temperatures the hole occupancy in the region around the test charge is reduced by thermal excitation and the resulting energy shift is smaller than that obtained at zero temperature. However, at high acceptor concentrations the carrier distribution and therefore the correlation of the hole gas is little different from that at zero temperature and the CH contributions are approximately equal.

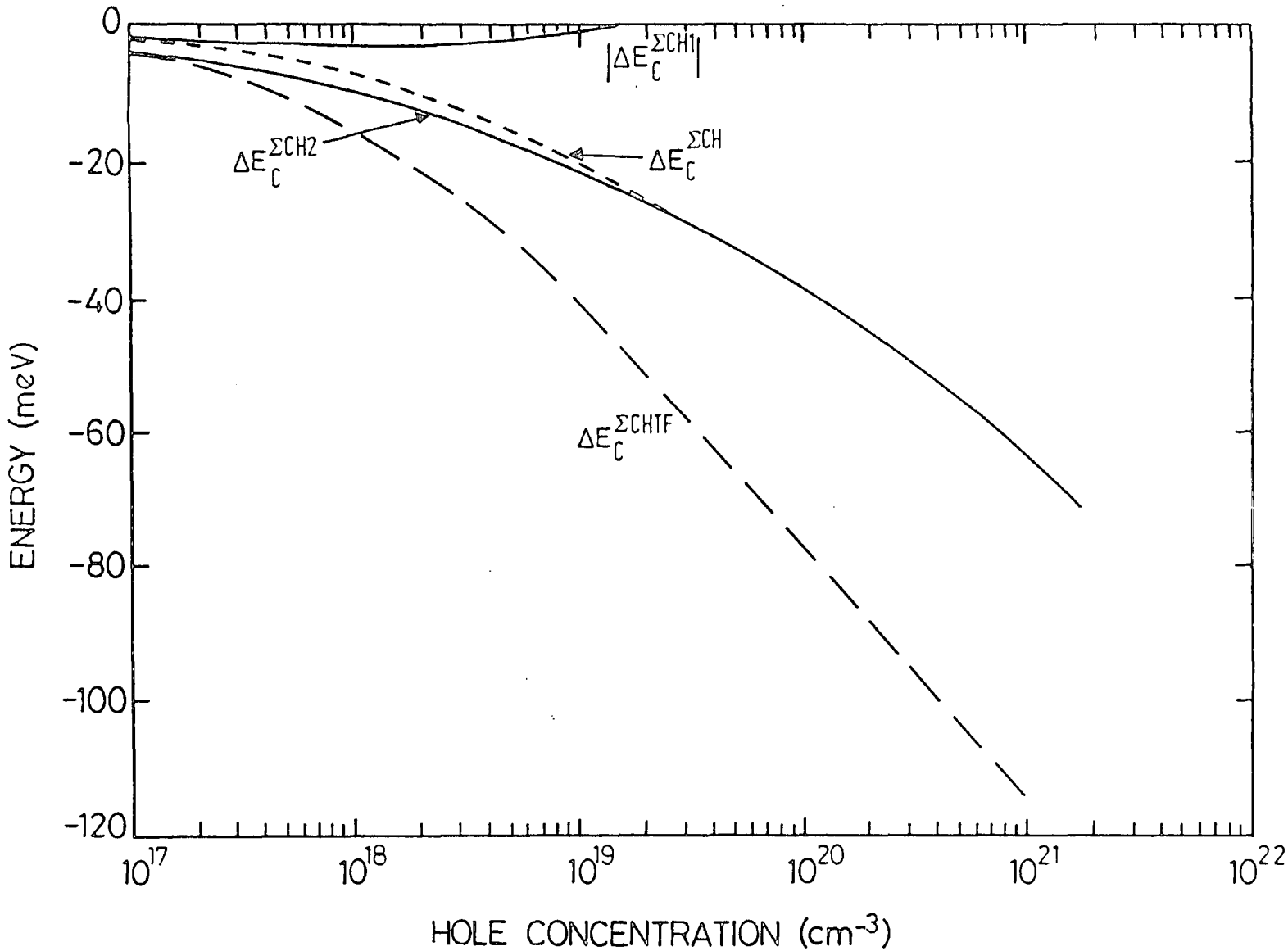

Figure 4.3: The hole concentration dependence of the energy shift in the conduction band edge of p-type Si due to the Coulomb-hole terms at T = 300 K. The conduction band edge shift derived in the Thomas-Fermi approximation $\Delta E_C^{\Sigma CHTF}$ is also shown.

4.3.3. Conduction Band Shift using the Thomas-Fermi Approximation for the Dielectric Function.

If the frequency independent, small wavevector T.F. approximation to the carrier screening is used in place of the plasmon pole dielectric function the conduction band CH term (4.33) reduces to

$$\Delta E_C^{\Sigma CHTF}(\underline{k}_o) = \frac{-e^2}{4\pi^2\varepsilon_o\varepsilon_r}\int_0^\infty \frac{\omega_p^2}{\omega_1^2(q)}\,dq \qquad (4.37)$$

where $\omega_1^2(q) = \omega_p^2\left(1 + \frac{q^2}{K^2}\right)$

giving

$$\Delta E_C^{\Sigma CHTF}(\underline{k}_o) = \frac{-e^2K}{8\pi\varepsilon_r\varepsilon_o} \qquad (4.38)$$

which is the same expression as derived for the zero temperature model with K replaced by its finite temperature value. The carrier concentration dependence of this term is given in figure 4.3 where at high carrier concentrations it is seen to overestimate the carrier screening effects and give much larger shifts than the plasmon pole approximation. At low concentrations, however, the screening is reduced substantially, this is quite marked in the T.F. approximation with its strong dependence on K. The resulting reduction in the T.F. CH term with increasing temperature then produces a more realistic approximation to the conduction band shift at low dopant concentrations.

4.3.4. Valence Band Shift - Introduction

The valence band shift is again derived by evaluating the difference between the real parts of the self energy for the screened interaction of the band edge test electron with the valence band occupied states and the unscreened interaction of the test electron with the full valence band, i.e.

$$\Delta E^{\Sigma}_{HH}(\underline{O}) = \left(\mathrm{Re}[E^{\Sigma CH}_{HH}(\underline{O})] + \mathrm{Re}[E^{\Sigma SX}_{HH}(\underline{O})]\right)\Big|_{\text{doped}} - \mathrm{Re}[E^{\Sigma I}_{HH}(\underline{O})]\Big|_{\text{intrinsic}} \qquad (4.39)$$

The above expression refers to the shift of the heavy hole band edge, the corresponding shift in the light hole band can be found by interchanging the relevant subscripts in the following expressions and is seen to be the same as the HH shift.

4.3.5. Derivation of the Valence Band CH Term

The CH term for the intrinsic material is zero so the only contribution comes from the CH shift in the doped material given by equation (4.30)

$$\Delta E^{\Sigma CH}_{HH}(\underline{O}) = \frac{e^2}{8\pi^3\varepsilon_o\varepsilon_r}\sum_{n''}\int_{\substack{\text{all } n''\\ \text{and } -q}} \frac{\omega_p^2}{2\omega_l(\underline{q})q^2}\left|I_{HH\underline{O},n''-\underline{q}}\right|^2\left[\frac{1+N_q}{\omega_{HH\underline{O}}-\omega_l(\underline{q})-\omega_{n''-\underline{q}}}\right.$$

$$\left. + \frac{N_q}{\omega_{HH\underline{O}}+\omega_l(\underline{q})-\omega_{n''-\underline{q}}}\right] d^3\underline{q} \qquad (4.40)$$

Substitution of the squared overlap integrals (2.40) and performing the resulting integral for the angular parts of the spherical polar wavevector term gives

$$E^{\Sigma CH}_{HH} = \frac{e^2}{4\pi^2\varepsilon_o\varepsilon_r}\sum_{n''}\int_0^{\infty}\frac{\omega_p^2}{2\omega_l(q)}\left[\frac{1+N_q}{\omega_{n''-\underline{q}}-\omega_l(q)} + \frac{N_q}{\omega_l(q)+\omega_{n''-\underline{q}}}\right]dq \qquad (4.41)$$

where the sum is now over $n'' \equiv$ HH or LH and the substitution

$$\omega_{HH\underline{O}} - \omega_{n''-\underline{q}} = \omega_{n''\underline{q}} = \frac{\hbar q^2}{2m_{n''}} \qquad (4.42)$$

has been made. In addition explicit mention of the wavevector $\underline{k} = \underline{O}$ has been dropped from $E^{\Sigma CH}_{HH}$.

The poles occurring in the integeral of the first term in square brackets, where the plasmon energy $\hbar\omega_1$ equals the band energy $\hbar\omega_{n''\underline{q}}$, make this integral difficult to evaluate. To overcome this problem the CH term is added to the SX term for the full valence band producing an easily evaluated integral. The value of the CH term can then be derived by subtracting the SX term which is also relatively easy to evaluate.

4.3.6. Derivation of Valence Band Screened Exchange Terms

The change in the heavy hole band SX term is given by

$$\Delta E_{HH}^{\Sigma SX} = E_{HH}^{\Sigma SX}\Big|_{doped} - E_{HH}^{\Sigma I} \tag{4.43}$$

where the real parts of the above terms are assumed. From expressions (4.29) and (4.31)

$$\Delta E_{HH}^{\Sigma SX} = \frac{-e^2}{8\pi^3\varepsilon_o\varepsilon_r}\sum_{n''}\int_{\substack{\text{all } n'' \\ \text{and } -\underline{q}}} \left|I_{HH\underline{0},n''-\underline{q}}\right|^2 \frac{f_{n''-\underline{q}}}{q^2}\cdot$$

$$\left[1 + \omega_p^2\left[\frac{1+N_{\underline{q}}}{((\omega_{HH\underline{0}}-\omega_{n''-\underline{q}})^2-\omega_1^2(q))} - \frac{N_{\underline{q}}}{((\omega_{HH\underline{0}}-\omega_{n''-\underline{q}})^2-\omega_1^2(q))}\right]\right] d^3\underline{q}$$

$$+ \frac{e^2}{8\pi^3\varepsilon_o\varepsilon_r}\sum_{n''}\int_{\substack{n'' \text{ and } -\underline{q} \\ \in \text{valence band}}} \left|I_{HH\underline{0},n''-\underline{q}}\right|^2 \frac{f^{int}_{n''-\underline{q}}}{q^2}\, d^3\underline{q} \tag{4.44}.$$

Substitution of the appropriate expressions for the overlap integrals (equations (2.40)) and performing the integral over the angular parts of the polar coordinate gives

$$\Delta E_{HH}^{\Sigma SX} = \frac{-e^2}{4\pi^2 \varepsilon_o \varepsilon_r} \sum_{n''} \int_0^{\infty} f_{n''-\underline{q}} \left[1 + \frac{\omega_p^2}{(\omega_{HH\underline{O}} - \omega_{n''-\underline{q}})^2 - \omega_1^2(q)} \right] dq$$

$$+ \frac{e^2}{4\pi^2 \varepsilon_o \varepsilon_r} \sum_{n''} \int_0^{\infty} f_{n''-\underline{q}}^{int} \, dq \qquad (4.45)$$

where $n'' \equiv HH$ or LH.

For the intrinsic material the electron occupation factor of the full valence band is unity. In the extrinsic material this occupation probability $f_{n''\underline{k}-\underline{q}} = 1 - f'_{n''\underline{k}-\underline{q}}$ where $f'_{n''\underline{k}-\underline{q}}$ is the hole occupation probability. Use of expression (4.42) for the energy eigenvalue difference in equation (4.45) gives

$$\Delta E_{HH}^{\Sigma SX} = \frac{-e^2}{4\pi^2 \varepsilon_o \varepsilon_r} \sum_{n''} \int_0^{\infty} \frac{\omega_p^2}{\omega_{n''q}^2 - \omega_1^2(q)} \, dq$$

$$+ \frac{e^2}{4\pi^2 \varepsilon_o \varepsilon_r} \sum_{n''} \int_0^{\infty} f'_{n''\underline{k}-\underline{q}} \left[1 + \frac{\omega_p^2}{\omega_{n''q}^2 - \omega_1^2(q)} \right] dq \qquad (4.46) .$$

That is $\Delta E_{HH}^{\Sigma SX} = \Delta E_{HH}^{\Sigma SXA} + \Delta E_{HH}^{\Sigma SXU}$ (4.47) .

The second term in this expression is equivalent to the zero temperature result (equation (3.28)). However, the integration is now over all states but limited by the Fermi occupation probability factor. The first term in equations (4.46) or (4.47) is equivalent to expression (3.17) for the difference in the exchange energies of the screened and unscreened interactions in the full valence band ($\Delta E_{HH}^{\Sigma SXA}$). For the reasons explained at the end of section 4.3.5 this term is added to the valence band CH term (4.41) to give

$$\Delta E_{HH}^{\Sigma SXA+CH} = \frac{e^2}{4\pi^2\varepsilon_o\varepsilon_r} \Sigma_{n''} \int \frac{\omega_p^2}{2\omega_1(q)} \left[\frac{2N_q\, \omega_{n''q}}{\omega_{n''q}^2 - \omega_1^2(q)} + \frac{1}{\omega_{n''q} + \omega_1(q)} \right] dq \qquad (4.48) .$$

The first term is equivalent to the conduction band term $\Delta E_C^{\Sigma CH1}$ and is evaluated in a similar manner. The contribution from this term is again found to be negligibly small at high carrier concentrations.

Similarly the second term is equivalent to the second conduction band CH term $\Delta E_C^{\Sigma CH2}$ and is therefore evaluated in the same way. The carrier concentration dependence of $\Delta E_{HH}^{\Sigma SXA+CH}$ for p-type Si at room temperature is given in figure 4.5 together with the individual contributions $\Delta E_{HH}^{\Sigma SXA}$ and $\Delta E_{HH}^{\Sigma CH}$ evaluated as described below.

4.3.7. Evaluation of $\Delta E_{HH}^{\Sigma SXA}$ and $\Delta E_{HH}^{\Sigma CH}$ Terms

Substitution of the plasmon dispersion relation (4.23) into the first term in equation (4.46),

$$\Delta E_{HH}^{\Sigma SXA} = \frac{-e^2}{4\pi^2\varepsilon_o\varepsilon_r} \Sigma_{n''} \int_0^\infty \frac{\omega_p^2}{\omega_{n''q}^2 - \omega_1^2(q)} dq , \qquad (4.49)$$

gives the expression

$$\Delta E_{HH}^{\Sigma SXA} = \frac{e^2K^2}{k_{fT}4\pi^2\varepsilon_o\varepsilon_r} \Sigma_{n''} \int_0^\infty \frac{dx}{k'^2 + x^2 + \alpha_{n''}x^4} \qquad (4.50)$$

where $x = \frac{q}{k_{fT}}$ $\quad k' = \frac{K}{k_{fT}}$ and $\alpha_{n''} = \frac{3m_{ov}}{4m_{Dv}} \left(1 - \frac{m_{Dv}^2}{m_{n''}^2} \right)$.

Solving this integral analytically using Gradshteyn and Ryshik (1980) formula numbers 2.161, 2.141/2 and 2.143/2 gives

$$\Delta E_{HH}^{\Sigma SXA} = \frac{e^2K^2}{k_{fT}4\pi^2\varepsilon_o\varepsilon_r} \sum_{n''} \frac{\pi\sqrt{-2\alpha_{n''}}}{2(1-4\alpha_{n''}k'^2)^{1/2}[(1-4\alpha_{n''}k'^2)^{1/2}-1]^{1/2}} \qquad (4.51) .$$

This SX term provides an upward shift of the heavy hole band edge while the valence band CH term gives a smaller opposite contribution which is evaluated through the equation

$$\Delta E_{HH}^{\Sigma CH} = \Delta E_{HH}^{\Sigma SXA+CH} - \Delta E_{HH}^{\Sigma SXA} \qquad (4.52) .$$

The hole concentration dependence of both CH and SXA terms for room temperature p-type Si is given in Figure 4.5. The valence band CH term is additionally compared with the corresponding zero temperature CH term and the finite temperature conduction band CH term in figure 4.4. For reasons already discussed in section 4.3.2 the finite temperature valence band CH term gives a lower energy shift than the zero temperature term but at high hole concentrations the shifts are approximately equal.

The only term still to be evaluated is that due to the SX interaction of the test electron with those electrons removed from the valence band by the hole gas occupation. This term is evaluated below.

4.3.8. Evaluation of $\Delta E_{HH}^{\Sigma SXU}$ and ΔE_{HH}^{Σ} Terms

From equation (4.46) and (4.47)

$$\Delta E_{HH}^{\Sigma SXU} = \frac{e^2}{4\pi^2\varepsilon_o\varepsilon_r} \sum_{n''} \int_0^{\infty} f'_{n''-\underline{q}} \left[1 + \frac{\omega_p^2}{\omega_{n''q}^2 - \omega_1^2(q)}\right] dq \qquad (4.53)$$

which separates into $\Delta E_{HH}^{\Sigma SXU} = \Delta E_{HH}^{\Sigma SXU1} + \Delta E_{HH}^{\Sigma SXU2}$ where

$$\Delta E_{HH}^{\Sigma SXU1} = \frac{e^2}{4\pi^2\varepsilon_o\varepsilon_r} \sum_{n''} \int_0^{\infty} f'_{n''-\underline{q}}\, dq = \frac{e^2}{4\pi^2\varepsilon_o\varepsilon_r} \sum_{n''} \int_0^{\infty} \frac{dq}{1+\exp\left[\left(\frac{\hbar q^2}{2m_{n''}} + E_{fv}\right)/kT\right]} \qquad (4.54)$$

and

$$\Delta E_{HH}^{\Sigma SXU2} = \frac{e^2}{4\pi^2 \varepsilon_o \varepsilon_r} \sum_{n''} \int_0^{\infty} \frac{\omega_p^2 f'_{n''-\underline{q}} \, dq}{(\omega_{n''\underline{q}}^2 - \omega_1^2(q))} \qquad (4.55) .$$

The term $\Delta E_{HH}^{\Sigma SXU1}$ resembles the first term of expression (3.28) for the integration over the states occupied by holes in the zero temperature extrinsic material. This integration is straightforward and was carried out using the NAG quadrature routine Dϕ1 AHF. The second term $\Delta E_{HH}^{\Sigma SXU2}$, however, contains a pole where the plasmon energy $\hbar\omega_1$ equals the band energy $\hbar\omega_{n''\underline{q}}$. Unlike the equivalent zero temperature term in which normally only the pole due to the light hole band falls within the integration range, the poles from both HH and LH bands are encountered in the infinite range integral of the present calculation. The integral for both HH and LH bands is therefore performed using the Cauchy principal part NAG routine Dϕ1 AQF. The carrier concentration dependence of the $\Delta E_{HH}^{\Sigma SXU}$ term for room temperature p-type Si is shown in figure 4.5. As with the zero temperature calculation this term provides only a small addition to the upward shift of the valence band edge, and once again this energy shift approaches that found at zero temperature and high carrier concentrations.

The resulting total upward shift of the valence band edge is given by

$$\Delta E_{HH}^{\Sigma} = \Delta E_{HH}^{\Sigma SXA+CH} + \Delta E_{HH}^{\Sigma SXU} \qquad (4.56)$$

and is also shown in figure 4.5.

For comparison the valence band edge shift derived in the T.F. approximation is evaluated in the next section.

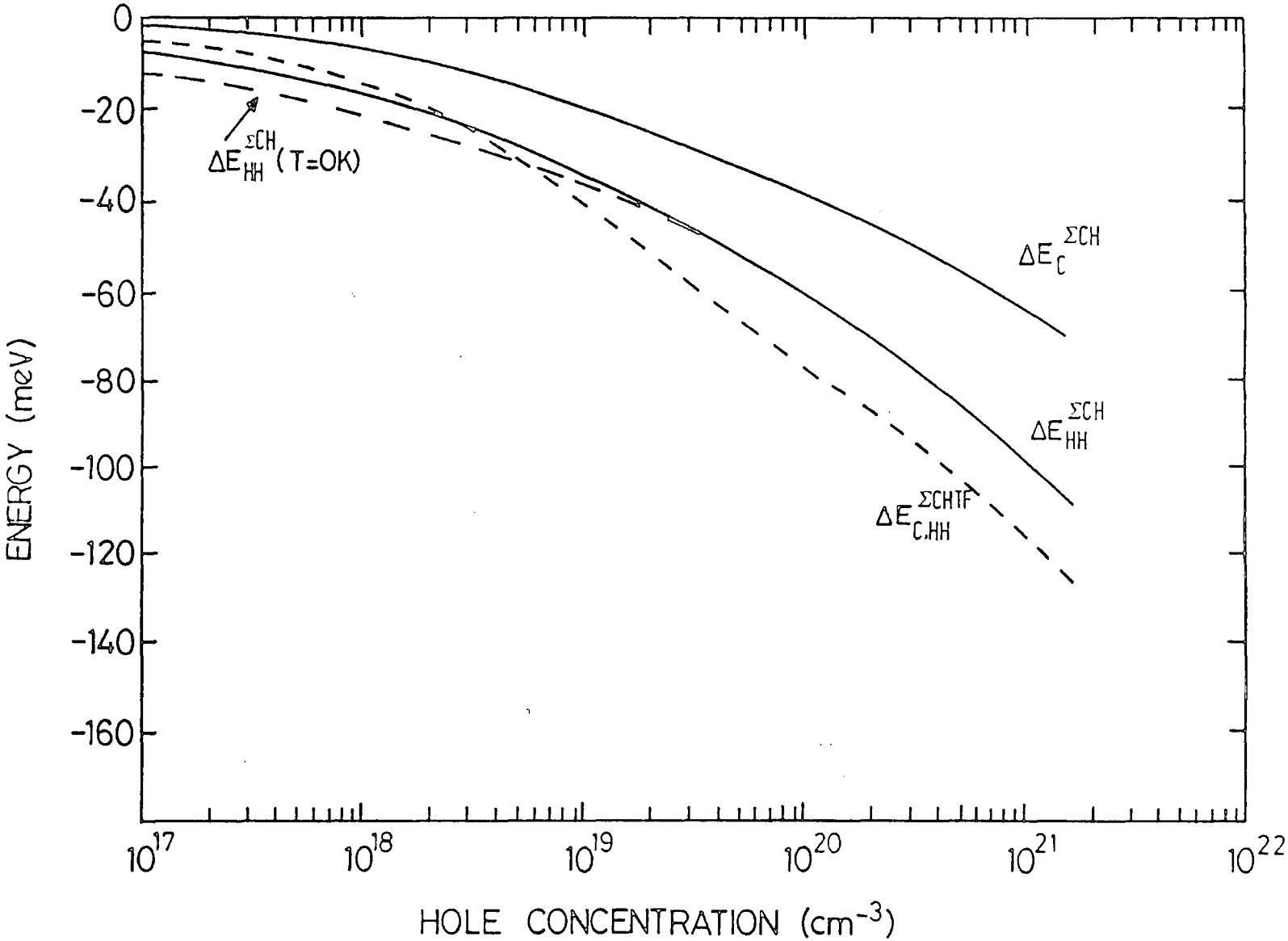

Figure 4.4: The hole concentration dependence of the Coulomb-hole energy shifts of the conduction and valence band edges of p-type Si at T = 300 K.

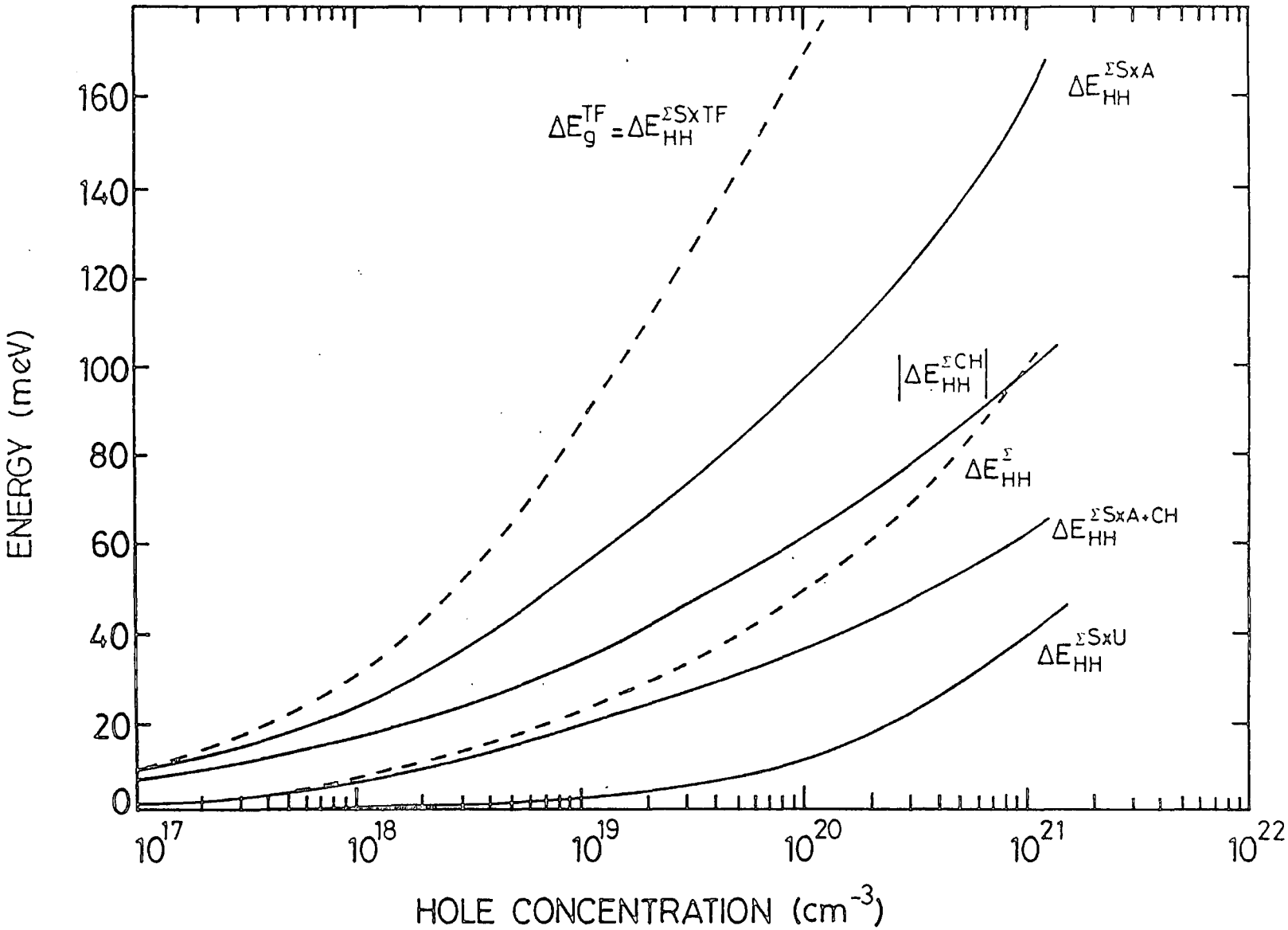

Figure 4.5: The hole concentration dependence of all terms contributing to the shift of the heavy-hole band edge in p-type Si at T = 300 K.

4.3.9. Valence Band Shift in the Thomas-Fermi Approximation

a) Coulomb Hole Term

Use of the frequency independent T.F. approximation for the carrier screening reduces the HH band CH term to the same form as expression (4.37) for the conduction band CH term except that the valence band coupling is now incorporated, giving,

$$\Delta E_{HH}^{\Sigma CHTF} = \frac{-e^2}{8\pi^2 \varepsilon_r \varepsilon_o} \Sigma_{n''} \int_0^{\infty} \frac{\omega_p^2 \, dq}{\omega_1^2(q)} \tag{4.57}$$

$$= \frac{-e^2 K}{8\pi \varepsilon_r \varepsilon_o} \tag{4.58}$$

which is the same downward energy shift as produced for the conduction band CH term and, as with the zero temperature model, the CH terms make no contribution to the band gap narrowing.

b) Screened Exchange Term

Evaluation of the heavy hole SX term is performed following the method of section 4.3.6. The difference between the screened exchange energy for the fully occupied valence band in the doped material and the exchange energy in the intrinsic material $\Delta E_{HH}^{\Sigma SXATF}$ reduces to

$$\Delta E_{HH}^{\Sigma SXATF} = \frac{e^2 K}{4\pi \varepsilon_r \varepsilon_o} \tag{4.59}$$

which relates directly to the first term of the zero temperature result of equation (3.33) but now K takes its finite temperature form.

The SX term for those states occupied by holes $\Delta E_{HH}^{\Sigma SXUTF}$ reduces from expression (4.46) to

$$\Delta E_{HH}^{\Sigma SXUTF} = \frac{e^2}{4\pi^2 \varepsilon_o \varepsilon_r} \sum_{n''} \int_0^{\infty} f'_{n''-q} \left[1 - \frac{\omega_p^2}{\omega_1^2(q)} \right] dq \qquad (4.60) .$$

Evaluation of this term is easily performed using the NAG integral routine Dϕ1 AHF.

The total SX contribution to the shift of the heavy hole band edge is given by the sum of equations (4.59) and (4.60) as:

$$\Delta E_{HH}^{\Sigma SXTF} = \Delta E_{HH}^{\Sigma SXA} + \Delta E_{HH}^{\Sigma SXU} \qquad (4.61) .$$

This term provides the only contribution to the band gap narrowing in the T.F. approximation as the CH terms produce equal downward shifts in both the valence and conduction bands. The carrier concentration dependence of the T.F. screened exchange term for room temperature p-type Si is shown in figure 4.5. This shift is seen to be larger than that produced for the more realistic plasmon pole approximation and is roughly equal to its zero temperature value, for high carrier concentrations. At low hole concentrations the finite temperature shift is significantly lower than the zero temperature value due to the sensitivity of the T.F. screening to the carrier distribution.

4.3.10. Results and Discussion

The hole concentration dependencies of the shifts in the conduction and valence band edges derived in the plasmon pole approximation, together with the resulting band gap narrowing in p-type Si, GaAs, $Ga_{0.47}In_{0.53}As$ and $Ga_{0.28}In_{0.72}As_{0.6}P_{0.4}$ at T = 300 K are illustrated in figures 4.6 - 4.9 respectively. For comparison the band gap narrowing at zero temperature is also shown.

The four materials considered have a similar valence band structure with little difference in the HH and LH effective masses. The shifts

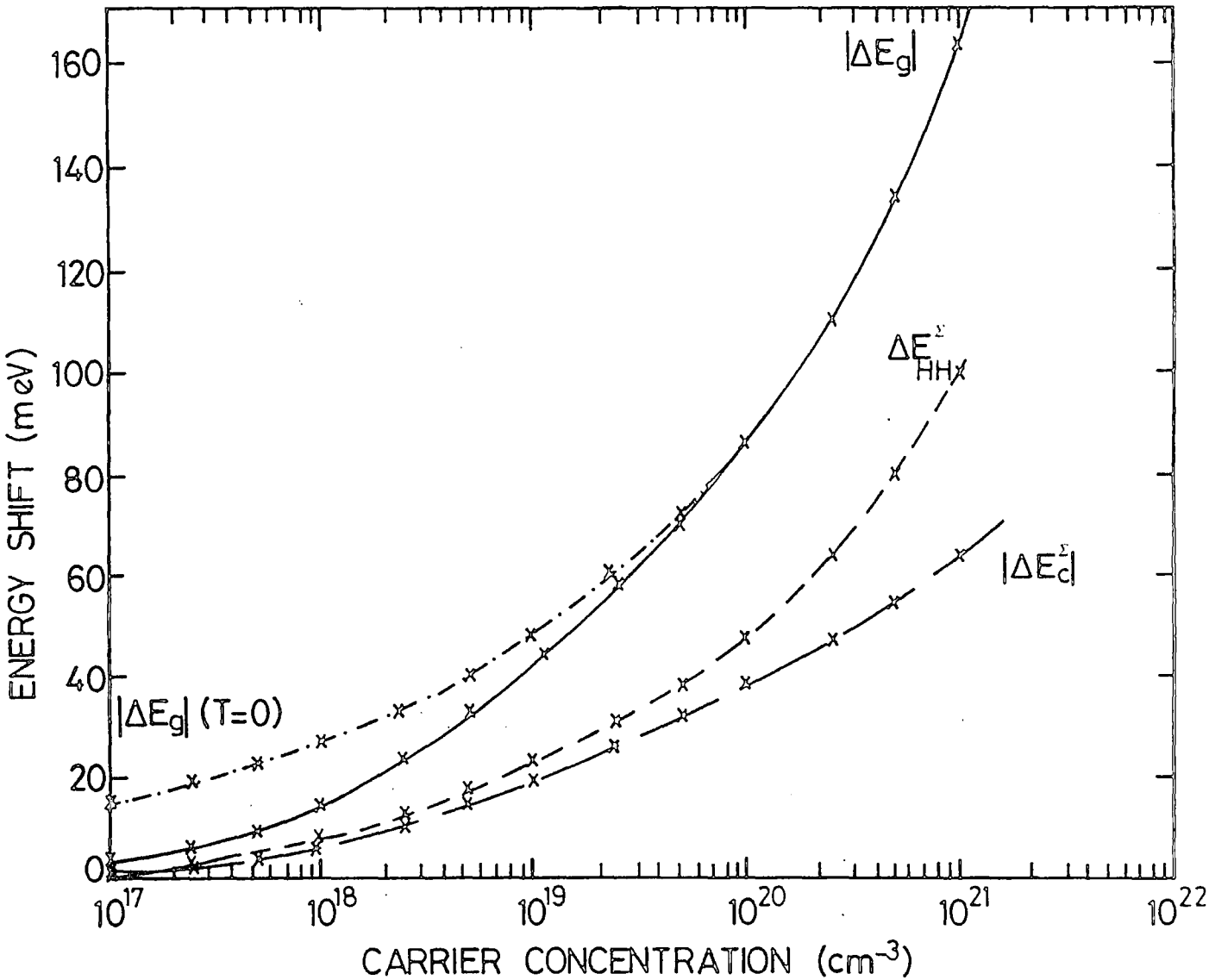

Figure 4.6: The hole concentration dependence of the energy shifts in the conduction and valence band edges and the corresponding band gap narrowing $|\Delta E_g|$ in p-type Si at T = 300 K. The band gap narrowing at T = OK

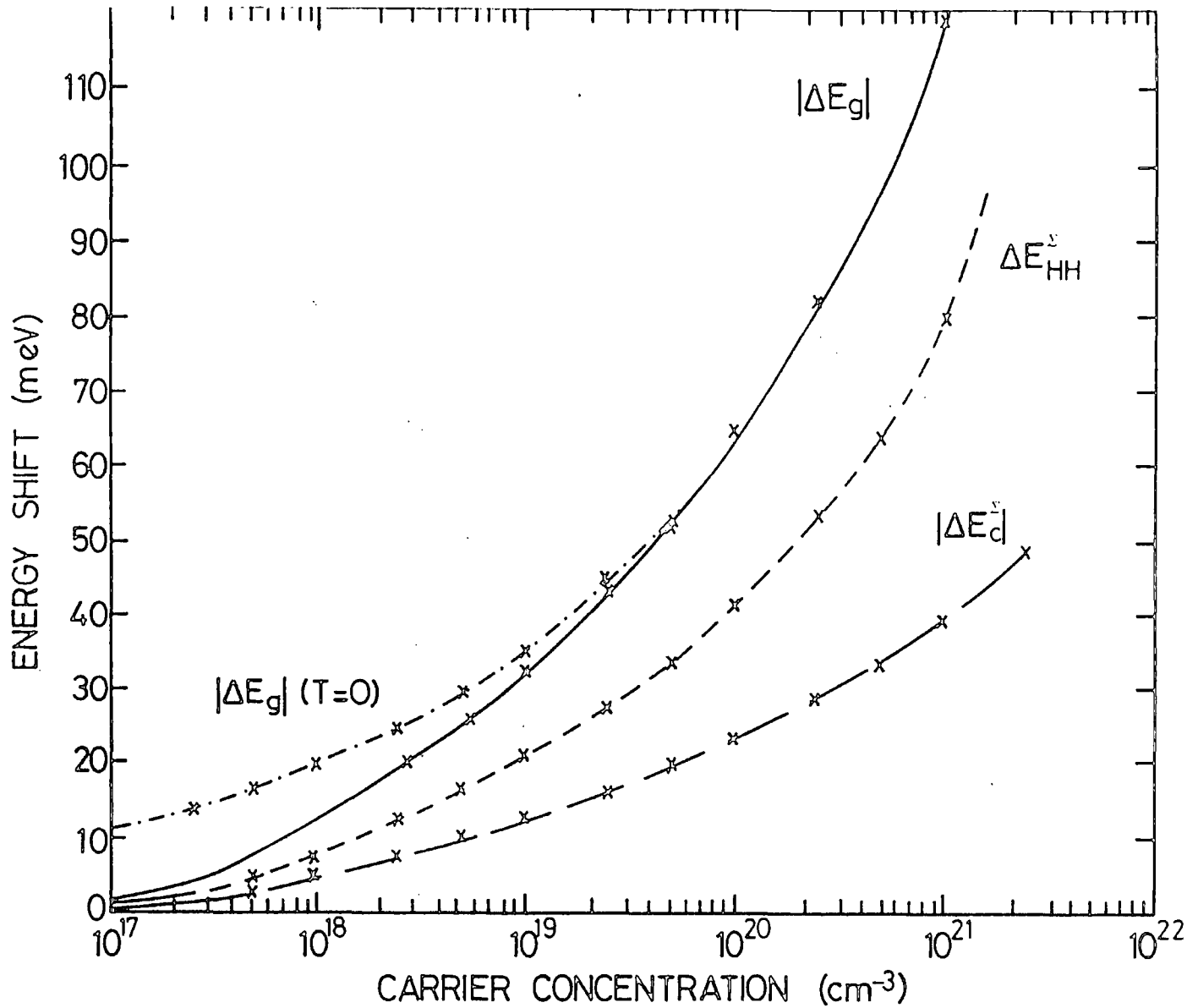

Figure 4.7: The hole concentration dependence of the energy shifts in the conduction and valence band edges and the corresponding band gap narrowing $|\Delta Eg|$ in p-type GaAs at T = 300 K.

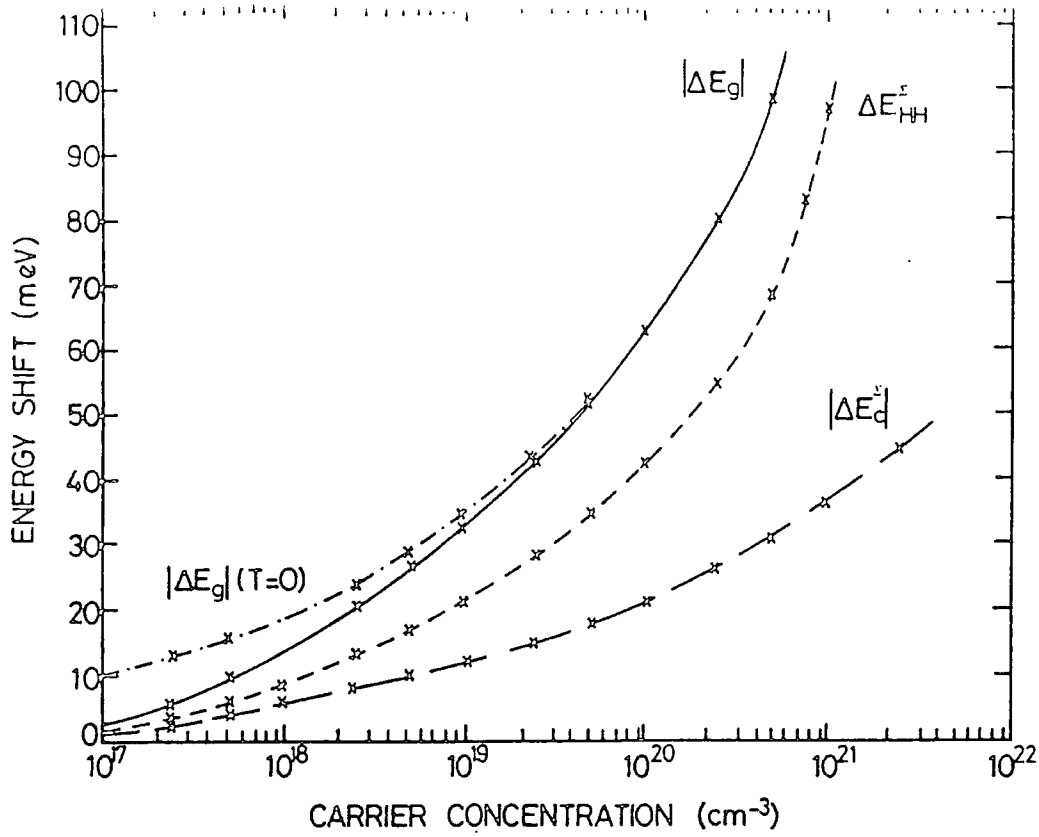

Figure 4.8: The hole concentration dependence of the energy shifts in the conduction and valence band edges and the corresponding band gap narrowing $|\Delta Eg|$ in p-type $Ga_{0.47}\ In_{0.53}\ As$ at T = 300 K.

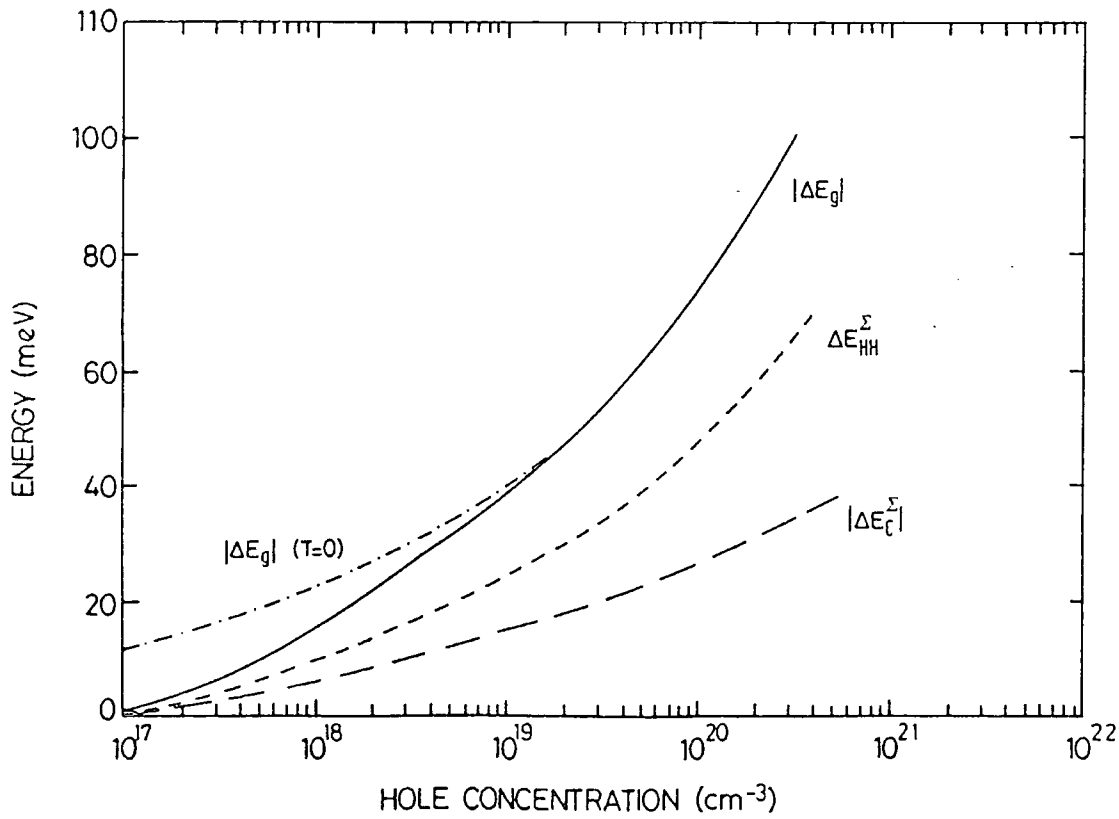

Figure 4.9: The hole concentration dependence of the energy shifts in the conduction and valence band edges and the corresponding band gap narrowing $|\Delta Eg|$ in p-type $Ga_{0.28}\ In_{0.72}\ As_{0.6}\ P_{0.4}$ at T = 300 K.

in the valence band edges are therefore similar in all four materials and represent the largest contribution to the band gap narrowing, due to the SX contribution which is not present in the conduction shift. The relatively large density of states effective mass of the valence band holes ensures large carrier concentrations ($\gtrsim 5 \times 10^{19}$ cm^{-3}) are required before the hole distribution resembles that at T = OK. At low carrier concentrations the main contribution to the reduction of the band edge shifts at room temperature from their zero temperature values comes from the valence band which is affected by changes in the CH and SX terms.

For comparison a brief description of the derivation of band edge shifts in n-type material is given below. This follows the work of Saunderson (1983) for n-type Si but is extended to include the results for the gallium compounds considered above.

4.4. Finite Temperature Band Gap Narrowing in n-type Material

4.4.1. Introduction

The analysis used here follows directly from that described for the zero temperature model in section 3.3. In the doped material the donor impurity band is considered to have merged with the host conduction band and each donor atom has contributed a single electron to the carrier gas.

4.4.2. Valence Band Shift

The Fermi level lies either close to or within the conduction band and the valence band is taken to be fully occupied. The resulting change in the exchange energy for a valence band edge electron is given through equations (4.29) and (4.31) as

$$\Delta E_{HH}^{\Sigma SX} = \frac{-e^2}{8\pi^3 \varepsilon_o \varepsilon_r} \sum_{n''} \int_{\substack{\text{all } n'' \\ \text{and } -q}} \left| I_{HHO,n''-\underline{q}} \right|^2 \frac{\omega_p^2}{q^2}$$

$$\left[\frac{1+N_q}{(\omega_{HHO}-\omega_{n''-\underline{q}})^2-\omega_1^2(q)} - \frac{N_q}{(\omega_{HHO}-\omega_{n''-\underline{q}})^2-\omega_1^2(q)} \right] d^3\underline{q} \qquad (4.62)$$

where $\omega_1(\underline{q})$ has its finite temperature form for an electron gas.

The valence band CH term is unaffected by carrier occupancy and is given directly by expression (4.41) as

$$\Delta_{HH}^{\Sigma CH} = \frac{e^2}{8\pi^2 \varepsilon_r \varepsilon_o} \sum_{n''} \int_0^\infty \frac{\omega_p^2}{\omega_1(q)} \left[\frac{1+N_q}{\omega_{n''q}-\omega_1(q)} + \frac{N_q}{\omega_1(q)+\omega_{n''q}} \right] dq \qquad (4.63)$$

4.4.3. Conduction Band Shift

The electrons in the newly occupied conduction band states of the doped material have a screened exchange interaction with the band edge test electron. The unoccupied conduction band states in the intrinsic material produce no such interaction so the change in the conduction band SX term is simply given by expression (4.29) in which the electron occupancy probability $f_{n''\underline{k}-\underline{q}}$ limits the integral to occupied states only.

$$\Delta E_C^{\Sigma SX}(\underline{k}_o) = \frac{-e^2}{2\pi^2 \varepsilon_o \varepsilon_r} \int_0^\infty f_{c\underline{k}_o-\underline{q}} \left\{ 1 - \frac{\omega_p^2}{\omega_1^2(q)-\omega_{cq}^2} \right\} dq \qquad (4.64)$$

where the appropriate substitution of overlap integrals has been made and the angular part of the polar coordinate wavevector integral performed. As $T \to 0K$ the occupancy probability takes the form of a step function and limits the upper range of the integral to k_{fe} so that the expression reduces to equation (3.46) of the zero temperature calculation.

The conduction band CH term can be derived directly from equation (4.30) which reduces to

$$\Delta E_C^{\Sigma CH}(\underline{k}_o) = \frac{e^2}{2\pi^2 \varepsilon_o \varepsilon_r} \int_0^\infty \left[\frac{N_q}{\omega_{\perp}(q)} \frac{\omega_{cq}}{} \frac{\omega_p^2}{(\omega_{\perp}^2(q) - \omega_{cq}^2)} - \frac{\omega_p^2}{2\omega_{\perp}(q)(\omega_{cq} + \omega_{\perp}(q))} \right] dq \quad (4.65) .$$

4.4.4. Results and Discussion

The electron concentration dependencies of the conduction and valence band shifts and the resulting band gap narrowing in n-type Si, GaAs, $Ga_{0.47}In_{0.53}As$ and $Ga_{0.28}In_{0.72}As_{0.6}P_{0.4}$ at T = 300 K are given in figures 4.10 to 4.13 respectively. The corresponding band gap narrowing results for T = OK are also shown for comparison.

The screening effect of the electrons is determined by their distribution in the conduction band which is in turn dependent on the density of states effective mass of the conduction band and the number of valleys occupied. In the case of silicon the relatively large density of states effective mass and six valley occupancy keeps the room temperature Fermi level in the band gap for electron concentrations $\lesssim 2 \times 10^{19}$ cm^{-3}. The screening effect of the electron gas is consequently much weaker than that produced by the strongly degenerate electron gas at T = OK. As a result the band gap narrowing is reduced by some 10 meV at an electron concentration of $n = 10^{18}$ cm^{-3}. At dopant concentration $\gtrsim 10^{20}$ cm^{-3} the Fermi level has entered the host conduction band, the electron gas is strongly degenerate and carrier distribution and screening resembles that at zero temperature. The resulting band gap narrowing is approximately equal to the zero temperature value. For the gallium compounds and alloys the single valley conduction band with very light density of states effective mass causes the room temperature Fermi level to enter

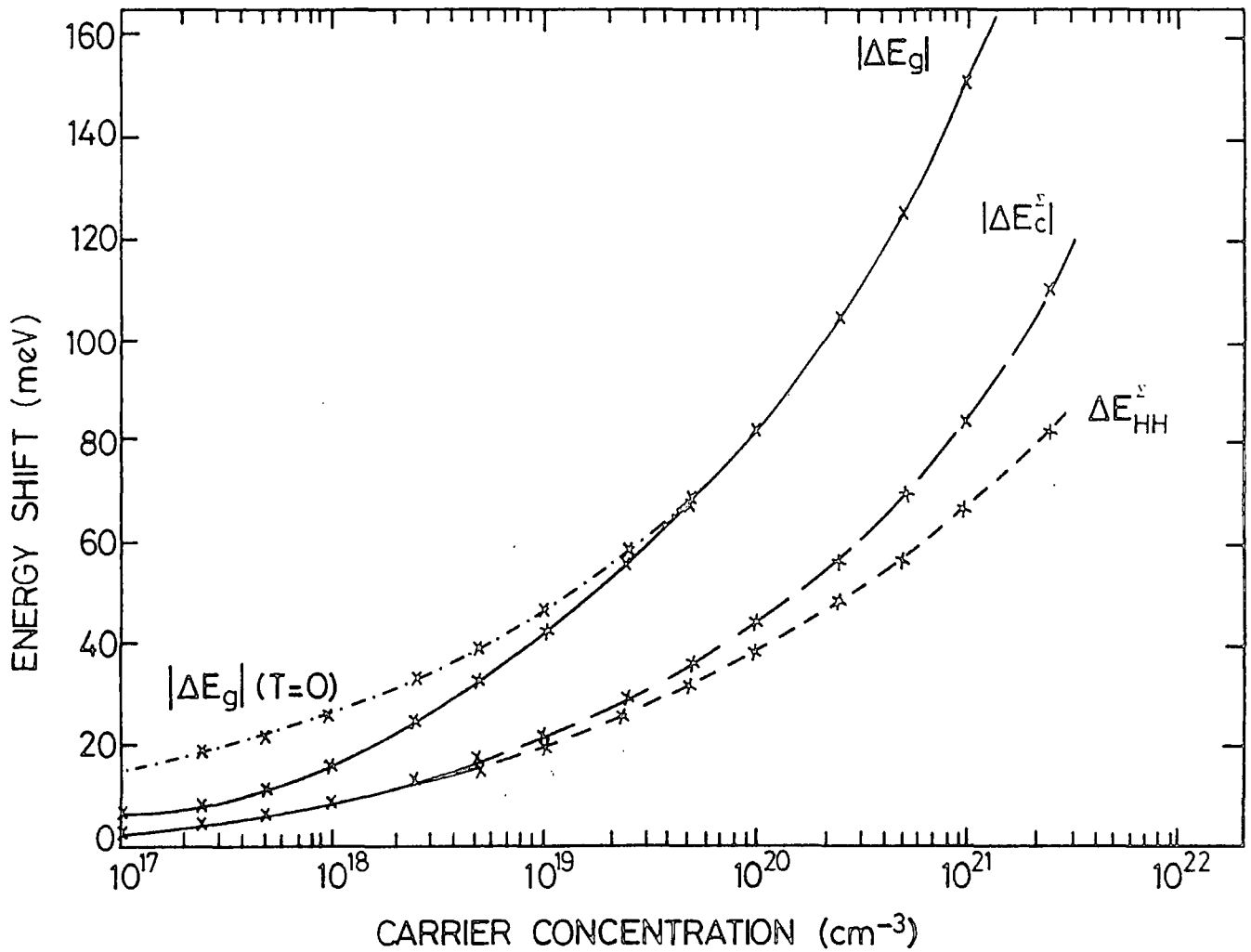

Figure 4.10: The electron concentration dependence of the energy shifts in the conduction and valence band edges and the corresponding band gap narrowing $|\Delta Eg|$ in n-type Si at T = 300 K and T = OK.

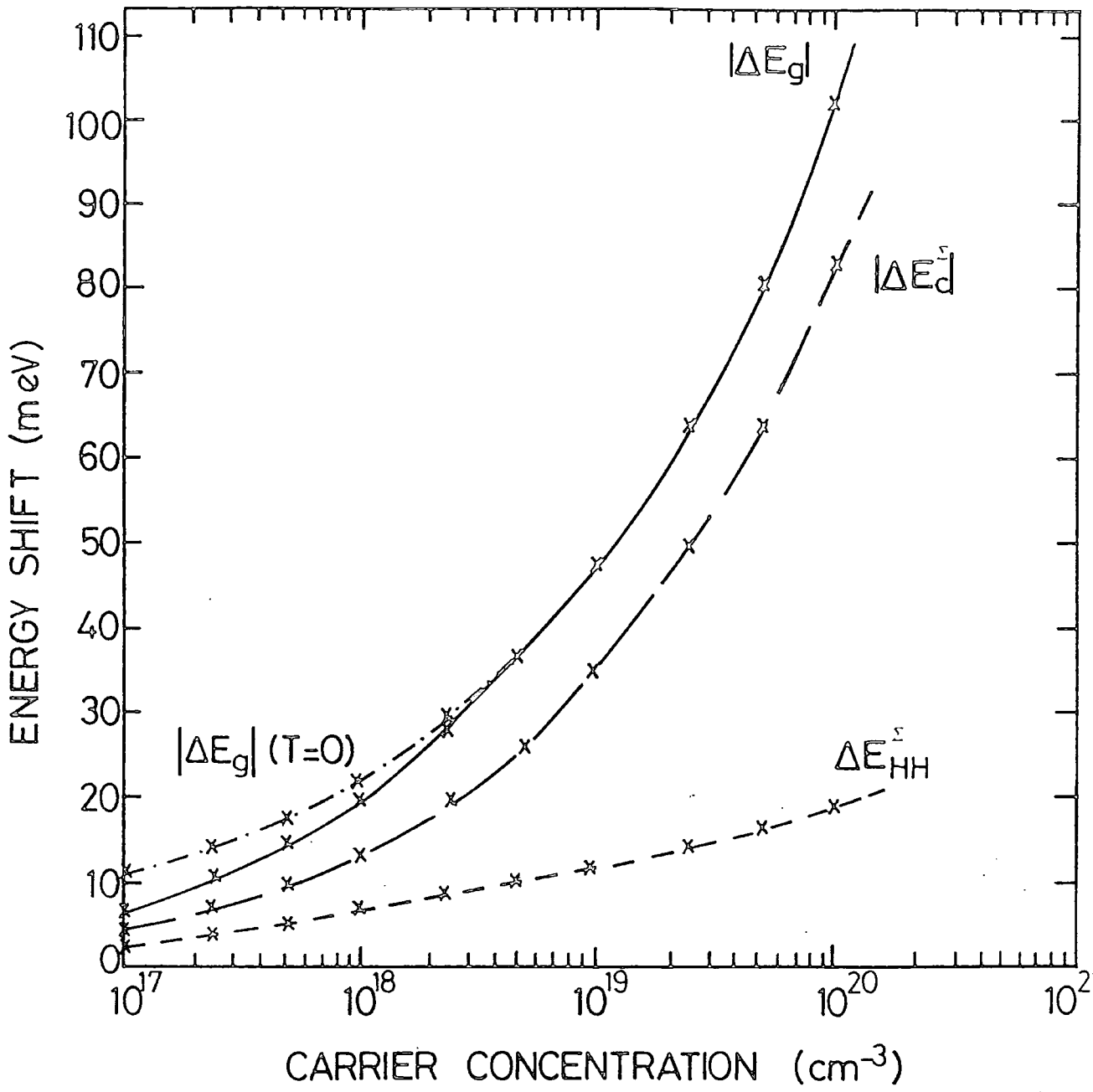

Figure 4.11: The electron concentration dependence of the energy shifts in the conduction and valence band edges and the corresponding band gap narrowing $|\Delta E_g|$ in n-type GaAs at T = 300 K and T = 0K.

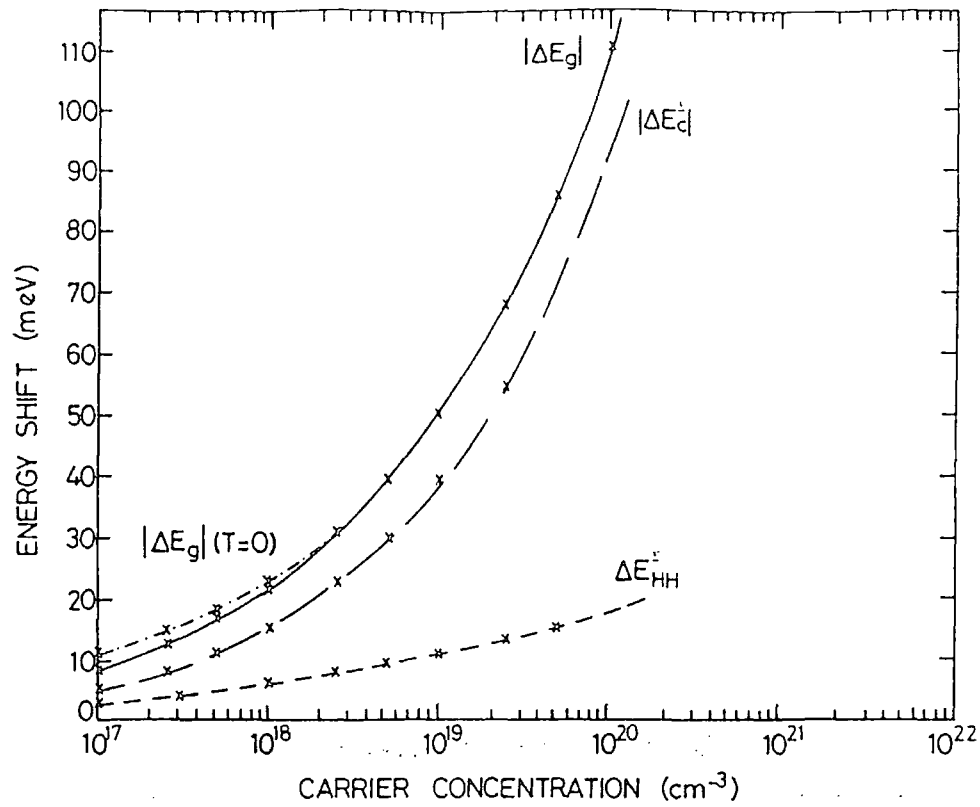

Figure 4.12: The electron concentration dependence of the energy shifts in the conduction and valence band edges and the corresponding band gap narrowing $|\Delta Eg|$ in n-type $Ga_{0.47}\ In_{0.53}\ As$ at T = 300 K and T = OK.

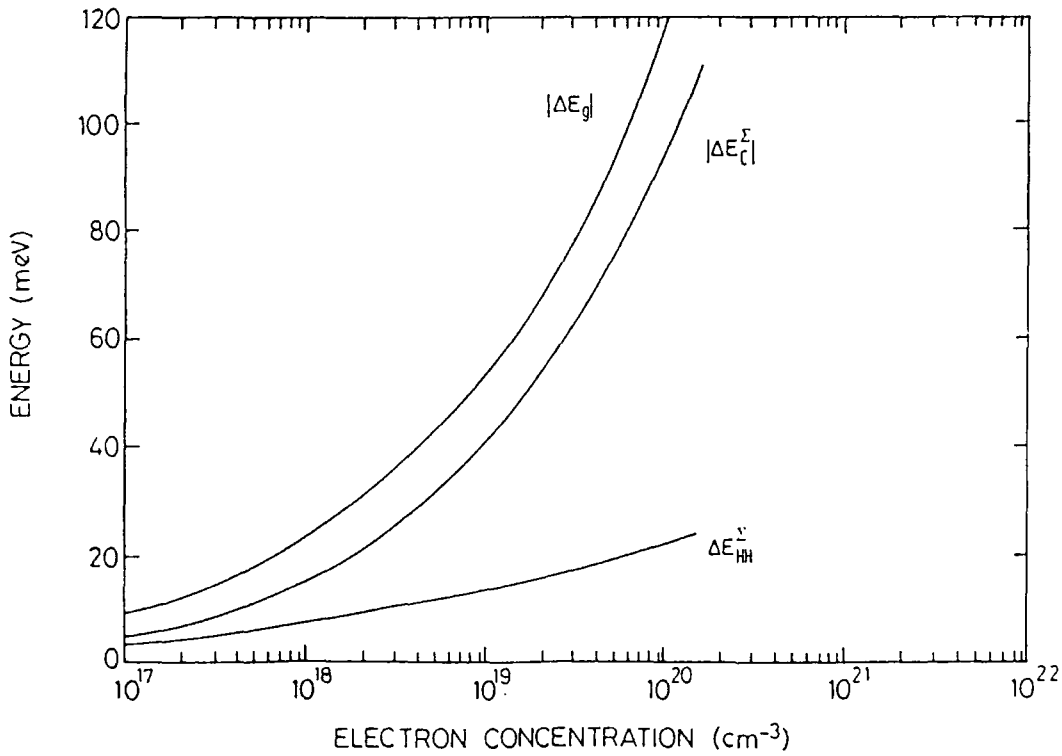

Figure 4.13: The electron concentration dependence of the energy shifts in the conduction and valence band edges and the corresponding band gap narrowing $|\Delta Eg|$ in n-type $Ga_{0.28}\ In_{0.72}\ As_{0.6}\ P_{0.4}$ at T = 300 K.

the host band at relatively low electron concentrations ($\simeq 3 \times 10^{17}$ cm^{-3} for GaAs). The carrier distribution is thus little different from that at zero temperatures for carrier concentrations $\gtrsim 5 \times 10^{18}$ cm^{-3} and the resulting band gap narrowing at finite and zero temperature are approximately equal.

Comparison of the formulae and results for n and p-type materials shows that there is a direct correspondence between the conduction band shift in n-type material and the valence band shift in p-type material and vice-versa, just as in the zero temperature case. However, the correspondence is somewhat obscured by the temperature distribution factors f and N_q.

4.5. Summary

The analysis of chapters 2 and 3 deriving the band gap narrowing due to electron-electron interactions at T = OK has been extended to finite temperature (T = 300 K). This extension is facilitated by the use of a finite temperature plasmon propagator which converts the zero temperature plasmon pole approximation of the carrier gas dielectric function to a suitable finite temperature form. All other terms in the self energy expression (including the Green's functions) are expressed in their finite temperature form but it turns out to be possible to evaluate the band edge shifts in a manner similar to that for T = OK.

The change in distribution of the carrier gas provides a physical explanation for the differences in the carrier concentration dependence of the band gap narrowing at finite and zero temperatures. At low carrier concentrations thermal excitation reduces the screening response to a perturbation and the band edge shifts are correspondingly lower than those produced at T = OK. As the dopant concentration is increased the carrier distribution and degeneracy resemble that at absolute zero and the band edge shifts at both T = OK and T = 300 K are very similar.

CHAPTER 5

INTERVALENCE BAND ABSORPTION AS A LOSS MECHANISM IN HETEROSTRUCTURE LASERS

5.0. Introduction

Low transmission loss and low dispersion are obtained in silica based optical fibres for wavelengths of 1.55 μm and 1.3 μm respectively. Double heterostructure lasers emitting within this range can be obtained by lattice matching $Ga_x In_{1-x} As_y P_{1-y}$ to InP and can be used as sources in optical fibre systems. However the threshold current density for these devices exhibits an exponential temperature dependence ($\sim \exp(T/T_o)$) where T_o has several constant values over different ranges of temperature. The higher the temperature range the lower is the value of T_o and hence the more rapid the variation of J_{th} with temperature. One such example of this behaviour is found in $Ga_{0.28} In_{0.72} As_{0.6} P_{0.4}$ (λ = 1.3 μm) for which $T_o \simeq 100$ K for $100 < T < 250$ K and $T_o \simeq 65$ K for 250 K < T < 350 K (ref. Casey (1984) and Henry et al (1983)).

Several loss mechanisms have been proposed to explain this temperature sensitivity: (i) Carrier leakage over the heterobarrier into the confining layers (Dutta et al (1980), Nahory et al (1979) and Yano et al (1981)), (ii) non radiative losses due to Auger recombination which both reduces the quantum efficiency and increases carrier leakage by exciting carriers above the heterostructure potential barrier (Dutta and Nelson (1981 and 1982) and Sugimura (1981)), (iii) non-radiative recombination at defects, and interface states, (Yano et al (1980) and Ettenberg and Kressel (1976)). (iv) intervalence band absorption (IVBA) causing optical losses, (Henry et al (1983), Mozer et al (1983), and Adams et al (1980)).

In view of the potential importance of the latter loss mechanism, IVBA coefficients for several laser materials have been evaluated at various temperatures and carrier concentrations.

5.1. The IVBA Mechanism

In an operational laser most photons emitted by electron transitions from the conduction to valence band will either leave the laser structure as part of the emitted radiation, often after stimulating more downward electron transitions, or be reabsorbed by causing the reverse transition. Some photons, however, are absorbed by other loss mechanisms. One such mechanism is the intervalence band absorption transition in which photons excite an electron from one valence band state into a higher energy state occupied by a hole in another valence band. If no phonon or other energy broadening mechanisms are considered in this process the transition is vertical in $\underline{k}$ space that is the electron wavevector $\underline{k}$ is conserved. This condition is assumed in the present calculations and all IVBA coefficients are evaluated for vertical transitions. The extent to which this simplification affects the calculated value of absorption coefficient has been shown in some detail by Takeshima (1984). By inclusion of phonon and impurity scattering processes, he has shown the principal effect of level broadening to be a reduction in the temperature dependence of IVBA coefficient over the range $T = 100\ K - 400\ K$ which correspondingly reduces the temperature dependence of threshold current density on the IVBA mechanism. The three possible types of vertical transition are illustrated in figure (5.1). The light-heavy hole band transition (A) is considered unimportant as the transition energies are small for all heavy hole states with a high probability of hole

occupancy. The spin split off-light hole band transition (B) is neglected on the basis of a low density of states in the light hole band and a very low hole occupancy of final states for transitions at the band gap energy. The larger density of states and hole occupancy in the heavy hole band produces much greater absorption at relevant wavelengths for the spin split off-heavy hole band transition (C) than for transition (B). IVBA coefficients are therefore only evaluated for the spin split off-heavy hole band transition.

The values of these absorption coefficients derived in the calculation are clearly dependent on the bandstructure and momentum matrix elements used. In the present work the absorption coefficients are derived using pseudopotential bandstructure and momentum matrix elements evaluated along 21 $\underline{k}$ space directions in an irreducible segment of the Brillouin zone. This good coverage of $\underline{k}$ space takes into account the variation of absorption coefficient with $\underline{k}$ space direction. The bandstructure and momentum matrix elements for alloy materials have been evaluated using a simple linear interpolation of the values obtained for the constituent compounds.

The absorption coefficients determined in the above model are compared with those derived using an approximation based on the same pseudopotential information in only three $\underline{k}$-space directions and also with a simple parabolic isotropic effective mass model.

5.2. Theory of Photon Absorption and the IVBA Transition

In a semiconductor laser photons are reflected by cleaved and mirrored surfaces at the opposite ends of the laser cavity. In traversing the cavity the photons induce electronic transitions across the semiconductor band gap. The electron-photon interaction can be considered

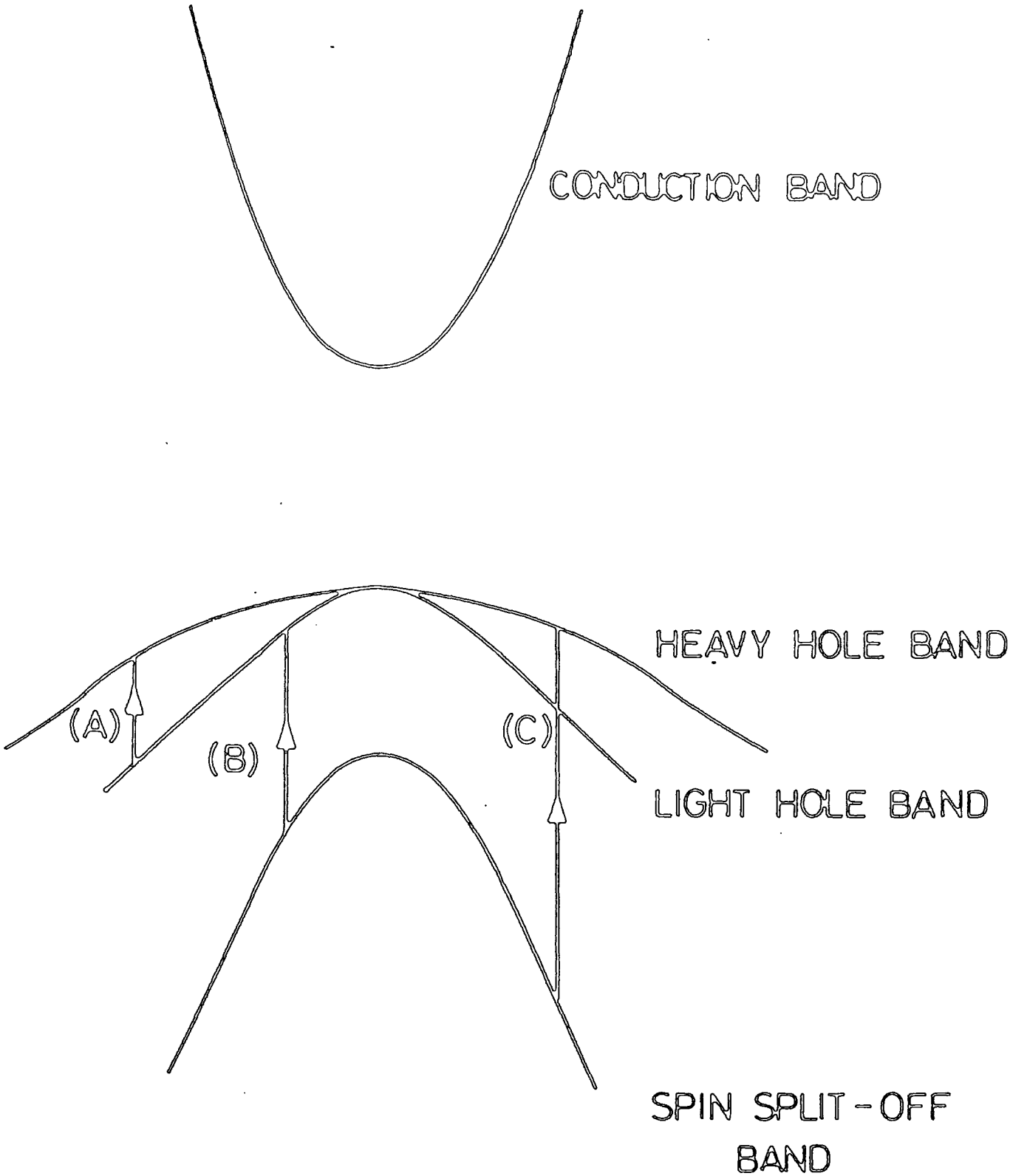

Figure 5.1: The three vertical (k-selection) types of IVBA transition. IVBA coefficients are only determined for the spin split off-heavy hole band transitions.

as the interaction of an electron of charge -e with an electromagnetic wave. The electric and magnetic fields of a plane electromagnetic wave can be represented in terms of the vector potential

$$\underline{A} = \frac{\underline{A}_o e^{-i(\underline{k}\cdot\underline{r}-\omega t)}}{2} + \frac{\underline{A}_o e^{i(\underline{k}\cdot\underline{r}-\omega t)}}{2} = \underline{A}_o \cos(\underline{k}\cdot\underline{r}-\omega t)$$

where

$$\underline{B} = \underline{\nabla}\times\underline{A} \qquad \underline{E} = -\frac{\partial \underline{A}}{\partial t} \tag{5.1}$$

The Hamiltonian for an electron subject to a regular periodic potential $V(\underline{r})$ and an electromagnetic field is then given by (Gasiorowicz (1974))

$$H = \frac{1}{2m_o}(\underline{p} + |e|\underline{A})^2 + V(\underline{r}) \tag{5.2}$$

on substitution into the Schrodinger equation and using $\underline{\nabla}\cdot\underline{A} = 0$ we obtain

$$\left(\frac{-\hbar^2}{2m_o}\nabla^2 - \frac{i|e|\hbar}{m_o}\underline{A}\cdot\underline{\nabla} + \frac{e^2A^2}{2m_o} + V(r)\right)\psi = E\psi \tag{5.3}$$

Of the terms in brackets the final term with the A^2 component can be shown to be several orders of magnitude smaller than the second term (assuming no large external fields are applied (ref. Gasiorowicz (1974)) and is therefore ignored. The second term can now be considered as a perturbation H' on the perfect crystal Hamiltonian where:

$$H' = -\frac{i|e|\hbar}{2m_o}[e^{-i(\underline{k}\cdot\underline{r}-\omega t)} + e^{i(\underline{k}\cdot\underline{r}-\omega t)}]\,\underline{A}_o\cdot\underline{\nabla} \tag{5.4}$$

The photon wavevector is very small compared with typical electron or hole wavevectors and in an expansion of $e^{-i\underline{k}\cdot\underline{r}}$,

$$e^{-i\underline{k}\cdot\underline{r}} = \sum_{n=0}^{\infty} \frac{(-i)^n}{n!} (\underline{k}\cdot\underline{r})^n \quad , \tag{5.5}$$

all terms higher than zeroth order can be neglected. In fact we take $\underline{k} = 0$.

Using time dependent perturbation theory the first time dependent term in equation (5.4) is proportional to $e^{i\omega t}$ and produces downward transitions and the second time dependent term, proportional to $e^{-i\omega t}$, produces upward transitions. The rates of transitions between states H and S in the heavy hole and spin split off bands are then given by Fermi's Golden Rule as:

$$R_{up} = \frac{2\pi}{\hbar} \sum_{S,H} f(E_S)(1-f(E_H)) \left|\langle H|H'|S\rangle\right|^2 \delta(E_H - E_S - \hbar\omega)$$

$$R_{down} = \frac{2\pi}{\hbar} \sum_{S,H} f(E_H)(1-f(E_S)) \left|\langle H|H'|S\rangle\right|^2 \delta(E_H - E_S - \hbar\omega) \tag{5.6}$$

where $f(E_{H,S})$ are the probabilities of electron occupancies in the relevant bands, and H' is now:

$$H' = -\frac{i|e|\hbar}{2m_o} \underline{A}_o \cdot \underline{\nabla} \tag{5.7} .$$

From equation (5.1) the direction of $\underline{A}$ is determined by the polarisation of the electric field, i.e. $\underline{A}_o = A_o\underline{\hat{e}}$ where $\underline{\hat{e}}$ is a unit vector in the polarisation direction. Now the intensity I of electromagnetic radiation is given by Poyntings vector as

$$I = \frac{1}{2} \frac{(\omega A_o)^2 \eta_r}{c\mu_o} = \frac{1}{2} \eta_r c\, \varepsilon_o\, \omega^2\, A_o^2 \tag{5.8}$$

where η_r is the refractive index of the semiconductor and the remaining constants take their usual meaning.

Substitution of equations (5.7) and (5.8) into the rate expressions (5.6) gives for the nett upward transition rate:

$$R_{\substack{\text{nett}\\ \text{up}}} = \frac{\pi e^2 \hbar I}{m_o^2 \varepsilon_o \omega^2 c \eta_r} \sum_{S,H} (f(E_S) - f(E_H)) |\langle H | \hat{e} \cdot \nabla | S \rangle|^2 \delta(E_H - E_S - \hbar\omega) \quad (5.9).$$

Now the energy density due to photons in the active region is given by

$$\text{Energy density} = \frac{\text{Irradiance}}{\text{photon velocity}} = \frac{I}{(c/\eta_r)} = \frac{N\hbar\omega}{\Omega} \quad (5.10)$$

where N is the number of photons in volume Ω.

The absorption coefficient is defined as the fractional loss of irradiance (intensity) per unit distance, which for a beam of photons in the x direction gives

$$\alpha(\omega) = -\frac{1}{I}\frac{dI}{dx} \quad (5.11)$$

(or equivalently $I(x) = I(0)e^{-\alpha x}$) which combined with equation (5.10) gives

$$\frac{1}{I}\frac{dI}{dx} = \frac{1}{I}\frac{dN}{dx}\frac{\hbar\omega c}{\Omega \eta_r} = \frac{1}{I}\frac{dN}{dt}\frac{\hbar\omega}{\Omega} \quad (5.12).$$

Now $-\frac{dN}{dt}$ is the photon loss per unit time which equals the nett rate of upward transitions. Hence

$$\alpha(\omega) = R_{\substack{\text{nett}\\ \text{up}}} \frac{1}{I}\frac{\hbar\omega}{\Omega} \quad (5.13)$$

which gives

$$\alpha(\omega) = \frac{\pi e^2 \hbar^2}{m_o^2 \varepsilon_o \omega c \eta_r \Omega} \sum_{S,H} (f(E_S) - f(E_H)) \left|\langle H|\hat{\underline{e}}\cdot\underline{\nabla}|S\rangle\right|^2 \delta(E_H - E_S - \hbar\omega) \qquad (5.14) .$$

By expanding the periodic parts of the carrier Bloch wave-function for states H and S in terms of reciprocal lattice vectors, it is shown in Appendix 4 that $\left|\langle H|\underline{e}\cdot\underline{\nabla}|S\rangle\right|^2$ averaged over all polarisations is

$$|M|^2 = \left|\langle H|\underline{e}\cdot\underline{\nabla}|S\rangle\right|^2 = |M|^2_{AV}\, \delta_{O,\underline{k}_H - \underline{k}_S} \qquad (5.15)$$

where $$|M|^2_{AV} = \frac{1}{3}\left[|M_x|^2 + |M_y|^2 + |M_z|^2\right] \qquad (5.16)$$

and M_i are the momentum matrix elements formed by the Bloch periodic parts for radiation polarised in the x, y, z directions

$$M_x = \int u_H^*(\underline{r})\hat{\underline{e}}_x \cdot \underline{\nabla}\, u_S(\underline{r}) d^3\underline{r} \qquad (5.17) .$$

The kronecker delta in equation (5.15) provides the $\underline{k}$ selection condition discussed previously. Using $\delta_{O,\underline{k}_H - \underline{k}_S} \equiv \frac{(2\pi)^3}{\Omega}\delta(\underline{k}_S - \underline{k}_H)$ and converting the sums over S and H states to integrals, expression (5.14) becomes:

$$\alpha(\omega) = \frac{\pi e^2 \hbar^2}{m_o^2 \varepsilon_o \omega c \eta_r \Omega} \frac{(2\pi)^3}{\Omega} \left(\frac{\Omega}{(2\pi)^3}\right)^2 \iint (f(E_S) - f(E_H)) |M|^2_{AVS} \delta(\underline{k}_S - \underline{k}_H)\, \delta(E_H - E_S - \hbar\omega)\, d^3\underline{k}_S d^3\underline{k}_H \qquad (5.18) .$$

Where to account for the two spin states in the heavy hole and splin split-off bands the transition matrix element has been summed over all possible transitions such that:

$$\sum_{\substack{\text{spin} \\ \text{states}}} |M|^2_{AV} = |M|_{AVS} \qquad (5.18a) .$$

Integration over $\underline{k}_S$ and dropping the subscript on $\underline{k}_H$ gives

$$\alpha(\omega) = \frac{\pi e^2 \hbar^2}{m_o^2 \varepsilon_o \omega c \eta_r (2\pi)^3} \int (f(E_S(\underline{k})) - f(E_H(\underline{k}))) |M|^2_{AV} \delta(E_H(\underline{k}) - E_S(\underline{k}) - \hbar\omega) d^3\underline{k} \quad (5.19) .$$

Now using the expression

$$\delta(E_{HS}(\underline{k}) - \hbar\omega) = \sum_{\ell} \frac{\delta(\underline{k}-\underline{k}_\ell)}{|\nabla_k E_{HS}|_{\underline{k}=\underline{k}_\ell}} \quad (5.20)$$

where $E_{HS}(\underline{k}) = E_H(\underline{k}) - E_S(\underline{k})$ and the $\underline{k}_\ell$ define surfaces in $\underline{k}$-space such that

$$E_{HS}(\underline{k}_\ell) - \hbar\omega = 0 . \quad (5.21) .$$

For isotropic $E - \underline{k}$ dispersion in both heavy hole and spin split-off bands such that the energy separation increases monotonically with $\underline{k}$, there is a single spherical surface defined by equation (5.21), and expression (5.19) reduces to

$$\alpha(\omega) = \frac{\pi e^2 \hbar^2}{m_o^2 \varepsilon_o \omega c \eta_r 8\pi^3} \left. \frac{(f(E_S(k)) - f(E_H(k))) |M|^2_{AVS} 4\pi k^2}{|\nabla_k E_{HS}(k)|} \right|_{k=k_\ell} \quad (5.22) .$$

However, to account for the non-isotropic $E - \underline{k}$ dispersion found in most semiconductors a surface integral over the defined surface must be performed. In the present calculation such a continuous surface is not defined, the band structure and momentum matrix elements being determined along only 21 k-space directions in an irreducible segment of the Brillouin Zone. Thus only 21 values of $\underline{k}$ are determined within this region. However, a good approximation to the surface can be made by assuming $\underline{k}$ has a constant value in each sector surrounding the chosen 21 directions. The derived surface area can then be used to evaluate the absorption coefficient for each sector.

If $d\Omega_i$ is the solid angle in $\underline{k}$-space of the sector i, the contribution to the absorption coefficient from the sector is given by

$$\alpha_i(\omega) = \frac{e^2\hbar^2}{m_o^2\varepsilon_o\omega c n_r 8\pi^2} \left. \frac{(f(E_S(k))-f(E_H(k))|M|^2_{AVS}k^2 d\Omega_i}{|\nabla_k E_{HS}(k)|} \right|_{k=k_{\ell_i}} \qquad (5.23) .$$

The total absorption coefficient is obtained by summing over i. The procedure for determining the appropriate solid angles is given in the next section.

In a simple isotropic, parabolic band effective mass approximation expression (5.22) reduces to:

$$\alpha(\omega) = \frac{e^2\hbar^2}{m_o^2\varepsilon_o\omega c n_r \pi 4}\left(\frac{2\mu}{\hbar^2}\right)^{3/2}[f(E_S(k))-f(E_H(k)]|M|^2_{AVS}(\hbar\omega-\Delta)^{1/2}$$

$$\text{where} \quad k = \left[\frac{2\mu}{\hbar^2}(\hbar\omega-\Delta)\right]^{1/2} \qquad (5.24)$$

$\frac{1}{\mu} = \frac{1}{m_S} - \frac{1}{m_H}$ is the reduced effective mass and Δ is the spin splitting energy.

5.3. Choice of Directions

Ideally a uniform distribution of points on a sphere in $\underline{k}$-space would be chosen to define the $\underline{k}$-space directions referred to in the last section. Each direction represented by the points could then be considered to represent equal solid angles in $\underline{k}$-space and correspondingly given an equal weighting in the absorption coefficient evaluation. However, as it is impossible to obtain a uniform distribution of a large number of points on a sphere, a convenient set of directions was chosen and the $\underline{k}$-space solid angle of the sectors represented by the chosen directions were then evaluated and the absorption coefficient weighted

accordingly. The Brillouin zone of the zinc-blende lattice is shown in Figure (5.2a) with the principal symmetry points and lines labelled by conventional notation. An irreducible segment (1/48th) of the zone is shown in Figure (5.2b) and represents the volume enclosed by appropriate planes passing through the Γ point and points L, K, W, X, U. This volume is also that enclosed by planes cutting the Γ-point and the lines along the [100], [110] and [111] directions. The region on the (100) face enclosed by these planes was divided into 21 equal area squares, as shown in Figure (5.3). Points in the centre of these squares joined to the Γ point then represent the k-space directions along which the band structure and momentum matrix elements were derived. The ratio of the k-space volumes represented by each direction was then determined from the solid angle subtended at the Γ-point by each chosen area. That is by $A \cos \theta / r^2$ where A is the area of the square, θ is the angle between the normal to the plane of squares and the line joining the square to the Γ-point, and r is the distance from the square to the Γ-point. For those squares along the diagonal C - B of Figure (5.3) for which the full area A is shared with a neighbouring irreducible segment, the derived ratio of solid angle is halved.

5.4. Evaluation of the Hole Quasi Fermi Level

Using the NAG routine Eϕ2 ADF a tenth order polynomial expression for the E - k dispersion relationship in the heavy hole, light hole and spin split off bands was determined along each of the 21 chosen k-space directions. As the hole occupancy of the spin split off band at the temperatures under consideration is neglible only the light and heavy hole bands were used to determine the quasi Fermi level. For a valence band hole concentration of $p\ (m^{-3})$ we have:

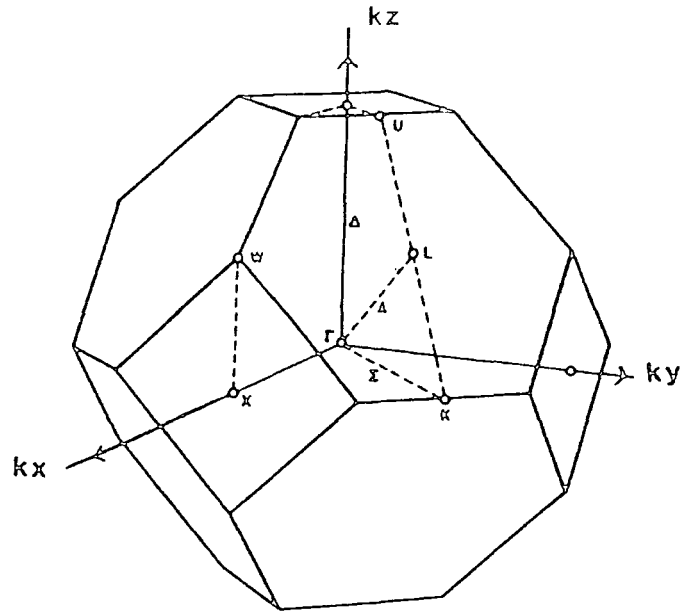

Figure 5.2a: The first Brillouin zone of the zinc blende lattice with the principal points and directions marked.

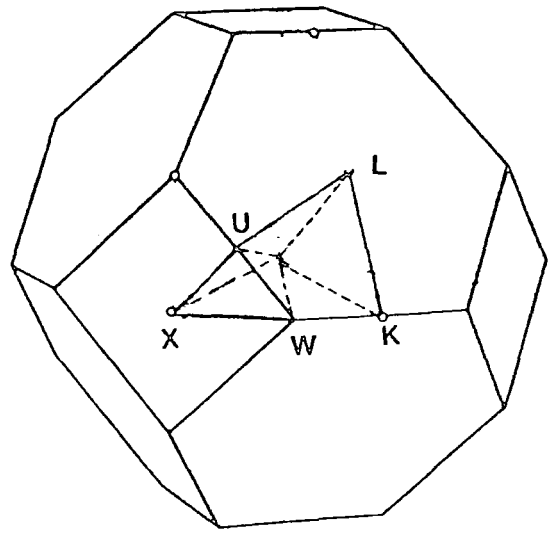

Figure 5.2b: An irreducible segment of the Brillouin zone occupying 1/48th of the total volume of k-space.

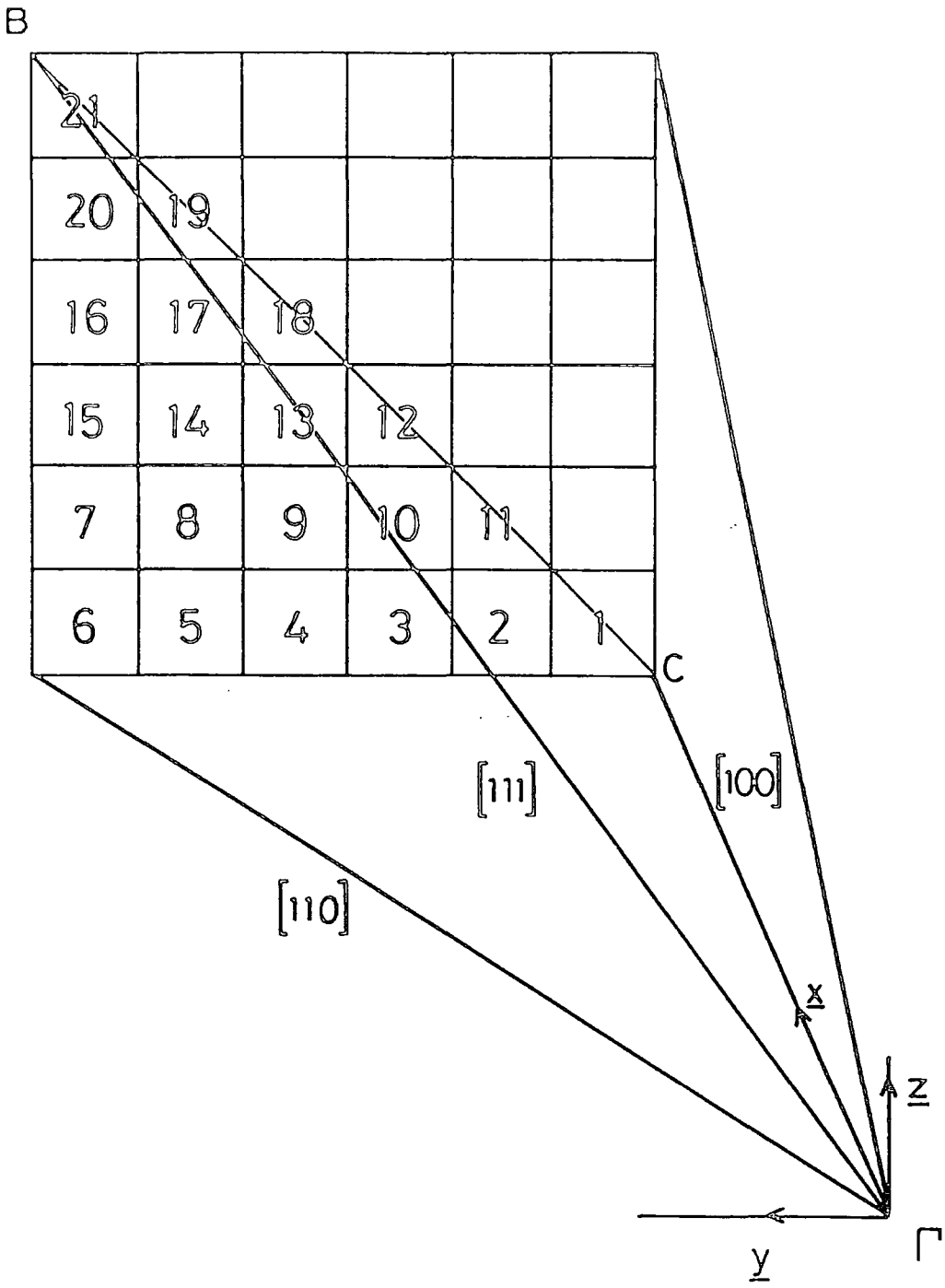

Figure 5.3: The section of the (100) plane divided into 36 equi-area squares, the lines joining the centres of the 21 marked squares to the Γ point define the directions for the bandstructure and matrix element derivation.

$$p = \frac{2}{(2\pi)^3} \sum_i \left[\int_0^{\text{ZONE EDGE}} f'(E_H(\underline{k}))d^3\underline{k} + \int_0^{\text{ZONE EDGE}} f'(E_L(\underline{k}))d^3\underline{k} \right] \frac{d\Omega_i}{4\pi} \qquad (5.25)$$

where $\frac{2}{(2\pi)^3}$ is the density of $\underline{k}$-states including a factor of 2 for spin and $d\Omega_i/4\pi$ is the fraction of the total volume of $\underline{k}$-space attributable to each of the 21 directions i, and $f'(E(\underline{k}))$ is the hole occupation factor for the relevant band. The above expression is equivalent to considering 21 isotropic systems and evaluating the hole quasi Fermi level using an average weighted by the appropriate $\underline{k}$-space volume for each direction.

The hole occupancy factor ensures rapid convergence of the integrals as $\underline{k}$ increases. Hence a value of $\underline{k} = 25\ \underline{k}_o$ where $\underline{k}_o = 2\pi/(100 \times \text{lattice constant})$ was used as the upper limit of the $\underline{k}$ integrals. Expression (5.25) then reduces to

$$p = \frac{2}{(2\pi)^3} 4\pi \left(\frac{2\pi}{100a}\right)^3 \sum_i \left[\int_0^{25} \frac{k'^2 dk'}{1+\exp\left(\frac{F+E_H(k')}{kT}\right)} + \int_0^{25} \frac{k'^2\, dk'}{1+\exp\left(\frac{F+E_L(k')}{kT}\right)} \right] \frac{d\Omega_i}{4\pi} \qquad (5.26)$$

where $k' = k/k_o$, a is the lattice constant and F is the hole quasi Fermi level, measured from the valence band edge. This expression was evaluated using the NAG root finding routine Cϕ5 ADF, together with the integral routine Dϕ1 AJF for which the quasi Fermi level is the determined root.

In a simple isotropic effective mass approximation (SEMA) for which the density of energy states has a $E^{1/2}$ dependence expression (5.25) reduces to:

$$p = \frac{1}{2\pi^2} \left(\frac{2m_H}{\hbar^2}\right)^{3/2} \int_{-\infty}^{0} \frac{-E^{1/2}dE}{1+\exp\left(\frac{F-E}{kT}\right)} + \frac{1}{2\pi^2} \left(\frac{2m_L}{\hbar^2}\right)^{3/2} \int_{-\infty}^{0} \frac{-E^{1/2}dE}{1+\exp\left(\frac{F-E}{kT}\right)} \qquad (5.27)$$

$$\text{or} \quad p = \frac{1}{2\pi^2}\left(\frac{2m_V}{\hbar^2}\right)^{3/2} \int_{-\infty}^{0} \frac{-E^{1/2}\,dE}{1+\exp\left(\frac{F-E}{kT}\right)} \tag{5.28}$$

where $m_V^{3/2} = m_H^{3/2} + m_L^{3/2}$ is the valence band density of states effective mass, and the valence band edge is taken as the zero of energy. A comparison of the hole quasi Fermi levels derived from 21-D pseudopotential and SEMA models for varying hole concentrations in GaAs at T = 300 K is given in figure (5.4). For both models the quasi Fermi level lies in the band gap for the carrier concentrations of interest (that is $p \leq 5 \times 10^{18}$ cm^{-3}.)

Discussion of these reults and their effect on the IVBA coefficients is given in the next section.

5.5. Bandstructure - Discussion and Comparison of Models Used

The bandstructure and momentum matrix elements were evaluated along the 21 $\underline{k}$-space directions using a Chelikowsy and Cohen (1976) pseudopotential calculation, an appropriate computer program for this evaluation being made available by S. Brand.

It is well known that for GaAs the [100] direction has a lighter effective mass and larger (S → H) momentum matrix elements (at a given $\underline{k}$) than the [110] and [111] directions. The use of many directions in the present calculation incorporates these differences and provides a good coverage of $\underline{k}$-space. Comparison of the main physical difference arising from the use of pseudopotential or effective mass bandstructure is best seen by examining their effect on the occupancy factor f_H which is the dominant term in the absorption coefficient expressions. The much larger heavy hole density of states derived in the pseudopotential calculation has three main effects which are shown diagrammatically in figure (5.5) and can be summarised as follows:

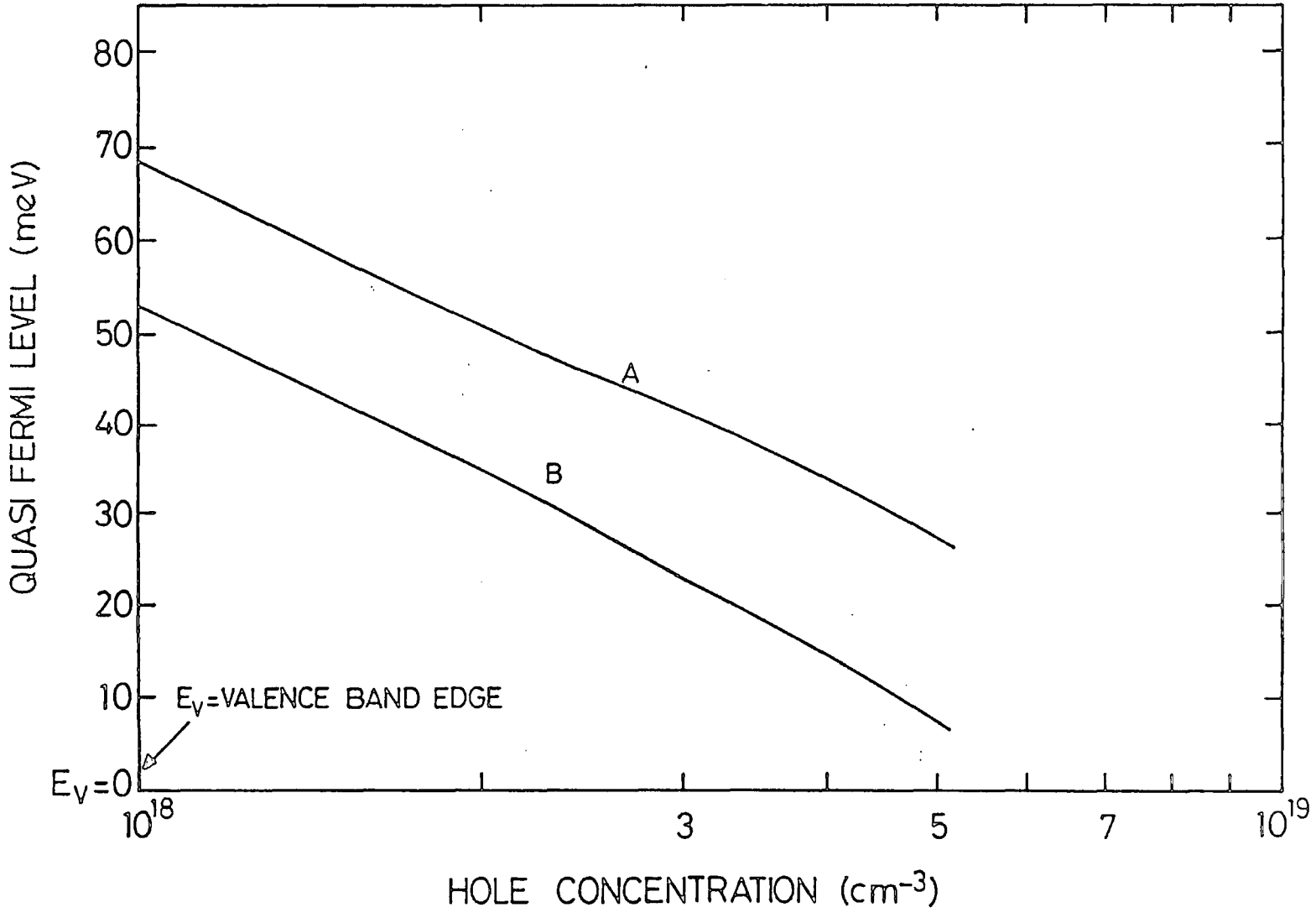

Figure 5.4: The position of the hole quasi-Fermi level relative to the valence band edge $E_v = 0$, for the 21-D pseudopotential (A) and simple effective mass (B) models.

For the pseudopotential bandstructure (i) the hole quasi Fermi level is further from the band edge, (ii) transitions at a given energy take place nearer the band edge, (iii) the heavy hole energy level at which a given energy transition takes place is higher so hole occupation is more likely. The effects are reflected in the absorption spectra for GaAs illustrated in figure (5.6) where absorption for high energy transitions is very small in the effective mass model due to low hole occupancy in the heavy hole band, and absorption for low energy transitions gives greater absorption than the pseudopotential calculation due to the relative positions of the quasi Fermi levels. To make the comparison more direct, the momentum matrix elements used in the effective mass calculation were the same as those used in the weighted average three direction (3-D) pseudopotential model discussed below.

To determine the effect of using a smaller number of directions, absorption coefficients were evaluated using a weighted average of results for isotropic systems based on the three symmetry directions [100], [110], and [111]. The weightings were taken as being proportional to the number of possible equivalent directions, i.e. [100]; [110]; [111]: 6, 12, 8. For higher energy transitions near the band gap energy the 3-D calculation gives greater absorption than the 21-D model, the reverse effect is seen for low energy transitions occurring near the band edge.

For both twenty-one and three $\underline{k}$ space direction calculations, the bandstructure and momentum matrix elements for alloys were determined using a simple linear interpolation of the values obtained for the constituent compounds.

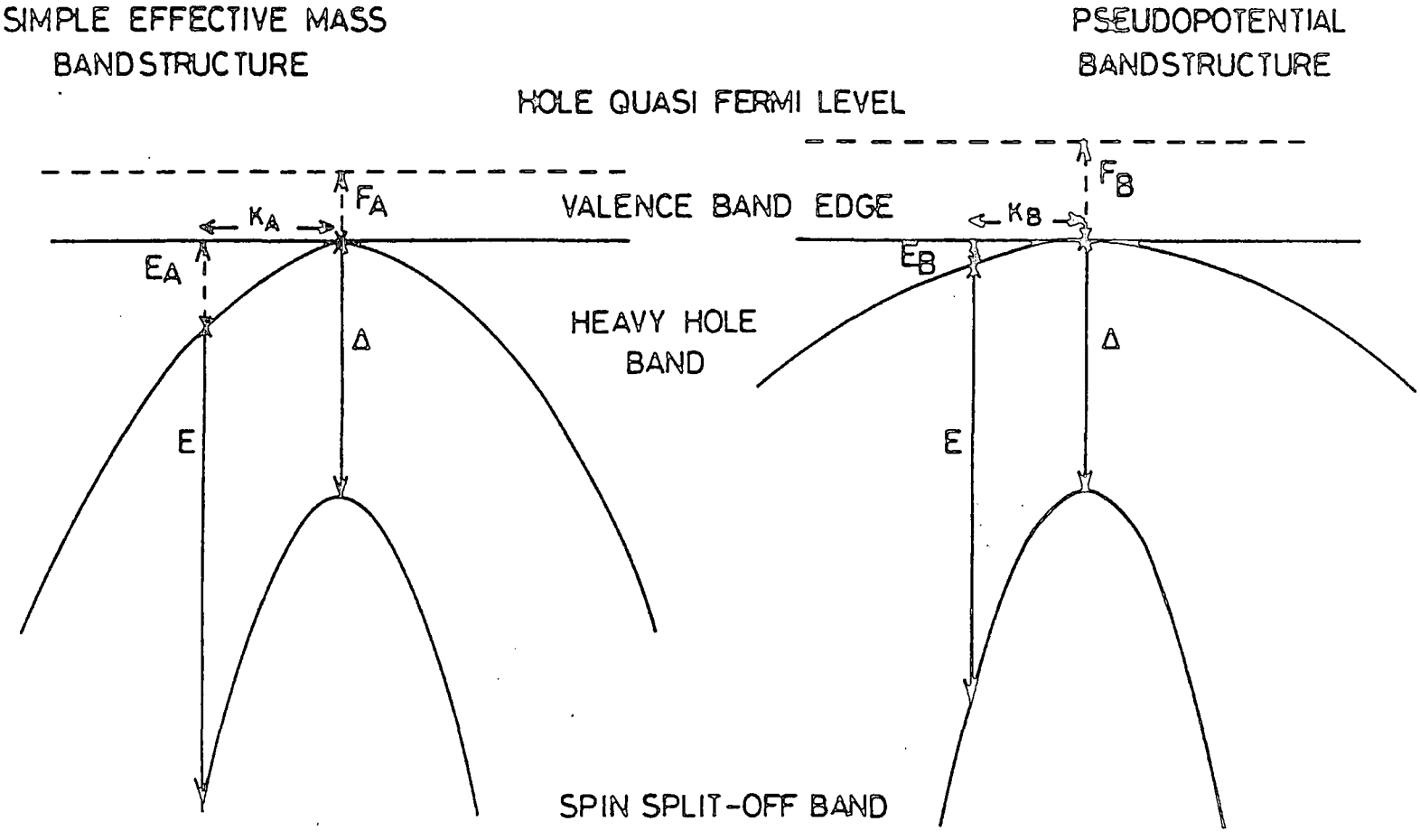

Figure 5.5: Comparison of the effect of different bandstructure for a transition energy E on (i) heavy hole energy level ($E_A > E_B$) (ii) k-value at which transition occurs ($k_A > k_B$) (iii) Fermi level ($F_B > F_A$).

5.6. Results and Discussion

5.6.1. Energy Dependence of the Absorption Coefficients

The calculated absorption coefficient versus wavelength for GaAs at a hole concentration of 10^{18} cm^{-3} and T = 300 K is shown in figure (5.6). For comparison the results of a simple effective mass model using $m_H = 0.45\ m_o$, $m_L = 0.085\ m_o$ and $m_s = 0.15\ m_o$ (ref. Landolt and Börnstein (1982) are also shown. The same weighted average matrix element was used in the pseudopotential 3-D and effective mass calculations, making comparison of the effects of different band structure more straightforward.

Low energy transitions give greater absorption in the 21-D calculation due to insufficient emphasis being placed on the 'heavy' [110] and [111] directions in the 3-D calculation, an effect which is also found for the other materials considered. The experimental work of Henry et al (1983) (which measured the resultant of all the possible types of IVBA transition shown in figure (5.1)) is also shown in figure (5.6) and compares well with both the 3-D and 21-D calculations. The large energy difference between the band gap and the spin splitting parameter in GaAs ensures transitions at the band gap energy take place at large $\underline{k}$ values where the hole occupancy of the heavy hole band is very low. The absorption coefficient at the band gap wavelength (0.87 μm) is therefore negligible.

Absorption coefficient versus wavelength results for $Ga_{0.47}\ In_{0.53}\ As$ (21-D and 3-D) at a hole concentration of 10^{18} cm^{-3} and T = 300 K are shown in figure (5.7) together with the experimental results of Henry et al (1984). The theoretical results are larger than the experimental results for all the wavelengths considered. Of the materials considered $Ga_{0.47}\ In_{0.53}\ As$ has the smallest band gap and largest spin splitting parameter and hence the largest band gap wavelength absorption

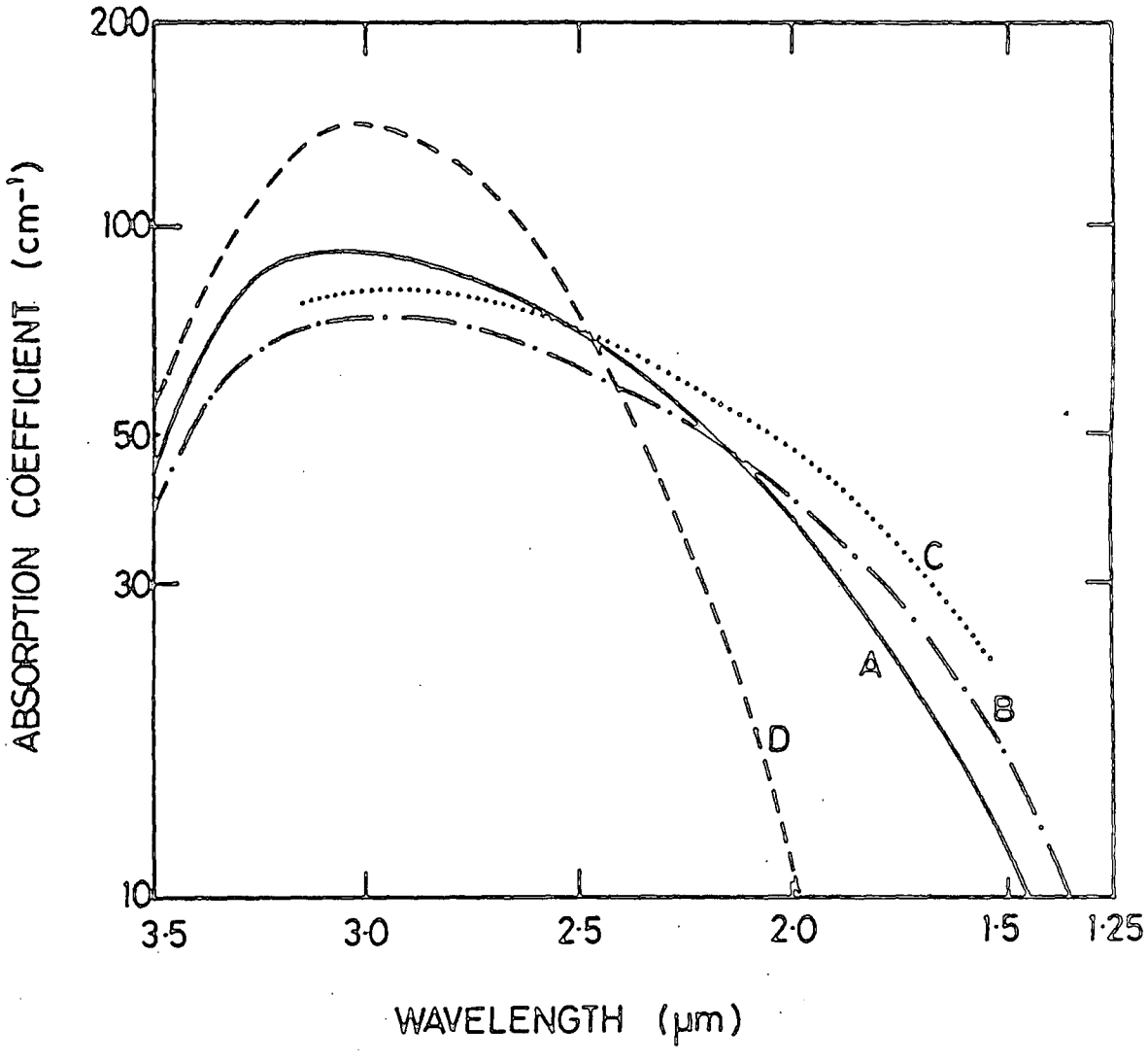

Figure 5.6: IVBA coefficient versus wavelength for GaAs. Results for twenty one and three k-space directions are shown in graphs (A) and (B) respectively. Graph (C) gives the experimental results of Henry et al and (D) represents a simple effective mass model.

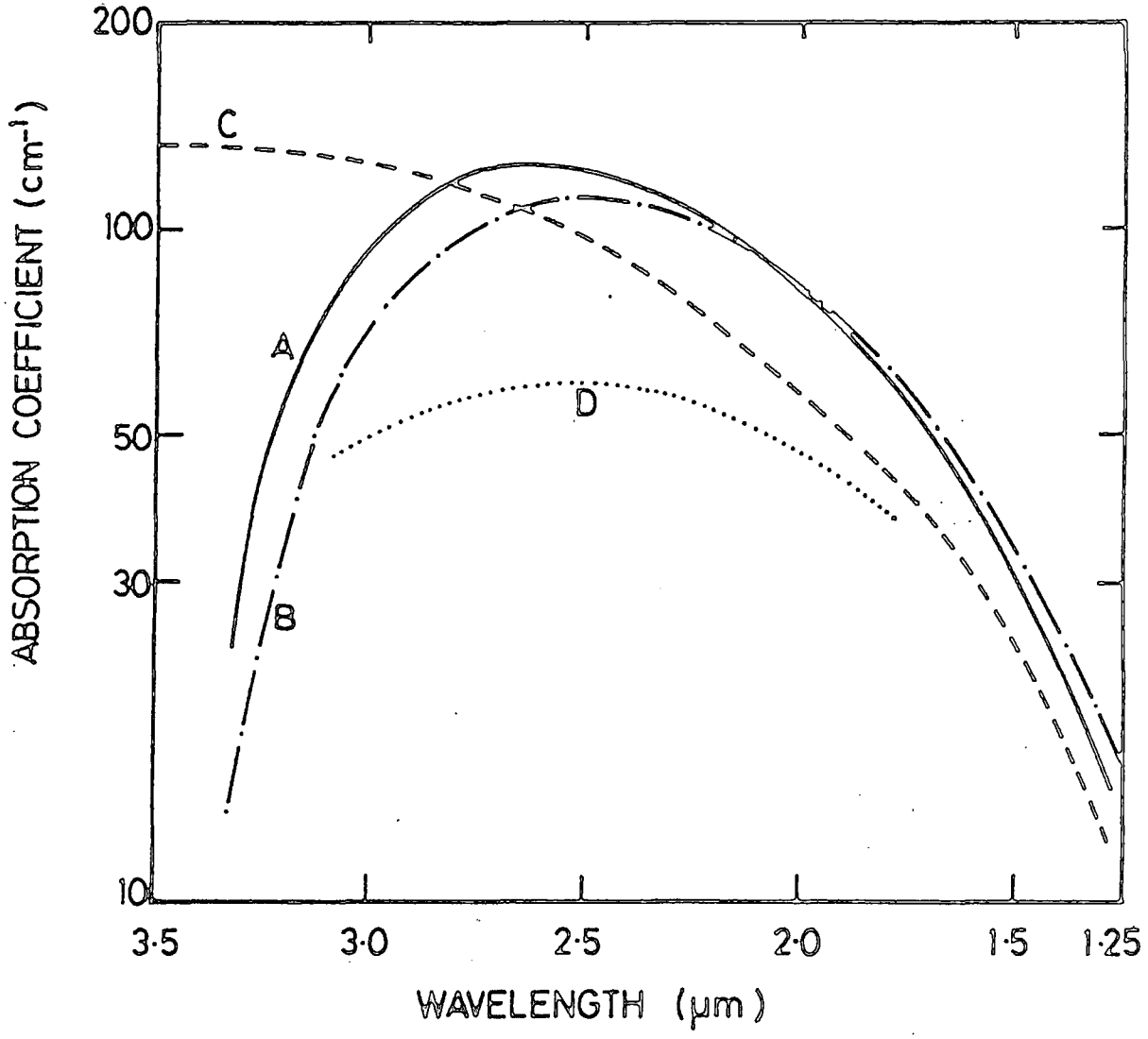

Figure 5.7: Graphs (A) and (B) show IVBA coefficients for $Ga_{0.47}\ In_{0.53}\ As$ for twenty one and three k-space directions respectively. Graph (C) shows results for $Ga_{0.28}\ In_{0.72}\ As_{0.6}\ P_{0.4}$ and (D) the experimental results of Henry et al for $Ga_{0.47}\ In_{0.53}\ As$.

coefficient (α (2l-D) = 39 cm^{-1} at λ = 1.6 μm). Results for the absorption coefficient as a function of wavelength (2l-D) for the quaternary material at the same temperature and hole concentration as used in the previous materials are also shown in figure (5.7). The relatively small spin splitting value (Δ = 0.26 eV) and larger band gap than the ternary material, results in lower absorption at the band gap energy (α (2l-D) = 13 cm^{-1} at λ = 1.3 μm) than is found in the ternary material.

5.6.2. Temperature Dependence

Calculated results (2l-D) of absorption coefficient versus temperature at the band gap wavelength for $Ga_{0.28}\ In_{0.72}\ As_{0.6}\ P_{0.4}$ and $Ga_{0.47}\ In_{0.53}\ As$ are shown in figure (5.8) (band gap wavelength absorption in GaAs is negligible at all temperatures considered). The ternary material exhibits a gradual increase in absorption coefficient with temperature with a decrease occurring for T > 350 K. This change occurs due to changes in the hole population as carriers are distributed further down the heavy hole band hence increasing the probability of high energy transitions and reducing the number of low energy transitions. The number of holes available for transitions at a given heavy hole energy level will hence show an initial increase with temperature then a decrease. This effect is not seen in the quaternary material which shows an initial rapid increase in absorption coefficient with temperature, the rate of increase falling at high temperatures. This again results from the large difference in energy between the band gap and the spin splitting parameter causing band gap energy transitions to take place well down the heavy hole band and ensuring much higher temperatures are needed before the carrier distribution changes can produce a negative

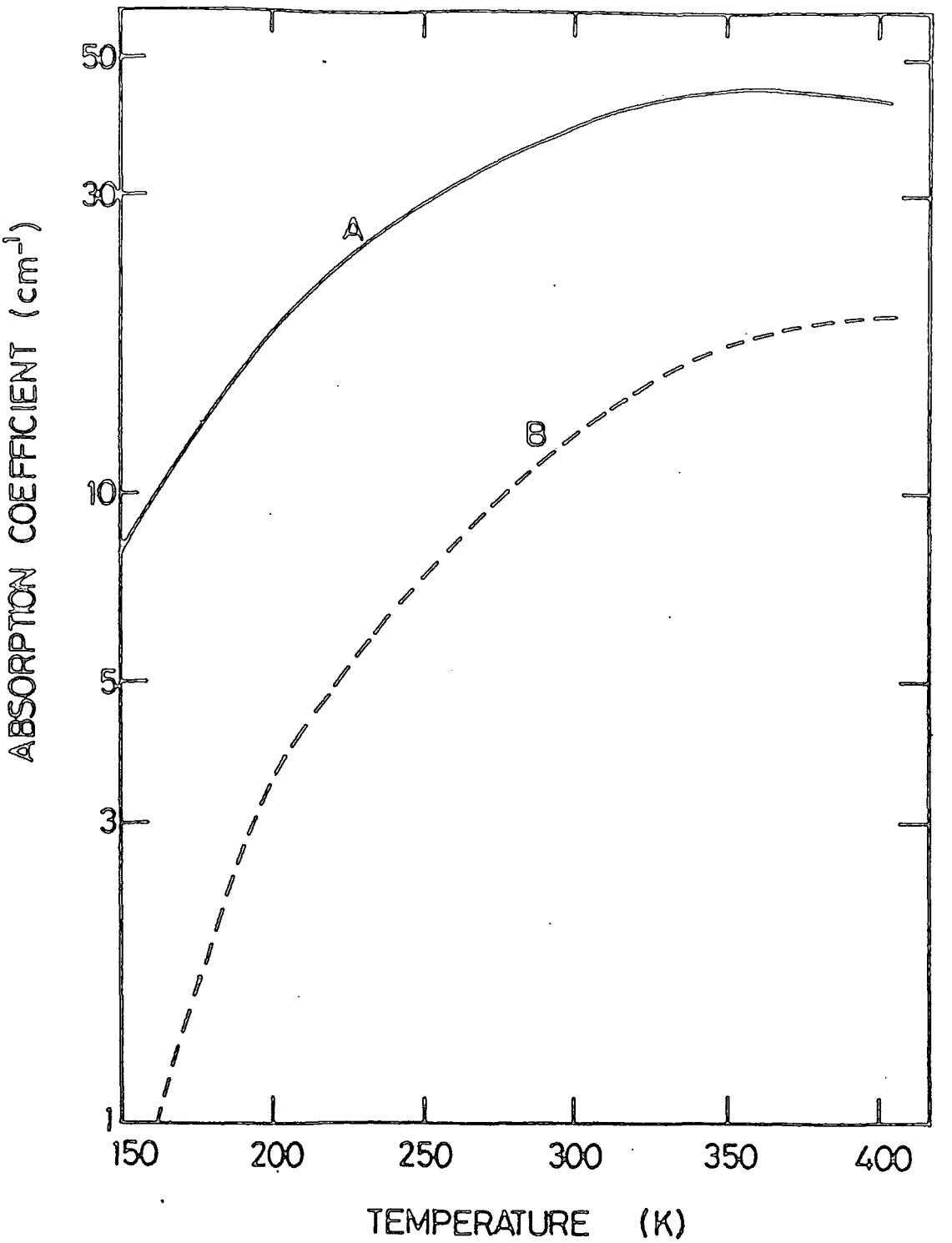

Figure 5.8: The temperature variation of IVBA coefficients for $Ga_{0.47}In_{0.53}As$ (graph (A)) and $Ga_{0.28}In_{0.72}As_{0.6}P_{0.4}$ (B) at wavelengths corresponding to their respective band gaps.

temperature coefficient of absorption. However, the absorption at the band gap energy in this material is small and would seem unable to contribute significantly to the total laser loss. The results for $Ga_{0.47}\ In_{0.53}\ As$ compare well with those of Takeshima (1984b). However, his use of a differently averaged bandstructure, and momentum matrix elements derived in the $\underline{k}\cdot\underline{p}$ method results in the temperature coefficient of absorption becoming negative at a lower temperature ($\simeq$ 250 K) than the present calculation.

5.6.3. Concentration Dependence

The concentration dependence of absorption coefficient at a given energy is found to be approximately linear for all the materials considered in the range $p = 7.5 \times 10^{17}\ cm^{-3} - 3 \times 10^{18}\ cm^{-3}$.

5.7. Summary

The wavelength, temperature, and concentration dependence of IVBA coefficients for three semiconductor laser materials have been evaluated using Chelikowsky and Cohen (1976) pseudopotential bandstructure and momentum matrix elements evaluated along twenty one $\underline{k}$ space directions in an irreducible segment of the Brillouin zone. Results obtained using only three $\underline{k}$ space directions compare well with the 21-D results but a simple parabolic, isotropic, effective mass approximation gives much smaller band gap energy absorption coefficients than the pseudopotential calculation. The temperature dependence of IVBA coefficients at wavelengths relevant to optical fibre transmission has been shown to be either small or where rapid variation does occur, the absorption itself is small.

CHAPTER 6

SUPERLATTICE AND QUANTUM WELL STRUCTURES

6.0. Introduction

Having described calculations of intervalence band absorption in bulk semiconductors a similar analysis is now performed for quantum well heterostructures. The optical losses produced by IVBA transitions can be an important intrinsic loss mechanism in quantum well lasers and as such these losses are evaluated for a single quantum well structure using several different bandstructure models.

The work in this chapter is concerned with the derivation of the electronic bandstructure and momentum matrix elements for the relevant optical transitions in quantum wells. The IVBA losses using this derived bandstructure together with corresponding losses derived using SEMA and pseudopotential bandstructures are evaluated in the next chapter.

6.1. Superlattices and Quantum Wells - Basic Theory

A conventional superlattice structure is composed of alternate layers (some 10 - 1000 Å thick) of two semiconductors. The materials are usually closely lattice matched to reduce strain at the layer interfaces. In the type I superlattice of interest in the present problem the band gap of one of the materials (say B) is larger than that of the other (say A) and the conduction and valence band edges in A lie within the band gap of B. This difference in band gap produces attractive potential wells for electrons in the conduction band and holes in the valence band (figure 6.1a), which act to restrict carrier motion in the direction perpendicular to the superlattice planes (the super-

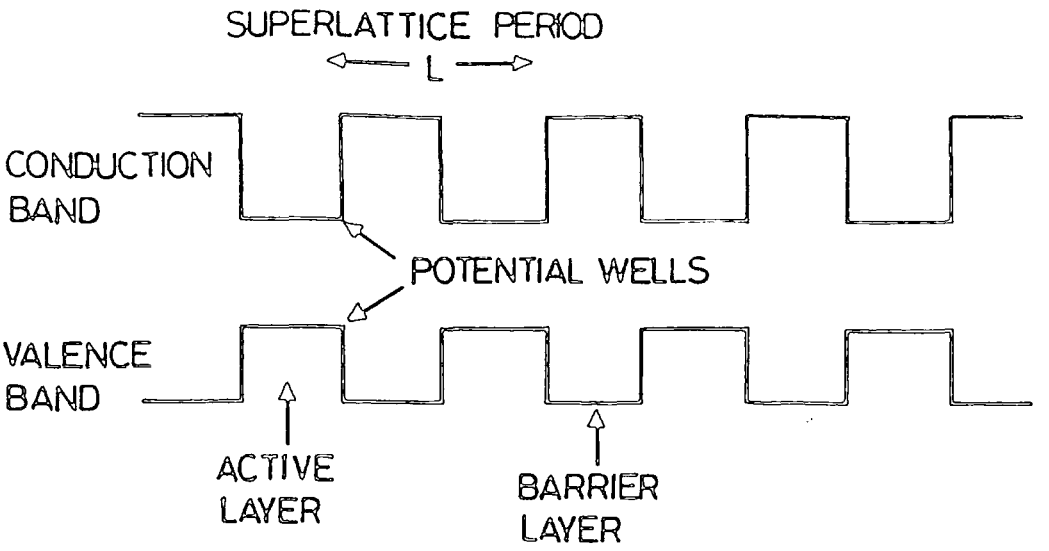

Figure 6.1a: The variation in bulk band edge energies forming the potential wells in a type I superlattice structure.

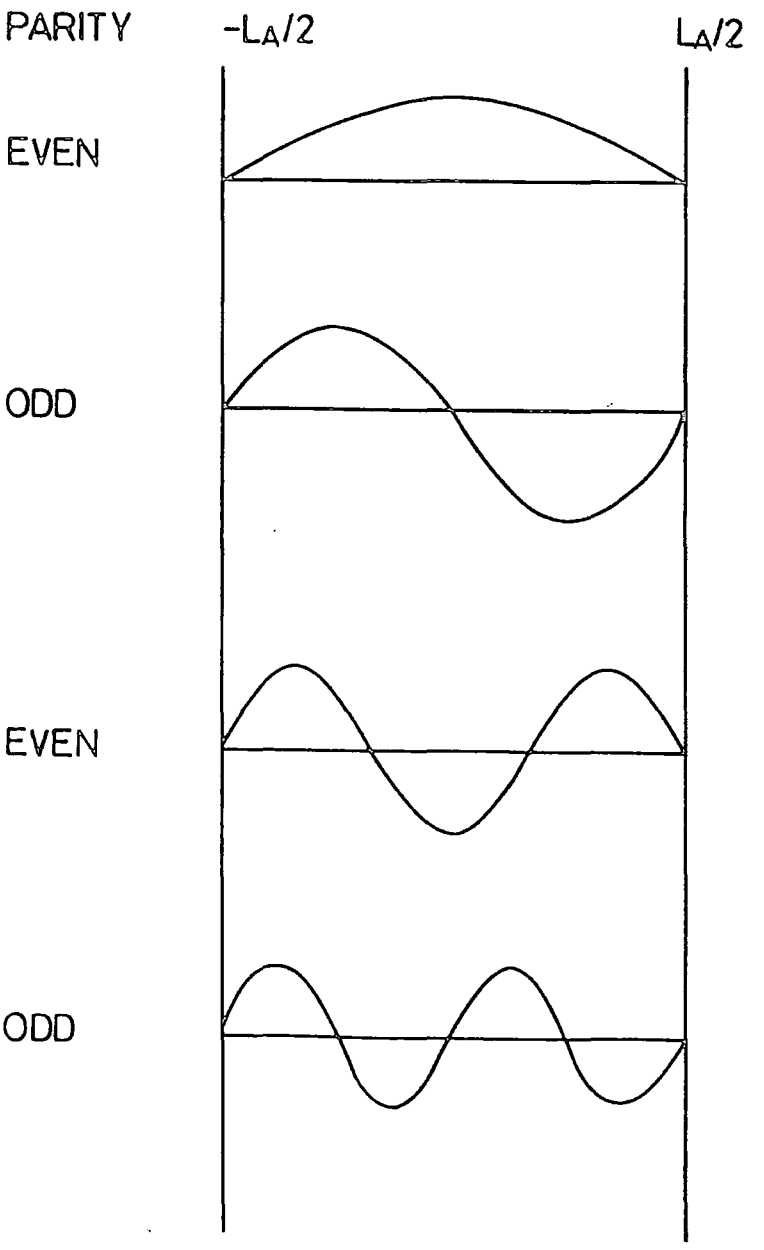

Figure 6.1b: The parity of the first four bound state wave functions for an electron confined to an infinite square well potential.

lattice direction - chosen as z). If a carrier is in a layer A and has an energy below that of the barrier presented by B and the width of layer A, L_A is less than the carrier de Broglie wavelength, quantisation of the particle motion in the z direction occurs, with motion in the layer planes remaining free. A series of quantised energy levels $E_n = \frac{\hbar^2 k_{zn}^2}{2m}$ (n is the nth bound state) for motion in the z direction is then produced, where to the simplest approximation k_{zn} is given by the solution of the infinite one dimensional well problem as $k_{zn} = \frac{\pi n}{L_A}$. Hence the allowed states form a series of sub-bands with edges defined by the E_n and energy dispersion relations for free motion in the x and y directions given by the simple effective mass model: $E = \frac{\hbar^2 k_{ll}^2}{2m}$ where $k_{ll}^2 = k_x^2 + k_y^2$, the total energy of a particle in state $\underline{k_{ll}}$ of the nth sub-band is then given by $E = E_n + \frac{\hbar^2 k_{ll}^2}{2m}$.

In optical emission carrier transitions can take place between conduction and valence sub-bands, the energy of the emitted photon (neglecting exitonic effects) being given by:

$$E = E_g + E_{cn} + E_{v\ell} + \frac{\hbar^2 k_{ll}^2}{2m_c} + \frac{\hbar^2 k_{ll}^2}{2m_v} \qquad (6.1)$$

where E_{cn} and $E_{v\ell}$ are the energies of the nth conduction and the ℓth valence sub-band edges (see figure 6.2) respectively, and m_c and m_v are the corresponding effective masses.

The form of a typical carrier wavefunction produced by the well confinement in the z-direction is a product of a slowly varying envelope function F(z) and a rapidly oscillating Bloch periodic part. In its simplest form for a quantum well of infinite depth the envelope function takes the form of a simple sine or cosine:

$$F(z) = \cos\left(\frac{n\pi x}{L_A}\right) \qquad n = 1,3,5,\ldots$$

$$= \sin\left(\frac{n\pi x}{L_A}\right) \qquad n = 2,4,6,\ldots \qquad (6.2)\ .$$

The cosine terms have even and the sine terms odd parity about the well centre; the first two envelope functions of each parity are illustrated in figure 6.1b. The definite parity and orthogonality of these functions results in a selection rule $\Delta n = 0$ for interband transitions (i.e. transitions are allowed between sub-bands $1 \rightarrow 1$, $2 \rightarrow 2$ etc). A full calculation for a finite quantum well shows that this rule is not generally valid and so called 'forbidden transitions' can be significant, as found for intervalence band transitions near the sub-band edges in the $\underline{k}\cdot\underline{p}$ model derived in this chapter. However, fundamental interband transitions and intervalence band transitions away from the band edge for which $\Delta n = 0$ still provide the dominant contributions to optical spectra. Expression (6.1) for the energies of emitted photons due to interband transitions must therefore be modified by the Δn selection rule. However, the energies of the remaining allowed transitions can be tuned by the variation of either the composition of the barrier material (altering the depth of the quantum wells) or the well width L_A (altering the carrier kinetic energy). An example of this compositional tuning is found in a $GaAs/Ga_{1-x}A\ell_x As$ superlattice. Where the aluminium content of the barrier material $Ga_{1-x}A\ell_x As$ can be varied resulting in an increase in band gap of $\simeq$ 560 meV at $T = 300$ K when x is changed from 0 to 0.45 (for $x \gtrsim 0.45$ the band gap is indirect). Variation of well width produces a more marked change in sub-band energies, well widening causing an increase in the number of sub-bands corresponding to confined states and a shift in their energies towards the bulk band edge.

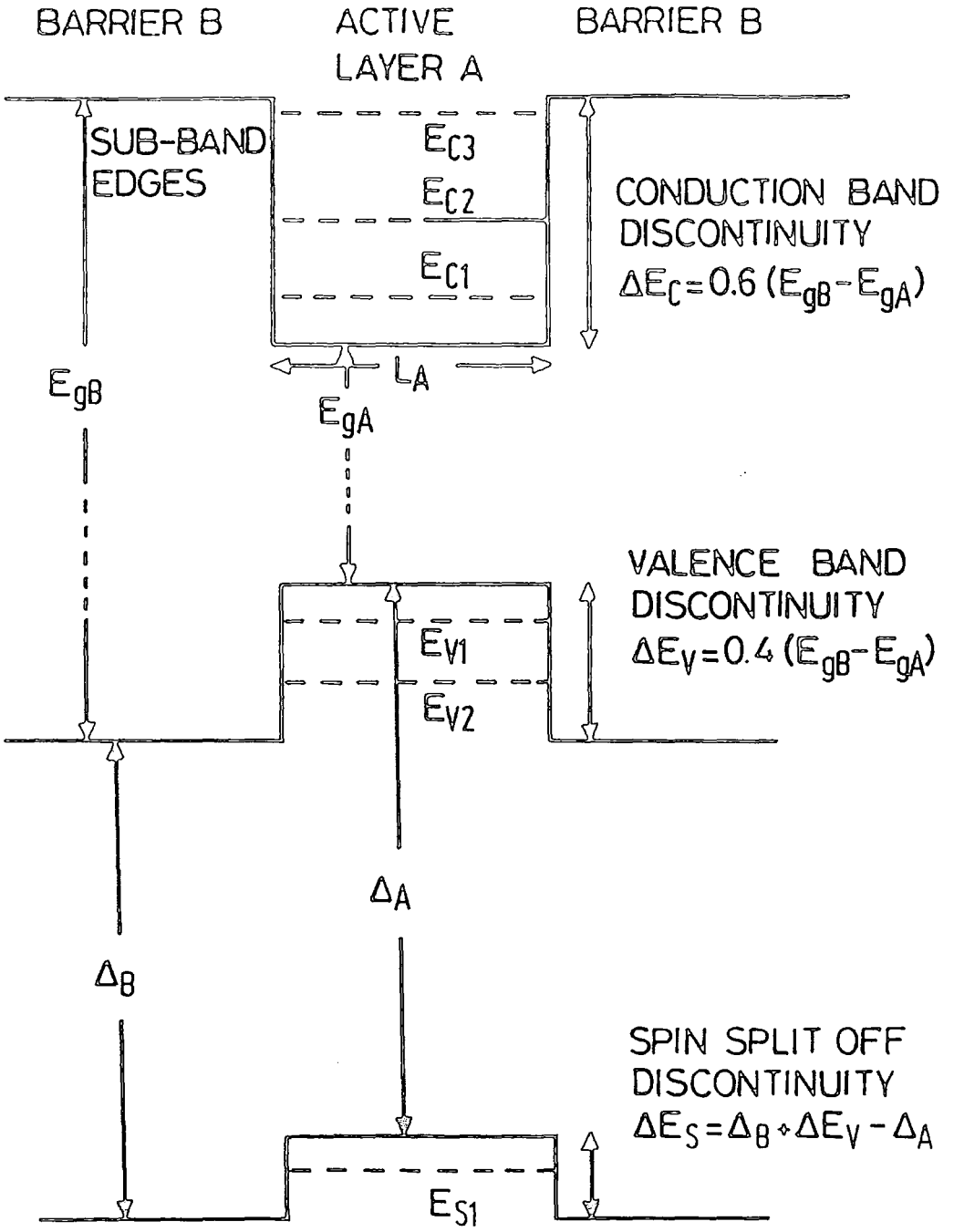

Figure 6.2: The potential wells and energy discontinuities in a super-lattice system with a 60/40 split in the band gap difference between materials A and B.

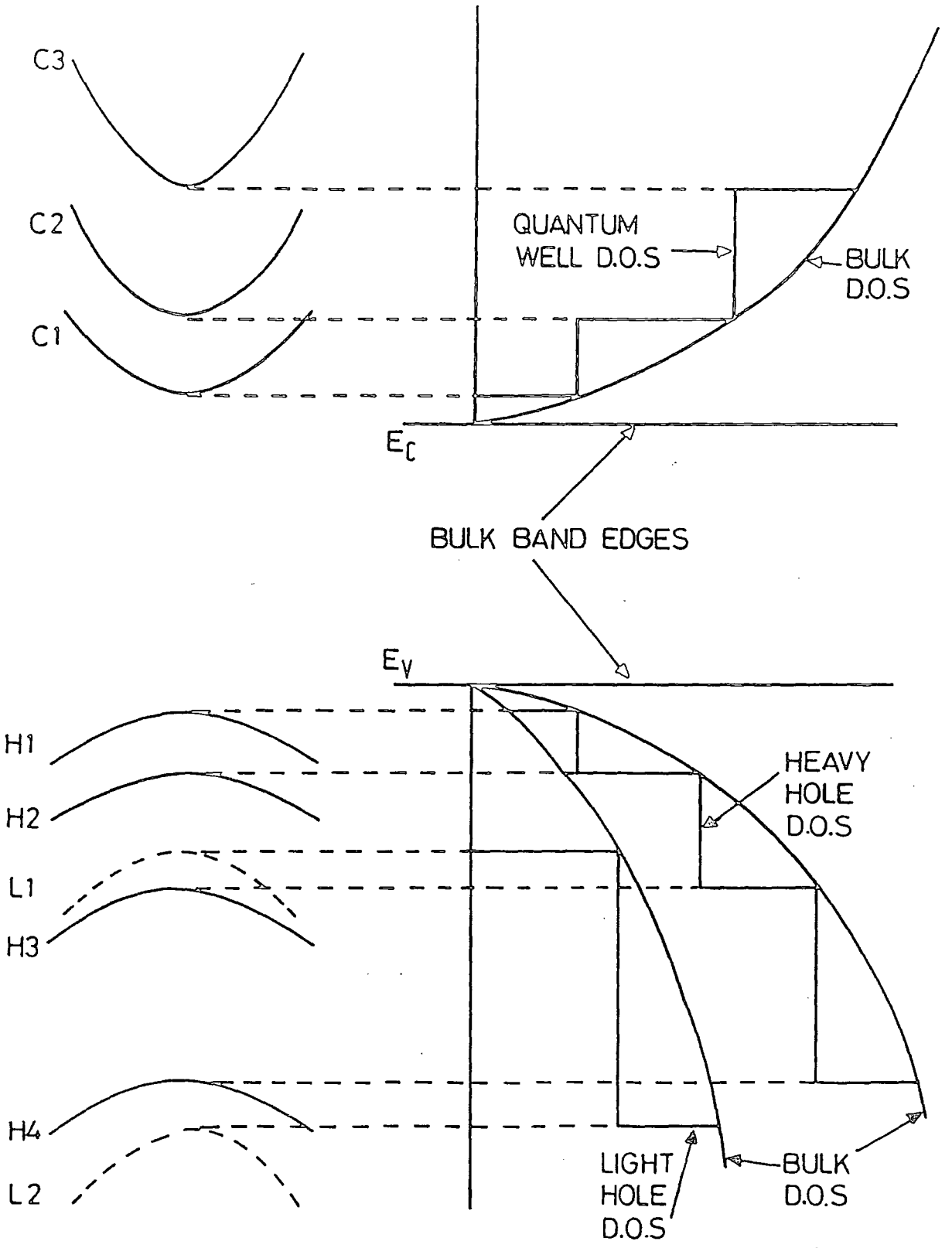

Figure 6.3: The step like form of the density of states produced in a quantum well structure, and compared with the density of states for bulk material in both conduction and valence bands.

Additional changes in the position and structure of the sub-bands can be made by reducing the width of the barrier material to give large coupling between adjacent wells. Each of the single well levels then splits into N closely spaced levels (where N is the number of wells) forming an essentially continuous band for large N as first discussed by Kronig and Penney (1931).

The depth of a quantum well in a given band is determined by the relative positions of the band edges in materials A and B. Early papers (Dingle et al 1974/75) gave the conduction band discontinuity ΔE_c (the well depth) as 85% of the band gap difference ($\Delta E_c = 0.85\ (E_{gB} - E_{gA})$) in a $GaAs/Ga_{1-x}\ A\ell_x\ As$ structure with x varying between 0.19 and 0.27. However, the trend in more recent papers (Batey et al 1985, and Miller et al 1984) is towards a 60/40 split (ΔE_c = 60% gap difference) in this structure, with different ratios occurring in other material systems. As the position of the sub-band levels is dependent on the well depth, any physical properties predicted using calculated energies for sub-bands, will be dependent on the choice of band offsets. In addition to the valence band edge energies the depth of the potential well in the spin split-off band is also dependent on the choice of splitting and is given by reference to figure (6.2) as:

$$\Delta E_S = \Delta_B + \Delta E_V - \Delta_A \qquad (6.3)$$

where Δ_A and Δ_B are the spin splitting parameters in A and B respectively.

The energy-wavevector dispersion relation for the system determines the form of the density of states function g(E). In a single quantum well and in the simplest effective mass model the density of states in all bands takes the form of a step or staircase function (as shown in figure (6.3)).

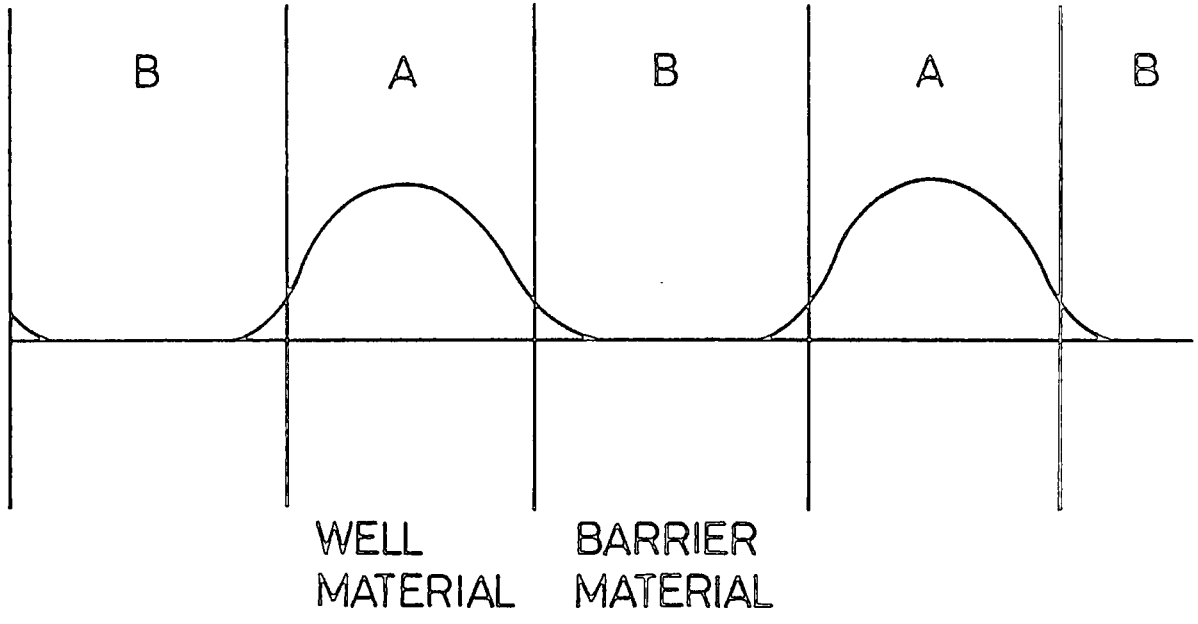

Figure 6.4: The envelope function of the ground state in an irregular superlattice, showing the continuity of the wave function at the A - B interface.

The discussion in this section has largely related to the simple effective mass model of superlattice and quantum well structures. In the next section a method for providing a more realistic approximation to the band structure in type I superlattices is considered. The dispersion relationships and the corresponding density of states derived from the calculation, differ in detail from the simple model, however there are some general similarities.

6.2. Derivation of Superlattice Bandstructure

6.2.1. Introduction

The technique described below gives the $E - \underline{k}$ relationship for $\underline{k}$ parallel to the well-barrier interface (in-plane $\underline{k}$) for a single quantum well superlattice. The approach adopted is to consider a superlattice, with barrier layers thick enough to essentially decouple adjacent wells so giving negligible $E - \underline{k}$ dispersion in the superlattice direction. The method is easily extended to superlattices with thin barriers and strongly coupled wells by a simple modification to the trial wave function and this procedure is outlined later. The periodic nature of the superlattice means we need only consider one period comprising a single well of material A and an adjacent barrier of material B and apply periodic boundary conditions. The problem then, is to solve the Schrodinger equation

$$\left[\frac{-h^2\nabla^2}{2m_o} + V\right]\psi = \varepsilon\psi \qquad (6.4)$$

where V is the periodic potential of the lattice in materials A or B as appropriate.

The method used to solve this expression is a variational technique derived by Schlosser and Marcus (1963) for the solution of the energy band problem in metals, and extended to the present problem by Altarelli (1983).

6.2.2. The Variational Technique

The standard Rayleigh-Ritz variational technique chooses a trial wave function ψ in terms of some variational parameters.

The expression $\varepsilon = \frac{\langle\psi|H|\psi\rangle}{\langle\psi\psi\rangle}$ where H is the Hamiltonian, is then minimised with respect to each of the variational parameters. The present problem however, is more complicated because we are dealing with two materials, and the wavefunctions in these materials must be matched at the A - B interfaces. Schlosser and Marcus have shown how the boundary conditions can be incorporated into a modified variational technique and their general method can be applied to a superlattice as follows (see Altarelli (1983)).

A rectangular box whose surface encloses a volume of the quantum well and barrier material (figure 6.5) is drawn such that S_1 and S_3 are interfaces between adjacent layers of well and barrier materials, S_2 is the interface between A and B materials, S_4, S_5 and S_6, S_7 are chosen to satisfy the cellular boundary conditions

$$\psi_w(\underline{r} + \underline{a},\underline{k}) = e^{i\underline{k}\cdot\underline{a}}\,\psi_w(\underline{r},\underline{k})$$

$$\nabla_n\psi_w(\underline{r} + \underline{a},\underline{k}) = -e^{i\underline{k}\cdot\underline{a}}\,\nabla_n\psi_w(\underline{r},\underline{k}) \qquad (6.5)$$

where ψ_w is the trial wave function in material w (A or B), n is the outward normal on the appropriate surface and a is the distance between opposite faces S_4 and S_5 of the box. Similar conditions

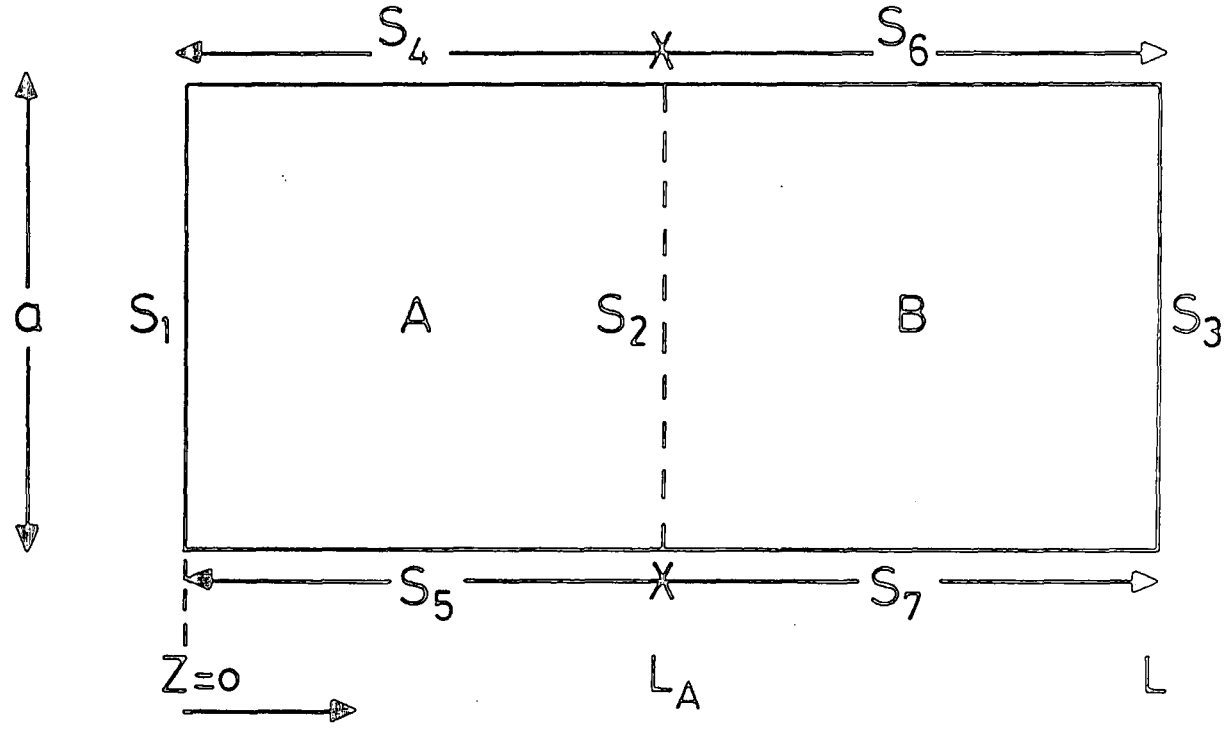

Figure 6.5: The surface surrounding a chosen volume of materials A and B. S_1, S_2 and S_3 are interfaces between adjacent material types. S_4 - S_7 are surfaces subject to the periodic boundary conditions imposed on the trial wave functions.

apply on the remaning parallel surfaces (not shown) on the box. Clearly we could choose $S_4 - S_7$ to be the outer surfaces of the material for which the boundary conditions (6.5) must apply. This choice of boundary conditions for the trial wave function ensures cancellation of some integral terms in the derivation of the variational expression in Appendix 5.

It is shown in Appendix 5 that ε differs only in second order from the true energy when derivations of the wavefunctions from the true functions are first order. The variational solution is therefore obtained by the condition that ε is stationary under independent variation of the parameters in the trial solutions in A and B. The modified variational expression derived in Appendix 5 is then given as

$$\varepsilon \int_{\Omega_{A+B}} \psi^* \psi \, d\Omega = \int_{\Omega_{A+B}} \psi^* H \psi \, d\Omega +$$

$$\frac{1}{4} \int_{S_2} [(\psi_B - \psi_A)(\nabla_n \psi_B^* + \nabla_n \psi_A^*) - (\psi_B^* + \psi_A^*)(\nabla_n \psi_B - \nabla_n \psi_A)] \, dS$$

$$- \frac{1}{4} \int_{S_4} [(\psi_B - \psi_A)(\nabla_n \psi_B^* + \nabla_n \psi_A^*) - (\psi_B^* + \psi_A^*)(\nabla_n \psi_B - \nabla_n \psi_A)] \, dS \qquad (6.6)$$

where ψ_A and ψ_B are trial wave functions in materials A and B respectively, ψ is ψ_A or ψ_B, H is the Hamiltonian in A or B as appropriate, and n is the outward normal on S_2 in material A (i.e. $\nabla_n \equiv \frac{\partial}{\partial z}$) .

The wavefunction continuity conditions at the A - B interface (which provided the necessity for a modified variational expression) are taken care of by the last two terms in equation (6.6).

It should be noted that atomic units for which $\hbar = m_o = 1$ have been used in expression (6.6) and the same prescription will be maintained throughout the remainder of this chapter. In addition the eigenvalue ϵ is shown in Appendix 6 to be always real as equation (6.6) reduces to a sum of conjugate pairs.

6.2.3. Choice of Trial Wave Function

We must now choose a trial wave function for the regions A and B. Following the standard procedure of $\underline{k}\cdot\underline{p}$ perturbation theory (Kane 1957) we can express the wave function of a state $\underline{k}$ in band n in terms of an expansion in the band edge Bloch functions u_j of the bulk material. To reduce the computational effort, wave functions for each material are expanded in terms of only the eight band edge Bloch functions $u_1 - u_8$ (two from each band allowing for spin) derived from the conduction, heavy hole, light hole and spin-split off bands. The effect of other bands on the wave function being accounted for by first order perturbation theory and on the energies by Löwdin (1951) renormalisation. The Bloch function basis states are chosen to diagonalise the spin-orbit interaction and are given as

$$
\begin{aligned}
& \overset{J,\ m_J}{} \\
u_1 &= 1/2 \quad 1/2 \qquad S\uparrow \\
u_5 &= 1/2 \quad -1/2 \qquad S\downarrow
\end{aligned}
\Bigg\} \text{ Conduction Band}
$$

$$
\begin{aligned}
u_2 &= 3/2,\ 3/2 \qquad (X + iY)\uparrow/\sqrt{2} \\
u_6 &= 3/2,\ -3/2 \qquad -(X - iY)\downarrow/\sqrt{2}
\end{aligned}
\Bigg\} \text{ Heavy Hole Band}
$$

$$
\begin{aligned}
u_3 &= 3/2,\ 1/2 \qquad -\sqrt{2}Z\uparrow/\sqrt{3} + (X + iY)\downarrow/\sqrt{6} \\
u_7 &= 3/2,\ -1/2 \qquad -(X - iY)\uparrow/\sqrt{6} - \sqrt{2}Z\downarrow/\sqrt{3}
\end{aligned}
\Bigg\} \text{ Light Hole Band}
$$

$$
\begin{aligned}
u_4 &= 1/2,\ 1/2 \qquad (X + iY)\downarrow/\sqrt{3} + Z\uparrow/\sqrt{3} \\
u_8 &= 1/2,\ -1/2 \qquad -(X - iY)\uparrow/\sqrt{3} + Z\downarrow/\sqrt{3}
\end{aligned}
\Bigg\} \text{ Spin Split Off Band} \qquad (6.7)
$$

The trial wave function for an electron in either material A or B is taken to be of the form

$$\psi = \sum_j u_j(\underline{r})F_j(\underline{z})e^{i\underline{k}_{ll}\cdot\underline{r}_{ll}} + \sum_j \sum_{i\neq j}\left(\frac{k\cdot p_{ij}}{E_j - E_i}\right) u_i(\underline{r})F_j(\underline{z})\ e^{i\underline{k}_{ll}\cdot\underline{r}_{ll}} \qquad (6.8)$$

where the summation over i refers to states in bands other than those forming the basis set (6.7), $\underline{k}_{ll}$ and $\underline{r}_{ll}$ are wavevector and position coordinates in the x - y plane, and $F_j(\underline{z})$ are envelope functions which along with the Bloch periodic parts give the z dependence of the wavefunction.

We are now in a position to evaluate the first term on the right hand side of equation (6.6). Using a wavefunction for material A of the form of equation (6.8) gives

$$\int_{\Omega_A} \psi^* H \psi \, d\Omega = \sum_{jj'} \int_0^{L_A} (F_j^* H^{oA}_{jj'} F_{j'})^A \, dz \qquad (6.9)$$

where $z = L_A$ is the location of the A - B interface shown on figure 6.5. and $H^{oA}_{jj'}$ is the Kane Hamiltonian matrix in which $\underline{k}$ takes its operator form $(\underline{k}_x, \underline{k}_y, -i\partial/\partial z)$. A similar expression can be derived for material B. Note the spin orbit splitting perturbation due to higher bands, the $\underline{k}$ dependent spin orbit splitting and the linear terms due to renormalised perturbations of the form $\sum_i \frac{\langle S|p_x|u_i\rangle\langle u_i|p_y|z\rangle}{(\frac{1}{2}(E_c+E_v)-E_i)}$ are all omitted from the Kane matrix, their values being negligibly small compared to the other energy terms. As a result the matrix possesses Kramer's symmetry and all eigenvalues subsequently derived occur in degenerate pairs.

The terms γ_1, γ_2 and γ_3 used in the Kane matrix are similar to the parameters used by Luttinger (1956) for the perturbations due to higher

bands. However, in the present model the basis states include the conduction band, and its contribuiton is therefore treated exactly, rather than as a perturbing higher band as in Luttinger's evaluation. The contributions of the conduction band are therefore subtracted from the Luttinger terms γ^L in the following way

$$\begin{aligned} \gamma_1 &= \gamma_1^L - \frac{2P^2}{3E_g} \\ \gamma_2 &= \gamma_2^L - \frac{P^2}{3E_g} \\ \gamma_3 &= \gamma_3^L - \frac{P^2}{3E_g} \end{aligned} \tag{6.10}$$

where E_g is the energy gap at $\underline{k} = 0$.

The operator function of $\underline{k}$ correspondingly applies to the first order perturbation expansion used in the trial wave function in A and B layers for the surface integrals in the variational expression (6.6). The explicit version of equation (6.8) for material A is

$$\psi_A = \sum_{j=1,8} e^{i\underline{k}_{11}\cdot\underline{r}_{11}} u_j^A(\underline{r})F_j^A(\underline{z}) + \sum_{j=1,8}\sum_{i\neq j}\left(\frac{\underline{k}\cdot p_{ij}}{E_j - E_i}\right)^A u_i^A(\underline{r})F_j^A(\underline{z})e^{i\underline{k}_{11}\cdot\underline{r}_{11}} \tag{6.11}$$

where $\underline{k} = (\underline{k}_x, \underline{k}_y, -i\partial/\partial z)$, the summation over i refers to the band index subscript (which is not to be confused with the complex number i), and again the spin-orbit coupling between the basis states j and the higher bands is neglected.

6.2.4. Evaluation of the Interface Integrals in Equation (6.6)

Expanding (6.11) gives

U_2	U_3	U_7	U_6	U_4	U_8	U_1	U_5
$E_v-\frac{1}{2}(\gamma_1-2\gamma_2)k_z^2$ $-\frac{1}{2}(\gamma_1+\gamma_2)\cdot(k_x^2+k_y^2)$	$\sqrt{3}(k_x-ik_y)k_z$	$\frac{\sqrt{3}}{2}\gamma_2(k_x^2-k_y^2)$ $-i\sqrt{3}\gamma_3 k_xk_y$	0	$\sqrt{\frac{3}{2}}\gamma_3\cdot(k_x-ik_y)k_z$	$\sqrt{\frac{3}{2}}\gamma_2(k_x^2-k_y^2)$ $-i\sqrt{6}\gamma_3 k_xk_y$	$-\sqrt{\frac{i}{2}}P(k_x-ik_y)$	0
$\sqrt{3}\gamma_2$ $(k_x+ik_y)k_z$	$E_v-\frac{1}{2}(\gamma_1-2\gamma_2)k_z^2$ $-\frac{1}{2}(\gamma_1-\gamma_2)\cdot(k_x^2+k_y^2)$	0	$\frac{\sqrt{3}}{2}\gamma_2(k_x^2-k_y^2)$ $-i\sqrt{3}\gamma_3 k_xk_y$	$-\frac{\gamma_2}{\sqrt{2}}$ $(k_x^2+k_y^2-2k_z^2)$	$-\frac{3}{\sqrt{2}}\gamma_3$ $(k_x-ik_y)k_z$	$i\sqrt{\frac{2}{3}}Pk_z$	$-\frac{iP}{\sqrt{6}}(k_x-ik_y)$
$\frac{\sqrt{3}}{2}\gamma_2(k_x^2-k_y^2)$ $+i\sqrt{3}\gamma_3 k_xk_y$	0	$E_v-\frac{1}{2}(\gamma_1+2\gamma_2)k_z^2$ $-\frac{1}{2}(\gamma_1-\gamma_2)\cdot(k_x^2+k_y^2)$	$-\sqrt{3}\gamma_3$ $(k_x-ik_y)k_z$	$\frac{3}{\sqrt{2}}\gamma_3$ $(k_x+ik_y)k_z$	$-\frac{\gamma_2}{\sqrt{2}}$ $(k_x^2+k_y^2-2k_z^2)$	$\frac{iP}{\sqrt{6}}(k_x+ik_y)$	$i\sqrt{\frac{2}{3}}Pk_z$
0	$\frac{\sqrt{3}}{2}\gamma_2(k_x^2-k_y^2)$ $+i\sqrt{3}\gamma_3 k_xk_y$	$-\sqrt{3}\gamma_3$ $(k_x+ik_y)k_z$	$E_v-\frac{1}{2}(\gamma_1-2\gamma_2)k_z^2$ $-\frac{1}{2}(\gamma_1+\gamma_2)\cdot(k_x^2+k_y^2)$	$\sqrt{\frac{3}{2}}\gamma_2(k_x^2-k_y^2)$ $+i\sqrt{6}\gamma_3 k_xk_y$	$\sqrt{\frac{3}{2}}\gamma_3\cdot(k_x+ik_y)k_z$	0	$\frac{iP}{\sqrt{2}}(k_x+ik_y)$
$-\sqrt{\frac{3}{2}}\gamma_3\cdot(k_x-ik_y)k_z$	$-\frac{\gamma_2}{\sqrt{2}}(k_x^2-k_y^2-2k_z^2)$	$\frac{3}{\sqrt{2}}\gamma_3(k_x-ik_y)k_z$	$\sqrt{\frac{3}{2}}\gamma_2(k_x^2-k_y^2)$ $-i\sqrt{6}\gamma_3 k_xk_y$	$-\gamma_1\frac{k^2}{2}-\Delta$	0	$-\frac{iPk_z}{\sqrt{3}}$	$-\frac{iP(k_x-ik_y)}{\sqrt{3}}$
$\sqrt{\frac{3}{2}}\gamma_2(k_x^2-k_y^2)$ $-i\sqrt{6}\gamma_3 k_xk_y$	$-\frac{3}{\sqrt{2}}\gamma_3$ $(k_x-ik_y)k_z$	$-\frac{\gamma_2}{\sqrt{2}}$ $(k_x^2-k_y^2-2k_z^2)$	$\sqrt{\frac{3}{2}}\gamma_3$ $(k_x-ik_y)k_z$	0	$-\frac{\gamma_1}{2}k^2-\Delta$	$\frac{iP}{\sqrt{3}}(k_x+ik_y)$	$-\frac{iPk_z}{\sqrt{3}}$
$\frac{iP}{\sqrt{2}}(k_x-ik_y)$	$-i\sqrt{\frac{2}{3}}Pk_z$	$-\frac{iP}{\sqrt{6}}(k_x-ik_y)$	0	$\frac{iPk_z}{\sqrt{3}}$	$-\frac{iP}{\sqrt{3}}(k_x-ik_y)$	$\frac{1}{2}k^2+E_c$	0
0	$\frac{iP}{\sqrt{6}}(k_x+ik_y)$	$-\sqrt{\frac{2}{3}}P(k_x-ik_y)$	$-\frac{iP}{\sqrt{2}}(k_x-ik_y)$	$\frac{iP}{\sqrt{3}}(k_x+ik_y)$	$\frac{iPk_z}{\sqrt{3}}$	0	$\frac{1}{2}k^2+E_c$

Figure 6.6: The Kane matrix derived from the band edge Bloch basis states for a bulk material.

See Appendix 10 for an enlarged version of this figure

$$\psi_A = \sum_j e^{i\underline{k}_{ll}\cdot\underline{r}_{ll}} u_j^A F_j^A + \sum_j \sum_{i\neq j} i\left(\frac{k_x P_{ij}^x + k_y P_{ij}^y}{E_j - E_i}\right)^A F_j^A u_i^A e^{i\underline{k}_{ll}\cdot\underline{r}_{ll}}$$

$$+ \sum_j \sum_{i\neq j}\left(\frac{P_{ij}^z}{E_j - E_i}\right)^A u_i^A \frac{\partial F_j^A}{\partial z} e^{i\underline{k}_{ll}\cdot\underline{r}_{ll}} \qquad (6.12)$$

where $P_{ij}^x = -ip_{ij}^x = \int_{\Omega_{cell}} u_i^* \left(\frac{-\partial}{\partial x}\right) u_j$, etc. and for brevity the z and $\underline{r}$ dependences of F and u have been omitted. Subtitutions of this equation into the surface integrals found in the variational expression (6.6) yields expressions involving products of Bloch periodic parts. To remain within the spirit of $\underline{k}\cdot\underline{p}$ theory these products are integrated over a unit cell at the interface. It is further assumed that the Bloch function periodic parts are the same for materials A and B. As the envelope functions vary little over a unit cell, they assume their values at the appropriate interface, and the integrals over Bloch function periodic parts are equal to paramters defined in $\underline{k}\cdot\underline{p}$ theory.

The detailed evaluation of the unit cell integrals is given in Appendix 7 from which we obtain the following expressions:

$$\int_{S_2} (\psi_A^* \nabla\psi_A - \psi_A \nabla\psi_A^*) dS = 2 \sum_{jj'} \left\{ F_j^* D_{jj'}^{zz} \frac{\partial F_{j'}}{\partial z} - F_{j'} D_{jj'}^{zz} \frac{\partial F_j}{\partial z} \right\}^A$$

$$+ 2 \sum_{jj'} F_j^{A*} [ik_y (D_{jj'}^{zy} + D_{jj'}^{yz})^A + ik_x (D_{jj'}^{xz} + D_{jj'}^{zx})^A - P_{jj'}^z] F_{j'}^A, \qquad (6.13)$$

$$\int_{S_2} (\psi_B^* \nabla\psi_A - \psi_A \nabla\psi_B^*) dS = 2 \sum_{jj'} [F_j^{B*} \frac{\partial F_{j'}^A}{\partial z} D_{jj'}^{Azz} - F_{j'}^A \frac{\partial F_j^{B*}}{\partial z} D_{jj'}^{Bzz}]$$

$$+ 2 \sum_{jj'} F_j^{B*} [ik_y (D_{jj'}^{Azy} + D_{jj'}^{Byz}) + ik_x (D_{jj'}^{Azx} + D_{jj'}^{Bxz}) - P_{jj'}^z] F_{j'}^A, \qquad (6.14)$$

where $D^{\alpha\beta}_{jj'} = \frac{\delta_{jj'}\delta_{\alpha\beta}}{2} + \sum_i \frac{p^{\alpha}_{ji}\, p^{\beta}_{ij'}}{E_{j'}-E_i}$ (6.15) .

Similar terms are formed for the remaining integrals by interchanging labels A and B

Note the $D^{\alpha\beta}_{jj'}$ are found in the Kane matrix of figure (6.6) which is of the form:

$$H^{o}_{jj'} = \sum_{\alpha\beta = x,y,z} D^{\alpha\beta}_{jj'}\, k_\alpha k_\beta + \sum_{\alpha = x,y,z} p^{\alpha}_{jj'}\, k_\alpha + E_{j'}\delta_{jj'} \qquad (6.16) .$$

No dependence of P on A or B is shown in the above expressions as the Bloch function periodic parts used in its evaluation are assumed to be the same in both materials.

An expression for the remaining normalisation term on the left hand side of the variational equation (6.6) is now derived, using the wave-function expression (6.8).

6.2.5. The Normalisation Term

The remaining term to be evaluated in the variational expression (6.6) is $\varepsilon \int_{\Omega_{A+B}} \psi^*\psi d\Omega$. Substitution of the trial wave functions into this expression yields an expression in terms of integrals over the envelope functions:

$$\varepsilon \int_{\Omega_{A+B}} \psi^*\psi d\Omega = \varepsilon \left[\sum_j \int_0^{L_A} F^{A*}_j F^{A}_j \, dz + \sum_j \int_{L_A}^{L} F^{B*}_j F^{B}_j \, dz \right] \qquad (6.17) .$$

A full derivation of this result is given in Appedix 8.

We must now consider the form of the envelope functions F_j used in the trial wave function.

6.2.6. The Envelope Function Expansion

Bloch's theorem requires that the envelope functions have the full periodicity of the superlattice (period L), and it is therefore convenient to express each F_j in terms of a Fourier series. The number of terms used in the expansion must be sufficiently large to provide a good representation of the envelope function, but too many terms requires excessive computational time in solving the variational expression. As such, an expansion in terms of thirteen basis states (a constant, 6 sines and 6 cosines) is used.

$$F_j^A = \frac{a_o}{2} + \sum_{\ell=1}^{6} a_{\ell j} \cos \frac{2\pi \ell z}{L} + \sum_{\ell=7}^{13} a_{\ell j} \sin \frac{2\pi(\ell-6)z}{L} \qquad (6.18)$$

$$F_j^B = \frac{b_o}{2} + \sum_{\ell=1}^{6} b_{\ell j} \cos \frac{2\pi \ell z}{L} + \sum_{\ell=7}^{13} b_{\ell j} \sin \frac{2\pi(\ell-6)z}{L} \qquad (6.19)$$

If the barrier thickness is reduced resulting in stronger coupling between adjacent wells the sub-band structure may then have significant dispersion in the z-direction. This dispersion is determined by multiplying the envelope terms F_j by a plane wave term $e^{ik_z z}$ where k_z is a wavevector in the superlattice Brillouin zone such that $(-\pi/L < k_z < \pi/L)$.

All terms in the variational expression (6.6) have now been evaluated and we must now consider the solution of this expression.

6.2.7. Solution of the Variational Expression

Each term of equation (6.6) has already been expressed in terms of envelope functions F_j^A, F_j^B etc. Use of equation (6.18) and (6.19) in these gives an equation, all terms of which are a product of a Fourier expansion coefficient (e.g. $a_{\ell j}$) and the complex conjugate of an expansion coefficient (e.g. $a^*_{\ell' j'}$)

$$\sum_{jj'} \sum_{\ell\ell'} a'^{*}_{\ell j} a'_{\ell' j'} (H^{1}_{jj'\ell\ell'} + H^{2}_{jj'\ell\ell'} - \varepsilon D_{jj'\ell\ell'}) = 0 \qquad (6.20) .$$

Here $a'_{\ell j}$ represents either $a_{\ell j}$ or $b_{\ell j}$, $H^{1}_{jj'\ell\ell'}$ represents terms from the Hamiltonian (first term on the right hand side of equation (6.6)), $H^{2}_{jj'\ell\ell'}$ represents terms from the interface integrals and $D_{jj'\ell\ell'}$ represents the normalisation terms. The variational character of energy ε means that equations for the coefficients $a'_{\ell j}$ and $a'^{*}_{\ell j}$ can now be obtained by the condition that ε is stationary as a function of the finite set of coefficients. Hence linear equations for the $a'_{\ell' j'}$ are obtained by differentiating with respect to the $a'^{*}_{\ell j}$. The linear equations can then be solved by matrix diagonalisation; the matrix in general is non-Hermitian. However we have proved quite generally in Appendix 6 that only real values of ε are valid solutions of expression (6.6) and it is convenient to cast the problem into a form that ensures real ε. Equation (6.20) is added to its complex conjugate (which is also variational) and the sum is then halved. On taking the j dependence as implicit the resulting expression gives:

$$\sum_{\ell\ell'} a'^{*}_{\ell} a'_{\ell'} \left[\frac{(J_{\ell\ell'} + J^{*}_{\ell'\ell})}{2} - \varepsilon \frac{(D_{\ell\ell'} + D^{*}_{\ell'\ell})}{2} \right] = 0 \qquad (6.21)$$

where $J_{\ell\ell'} = H^{1}_{\ell\ell'} + H^{2}_{\ell\ell'}$.

As the above sum is still variational, differentiation w.r.t. a'^{*}_{ℓ} yields a system of linear equations of the form:

$$\sum_{\ell'} a'_{\ell'} \left[\frac{(J_{\ell\ell'} + J^{*}_{\ell'\ell})}{2} - \varepsilon \frac{(D_{\ell\ell'} + D^{*}_{\ell'\ell})}{2} \right] = 0 \qquad (6.22) .$$

These equations have non-trivial solutions if

$$\det \left| \frac{(J_{\ell\ell'} + J^*_{\ell'\ell})}{2} - \varepsilon \frac{(D_{\ell\ell'} + D^*_{\ell'\ell})}{2} \right| = 0 \qquad (6.23) \ .$$

The solution of this will now yield only real eigenvalues due to the Hermitian nature of the terms.

The J matrix can be seen to fall into 4 blocks corresponding to the various combinations of the expansion coefficients:

$$\left(\begin{array}{c|c} a^*_{\ell j} \, a_{\ell' j'} & a^*_{\ell j} \, b_{\ell' j'} \\ \hline b^*_{\ell j} \, a_{\ell' j'} & b^*_{\ell j} \, b_{\ell' j'} \end{array} \right) \qquad (6.24) \ .$$

Each of these main blocks can be further subdivided into 64 small blocks corresponding to matrix elements involving the Bloch functions u_j and $u_{j'}$. For $j = 1 - 8$ and $j' = 1 - 8$. The upper left and lower right blocks contain terms due to the Kane Hamiltonian matrices (figure (6.6)) for material A and B respectively, plus terms from the interface integrals. The other blocks contain interface integral terms only.

Thus symbolically

$$J = \left(\begin{array}{c|c} H^1 + H^2 & H^2 \\ \hline H^2 & H^1 + H^2 \end{array} \right) \qquad (6.25) \ .$$

The D matrix is real and contains terms only in the upper left and lower right blocks and only for $j = j'$ but it should be noted that it is not a unit matrix. The system of linear equations (6.21) thus takes the matrix form

$$JX = \varepsilon DX \qquad (6.26)$$

where X is the vector formed from the a'_ℓ coefficients, and J and D are square matrices of dimension 208 × 208. As D is not a unit matrix, evaluation of (6.26) requires the use of NAG routine Fϕ2 GJF for solution of a generalised eigenvalue problem.

6.3. Results and Discussion

6.3.1. Introduction

The solution of expression (6.30) demands considerable amounts of c.p.u. time on a large mainframe computer due to the large dimensions (208 × 208) of the complex square matrices J and D. With the limitation on computer facilities the sub-band structures and momentum matrix elements for a single well width in only one superlattice system have been determined. In view of the considerable attention devoted to the $GaAs/Ga_{1-x}Al_xAs$ quantum well system in heterostructure studies the bandstructure for this system has been evaluated using the material parameters listed in table 6.1. The relatively wide $Ga_{1-x}Al_xAs$ barrier layers (200 Å) essentially decouples adjacent wells giving negligible $E - \underline{k}_z$ dispersion and the in-plane bandstructure corresponds to that found in a single quantum well.

6.3.2. Bandstructure

The solution of equation (6.26) for a given wavevector $\underline{k}_{11}$ in the layer plane produces 104 doubly degenerate (i.e. 208) eigenvalues. Of these solutions only a small number (usually less than 15 degenerate pairs) correspond to the bound state solutions for carriers confined to the quantum well regions. For example in the 100/200 Å well/barrier system considered in the present work there are 6 doubly degenerate heavy and light hole confined states and 2 doubly degenerate states in both the

Table 6.1: Parameters used in Bandstructure Evaluation

Parameter	GaAs	Ga_{1-x} Al_x As
Percentage Aluminium content	-	30% (x = 0.3)
Material width	100 Å	200 Å
Band Gap E_g (eV)	1.424	$1.424 + 1.247x$ [a]
Spin orbit splitting Δ (eV)	0.34	$0.34 - x(0.34 - 0.275)$ [a]
P (a.u) [b]	0.636	0.636
γ_1^L [c]	6.85	3.45
γ_2^L [c]	2.1	0.68
γ_3^L [c]	2.9	1.29

The ratio of conduction to valence band discontinuity is taken as $\Delta E_c/\Delta E_v = 60/40$.

References

(a) Casey and Panish (1978) and Adachi (1985).

(b) Alavi and Aggarwal (1978) give P for GaAs,, the same value is assumed for the alloy material.

(c) Altarelli and Ekenberg (1985).

the conduction and spin split off wells for a given value of $\underline{k}_{11}$. The remaining solutions correspond to unbound states of the conduction and valence bands. The unbound states are not studied here but it should be recognised that their energies are likely to show considerable dependence on the wavevector component k_z. In contrast and as explained earlier bound state energies will have a negligible dependence on k_z because of the lack of significant coupling between wells for these states. The relevant bound states of the system are obtained by examination of the relative amplitudes of the wavefunctions in regions A and B and the form of the appropriate envelope parts of the wavefunction. Some spurious solutions where the variational wavefunctions show poor matching at the interfaces are also rejected by examining the relative magnitudes of the energy contribuiton from the interface matching conditions and the Kane matrix terms.

The sub-band dispersion for bound states with $\underline{k}_{11}$ in the [100] and [110] directions are shown in figures (6.7) (with predominant heavy and light hole character) (6.8) (with predominant conduction band character) and (6.9) with predominant spin split-off character). The spin split-off and conduction sub-bands are almost parabolic in nature and approximate closely to the effective mass theory sub-bands obtained using $m_X = 0.15\ m_o$ and $m_c = 0.067\ m_o$. In addition in each case the dispersion along the two k_{11} directions differs little. The only obvious comparison that can be drawn between simple effective mass theory results and those illustrated in Figure 6.7 for the heavy and light hole sub-bands is the approximate n^2 relationship in the energies of the heavy hole sub-band edges. Unlike the simple uncoupled band calculation these sub-bands have a distinctly non-parabolic E - $\underline{k}_{11}$ dispersion resulting from band mixing. The small energy separation between some of these sub-bands causes distinct band bending effects and anticrossing behaviour. This is particularly noticeable between sub-bands H1 and L1 at

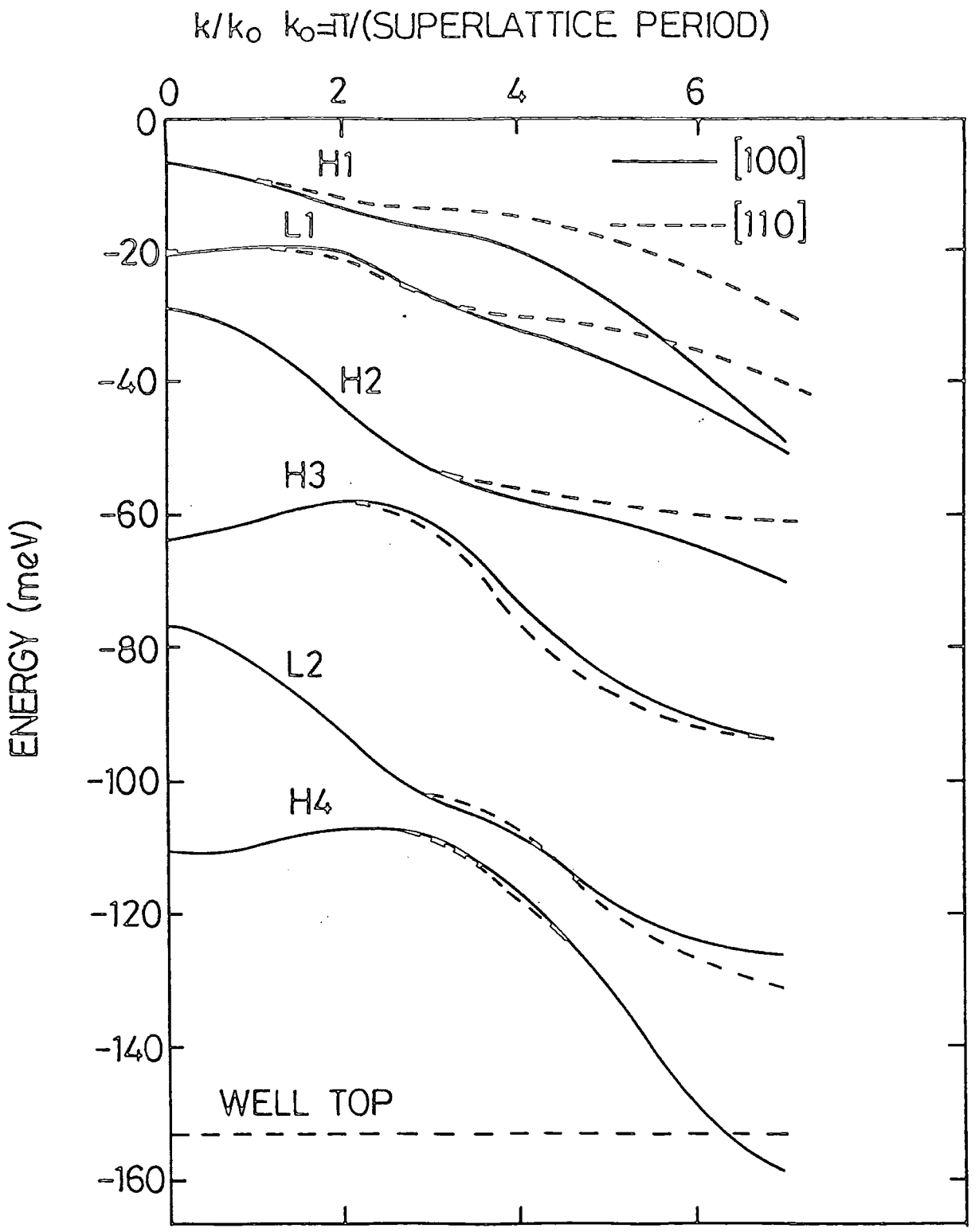

Figure 6.7: The heavy and light hole sub-band dispersion derived for in-plane wavevectors in the [100] and [110] directions.

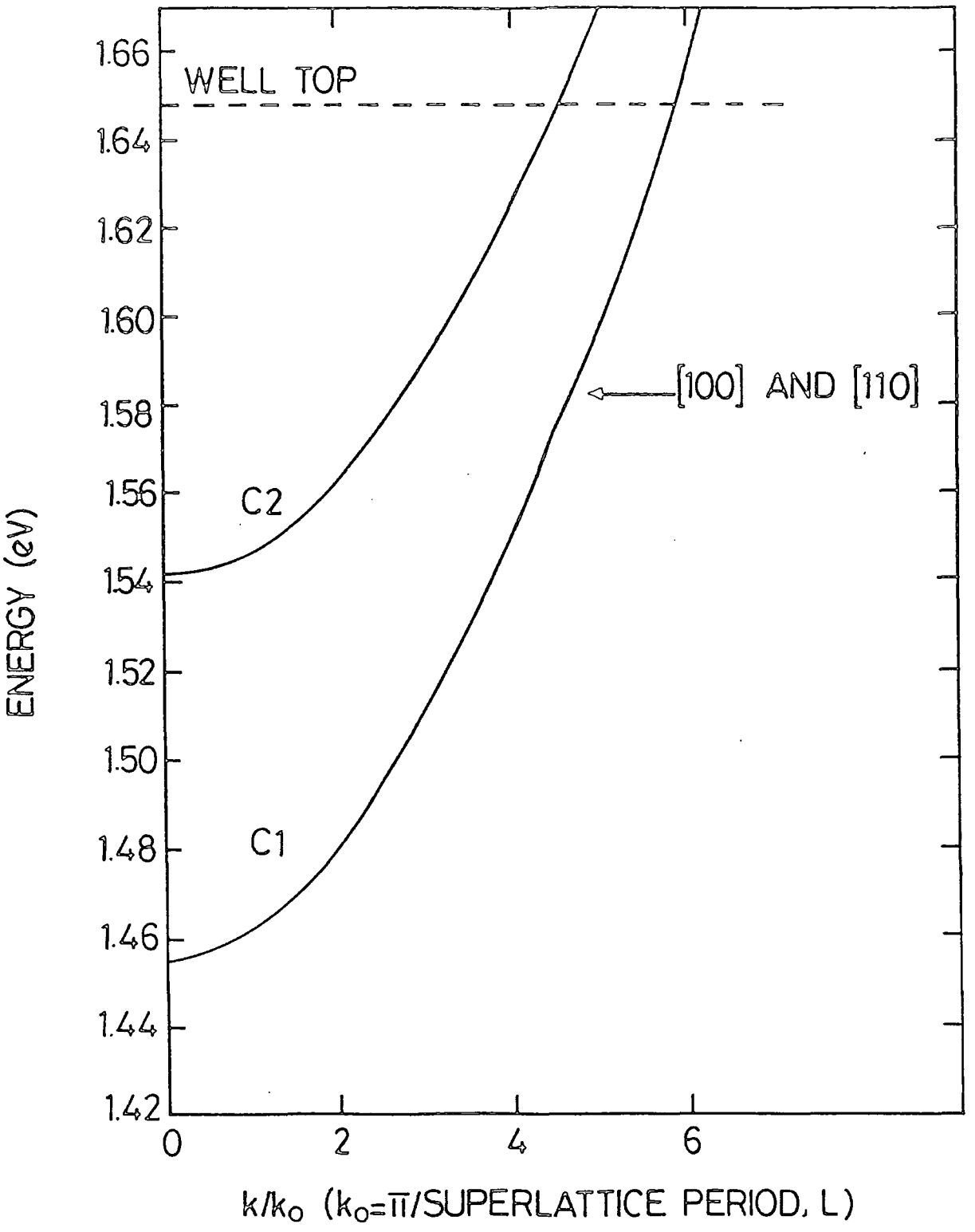

Figure 6.8: The conduction sub-band dispersion derived for in-plane wavevectors in the [100] and [110] directions. No significant energy difference is found in the two directions over the range of k_{11} shown.

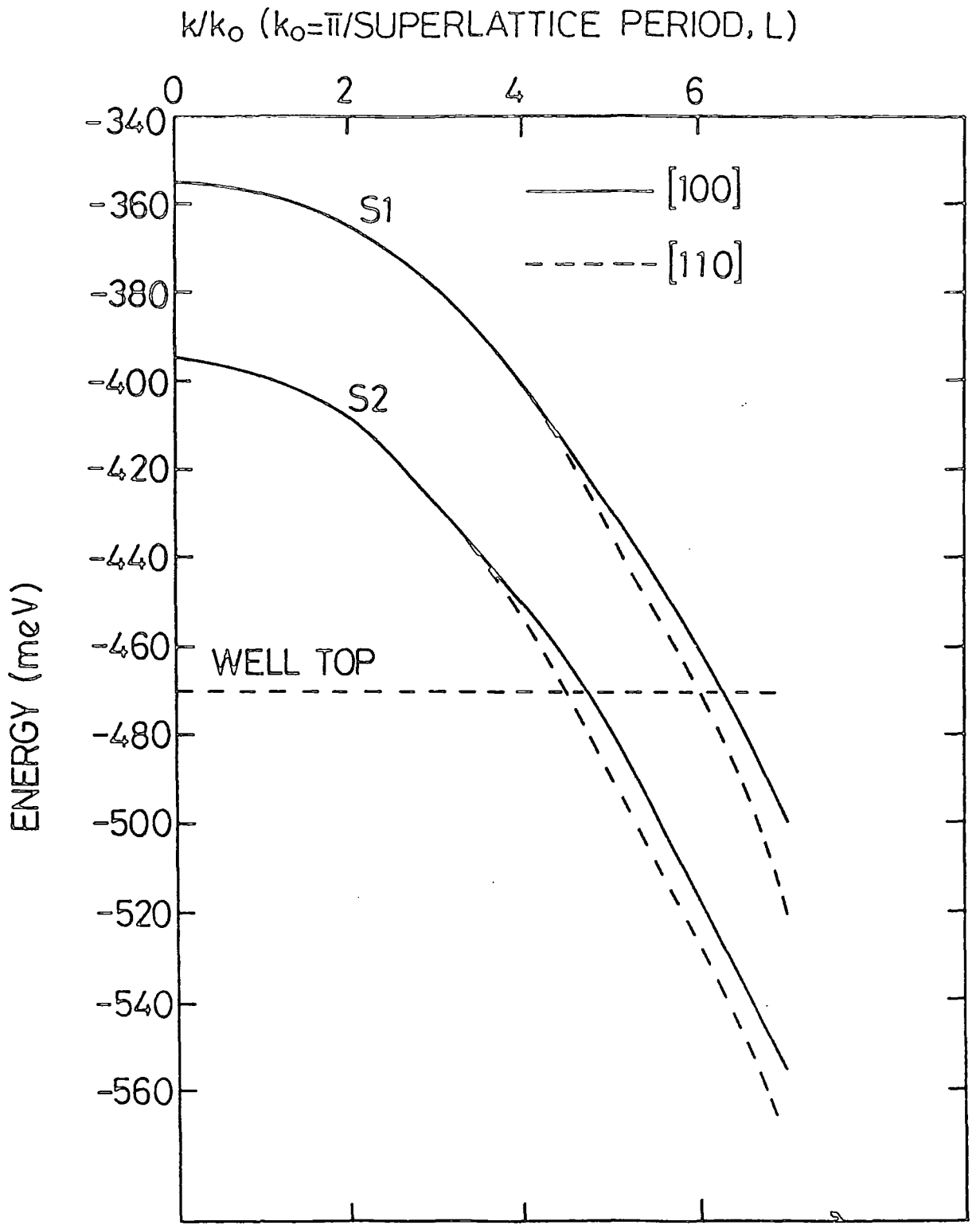

Figure 6.9: Dispersion of the spin split-off sub-bands for in-plane wavevectors in the [100] and [110] directions.

$\underline{k}_{11} \approx 2\underline{k}_{o}$ ($k_o = \pi/300$ Å) and subbands H2 and H3 at $\underline{k}_{11} \approx 3\underline{k}_{o}$ at which points the hole effective mass in bands L1 and H3 is seen to change sign. These results are in excellent agreement with those derived from a pseudopotential complex bandstructure calculation by Monaghan et al (1986) and in good quantitative agreement with the results of Sanders and Chang (1985) derived using a two band $\underline{k}\cdot\underline{p}$ model. It should be noted here that the absence of similar effects in the conduction and spin split-off bands results from the small inter-sub-band coupling.

The non-parabolic nature of the heavy and light hole sub-bands has marked effects on their density of states and corresponding hole occupancy. The most noticeable and important difference (relevant to optical transitions) between this bandstructure and a simple effective mass model occurs in the first light hole sub-band which exhibits a much larger density of states in the present model. These changes and their effects on the IVBA transition are discussed in detail in the next chapter.

Band mixing affects not only the energy of a given state but produces significant changes in the state wavefunction. The change in character of a band wave function with increasing in-plane wave vector $\underline{k}_{11}$ and the resulting effects on the optical transition matrix elements is discussed in the next section.

6.3.3. Wavefunctions and Momentum Matrix Elements

6.3.3 a) Preliminary Discussion

The determinantion of absorption coefficients such as those due to the intervalence band absorption transitions evaluated in the next chapter require knowledge of the momentum matrix elements as a function of in-plane ($\underline{k}_{11}$) wavevector and the dispersion relations of the sub-bands.

The value of these matrix elements at a given k_{ll} is dependent on the form of the wavefunctions of the initial and final states of the transition. Therefore, in the next section we examine the nature of the wavefunctions for relevant transitions and relate these to the magnitude of the derived matrix element.

In view of the periodicity of the superlattice structure it is sensible to normalise the state wavefunctions to a single period (a well with an adjacent barrier). The normalised wavefunction of equation (6.8) ignoring terms from higher bands is shown in Appendix 8 to be

$$\psi = \left(\frac{N\Omega_{cell}}{A}\right)^{1/2} \sum_j F_j u_j e^{i\underline{k}_{ll}\cdot\underline{r}_{ll}} \tag{6.27}$$

where $N^{1/2}$ is the normalisation factor for the envelope terms such that

$$N \sum_j \int_0^L F_j^* F_j \, dz = 1 \tag{6.28}$$

and A is the area of the layer plane.

It is also shown in appendix 8 that the same normalisation factor is correct to first order for the wave function including the effects of higher bands.

The normalised perturbed wavefunction can then be used in the determination of momentum matrix elements for the optical transitions. Expressions for the matrix elements for transitions between the spin split-off and heavy hole sub-bands (the corresponding expressions for transitions to the light hole band is given by replacing subscript H with L) are derived in appendix 9. This is done for radiation polarised in both the x-direction and the z-direction. In the IVBA calculations of chapter 7 and the remainder of the chapter the matrix elements are evaluated assuming the radiation is polarised in the in-plane

x direction which corresponds to a quantum well laser operating in the TE mode. The resulting expression for the momentum matrix elements is given by equation (A9.16) as

$$M_x = (N_H N_S)^{1/2} \delta_{o,\underline{k}_{llH}-\underline{k}_{llS}} \sum_j \sum_{j'} [\langle F^*_{jH} F_{j'S}\rangle [iP^x_{jj'} + 2k_x D^{xx}_{jj'} + k_y (D^{xy}_{jj'} + D^{yx}_{jj'})] - \langle F^*_{jH} \frac{\partial F_{j'S}}{\partial z}\rangle iD^{xz}_{jj'} + \langle \frac{\partial F^*_{jH}}{\partial z} F_{j'S}\rangle iD^{zx}_{jj'}] \quad (6.29)$$

where $\langle F^*_{jH} F_{j'S}\rangle$ implies integration over the length L_A of region A.

6.3.3. b) Transitions Between the Spin Split-Off and Heavy/Light Hole Sub-Bands at $\underline{k}_{ll} = 0$

Examination of the Kane matrix figure (6.6) indicates that at the band edge ($k_{ll} = 0$) the heavy hole band is completely decoupled from all other bands whereas the light hole and spin split off bands are coupled by the k_z operator. The wavefunction of a bound state therefore consists of either a single HH component or components from each of the other three bands in the basis set, one of which may give the dominant contribution to the state. Examination of the wavefunction components therefore provides the means of associating a derived eigenvalue with a particular sub-band. The envelope functions of the dominant component of each wavefunction (at $\underline{k}_{ll} = 0$) take the form appropriate to the quantum number n of the sub-band. Ideal examples of this for an infinite square well potential are shown in figure (6.1b). In the present model the finite depth of the potential well allows some penetration of the wavefunction into the barrier material as shown in figures 6.10a and 6.10b for the suitably normalised envelope functions of sub-bands H1 and H2. It should be noted that the periodicity of these

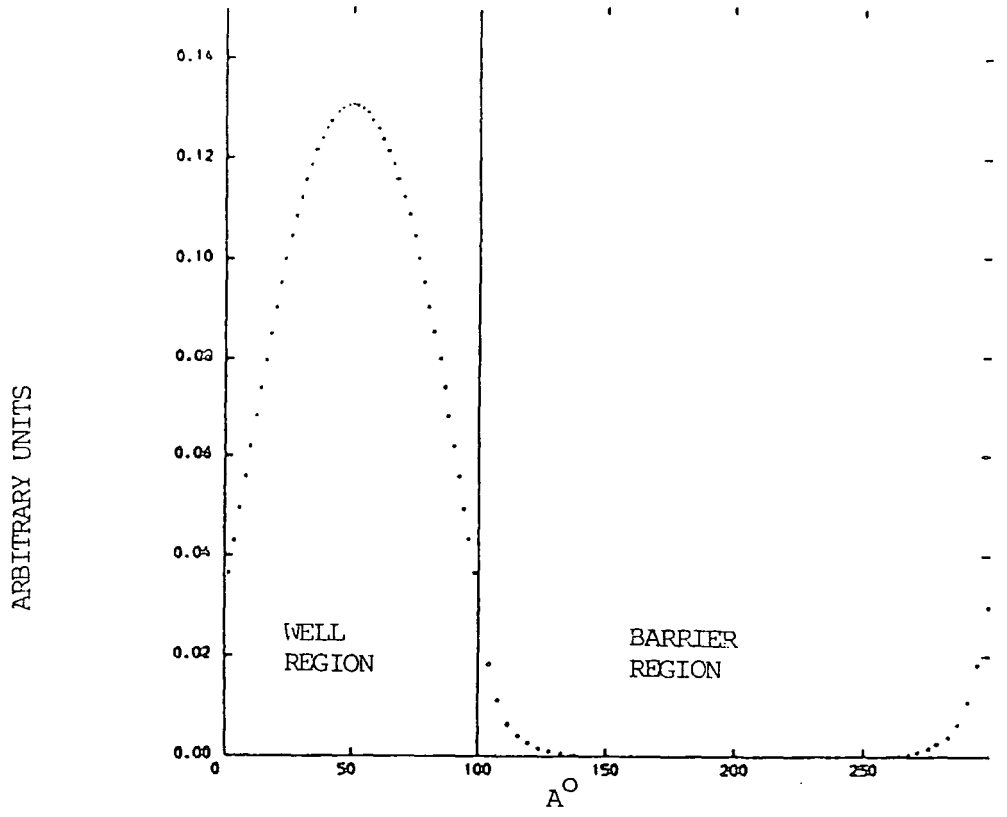

Figure 6.10a: The even parity envelope function of the heavy hole component of the sub-band H1 (at $k_{11} = 0$) showing the periodicity of the wavefunction.

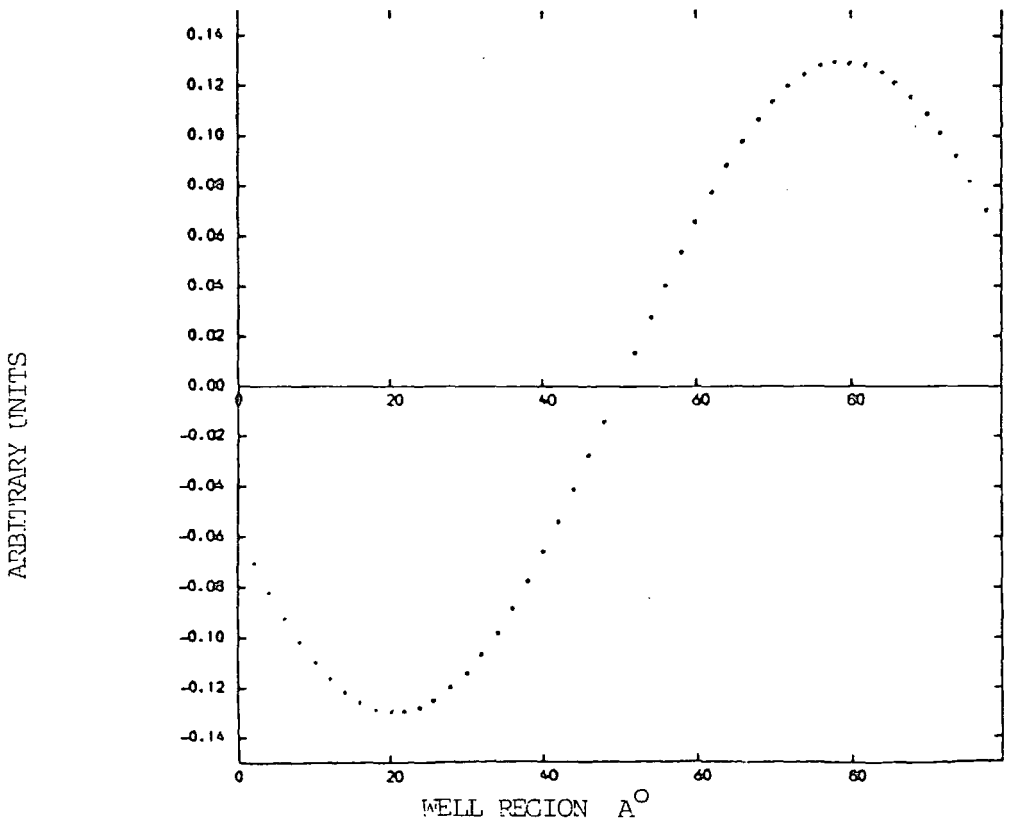

Figure 6.10b: The odd parity envelope function of the heavy hole component of sub-band H2 at $k_{11} = 0$.

functions is reflected in the behaviour of the function in figure 6.10a at the R.H.S. of the barrier material.

This straightforward situation however is found not to hold for the envelope function of the spin split-off component of sub-band S1 (the first spin split-off sub-band). This envelope function (shown in figure 6.11a), although of definite parity is seen to have distinct secondary peaks. These peaks result from a coupling-in of the SS component of an unbound light hole state (see Figure 6.11 b) occurring some 8meV higher in energy than the bound SS state. The relatively large SS component of this unbound state appears to perturb the corresponding component of the bound S1 state producing an envelope function of the form shown in figure 6.11a. Similar perturbations of the SS envelope function in sub-bands S1 and S2 occur for $\underline{k}_{11} \neq 0$ and while the relevant parity of the SS envelope function is retained these perturbations clearly have some effect on the value of momentum matrix elements derived for transitions to or from these sub-bands.

The parity of the envelope function of the smaller components of Bloch functions coupled-in with the dominant contributions of the LH, SS and C sub-bands can be determined by examination of the Kane matrix figure (6.6). Taking for example the light hole Bloch function u_3, at $\underline{k}_{11} = 0$ this is coupled with an even parity envelope function of the SS Bloch function u_4 and an odd parity envelope function from the conduction band Bloch function u_1. Similar couplings are found in the conduction and SS sub-bands. The wavefunction of a degenerate state in sub-band L1 is therefore composed of a dominant LH component with an even parity envelope function (n = 1) coupled with small amounts of SS and C band components with even and odd parity envelope functions respectively.

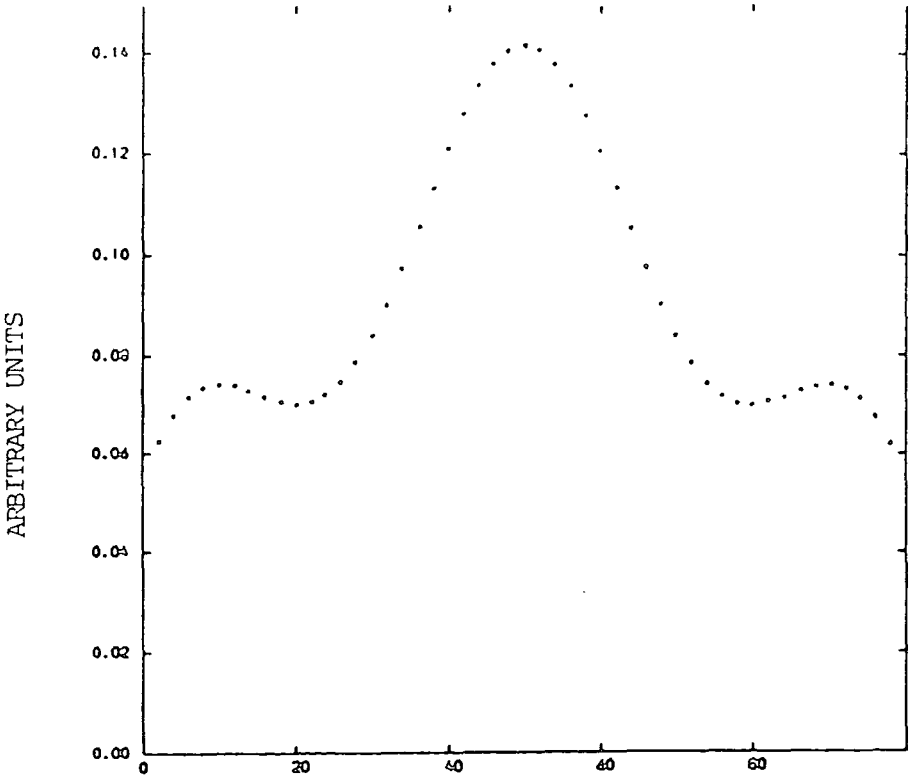

Figure 6.11a.

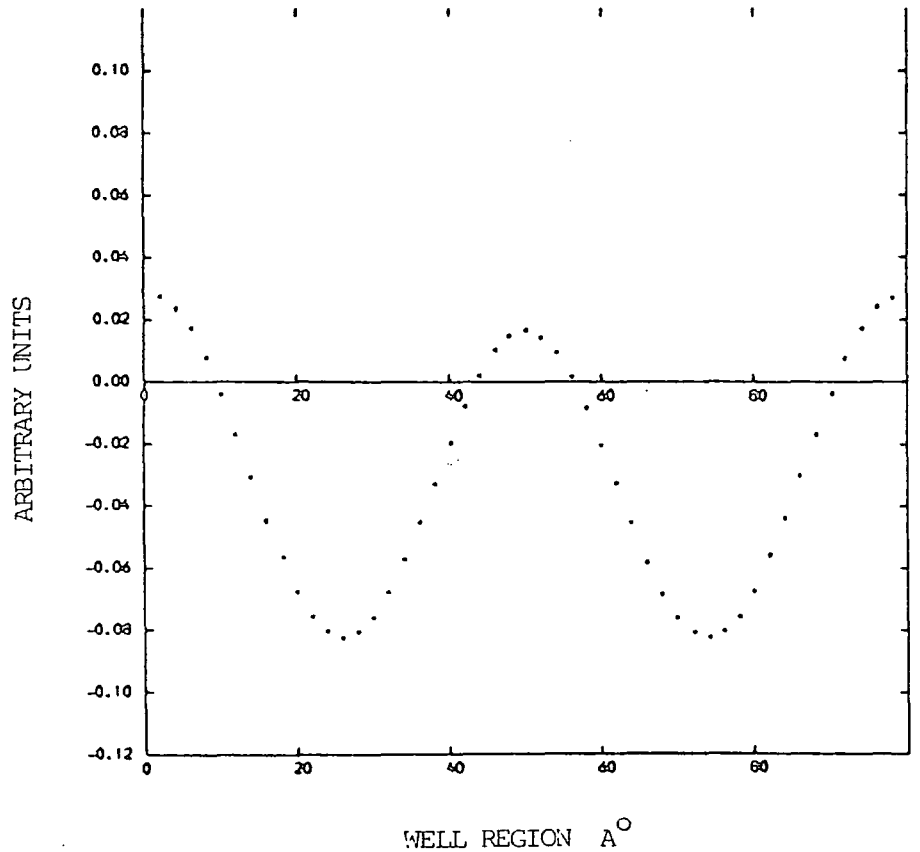

Figure 6.11b.

Figures 6.11a & b: The even parity envelope function (figure (a)) of the spin split-off component of sub-band S_1, with the coupled-in spin split-off component (figure (b)) of an unbound state with a dominant light hole component.

As we shall see this coupling of different parity envelope functions results in a $\Delta n = 1$ selection rule for SS to HH or LH transitions at $\underline{k}_{ll} = 0$.

The dominant terms in the matrix element expression (6.29) are of the form $P^{x}_{jj'}$, arising from the coupling of orbital (Bloch function periodic parts at the band edge) wavefunctions of s and p like symmetry. These terms are multiplied by the overlap integrals of the envelope term $\langle F_j F_{j'} \rangle$ and their contributions are therefore negligibly small for envelope functions F_j and $F_{j'}$ of opposite parity. As the heavy hole sub-band states are of purely p like symmetry at the band edge, terms of the form $P^{x}_{jj'}$, for transitions from SS to HH sub-bands at the band edge only arise due to small amounts of conduction band s like orbital mixed into SS states. However this s-like orbital has an envelope function of opposite parity to the dominant SS component. Hence the envelope function overlap integral between HH and SS sub-bands with the same quantum number n (and hence the same parity envelopes) is small, close to $\underline{k}_{ll} = 0$. The contributions from other terms in the matrix element expression (6.29) are generally quite small and as a result transitions from the SS to HH sub-bands for which $\Delta n = 0$ are small. However, transitions for which $\Delta n = 1$ are possible due to the equal parity of the envelope function of the HH band (sub-band quantum number n) and the SS band (sub-band quantum number $n \pm 1$). A similar effect occurs from transitions between the SS and LH sub-bands, however, in this case both states have s-like orbital components.

The $\underline{k}_{ll}$ dependence of the momentum matrix elements averaged along the [100] and [110] direction for transitions between sub-bands (S1, S2) and (H1, L1, H2) is shown in figure (6.14). As each state derived from the solution of expression (6·26) is doubly degenerate, the results shown in figure (6.14) are determined from the expression

$$|M|^2 = [|M_{i1f1x}|^2 + |M_{i2f1x}|^2 + |M_{i1f2x}|^2 + |M_{i2f2x}|^2] \, \delta_{o,\underline{k}_{11H}-\underline{k}_{11S}} \qquad (6.30)$$

where the subscripts i and f refer to the initial and final states of the transition repsectively, and each individual term is of the form given in equation (6.29).

6.3.3 c) Transitions Between the Spin Split-Off and Heavy/Light Hole Sub-Bands at $\underline{k}_{11} \neq 0$

At non-zero values of $\underline{k}_{11}$ the wave function of a given state contains components of all eight basis states given in expression (6.7). That is each state is composed of the two spin components of the band edge Bloch functions of the four bands considered. The mixing of the different basis states becomes more marked with increasing $\underline{k}_{11}$ and the magnitude of the compoment due to the s-like orbitals u_1 and u_5 in the valence band states tends to increase. In a simple $\underline{k}\cdot\underline{p}$ calculation in the bulk material this would lead to an increase in the intervalence band transitions. However, this situation is complicated in the present model by the differing parities of envelope functions and the change in character of the sub-bands, such as in the case of H1 and L1 as discussed below.

As seen in figure (6.7), with increasing $\underline{k}_{11}$ the sub-bands H1 and L1 approach each other in energy and then move apart exhibiting a distinct anticrossing behaviour. Examination of the wavefunctions of states in sub-bands H1 and L1 (for $\underline{k}_{11}$ along the [100] direction) indicates a change in wavefunction character in the region $\underline{k}_{11} = 2 - 3\underline{k}_o$. For values of $\underline{k}_{11} < 2\underline{k}_o$ the wavefunction of the H1 state has a large HH component and a smaller LH component, a complementary situation

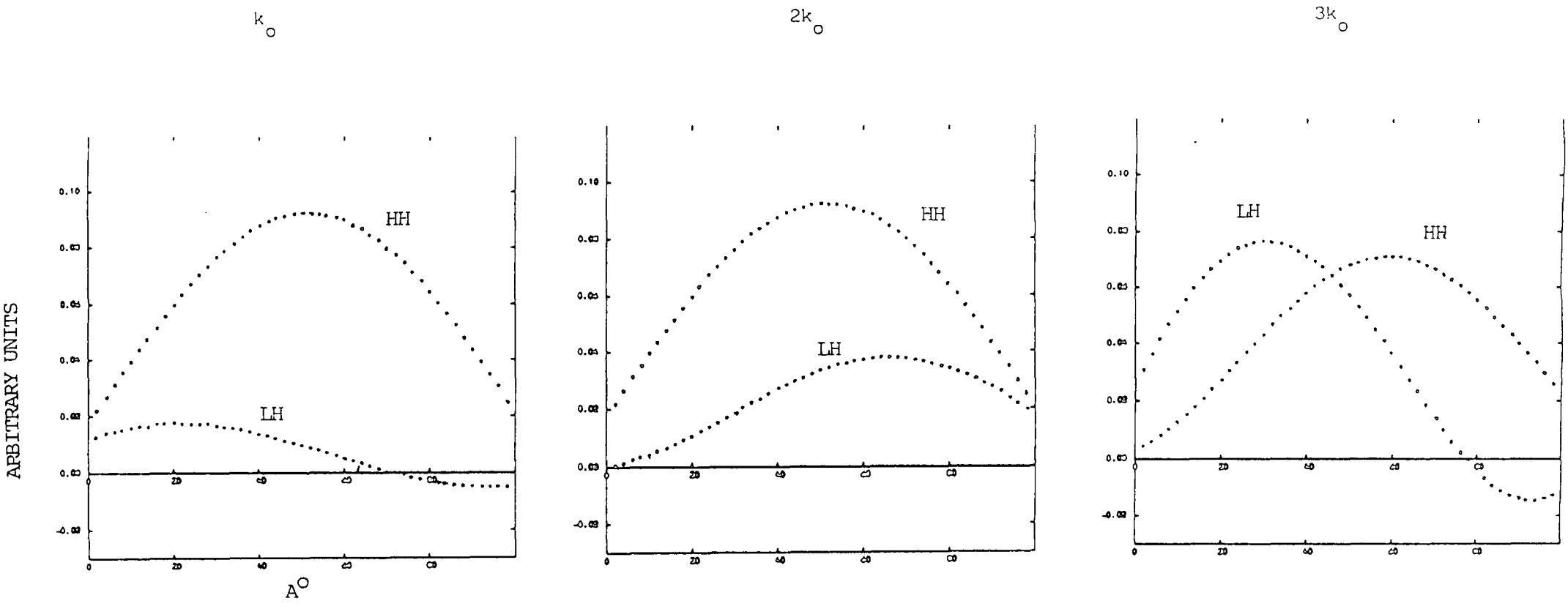

Figure 6.12: The envelope functions of the heavy hole and light hole components of sub-band H1 for $k_{11} = k_o - 3k_o$ along the [100] direction.

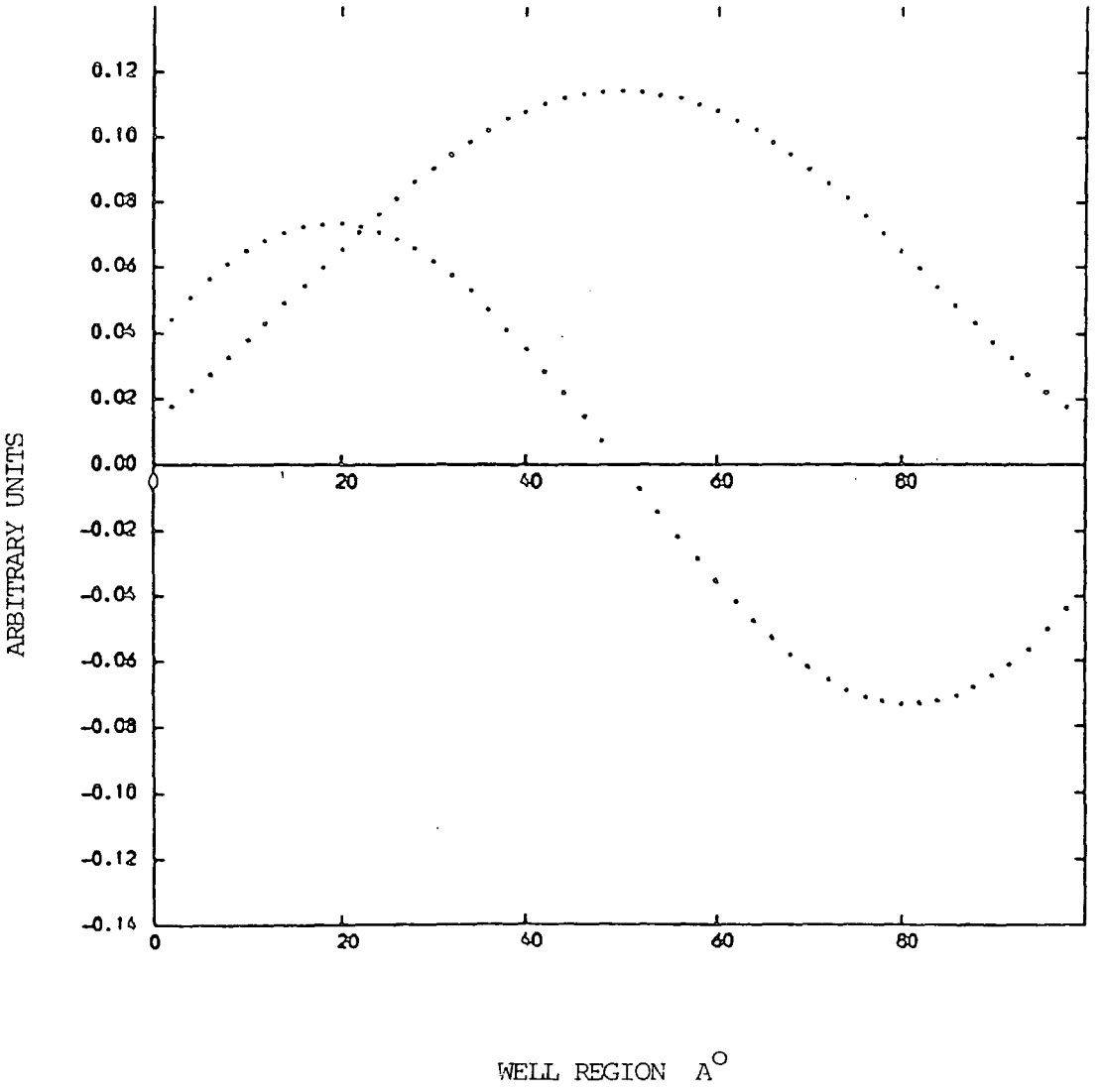

Figure 6.13: The symmetrical and anti-symmetrical components of the heavy hole envelope function of sub-band H1 at $k = 3k_o$.

exists in the L1 state. With increasing $\underline{k}_{11}$ the LH component of the H1 state increases and the HH component reduces, and for $\underline{k} \gtrsim 3\underline{k}_o$ the LH component is dominant. Once again a complementary effect occurs in sub-band L1. The sub-bands have thus essentially changed character. The relative magnitudes of the HH and LH components of one particular spin state of the wavefunction in the H1 sub-band for $\underline{k}_{11} = \underline{k}_o - 3\underline{k}_o$ along the [100] direction is shown in figure (6.12), and clearly indicate the changes discussed above.

A further change in the wavefunctions which can be clearly seen from figure (6.12) is the increasing asymmetry of the envelope functions as $\underline{k}_{11}$ increases. The asymmetric envelope functions can be re-expressed as symmetric and antisymmetric functions by adding or subtracting the contribution of the same spin basis form the other degenerate state in the band considered. The relative magnitudes of the symmetric and anti symmetric components can then be compared with such components for the states to (from) which transitions occur. This then provides a good indication of the overlap integrals of the transition matrix elements. For example an increase in antisymmetric (odd parity) component of the HH envelope functions leads to a reduction in the overlap with the even parity envelope functions of another state but an increase in the overlap integrals with odd parity envelope functions. These changes in symmetry which are also found in the s-like components of the HH, LH and SS sub-bands are partially responsible for the variation with $\underline{k}_{11}$ of the matrix elements of the intervalence band transtions. The symmeterised forms of the HH components of sub-band H1 for $\underline{k}_{11} = 3\underline{k}_o$ along the [100] direction are shown in figure (6.13). The antisymmetric (odd parity) component of the HH envelope has significant amplitude.

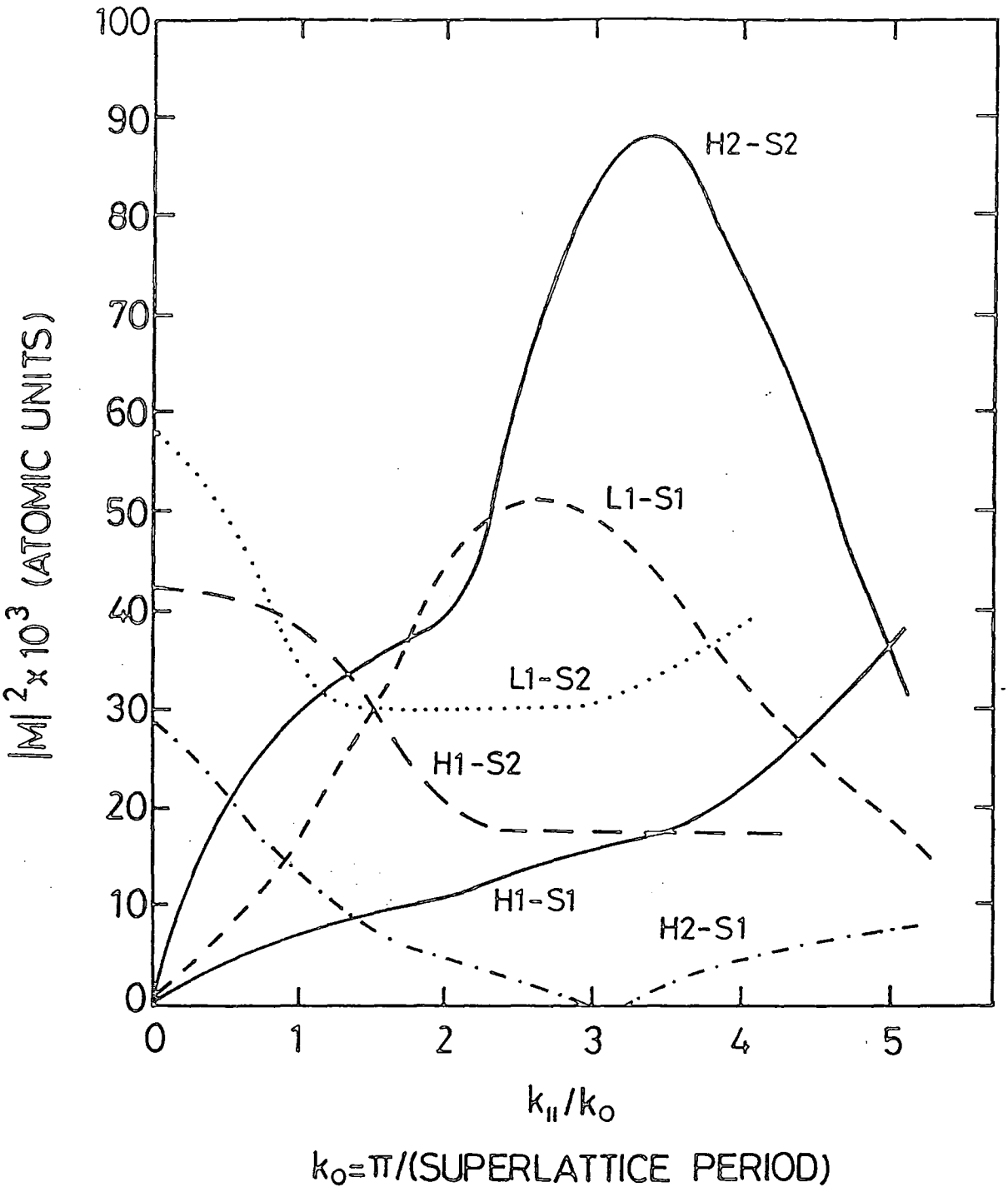

Figure 6.14: Dispersion of the squared momentum matrix elements $|M|^2$ for transitions from the spin split-off to the heavy and light hole sub-bands. The matrix elements shown are averaged over results derived for in-plane wavevectors along the [100] and [110] directions.

In summary the various wave function properties affecting the momentum matrix elements between states relevant to IVBA transitions are as follows: a) the magnitude of the symmetrical and antisymmetrical components of each basis state (that is the form and amplitude of the envelope function of each basis state), b) the coupling of unbound light and heavy hole states to the bound SS states. All these effects to some extent influence the magnitude of the intervalence band matrix elements (averaged over the [100] and [110] direction) shown in figure (6.14). The combination of these factors leads to a general increase with $\underline{k}_{11}$ of transitions for which $\Delta n = 0$ and a decrease in transitions for which $\Delta n = 1$ over the small range of $\underline{k}_{11}$ considered. The effects of these changes on the derived values of absorption coefficients is given in the next chapter.

6.4. Summary

A technique for the derivation of quantum well or superlattice band-structure has been described. The method used is a variational approach first devised by Schlosser and Marcus (1963) for solution of the energy band problem in metals, and extended to the present model by Altarelli (1983). In this approach a trial wave function is matched at the interfaces of the quantum well. The trial wavefunction is expanded in terms of eight Bloch basis states each weighted by an envelope term expressed as a Fourier expansion of sines and cosines. The Bloch periodic parts of the wavefunction in both well and barrier material are considered to be the same.

Using this model the in-plane bandstructure for a $GaAs/Ga_{0.7}Al_{0.3}As$ 100/200 Å quantum well structure has been evaluated. The $E - \underline{k}_{11}$ dispersion in the conduction and spin split-off bands is similar to that

used in a simple effective mass model, whereas the heavy and light hole bands show marked non-parabolicity due to band mixing.

The wavefunctions determined from the bandstructure calculation are used to evaluate the momentum matrix elements of transitions relevant to the IVBA calculations. These matrix elements exhibit a $\Delta n = 1$ selection rule for transitions at the sub-band edges with $\Delta n = 0$ transitions becoming more important with increasing in-plane wavevector.

CHAPTER 7

INTERVALENCE BAND ABSORPTION IN QUANTUM WELL LASERS

7.0. Introduction

The IVBA coefficients of some bulk semiconductor materials used in double heterostructure (DH) lasers were evaluated in chapter 5. As explained there, IVBA is one of the mechanisms responsible for the temperature dependence of semiconductor laser threshold current densities. The threshold current temperature dependence normally takes the form $J_{th} \propto \exp(T/T_o)$ and a similar exponential temperature dependence is found in quantum well lasers (Resek (1980) and Chin (1980)). For quantum well lasers several loss mechanisms have been suggested (see Dutta (1983)) as the possible cause of this temperature dependence of the threshold current, with the emphasis falling largely on Auger recombination in the longer wavelength (λ = 1.3. - 1.6 μm) devices. While IVBA may not be a significant mechanism for the temperature dependence of threshold currents in the longer wavelength lasers, it is expected to be important in the $GaAs / Ga_{0.7} Al_{0.3} As$ quantum well structure where Auger recombination is considered to be small. Therefore some model calculations of absorption in this system have been carried out. In the process of doing this, some important parameters such as the hole occupation of different sub-bands and the Fermi energy have been evaluated in the models considered.

7.1. The Intervalence Band Absorption Transitions

The absorption coefficients evaluated in this chapter are obtained by considering only transitions occurring between bound states of the valence band quantum well. The results are therefore based on the

assumption that the bound-unbound and unbound-unbound transitions are responsible for only a small proportion of the total intervalence band absorption.

The number of bound states of a well is basically determined by the well depth, well width and the light, heavy and spin split-off effective masses at the sub-band edges. In the $GaAs/Ga_{0.7}Al_{0.3}As$ structure of interest here the well depths in the spin split-off and in the heavy and light hole valence bands differ by only a few hundred meV on the basis of a discontinuity ratio $\Delta E_c/\Delta E_v = 60/40$. For a fixed well width therefore the number of bound states in each well is determined by the hole effective mass. The relatively small effective masses of the holes in the spin split-off (SS) and light hole (LH) bands implies very few bound states (for example in the $\underline{k}\cdot\underline{p}$ calculation only two bound states are produced in a 100 A^{o} GaAs well). The large heavy hole (HH) effective mass correspondingly produces many more bound states.

Although IVBA transitions may occur between any bound valence band states, the lasing wavelength transitions of interest in the present work will come from the excitation of electrons from the SS to LH or HH states occupied by holes. Other IVBA transitions are therefore not considered in the following analysis.

The number of possible SS, HH or LH transitions is equal to the product of the number of bound states in each well. This simple rule, however, ignores the form of the envelope term modulating the Bloch periodic part of the bound state wave function. As explained in Section 6.1, in its simplest form, this envelope has a pure sine or cosine character. The orthogonality of these envelope functions imposes a $\Delta n = 0$ selection rule on the IVBA transitions (that is transitions only occur between sub-bands with the same quantum number n). This selection rule is applied in the evaluation of the IVBA coefficients in

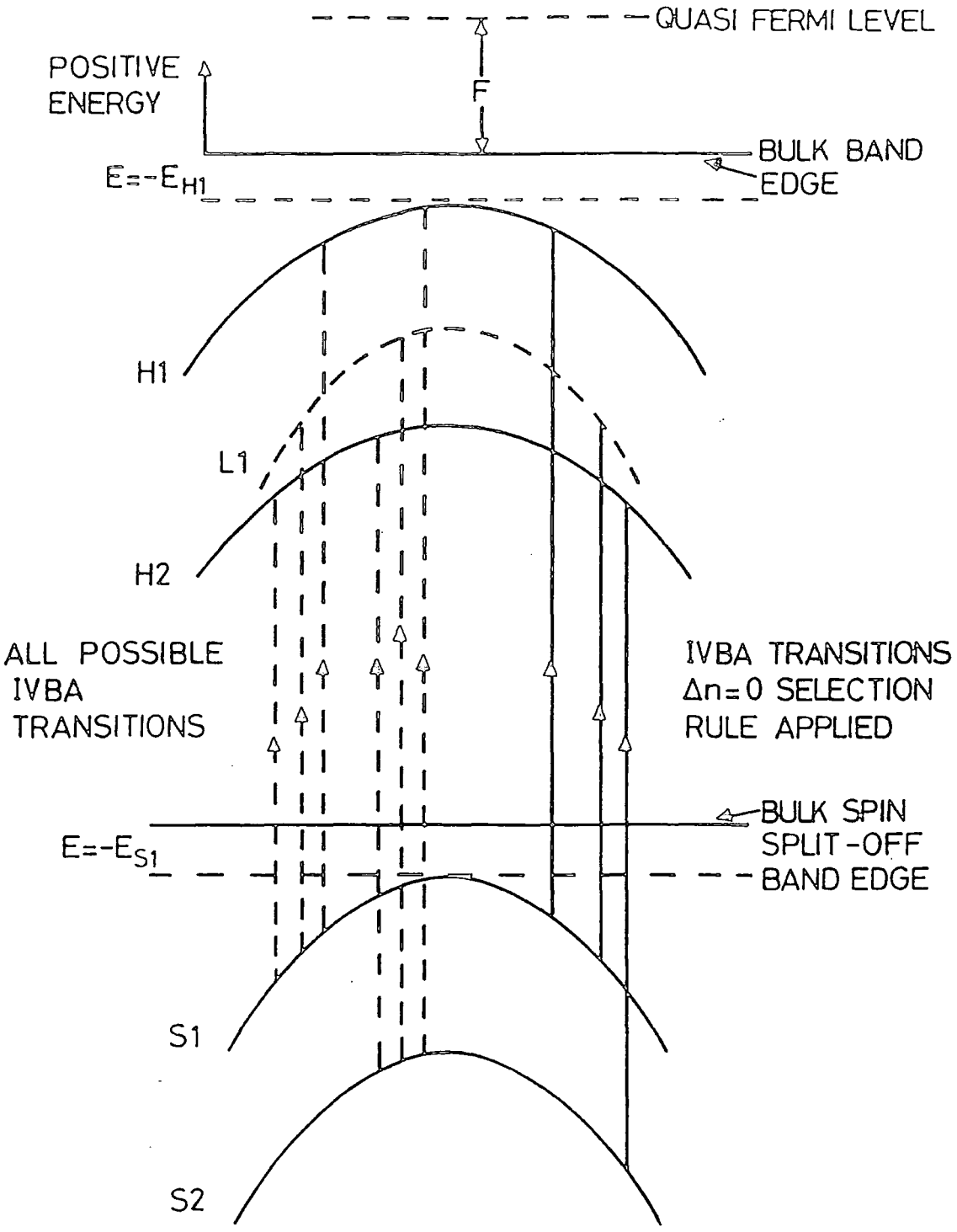

Figure 7.1: Possible IVBA transitions (with and without the $\Delta n = 0$ selection rule) between sub-bands S1, S2 and H1, L1, H2. The diagram also defines the positive energy direction for evaluation of the hole quasi-Fermi level.

the simple effective mass (SEMA) and pseudopotential calculations of section 7.5. However, it was shown in chapter 6 that a more realistic determination of bandstructure and wavefunctions based on a $\underline{k}\cdot\underline{p}$ approach produces momentum matrix elements for which the selection rule no longer applies. Hence in the evaluation of the IVBA coefficients using the $\underline{k}\cdot\underline{p}$ bandstructure contributions to the absorption from all possible transitions from the SS to HH and LH sub-bands with significant hole occupancy are considered. The possible transitions between SS and HH and LH sub-bands for a simplified model with two HH, two SS and one LH sub-band is shown in figure 7.1. The effect on these transitions of applying the $\Delta n = 0$ selection rule is also shown.

7.2. Bandstructure Models

Three bandstructure models (SEMA, pseudopotential and $\underline{k}\cdot\underline{p}$) are used to calculate IVBA coefficients. The essential difference between the models is in the form of the in-plane bandstructure. In the SEMA model the sub-band edges are derived using a simple wave function matching technique described in the next section. Away from these sub-band edges each sub-band $E - \underline{k}_{11}$ dispersion relation takes the familiar parabolic form $E = \hbar^2 k_{11}^2 / 2m_x$ where m_x is the effective mass of the relevant bulk band. For the intersub-band momentum matrix elements simple averages of the Bloch function matrix elements for the [100] and [110] directions from the bulk pseudopotential calculation of chapter 5 are used.

To provide what might be expected to be a better approximation to the sub-band structure, the pseudopotential model uses a simple average of the bulk pseudopotential bandstructure for the [100] and [110] directions. The same sub-band edges as derived for the SEMA model are used.

The third evaluation of IVBA coefficient is performed using an average of the bandstructure and momentum matrix elements derived in the [100] and [110] directions from the $\underline{k}\cdot\underline{p}$ calculation of chapter 6. As this model is expected to provide a good representation of the quantum well bandstructure, the IVBA coefficients derived from it should provide a more realistic estimate than the other two models. However, the complexities and limitations of this model greatly restrict the region of k-space over which bandstructure and momentum matrix elements can be accurately determined and, as such, the absorption coefficients derived in this model only cover the low energy transitions near the sub-band edges.

Having briefly described the three bandstructure models to be used, a comparison of some important parameters derived from them is now given.

7.3. Determination of Sub-Band Edges

The sub-band edges for the SEMA and pseudopotential models are evaluated using the familiar quantum mechanical solution for a particle confined to a 1-D potential well (Schiff (1955)). In the present model where the particle wavefunction is a product of a Bloch periodic part and an envelope function, the Bloch term is assumed to be the same in both well and barrier regions. The solution of the potential well problem then amounts to solving the Schrödinger equation for the envelope parts (F_1 and F_2) of the particle wavefunction inside and outside the well, as:

$$-\frac{\hbar^2}{2m_1}\frac{d^2F_1}{dz^2} = EF_1 \qquad \text{inside well}$$

$$-\frac{\hbar^2}{2m_2}\frac{d^2F_2}{dz^2} = (E - V)F_2 \qquad \text{outside well} \tag{7.1}$$

where V is the depth of the potential well and m_1 and m_2 are the effective masses in the well and barrier region respectively.

These wavefunctions are also subject to the current continuity condition (Bastard (1981))

$$\frac{1}{m_1}\frac{dF_1}{dz} = \frac{1}{m_2}\frac{dF_2}{dz} \tag{7.2}$$

at the well boundaries. A further condition that the wavefunctions are matched a single band at a time, for example HH - HH is also applied. Thus, no band mixing is included in this simple model.

Solution of equations (7.1) and (7.2) in the usual way gives:

$$\tan\left[\frac{(2m_1E)^{1/2}L_A}{2\hbar}\right] = \left[\frac{m_1(V-E)}{m_2E}\right]^{1/2}$$

and

$$\tan\left[\frac{(2m_1E)^{1/2}L_A}{2\hbar}\right] = -\left[\frac{m_2E}{m_1(V-E)}\right]^{1/2} \tag{7.3}$$

where E is the energy of the sub-band edge, and L_A is the well width. The well width dependence of the band edges for the SS sub-bands and the HH and LH sub-bands are shown in figures 7.2 and 7.3 respectively. Both diagrams give a clear indication of the increase in the number of bound states as the well width increases.

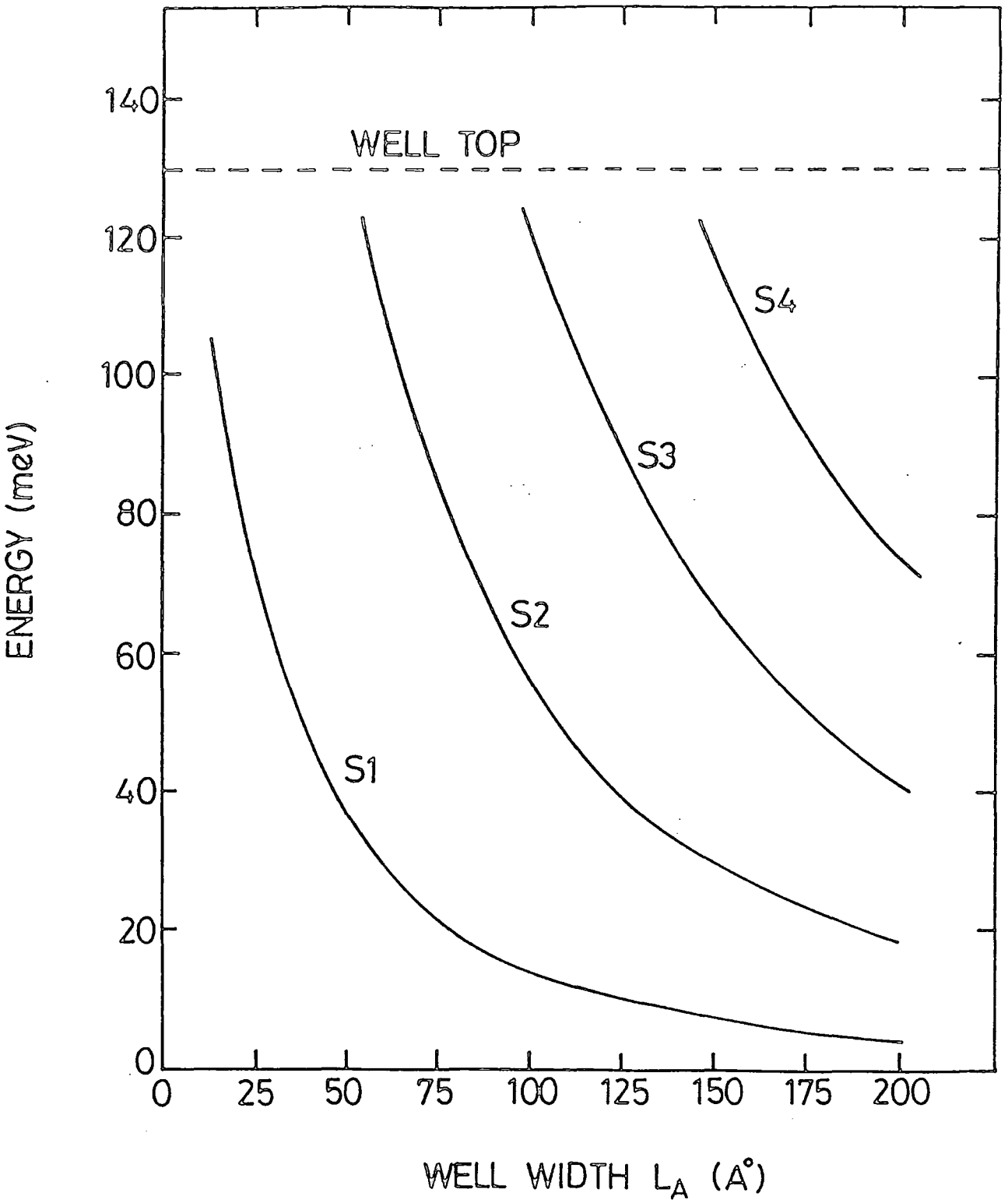

Figure 7.2: The well width variation of the spin split-off sub-band edges in a $GaAs/Ga_{0.7}Al_{0.3}As$ quantum well structure.

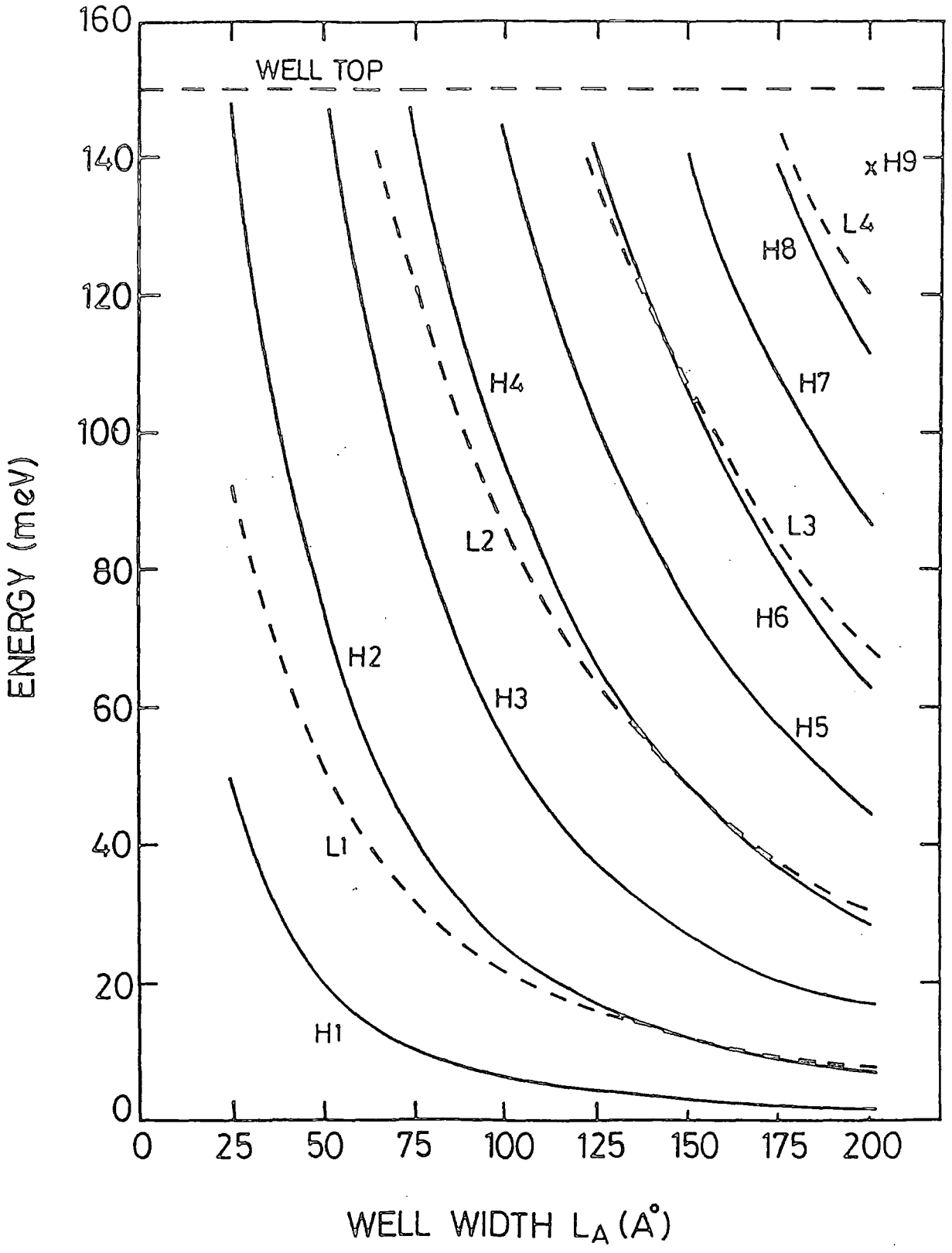

Figure 7.3: The well width variation of the heavy and light hole sub-band edges in a $GaAs/Ga_{0.7}Al_{0.3}As$ quantum well structure.

The energies of all the sub-band edges obtained are approximately equal to those derived from the $\underline{k}\cdot\underline{p}$ calculation for $L_A = 100\ A^{\circ}$, and the kinetic energies are seen to be roughly proportional to n^2 as would be predicted by the infinite square well model for which $E = \frac{n^2\pi^2\hbar^2}{2m_x L_A^2}$. Figure 7.3 also reveals a crossing of sub-bands H2 and L1 in the region $L_A = 150 - 200\ A^{\circ}$. In a bandstructure model incorporating band coupling effects (e.g. the $\underline{k}\cdot\underline{p}$ model) these sub-bands would exhibit strong anticrossing behaviour and the heavy (H2) and light (L1) hole wavefunctions would change character as the well width was increased from $150 - 200\ A^{\circ}$. This effect is discussed in some detail by Chang and Schulman (1985) and Schulman and Chang (1985).

Having derived the sub-bandstructure for the SEMA and pseudopotential models (see section 7.2) and the $\underline{k}\cdot\underline{p}$ model (see chapter 6) it is now possible to evaluate the position of the hole quasi Fermi level for each sub-bandstructure in the next section.

7.4. Determination of Hole Quasi Fermi Level

The assumption is made of carrier thermalisation between all valence sub-bands. That is it is assumed the holes produced by optical excitation or electric injection have lifetimes sufficiently long that thermalisation between all valence sub-bands occurs and the carriers are in equilibrium with the lattice so that the hole temperature equals the lattice temperature. This is a standard assumption in the calculation of optical spectra in the bulk and is based on a comparison of optical transition and carrier relaxation times. Its validity in quantum wells is not so clearly established but it will be used as a matter of expediency. Under these conditions only one quasi Fermi level need be calculated and Fermi-Dirac statistics can be used.

For each of the heavy and light hole sub-bands a tenth order polynomial approximation $E_{H,Ln}(\underline{k}_{ll})$ to the $E - \underline{k}_{ll}$ dispersion relationship was obtained using NAG routine Eϕ2 ADF. Then choosing the bulk valence band edge as the zero of energy and defining the positive energy direction as shown in figure (7.1) the hole occupation per unit volume p is given by

$$p = \frac{1}{AL_A}\frac{2A}{(2\pi)^2}\left[\sum_n \int_0^{\text{ZONE EDGE}} f(E_{Hn}(\underline{k}_{ll}))d\underline{k}_{ll} + \sum_{n'} \int_0^{\text{ZONE EDGE}} f(E_{Ln'}(\underline{k}_{ll}))d\underline{k}_{ll}\right] \qquad (7.4)\ .$$

Where $2A/(2\pi)^2$ is the 2 - D density of $\underline{k}$-states including a factor of two for spin degeneracy, AL_A is the volume of well material containing the holes ((L_A = well width), $f(E_{H,Ln}(\underline{k}_{ll}))$ is the hole occupation probability, and the sums are taken over all relevant sub-bands (unbound sub-bands are not considered due to their negligibly small hole occupancy).

Clearly the hole occupation of the higher sub-bands at large k_{ll} values is very small, and the integrals in equation (7.4) converge rapidly for values of $k_{ll} > 10\ k_o$ ($k_o = \pi/L \simeq 0.094 \times$ ZONE EDGE, where L is the superlattice period). Thus taking the upper limit of the integrals as $k_{ll} = 15\ k_o$ and using dimensionless parameters we obtain

$$p = \frac{1}{L_A\pi}\left(\frac{\pi}{L}\right)^2\left[\sum_n \int_0^{15} \frac{k\ dk}{1+\exp\left(\frac{F+E_{Hn}(k)}{kT}\right)} + \sum_{n'} \int_0^{15} \frac{k\ dk}{1+\exp\left(\frac{F+E_{Ln'}(k)}{kT}\right)}\right] \qquad (7.5)\ .$$

where $k = k_{ll}/k_o$

Equation (7.5) is solved for F using the NAG root finding routine Cϕ5 ADF together with the integral routine Dϕ1 AJF.

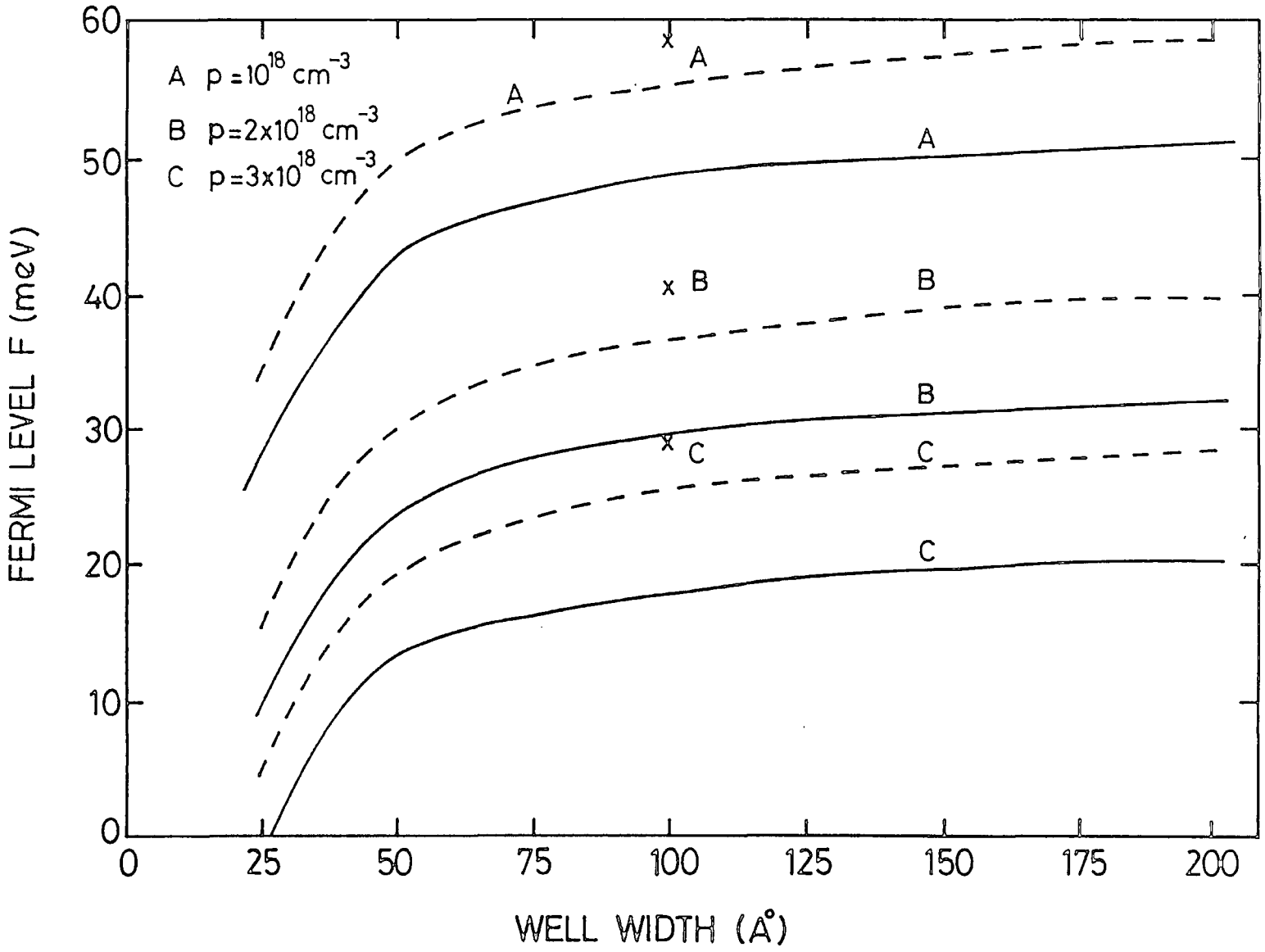

Figure 7.4: Well width and concentration dependence of the hole quasi-Fermi level derived using SEMA (sold lines), pseudopotential (dashed lines) and k•p (crosses) bandstructures.

In the simple effective mass approximation (SEMA) for which $E_{H,L} = \hbar^2 k_{11}^2 / 2m_{H,L}$ for all sub-bands, equation (7.4) reduces to:

$$p = \frac{m_H}{\pi L_A \hbar^2} \sum_n \int_{-\infty}^{-E_{Hn}} \frac{dE}{1+\exp\left(\frac{F-E}{kT}\right)} + \frac{m_L}{\pi L_A \hbar^2} \sum_{n'} \int_{-\infty}^{-E_{Ln'}} \frac{dE}{1+\exp\left(\frac{F-E}{kT}\right)} \qquad (7.6)$$

where $\frac{m_{H,L}}{\pi L_A \hbar^2}$ is the density of energy states in the relevant sub-band (including a factor of two for spin) and the $E_{H,Ln}$ are the energies of the nth sub-band edges.

The integrals in expression (7.6) can be carried out analytically by substitution giving:

$$p = \frac{m_H kT}{\pi \hbar^2 L_A} \sum_n \ln[1+\exp[-(F+E_{Hn})/kT]] + \frac{m_L kT}{\pi \hbar^2 L_A} \sum_{n'} \ln[1+\exp[-(F+E_{Ln'})/kT]] \qquad (7.7)$$

Substitution of Boltzmann statistics for the Fermi Dirac (F-D) factors in expression (7.6) immediately yields:

$$p = \frac{m_H kT}{\pi L_A \hbar^2} \sum_n \exp\left(\frac{-F-E_{Hn}}{kT}\right) + \frac{m_L kT}{\pi L_A \hbar^2} \sum_{n'} \exp\left(\frac{-F-E_{Ln'}}{kT}\right) \qquad (7.8)$$

$$\text{or} \quad F = -kT \ln\left[\frac{p}{N_H \sum_n \exp\left(\frac{-E_{Hn}}{kT}\right) + N_L \sum_{n'} \exp\left(\frac{-E_{Ln'}}{kT}\right)}\right] \qquad (7.9)$$

where $N_{H,L}$ is the effective density of states:

$$N_{H,L} = \frac{m_{H,L} kT}{\pi L_A \hbar^2} \qquad (7.10)$$

This Boltzmann approximation is good for relatively wide wells $L_A \gtrsim 75\ A^o$ and hole concentrations $p \lesssim 3 \times 10^{18}\ cm^{-3}$ where the hole quasi Fermi level is well into the band gap, however Fermi-Dirac statistics have been used for all numerical results given in this chapter.

In figure (7.4) the carrier concentration and well width dependence of the hole quasi Fermi level F in the SEMA and pseudopotential models are compared. A comparison is also made with the values of F obtained using the $\underline{k}\cdot\underline{p}$ model for $L_A = 100\ A^o$. As pointed out in chapter 5, the pseudopotential bandstructure calculation produces sub-bands which are non-parabolic and give larger densities of states than is found in the SEMA model. The increased density of states is reflected in the position of the hole quasi Fermi level which is deeper into the band gap. This effect is clearly illustrated in figure (7.4) with the quasi Fermi level in the pseudopotential model having a higher energy than for the SEMA model for all concentrations and well widths. With increasing hole concentration the Fermi level crosses the bulk the band edge, this crossing occurs for $p < 2 \times 10^{18}\ cm^{-3}$ for the narrow $L_A = 25\ A^o$ well. As the well width increases the quasi Fermi level in the SEMA model tends towards that evaluated using a parabolic band effective mass approximation in the bulk material. A similar effect would be seen for the pseudopotential calculation if the same average of bandstructure directions was used in the bulk and quantum well models. The quasi Fermi level evaluated using the $\underline{k}\cdot\underline{p}$ bandstructure for $L_A = 100\ A^o$ is very similar to that derived in the pseudopotential model. However, these similar results occur for very different reasons. The pseudopotential model gives a larger density of states in the heavy hole sub-bands than does the $\underline{k}\cdot\underline{p}$ model. However the distinct non-parabolicity and change in sign of the hole effective mass in the first light hole sub-band of the $\underline{k}\cdot\underline{p}$ model gives this band a very large density of states compared with the corresponding sub-bands in the other models. Unlike the other models, therefore, the light hole sub-band has a strong influence on the position of the hole quasi Fermi level. This influence is reflected in hole occupation of the different sub-bands, discussed in the next section.

7.5. Distribution of Holes between Sub-Bands

In the comparison of the different bandstructure models one of the most significant features is the change in hole occupation of each sub-band. To derive these occupation numbers the assumption of carrier thermalisation is maintained and the quasi Fermi levels derived in the previous section are used.

The hole occupancy per unit volume $p_{H,Ln}$ of a given sub-band n is given by:

$$p_{H,Ln} = \frac{2}{AL_A} \int_0^{\text{ZONE EDGE}} (\text{Density of states}) \times (\text{occupation factor})\, dk_{ll} \qquad (7.11)$$

where the factor of 2 accounts for spin degeneracy. Assuming in-plane isotropy gives

$$p_{H,Ln} = \frac{2}{AL_A} \frac{A}{(2\pi)^2} \int_0^{\text{ZONE EDGE}} 2\pi\, k_{ll}\, f(E_{H,Ln}(k_{ll}))\, dk_{ll} \qquad (7.12)$$

following the prescription used in the previous section; using dimensionless integral parameters, reducing the upper limit of the integral to 15 k_o ($k_o = \pi/L$), and substituting the relevant polynomial expansion we obtain:

$$p_{H,Ln} = \frac{1}{L_A \pi} \left(\frac{\pi}{L}\right)^2 \int_0^{15} \frac{k\, dk}{\exp\left(\frac{F+E_{H,Ln}(k)}{kT}\right)+1} \qquad (7.13)$$

where again $k = k_{ll}/k_o$.

In the SEMA model the polynomial $E_{H,Ln}(k)$ takes the form:

$$E_{H,Ln}(k) = E_{H,Ln} + \frac{\hbar^2 k^2}{2m_{H,L}}$$

or alternatively using the energy density of states in expression (7.11) gives

$$p_{H,Ln} = \int_{-\infty}^{-E_{H,Ln}} \frac{m_{H,L}}{\pi L_A \hbar^2} \frac{dE}{\left[\exp\left(\frac{F-E}{kT}\right)+1\right]} \qquad (7.14)$$

which reduces to

$$p_{H,Ln} = \frac{m_{H,L} kT}{\pi L_A \hbar^2} \ln\left[1 + \exp\left(\frac{-F-E_{H,Ln}}{kT}\right)\right] \qquad (7.15) \ .$$

If the Fermi level is well into the band gap and the Boltzman approximation can be used, then

$$p_{H,Ln} = N_{H,L} \exp\left(\frac{-F-E_{H,Ln}}{kT}\right) \qquad (7.16)$$

where $N_{H,L}$ is the effective density of states defined in expression (7.10).

Variation of sub-band occupation with well width for the SEMA model with a hole concentration of $p = 10^{18}$ cm^{-3} at $T = 300$ K is shown in figure (7.5). These results are derived using expression (7.15) and compared with the corresponding hole densities derived using the more realistic $\underline{k}\cdot\underline{p}$ bandstructure for $L_A = 100$ A°.

The hole occupancies given by the curves shown in figure (7.5) for the SEMA model can be explained in terms of the well width dependence of the sub-band edge energies. In very narrow wells (e.g. 25 A°) the sub-band edges are widely separated in energy and nearly all holes are found in the highest sub-band H1. As the well width increases the energy separation of sub-bands reduces and more sub-bands are found near the bulk band edge. This results in a depopulation of sub-band H1 and an increase in population of other sub-bands. The low hole occupancy of LH sub-bands for all well widths is a direct result of the small light hole density of states.

In comparing the results of the SEMA and $\underline{k}\cdot\underline{p}$ models the most significant difference between the two is found in the population of the

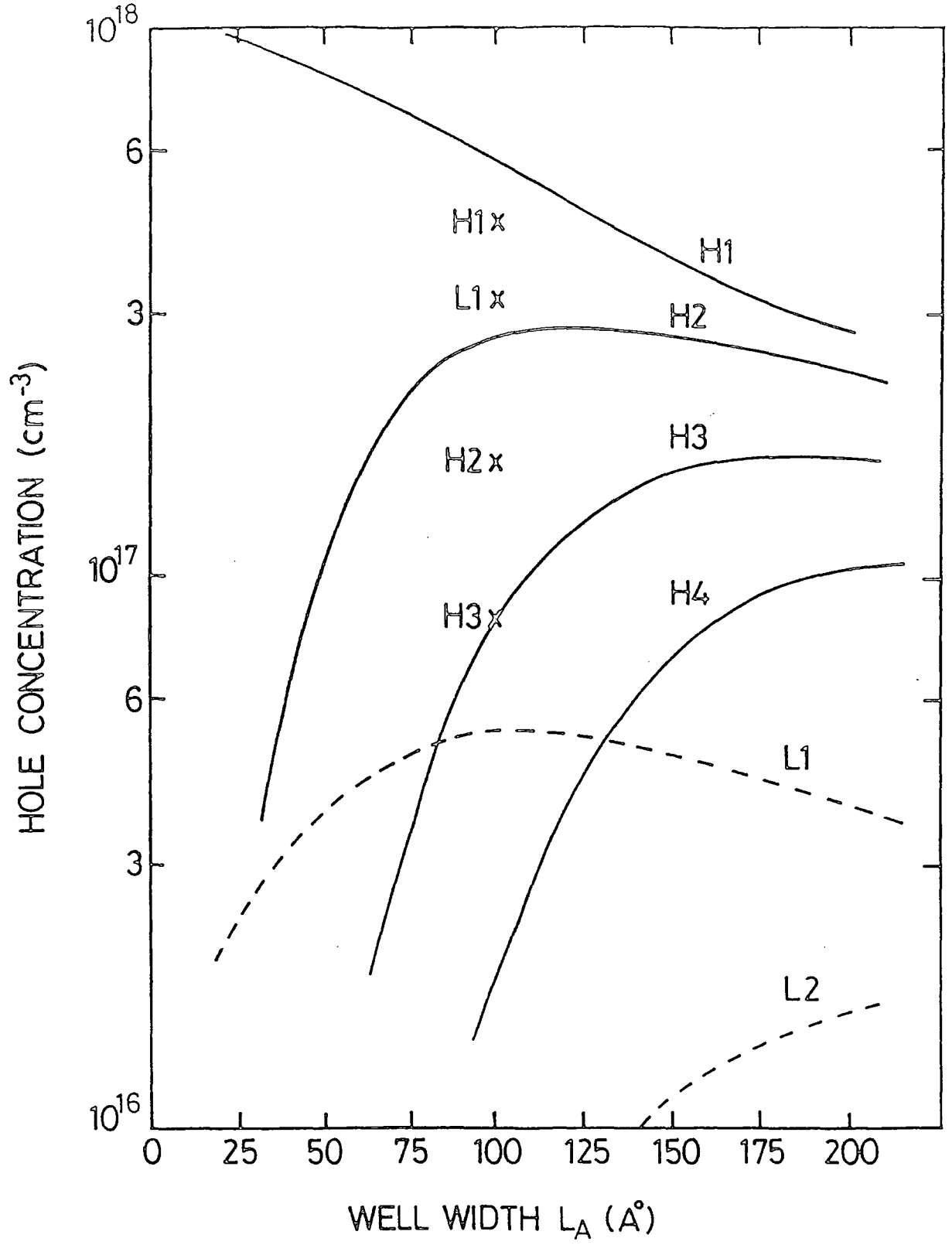

Figure 7.5: Well width variation of valence sub-band hole occupancies, derived using SEMA (lines) and $\underline{k}\cdot\underline{p}$ (crosses) bandstructures for a total hole concentration of 10^{18} cm^{-3} at T = 300K.

first light hole sub-band which is $\simeq 5 \times 10^{16}$ cm^{-3} (SEMA) and some five times larger $\simeq 3 \times 10^{17}$ cm^{-3} in the $\underline{k}\cdot\underline{p}$ model. A complementary effect occurs in the first two heavy hole sub-bands for which the hole occupation is lower in the $\underline{k}\cdot\underline{p}$ model. The large hole concentration in the light hole sub-band of the $\underline{k}\cdot\underline{p}$ model is a result of its large density of states.

With such a low hole occupancy of sub-band L1 in the SEMA model, it is justifiable to neglect IVBA transitions to this sub-band. (Note a similar hole distribution occurs in the pseudopotential model and transitions to the LH sub-bands can also be ignored there). However, this is clearly not a useful approximation in the $\underline{k}\cdot\underline{p}$ model for which a substantial proportion ($\gtrsim$30%) of the hole population is found in sub-band L1 (for $L \doteq 100$ A^{o}). Thus in the evaluation of the IVBA coefficients, transitions to the light hole sub-bands are accounted for in the $\underline{k}\cdot\underline{p}$ model but ignored in the SEMA and pseudopotential models.

7.6. Evaluation of the IVBA Coefficients

The equation for the IVBA coefficient in the quantum well system is derived in a similar way to that for the bulk. The result is

$$\alpha(\omega) = \frac{\pi e^2 \hbar^2}{m_o^2 \varepsilon_o \omega c \eta \Omega_{WELL}} \sum_{n_S n_{H,L}} \sum_{SH,L} (f_{H,L} - f_S) |\langle H,L | \hat{\underline{e}}\cdot\underline{\nabla} | S\rangle|^2 \delta(E_{H,L} - E_S - \hbar\omega) \qquad (7.17)$$

(where $f_{H,L,S}$ are hole occupation factors). Note the expression for $\alpha(\omega)$ now contains sums over all sub-bands (n_S and $n_{H,L}$) and sums over the states within each sub-band (S,L,H).

Converting the sums over states within each sub-band to integrals over $\underline{k}$ using $\sum_S \equiv \frac{A}{(2\pi)^2} \int \underline{d^2k}$, and using $\Omega_{WELL} = AL_A$ gives

$$\alpha(\omega) = \frac{\pi e^2 \hbar^2}{m_o^2 \varepsilon_o \omega c \eta A L_A} \frac{A^2}{(2\pi)^4} \sum_{n_S n_{H,L}} \iint (f_{H,L} - f_S) \left| \langle H,L | \hat{\underline{e}} \cdot \underline{\nabla} | S \rangle \right|^2$$

$$\delta(E_{H,L} - E_S - \hbar\omega)\, d^2\underline{k}_{\parallel H,L}\, d^2\underline{k}_{\parallel S} \qquad (7.18)$$

where the degeneracy of the states involved in the transition is incorporated in the squared matrix element which is summed over all transitions. For the SEMA and pseudopotential models transitions to the LH band have been ignored due to the low density of states in these sub-bands. For the quantum well the momentum matrix element in the SEMA and pseudopotential models is given by the 2-D equivalent of the transition matrix elements used in the bulk material (see Appendix 4) that is:

$$|M|^2 = |M|^2_{AV}\, \delta_{o,\underline{k}_{\parallel S} - \underline{k}_{\parallel H}}\, \delta_{n_S n_H} \equiv |M|^2_{AV}\, \frac{(2\pi)^2}{A}\, \delta(\underline{k}_{\parallel S} - \underline{k}_{\parallel H})\, \delta_{n_S n_H} \qquad (7.19)\ .$$

The average over all polarisation directions is retained to give comparison with the IVBA results for bulk material. The Kronecker delta δ_{n_S, n_H} comes from the orthogonality of the envelope functions and provides the $\Delta n = 0$ selection rule.

For the $\underline{k} \cdot \underline{p}$ model the squared momentum matrix element for light polarised in the x-direction (T.E. mode of the laser) is given by expression (6.30) for the four possible transitions between two doubly degenerate states, that is

$$|M|^2 = \left[|M_{ilflx}|^2 + |M_{i2flx}|^2 + |M_{ilf2x}|^2 + |M_{i2f2x}|^2 \right] \delta_{o,\underline{k}_{\parallel H} - \underline{k}_{\parallel S}} \qquad (7.20)$$

$$\text{or} \quad |M|^2 = |M|^2_{TOT}\, \frac{(2\pi)^2}{A}\, \delta(\underline{k}_{\parallel S} - \underline{k}_{\parallel H}) \qquad (7.21)$$

where

$$|M|^2_{TOT} = |M_{i1f1x}|^2 + |M_{i2f1x}|^2 + |M_{i1f2x}|^2 + |M_{i2f2x}|^2 \qquad (7.21a)$$

Substitution in equation (7.18) of the relevant expression (7.19 or 7.21) for the squared momentum matrix element gives

$$\alpha(\omega) = \frac{\pi e^2 \hbar^2}{m_o^2 \varepsilon_o \omega c \eta L_A 4\pi^2} \sum_{n_S n_{H'}} \iint |M_1|^2 [f_{H'}(E_{H'}(\underline{k}_{11H'})) - f(E_S(\underline{k}_{11S}))]$$

$$\delta(E_{H'}(\underline{k}_{11H'}) - E_S(\underline{k}_{11S}) - \hbar\omega)) \delta(\underline{k}_{11S} - \underline{k}_{11H'}) d^2\underline{k}_{11H'} d^2\underline{k}_{11S} \qquad (7.22)$$

where $|M_1|^2 = \begin{cases} \delta_{n_H n_S} |M|^2_{AV} & \text{SEMA and pseudopotential models} \\ |M|^2_{TOT} & \underline{k}\cdot\underline{p} \text{ model} \end{cases}$

and $H' = \begin{cases} H & \text{SEMA and pseudopotential models} \\ H \text{ and } L & \underline{k}\cdot\underline{p} \text{ model} \end{cases} \qquad (7.23)$.

Integrating over $\underline{k}_{11S}$ and dropping the 11 subscript to shorten the notation gives

$$\alpha(\omega) = \frac{e^2 \hbar^2}{m_o^2 \varepsilon_o \omega c \eta L_A 4\pi} \sum_{n_S n_{H'}} \int |M_1|^2_{\underline{k}} [f_{H'}(E_{H'}(\underline{k}) -$$

$$f_S(E_S(\underline{k}))] \delta(E_{H'}(\underline{k}) - E_S(\underline{k}) - \hbar\omega) d^2\underline{k} \qquad (7.24) .$$

Now the prescription used in chapter 5. For evaluation of bulk IVBA coefficients is followed, in particular we makeuse of the relation

$$\delta(E_{H'S}(\underline{k}) - \hbar\omega) = \sum_{\ell} \frac{\delta(\underline{k}-\underline{k}_{\ell})}{|\nabla_k E_{H'S}|_{\underline{k}=\underline{k}_{\ell}}} \qquad (7.25)$$

where $E_{H'S} = E_{H'}(\underline{k}) - E_S(\underline{k})$ and the $\underline{k}_{\ell}$ define surfaces in 2-D $\underline{k}$-space such that

$$E_{H'S}(\underline{k}) - \hbar\omega = 0 \qquad (7.26)\ .$$

On assuming an isotropic $E - \underline{k}$ dispersion over the layer plane, equation (7.24) reduces to

$$\alpha(\omega) = \frac{e^2\hbar^2}{m_o^2\varepsilon_o\omega c\eta L_A 4\pi} \sum_{n_S n'_H} \left. \frac{|M_1|^2[f_{H'}(E_{H'}(k)-f_S(E_S(k))]2\pi k}{|\nabla_k E_{H'S}|} \right|_{E_{HS}=\hbar\omega} \qquad (7.27)\ .$$

Bandstructure and momentum matrix elements are evaluated along two directions ([100] and [110]) and the absorption coefficients are obtained using a simple average based on the two directions in a similar way to the bulk calculation.

The numerical evaluation of $\alpha(\omega)$ in equation (7.27) was performed using the NAG root finding routine Cϕ5 ADF to determine the solutions of $E_{H'S}(k) - \hbar\omega = 0$ for a given ω, where $E_{H'S}(k)$ is a tenth order polynomial. Similar polynomials are derived for the $|M_1|^2 - k$ relations between the relevant sub-bands, into which the root solutions of k are substituted.

In the SEMA model equation (7.27) can be simplified using:

$$H' = H$$

$$E_H(k) = -E_{Hn} - \frac{\hbar^2k^2}{2m_H}$$

$$E_S(k) = -\Delta - E_{Sn} - \frac{\hbar^2k^2}{2m_S}$$

$$E_{HS}(k) = \Delta + E_{Sn} - E_{Hn} + \frac{\hbar^2 k^2}{2\mu} - \hbar\omega = 0$$

so $$k = \left[\frac{2\mu}{\hbar^2}(\hbar\omega - \Delta + E_{Hn} - E_{Sn})\right]^{1/2}$$

where $$\frac{1}{\mu} = \frac{1}{m_S} - \frac{1}{m_H} \qquad (7.28)\ .$$

Hence

$$\alpha(\omega) = \frac{e^2\mu|M|^2_{AV}}{m_o^2\varepsilon_o\omega\eta c L_A 2\, n_H n_S} \sum (f_H - f_S)\delta_{n_H n_S} \qquad (7.29)\ .$$

The IVBA coefficients derived from expressions (7.27) and (7.29) are now given and comparison is made between the three models.

7.7. Results and Discussion

7.7.1. Introduction

As the SEMA and pseudopotential models both use the same $\underline{k}_{11}$ dependence of the momentum matrix elements and also the $\Delta n = 0$ selection rule, it is straightforward to give a comparison of results for these two models and that forms the initial part of this section.

7.7.2. SEMA and Pseudopotential Models

a) Wavelength Dependence: The wavelength dependence of the IVBA coefficients derived in the two models for a $GaAs/Ga_{0.7}Al_{0.3}As$ quantum well structure with well width $L_A = 100\ A^o$, $p = 10^{18}\ cm^{-3}$ and $T = 300\ K$ are shown in figures (7.6) (SEMA) and (7.7) (pseudopotential). The three spin split-off sub-bands S1 - S3 allow hole transitions from the heavy hole sub-bands H1 - H3 under the $\Delta n = 0$ selection rule.

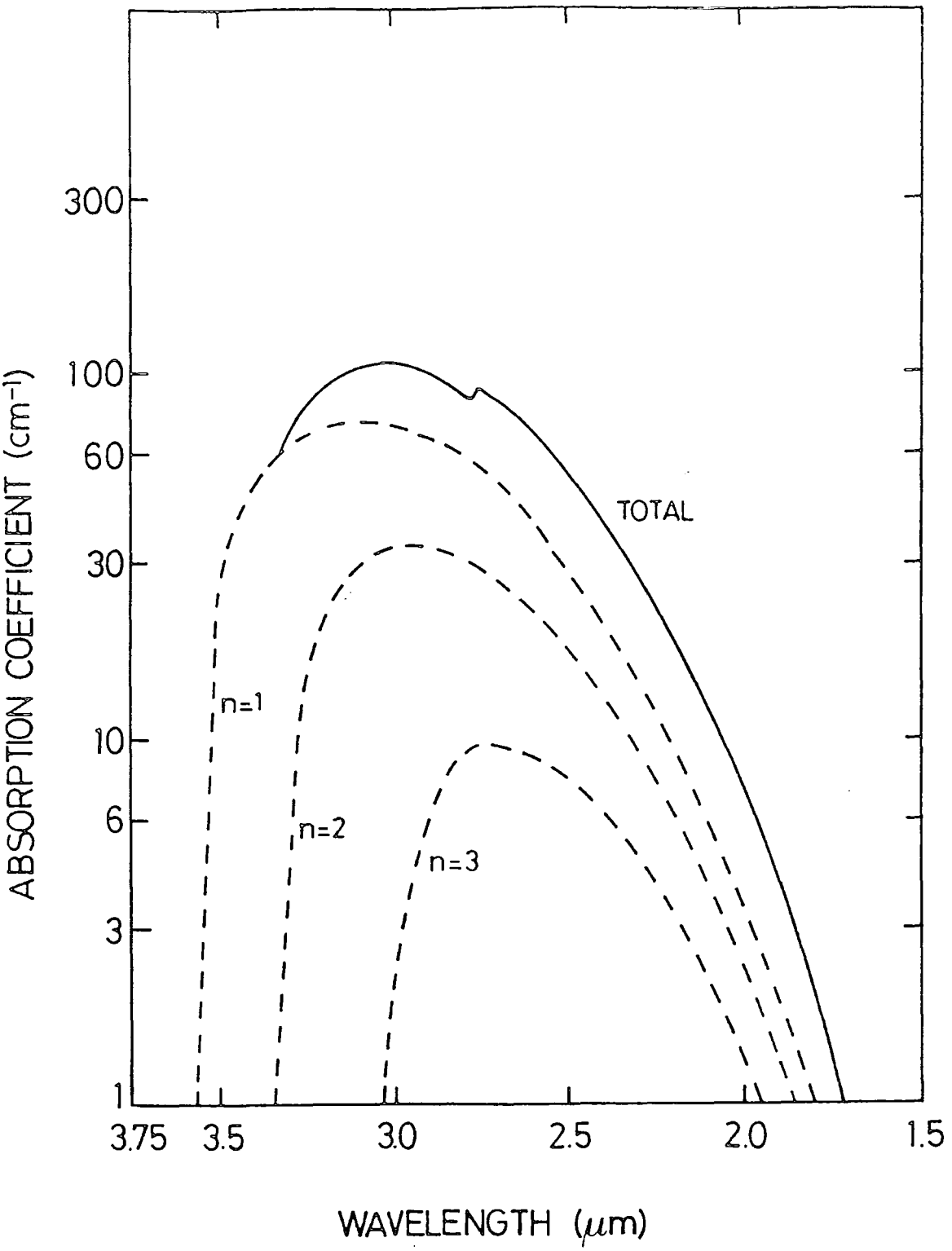

Figure 7.6: The wavelength dependence of the IVBA coefficients derived using a simple effective mass bandstructure for a $GaAs/Ga_{0.7}Al_{0.3}As$ quantum well structure with 100 A^{o} well and a hole concentration of 10^{18} cm^{-3} at T = 300 K.

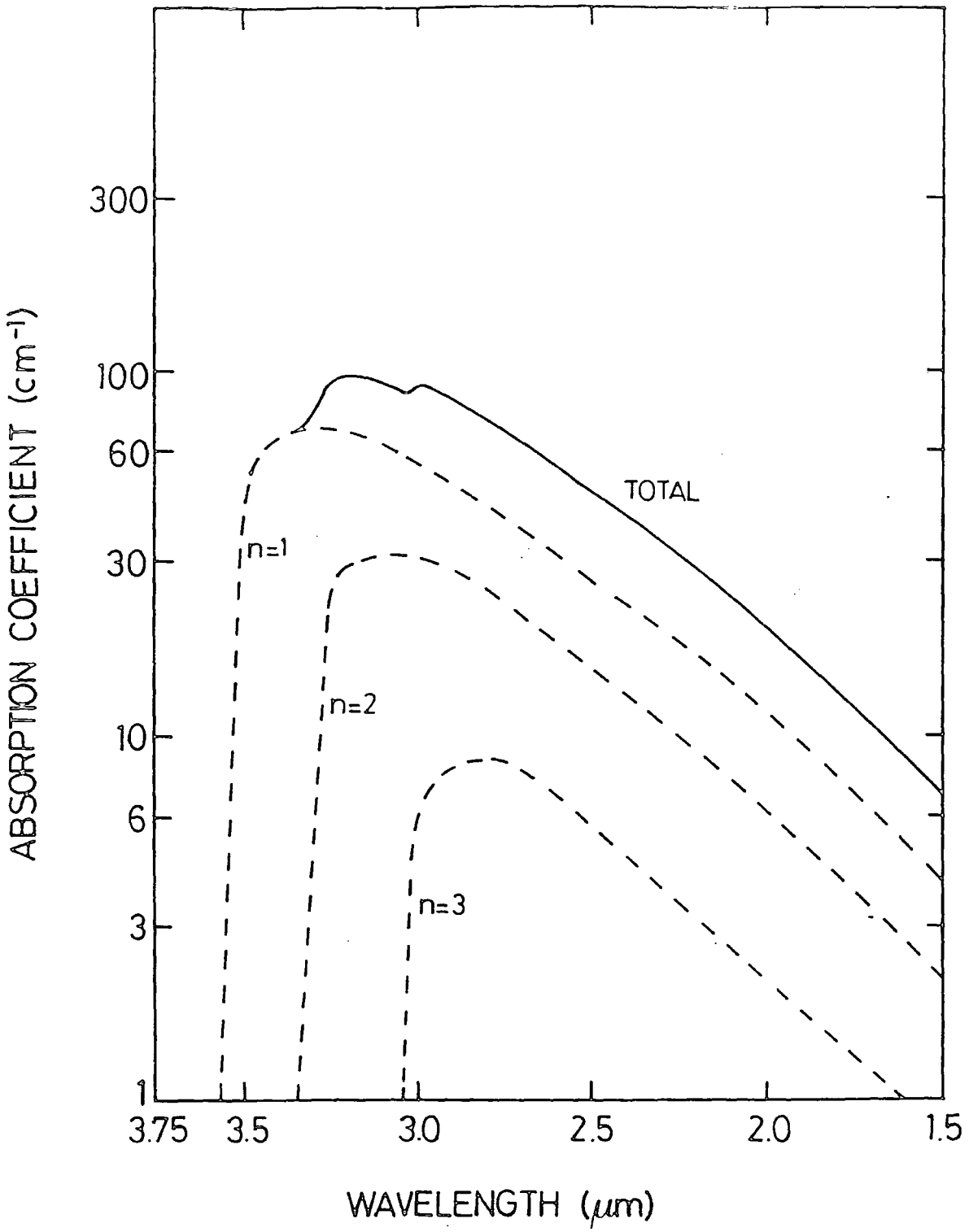

Figure 7.7: The wavelength dependence of the IVBA coefficients for a well width of 100 A^{o} in a $GaAs/Ga_{0.7}Al_{0.3}As$ quantum well structure. The results are based on a sub-band structure derived from an average of the bulk pseudopotential bandstructure evaluated along the [100] and [110] directions.

The IVBA coefficients derived for each value of n is shown together with the total absorption coefficient. The very small absorption due to the S3 - H3 transitions reflects the low hole occupancy of the H3 sub-band. The low hole occupancy of all the heavy hole sub-bands at the large $\underline{k}_{11}$ values required for transitions of energy equal to the band gap, also causes absorption in this part of the wavelength range to be negligibly small. The result is similar to that derived for bulk GaAs.

The total absorption coefficient given in figures 7.6 and 7.7 shows several rapid increases at wavelengths corresponding to the onset of transitions between sub-bands with increasing n values. However, these curves lack the sharp step-like increases found in fundamental absorption transitions due to the vanishing momentum matrix elements at the sub-band edges. Comparison of the total absorption coefficient for both models clearly indicates the changes induced by the different band-structure. In the SEMA model the high energy transitions occurring at large $\underline{k}_{11}$ give much smaller absorption than the pseudopotential model due to the very low hole occupancy of the heavy hole sub-bands. However, the low energy transitions are more pronounced in the SEMA model because the hole quasi Fermi level is closer to the bulk band edge. These effects mirror the corresponding results derived in chapter 5 for the bulk material.

b) Temperature Dependence: In figure (7.8) the temperature dependence of the IVBA coefficients derived in the pseudopotential model for several wavelengths, is illustrated. The well width of 100 A^{o} and the hole concentration $p = 10^{18}$ cm^{-3} are retained. As the temperature increases the absorption due to low energy transitions decreases while absorption due to high energy transitions increases. A similar effect was observed in absorption coefficients derived for bulk material (see figure 5.8).

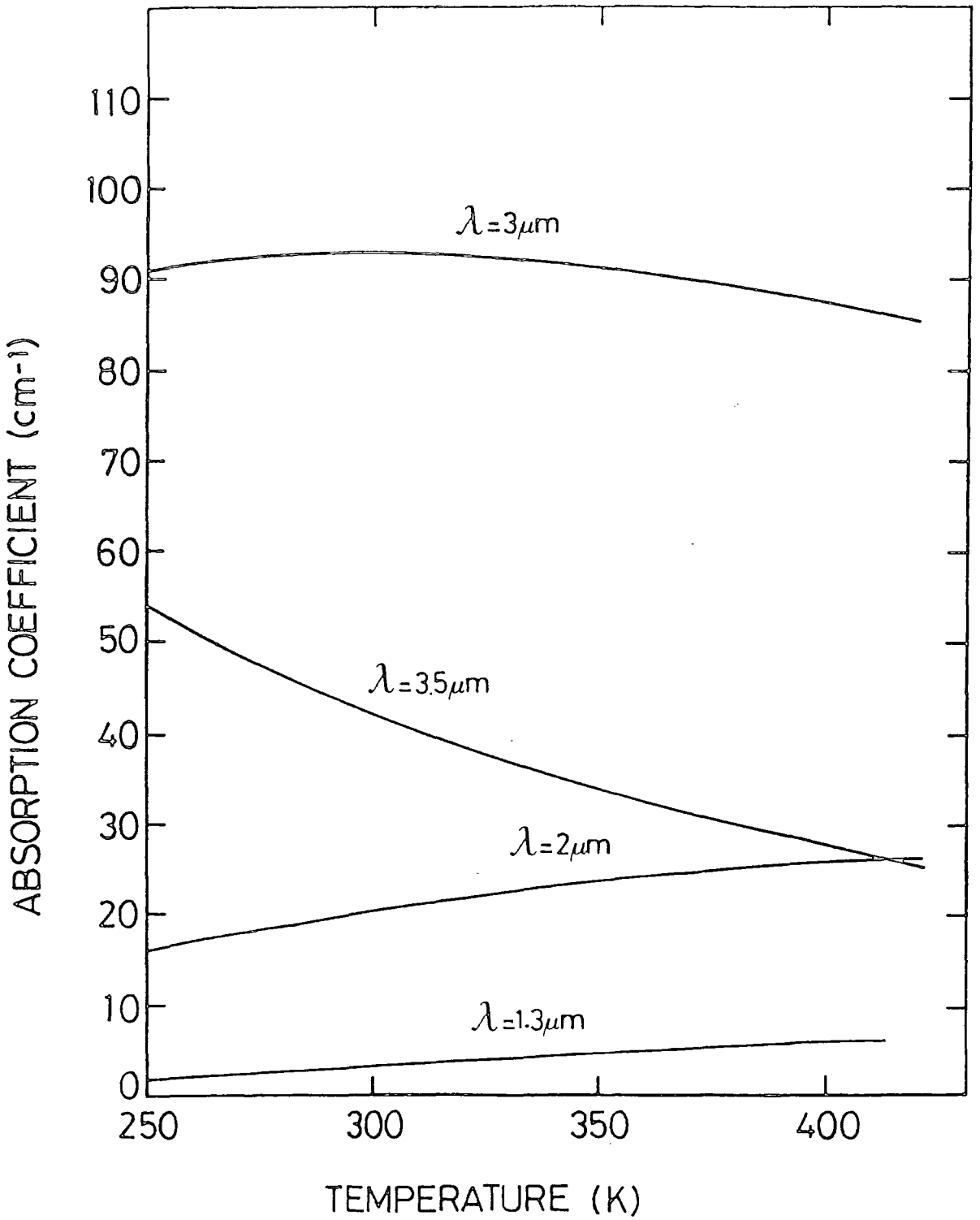

Figure 7.8: The temperature dependence of the IVBA coefficients for several wavelengths. Results are derived using the bulk pseudopotential bandstructure approximation for the sub-band E-k dispersion.

These changes can be understood in terms of an increase in the hole population at larger $\underline{k}_{ll}$ values as holes are thermally excited away from the lowest sub-band edge (hence reducing the low energy absorption transitions).

c) Concentration Dependence: The hole concentration dependence of the absorption coefficients for a given well width and temperature is approximately linear for all wavelengths considered, a result which again is similar to that found in bulk material.

d) Well Width Dependence: As the well width increases and sub-bands are pushed closer to the bulk band edges the energy separation of the sub-bands H1 and S1 is reduced resulting in an increase of absorption due to low energy transitions.

For a given high energy transition, increasing the well width lowers the absorption due to S1 - H1 transitions as these now take place further out in $\underline{k}$-space and also the hole population of H1 is lowered by the increasing population of the higher energy sub-bands. However, the absorption due to higher sub-bands increases and tends to compensate for the reduction in the process involving the lowest sub-band.

7.7.3. The $\underline{k}\cdot\underline{p}$ model

As explained in section 7.2 the bandstructure derived for the 100 A^{o} GaAs quantum well using the modified $\underline{k}\cdot\underline{p}$ calculation, has only been determined for the region of $\underline{k}$-space close to the sub-band edge. Only low energy IVBA transitions can occur within this region and these do not contribute to the optical loss at lasing wavelengths. However, a useful

comparison can be made in the limited energy range with the other two bandstructure models. The wavelength dependence of the IVBA coefficients has been derived in the $\underline{k}\cdot\underline{p}$ model again using a simple average of results calculated for the [100] and [110] directions. The absorption coefficient $\alpha(\omega)$ for a hole concentration of 10^{18} cm^{-3} at T = 300 K, is shown in figure 7.9. As discussed in section 7.1 the $\Delta n = 0$ selection rule does not apply to the intervalence band transitions in this model and band edge transitions for which $\Delta n = 1$ are in fact significant. These transitions provide absorption which would not otherwise occur. Transitions obeying the $\Delta n = 0$ selection rule (as in the other models) become more significant, and others less so, with increasing $\underline{k}_{11}$. The absorption coefficients shown in figure 7.9 generally reflect the bandstructure and momentum matrix elements shown in figures 6.7 and 6.14 and as such the absorption due to the H2 - S1 transition is not shown, the matrix elements for these transitions being very small.

The large density of states in sub-band L1 (resulting from the band curvature) produces significant absorption for transitions to this band. This contrasts markedly with the SEMA and pseudopotential models in which these transitions are ignored due to the relatively low density of states in the light hole sub-bands. The absorption coefficients for transitions from the SS to HH sub-bands for which $\Delta n = 0$ are notably smaller than those derived in the other two bandstructure models, a result partly due to the lower hole occupancy of the HH sub-bands. The transitions to the L1 sub-band to some extent compensate for this, however the total absorption coefficient in the $\underline{k}\cdot\underline{p}$ model remains lower than that derived in the other models for all the wavelengths shown.

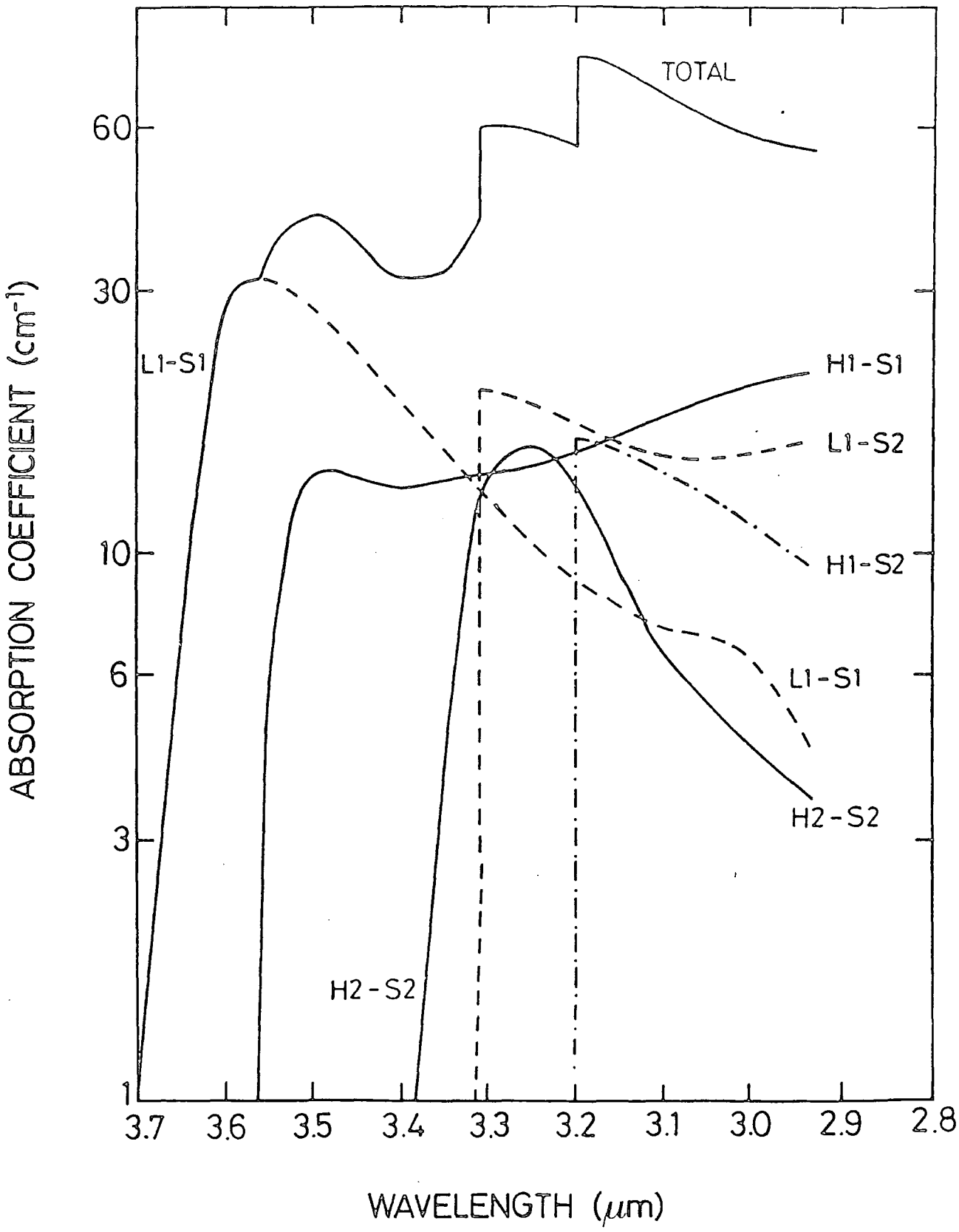

Figure 7.9: The wavelength dependence of the IVBA coefficients derived in the $\underline{k}\cdot\underline{p}$ model. The $\Delta n = 0$ selection rule is not applied and significant contributions arise from 'forbidden' transitions.

7.8. Summary

The IVBA coefficients for a 100 A^{o} GaAs quantum well structure have been evaluated using three different bandstructure models. The absorption coefficients derived using simple effective mass and pseudo-potential bandstructures show wavelength, temperature and concentration dependence similar to that found in bulk material. These dependencies can be summarised as:

a) absorption at lasing wavelength is small but low energy transitions give significant absorption,

b) the concentration dependence is approximately linear,

c) low energy transitions decrease with increasing temperature while high energy transitions increase.

The absorption coefficients derived using the $\underline{k}\cdot\underline{p}$ bandstructure and momentum elements determined in chapter 6 are limited to the low energy part of the spectrum involving transitions close to the sub-band edges, and as such the results are not really relevant to the operation of the GaAs QW laser. However, the trends shown in this model could be important in longer wavelength lasers for which IVBA transitions occurring near the band edge provide a significant optical loss. The effect of particular importance shown in this model is the contribution to the absorption of transitions that are forbidden in the simpler models.

CHAPTER 8

CONCLUSIONS AND SUGGESTIONS FOR FUTURE WORK

8.0. Conclusions

The aim of the work in this thesis has been to evaluate some fundamental effects relevant to the optical properties of semiconductors resulting from the presence of high concentrations of free carriers. The two important effects considered are the band gap narrowing, producing changes in the emission and absorption spectra, and the optical absorption produced in semiconductor laser material due to intervalence band transitions.

In chapter 2 a model was developed for the evaluation of band edge shifts (at $T = 0K$) due to changes in electron-electron interactions resulting from the introduction of extra carriers. This model incorporated coupling between the heavy and light hole valence bands and used a plasmon-pole approximation for the dielectric function of the carrier gas. The band gap narrowing in p-type Si and p- and n-type Si, GaAs $Ga_{0.47}\ In_{0.53}\ As$ and $Ga_{0.28}\ In_{0.72}\ As_{0.6}\ P_{0.4}$ was evaluated using this model, as described in chapter 3. A typical example of a band gap reduction predicted by this calculation was 88 meV in p-type Si for a hole concentration of $10^{20}\ cm^{-3}$. This narrowing of the band gap leads to a shift to lower energies of the band to band features in the luminescence spectra. A corresponding effect in the absorption spectra is normally not found due to the Moss-Burstein shift which produces an opposing increase in the absorption energy. For materials with very light conduction band effective masses (e.g. GaAs) the Moss-Burstein shift is much larger than the band gap narrowing for most concentrations of interest in the n-type materials considered in the present work.

In chapter 4 the model for evaluation of the energy shift of a state due to many body effects, was extended to finite temperature (T = 300 K) through the use of a finite temperature plasmon-pole approximation. For large free carrier concentrations (> 10^{20} cm^{-3}) the carrier distributions at T = 0 and 300 K differ little in all the materials considered, and for a given carrier concentration the band gap narrowing at these temperatures is approximately the same. For lower carrier concentrations (or higher temperatures) the thermal excitation of the carriers reduces their screening effect producing a smaller band gap narrowing than at T = OK. This effect is least noticeable in n-type materials with low conduction band effective masses (e.g. GaAs) in which the carrier gas becomes strongly degenerate resembling that at T = OK even at quite low carrier concentrations (eg. $n = 5 \times 10^{18}$ cm^{-3} in GaAs) .

Optical losses due to IVBA transitions were evaluated in chapter 5 for materials used in double heterostructure lasers: that is GaAs, $Ga_{0.47}$ $In_{0.53}$ As and $Ga_{0.28}$ $In_{0.72}$ $As_{0.6}$ $P_{0.4}$. The wavelength dependence of the IVBA coefficient evaluated using a pseudopotential bandstructure model compared well with the experimental results of Henry et al (1983). In each case the temperature dependence of IVBA coefficients was shown to be either small or if rapid variation did occur the absorption itself was small. This would seem to imply that IVBA is not responsible for the temperature dependence of laser threshold current densities. However, a full self consistent laser rate calculation would be needed to confirm this suggestion.

In Chapter 6 a variational technique for the derivation of quantum well bandstructure was described. The method based on a modified $\underline{k} \cdot \underline{p}$ approach can also with small alterations be used to determine superlattice bandstructure.

For the 100 A° GaAs quantum well considered, insufficient bandstructure was evaluated to enable the determination of IVBA coefficients at wavelengths relevant to laser operation. The model could however be used to evaluate IVBA in longer wavelength lasers for which intervalence band transitions occurring near the sub-band edge may be close to lasing energies.

The results derived from the $\underline{k}\cdot\underline{p}$ model for the wavelength dependence of IVBA coefficients were compared with corresponding results derived using simple effective mass and pseudopotential bandstructures. These models which are easily extended to high energy transitions were used to determine the concentration and temperature dependence of IVBA coefficients at various wavelengths.

8.1. Suggestions for Future Work

The band gap narrowing derived in chapters 3 and 4 for p-type material was evaluated using a plasmon-pole approximation for the Lindhard dielectric function. An improvement on this model through the use of the full Lindhard dielectric function including coupled valence bands, was discussed in section 2.6. This modification would then complement the work of Berggren and Sernelius (1981) who used the Lindhard dielectric function for electrons in evaluating the band gap narrowing in n-type materials.

A further extension of the plasmon-pole model could be made through the use of a realistic bandstructure derived in a pseudopotential calculation, and by evaluation of band shifts at non-zero k-values.

The band gap narrowing work could also be extended to the derivation of band shifts in low dimensional structures. This is particularly important in the quantum laser systems considered in chapters 6 and 7 for which band gap renormalisation would produce changes in the band to band emission spectra.

While the real part of the electron-electron self energy provides the shift in the energy of an electronic state the imaginary part determines the energy broadening of states. Evaluation of the imaginary part of the self energy would provide a straightforward extension of the present work and a useful contribution to the understanding of some aspects of optical spectra.

These energy level broadening effects could also be incorporated into the IVBA calculations in bulk and quantum well lasers. This would then provide a comparison with broadening mechanisms considered by other authors for IVBA in bulk materials (e.g. Takeshima (1984a)).

Finally as mentioned in section 7.8 the $\underline{k}\cdot\underline{p}$ bandstructure model could be used to determine fundamental and intervalence band absorption coefficients in alloy materials used for long wavelength lasers.

APPENDIX 1

PARAMETER VALUES

	Si	GaAs	$Ga_{0.47}In_{0.53}As$	$Ga_{0.28}In_{0.72}As_{0.6}P_{0.4}$
m_H/m_o	0.5	0.45*	0.47	0.466
m_L/m_o	0.16	0.085	0.055	0.075
m_S/m_o	0.24	0.15	0.12	0.14
m_ℓ/m_o	0.98	0.067	0.041	0.056
m_t/m_o	0.19	0.067	0.041	0.056
E_g (ev) T=300k	1.12	1.42	0.78	0.96
Δ (ev) T=300k	0.045	0.34	0.38	0.262
ε_r	11.8	12.35	11.67	11.18

* 0.52 in chapters 3 and 4.

APPENDIX 2

EVALUATION OF INTEGRAL EXPRESSION (2.36)

Expression (2.36) is writen as

$$\int \phi^{*}_{n\underline{k}}(\underline{r})\ \phi_{n''\underline{k}''}(\underline{r})e^{i\underline{q}\cdot\underline{r}} = \frac{\Omega_{cell}}{\Omega}\int u^{*}_{n\underline{k}}(\underline{r})u_{n''\underline{k}''}(\underline{r})e^{i(\underline{k}''+\underline{q}-\underline{k})\cdot\underline{r}}\, d^{3}\underline{r} \quad (A2.1)\ .$$

The product of Bloch periodic parts may be expanded in terms of reciprocal lattice vectors as:

$$u^{*}_{n\underline{k}}(\underline{r})u_{n''\underline{k}''}(\underline{r}) = \sum_{\underline{g}} C_{\underline{g}}e^{i\underline{g}\cdot\underline{r}} \quad (A2.2)\ .$$

where

$$C_{\underline{g}} = \frac{1}{\Omega_{cell}}\int_{\text{unit cell}} u^{*}_{n\underline{k}}(\underline{r})u_{n''\underline{k}''}(\underline{r})e^{-i\underline{g}\cdot\underline{r}}\, d^{3}\underline{r} \quad (A2.3)\ .$$

Substitution of (A2.2) into (A2.1) gives

$$\int \phi^{*}_{n\underline{k}}(\underline{r})\phi_{n''\underline{k}''}(\underline{r})e^{i\underline{q}\cdot\underline{r}}d^{3}\underline{r} = \frac{\Omega_{cell}}{\Omega}\int \sum_{\underline{g}} C_{\underline{g}}e^{i(\underline{k}''+\underline{g}+\underline{q}-\underline{k})\cdot\underline{r}}\, d^{3}\underline{r} \quad (A2.4)$$

$$= \Omega_{cell}\sum_{\underline{g}} C_{\underline{g}}\delta_{\underline{g},\underline{k}-\underline{k}''-\underline{q}} \quad (A2.5)\ .$$

The only significant contribution to the energy shifts evaluated using equation (2.39) are those for which $\underline{g} = 0$. Retaining only this term in (A2.5) gives:

$$\int \phi^{*}_{n\underline{k}}(\underline{r})\phi_{n''\underline{k}''}(\underline{r})e^{i\underline{q}\cdot\underline{r}}d^{3}\underline{r} = \Omega_{cell}\, C_{o}\delta_{o,\underline{k}-\underline{k}''-\underline{q}} \quad (A2.6)$$

which on using (A2.3) gives

$$\int \phi^*_{n\underline{k}}(\underline{r})\phi_{n''\underline{k}''}(\underline{r})e^{i\underline{q}\cdot\underline{r}}d^3r = \delta_{o,\underline{k}-\underline{k}''-\underline{q}}\int u^*_{n\underline{k}}(\underline{r})u_{n''\underline{k}''}(\underline{r})d^3\underline{r}$$

$$= \delta_{o,\underline{k}-\underline{k}''-\underline{q}}\ I_{n\underline{k},n''\underline{k}''} \qquad \text{(A2.7)}$$

where

$$I_{n\underline{k},n''\underline{k}''} = \int u^*_{n\underline{k}}(\underline{r})u_{n''\underline{k}''}(\underline{r})d^3\underline{r} \qquad \text{(A2.8)}$$

APPENDIX 3

CLASSICAL DERIVATION OF PLASMA FREQUENCY

a) Six Valley Silicon Conduction Band

Assume the carriers are distributed equally between the six valleys shown in Figure (A3.1) and an electric field is applied along the x-direction. The applied field causes electron motion in the x-direction.

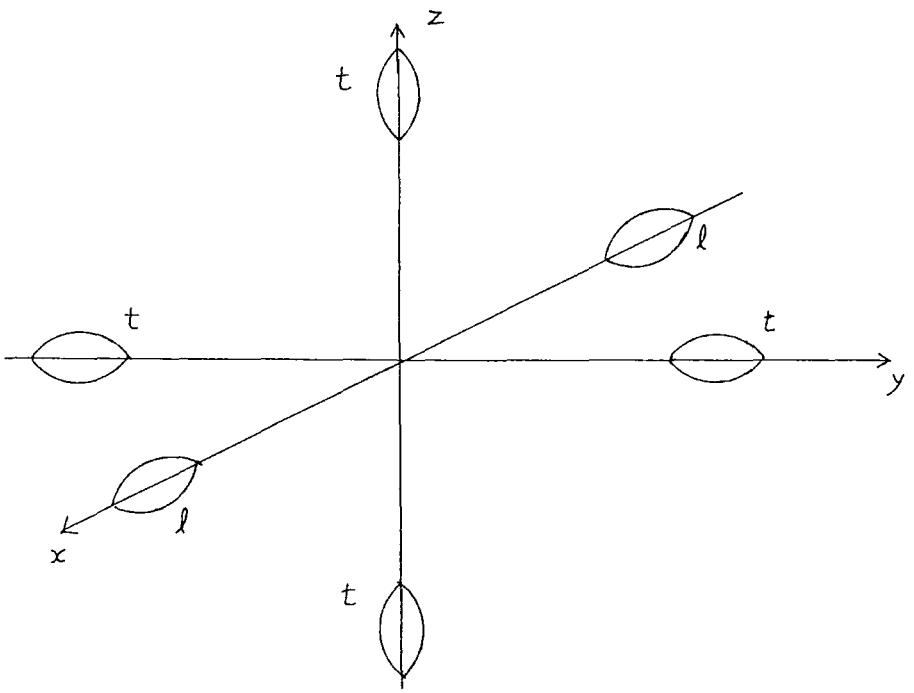

Figure (A3.1)

In four of the valleys this direction corresponds to the transverse direction t with displacements x_t. The other two valleys have their longitudinal axes in the x direction and corresponding displacements x_ℓ. On removing the driving force, the force F felt by each electron is $F = -Ee$ where

$$E = \frac{1}{3}\,\frac{ne\,x_\ell}{\varepsilon_o\varepsilon_r} + \frac{2}{3}\,\frac{ne\,x_t}{\varepsilon_o\varepsilon_r} \quad . \tag{A3.1}$$

The acceleration of particles with mass m_ℓ and m_t is then given as:

$$m_\ell \frac{d^2x_\ell}{dt^2} = -\frac{ne^2x_\ell}{3\varepsilon_o\varepsilon_r} - \frac{2}{3}\frac{ne^2x_t}{\varepsilon_o\varepsilon_r} \tag{A3.2}$$

$$m_t \frac{d^2x_t}{dt^2} = -\frac{ne^2x_\ell}{3\varepsilon_o\varepsilon_r} - \frac{2}{3}\frac{ne^2x_t}{\varepsilon_o\varepsilon_r} \quad . \tag{A3.3}$$

Using trial solutions of the form $x_\ell = x_{\ell o}\, e^{i\omega t}$ and $x_t = x_{to}\, e^{i\omega t}$ gives

$$\left(-m_\ell\omega^2 + \frac{1}{3}\frac{ne^2}{\varepsilon_r\varepsilon_o}\right) x_{\ell o} + \left(\frac{2}{3}\frac{ne^2}{\varepsilon_o\varepsilon_r}\right) x_{to} = 0$$

$$\left(\frac{1}{3}\frac{ne^2}{\varepsilon_o\varepsilon_r}\right) x_{\ell o} + \left(-m_t\omega^2 + \frac{2}{3}\frac{ne^2}{\varepsilon_o\varepsilon_r}\right) x_{to} = 0 \tag{A3.4}$$

For non-trivial solutions the determinant of the coefficients of $x_{\ell o}$ and x_{to} must vanish. Solving this determinant gives

$$\omega^2 = \frac{ne^2}{\varepsilon_o\varepsilon_r m_{ope}} \quad \text{where} \quad m_{ope} = \frac{3m_\ell m_t}{2m_\ell + m_t}$$

or $$\frac{1}{m_{ope}} = \frac{1}{3}\left(\frac{1}{m_\ell} + \frac{2}{m_t}\right) \tag{A3.5}$$

b) Heavy and Light Hole Valence Band

A similar analysis to above gives:

$$m_H \frac{d^2x_H}{dt^2} = -\lambda_H \frac{pe^2}{\varepsilon_o\varepsilon_r} x_H - \lambda_L \frac{pe^2}{\varepsilon_o\varepsilon_r} x_L$$

$$m_L \frac{d^2x_L}{dt^2} = -\lambda_H \frac{pe^2}{\varepsilon_o\varepsilon_r} x_H - \lambda_L \frac{pe^2}{\varepsilon_o\varepsilon_r} x_L \tag{A3.6}$$

where λ_H = heavy hole fraction of total hole concentration

$$\lambda_H = \frac{m_H^{3/2}}{m_H^{3/2}+m_L^{3/2}}$$

λ_L = light hole fraction of total hole concentration

$$\lambda_L = \frac{m_L^{3/2}}{m_H^{3/2}+m_L^{3/2}} \qquad \text{(A3.7)} .$$

Again using the trial solution $x_H = x_{Ho}\, e^{i\omega t}$, $x_L = x_{Lo}\, e^{i\omega t}$ gives

$$\omega^2 = \left(\frac{\lambda_H m_L + \lambda_L m_H}{m_H m_L}\right) \frac{pe^2}{\varepsilon_o \varepsilon_r}$$

$$= \left[\frac{m_H^{1/2}}{m_H^{3/2}+m_L^{3/2}} + \frac{m_L^{1/2}}{m_H^{3/2}+m_L^{3/2}}\right] \frac{pe^2}{\varepsilon_o \varepsilon_r}$$

thus $\omega_p^2 = \dfrac{pe^2}{\varepsilon_o \varepsilon_r m_{ov}}$ where $\dfrac{1}{m_{ov}} = \dfrac{m_H^{1/2}+m_L^{1/2}}{m_H^{3/2}+m_L^{3/2}}$ (A3.8) .

c) Electron-Hole Plasma

A similar analysis to the above for a single conduction band and a heavy and light hole valence band yields

$$\omega^2 = \frac{ne^2}{\varepsilon_r \varepsilon_o \mu} \quad \text{where} \quad \frac{1}{\mu} = \frac{1}{m_{De}} + \frac{\lambda_L}{m_L} + \frac{\lambda_H}{m_H} \qquad \text{(A3.9)}$$

where n = concentration of electrons or holes, i.e.

$$\omega_p^2 = \omega_p^2(\text{electrons}) + \omega_p^2(\text{holes}) .$$

APPENDIX 4

DERIVATION OF THE AVERAGED MOMENTUM MATRIX ELEMENTS IN A BULK SEMICONDUCTOR

The momentum matrix element between states in the spin split-off and heavy hole bands is given by

$$M = \int_{\Omega} \psi_H^*(\underline{r}) \left| \hat{\underline{e}} \cdot \underline{\nabla} \right| \psi_S(\underline{r}) \, d^3\underline{r} \qquad \text{(A4.1)}$$

where the volume integral covers the active lasing material and the unit polarisation vector is defined as:

$$\hat{\underline{e}} = \underline{e}_x + \underline{e}_y + \underline{e}_z \quad \text{where} \quad \hat{e}^2 = e_x^2 + e_y^2 + e_z^2 = 1 \qquad \text{(A4.2)} \; .$$

The Bloch functions ψ_H and ψ_S can be expressed as

$$\psi_H = \left(\frac{\Omega_{cell}}{\Omega}\right)^{1/2} u_H(\underline{r}) e^{i\underline{k}_H \cdot \underline{r}} \qquad \psi_S = \left(\frac{\Omega_{cell}}{\Omega}\right)^{1/2} u_S(\underline{r}) e^{i\underline{k}_S \cdot \underline{r}} \qquad \text{(A4.3)} \; .$$

Substitution of (A4.3) into (A4.1) gives

$$M = \frac{\Omega_{cell}}{\Omega} \int_{\Omega} u_H^*(\underline{r}) e^{-i\underline{k}_H \cdot \underline{r}} \left| \hat{\underline{e}} \cdot \underline{\nabla} \right| u_S(\underline{r}) e^{i\underline{k}_S \cdot \underline{r}} \, d^3\underline{r} \qquad \text{(A4.4)}$$

$$\text{or} \quad M = \frac{\Omega_{cell}}{\Omega} \int_{\Omega} u_H^*(\underline{r}) e^{-i\underline{k}_H \cdot \underline{r}} \left| e_x \frac{\partial}{\partial x} + e_y \frac{\partial}{\partial y} + e_z \frac{\partial}{\partial z} \right| u_S(\underline{r}) e^{i\underline{k}_S \cdot \underline{r}} \, d^3\underline{r} \qquad \text{(A4.5)} \; .$$

Applying the differential operators and ignoring the small terms arising from differentiation of the exponential factor gives

$$M = \frac{\Omega_{cell}}{\Omega} \int (u_H^*(\underline{r}) \left| e_x \frac{\partial}{\partial x} + e_y \frac{\partial}{\partial y} + e_z \frac{\partial}{\partial z} \right| u_S(\underline{r})) e^{-i(\underline{k}_H - \underline{k}_S)\cdot\underline{r}} d^3\underline{r} \qquad (A4.6)$$

$$\text{or} \quad M = e_x M'_x + e_y M'_y + e_z M'_z \qquad (A4.7)$$

$$\text{where} \quad M'_x = \frac{\Omega_{cell}}{\Omega} \int (u_H^*(\underline{r}) \frac{\partial}{\partial x} u_S(\underline{r})) e^{-i(\underline{k}_H - \underline{k}_S)\cdot\underline{r}} d^3\underline{r} \qquad (A4.8) .$$

As $(u_H^*(\underline{r}) \frac{\partial}{\partial x} u_S(\underline{r}))$ is lattice periodic it can be expanded as a sum or reciprocal lattice vectors,

$$u_H^*(\underline{r}) \frac{\partial}{\partial x} u_S(\underline{r}) = \sum_{\underline{g}} C_{\underline{g}} e^{i\underline{g}\cdot\underline{r}} \qquad (A4.9) .$$

Then

$$M'_x = \frac{\Omega_{cell}}{\Omega} \int_{\Omega} \sum_{\underline{g}} C_{\underline{g}} e^{i\underline{g}\cdot\underline{r}} e^{-i(\underline{k}_H - \underline{k}_S)\cdot\underline{r}} d^3\underline{r} \qquad (A4.10)$$

$$M'_x = \Omega_{cell} \sum_{\underline{g}} C_{\underline{g}} \delta_{\underline{g},\underline{k}_H - \underline{k}_S} \qquad (A4.11)$$

$$\text{so} \quad M'_x = \Omega_{cell} C_{\underline{o}} \delta_{\underline{o},\underline{k}_H - \underline{k}_S} \qquad (A4.12)$$

as $\underline{k}_H$ and $\underline{k}_S$ will always be much smaller than the smallest non-zero reciprocal lattice vector.

Now

$$C_{\underline{g}} = \frac{1}{\Omega_{cell}} \int u_H^*(\underline{r}) \frac{\partial}{\partial x} u_s(\underline{r}) e^{-i\underline{g}\cdot\underline{r}} d^3\underline{r} \qquad (A4.13) .$$

$$\text{So} \quad C_{\underline{o}} = \frac{1}{\Omega_{cell}} \int u_H^*(\underline{r}) \frac{\partial}{\partial x} u_s(\underline{r}) \, d^3\underline{r} \qquad (A4.14)$$

then $$M'_x = M_x \, \delta_{\underline{o},\underline{k}_H-\underline{k}_S} \qquad \text{(A4.15)}$$

where $$M_x = \int u^*_H(\underline{r}) \, \frac{\partial}{\partial x} u_S(\underline{r}) \, d^3\underline{r} \qquad \text{(A4.16)} \; .$$

Similar expressions are found for M'_y and M'_x giving

$$M = (e_x M_x + e_y M_y + e_z M_z) \, \delta_{\underline{o},\underline{k}_H-\underline{k}_S} \qquad \text{(A4.17)}$$

and $$|M|^2 = |e_x M_x + e_y M_y + e_z M_z|^2 \, \delta_{\underline{o},\underline{k}_H-\underline{k}_S} \qquad \text{(A4.18)} \; .$$

Now an integral over all polarisation space normalised to unit volume gives

$$|M|^2 = \frac{1}{4\pi} \int |e_x M_x + e_y M_y + e_z M_z|^2 \, \delta_{\underline{o},\underline{k}_H-\underline{k}_S} \, de \qquad \text{(A4.19)} \; .$$

Using the coordinate system

$$e_x = e \sin\theta \cos\phi \qquad e_y = e \sin\theta \sin\phi \qquad e_z = e \cos\theta$$

on substitution into (A4.19) only terms of the form e_x^2, e_y^2, e_z^2 contribute towards the integral, for example

$$\int e_x^2 de = \int_{\theta=0}^{\pi} \int_{\phi=0}^{2\pi} \sin^2\theta \cos^2\phi \sin\theta \, d\theta \, d\phi = \frac{4\pi}{3} \qquad \text{(A4.20)} \; .$$

Hence

$$|M|^2 = \frac{1}{3}[|M_x|^2 + |M_y|^2 + |M_z|^2] \, \delta_{\underline{o},\underline{k}_H-\underline{k}_S} \qquad \text{(A4.21)} \; .$$

APPENDIX 5

Derivation of the Variational Expression (6.6)

Taking the trial wave functions and energy to be different from their true values by a small amount, i.e.

$$\psi = \psi_t + \delta\psi \qquad \psi_A = \psi_t + \delta\psi_A$$

$$\psi_B = \psi_t + \delta\psi_B \qquad \varepsilon = \varepsilon_t + \delta\varepsilon \tag{A5.1}$$

where ψ_t and ε_t are the true wavefunction and eigenvalue respectively, ψ_A and ψ_B are trial wavefunctions in regions A and B.

Note the above expressions for ψ_A and ψ_B imply that the trial wavefunctions in regions A and B are varied independently, i.e. $\delta\psi_A \neq \delta\psi_B$.

We substitute these trial functions into the normal variational expression, (using atomic units throughout).

$$\int_{\Omega_{A+B}} \psi^* H \psi \, d\Omega = \varepsilon \int_{\Omega_{A+B}} \psi^* \psi \, d\Omega \tag{A5.2}$$

which on ignoring terms of second order in small quantities gives

$$\int_{\Omega_{A+B}} (\psi_t^* H \delta\psi + \delta\psi^* H \psi_t + \psi_t^* H \psi_t) d\Omega =$$

$$\varepsilon_t \int_{\Omega_{A+B}} (\psi_t^*\psi_t + \psi_t^*\delta\psi + \delta\psi^*\psi_t) d\Omega + \delta\varepsilon \int_{\Omega_{A+B}} \psi_t^* \psi_t \, d\Omega \tag{A5.3}$$

subtracting terms on L.H.S. from the R.H.S. gives

$$\delta\varepsilon \int_{\Omega_{A+B}} \psi_t^* \psi_t \, d\Omega = \int_{\Omega_{A+B}} \psi_t^* (H - \varepsilon_t) \delta\psi \, d\Omega \qquad (A5.4)$$

We now separate the volume integrals into integration over distinct volumes of material A and B and use Green's Theorem for a region Ω bounded by a surface S

$$\int_{\Omega} (\psi \nabla^2 \phi - \phi \nabla^2 \psi) d\Omega = \int_{S} (\psi \nabla_n \phi - \phi \nabla_n \psi) dS \qquad (A5.5)$$

n being the outward normal to surface S.

This is applied to the R.H.S. of equation (A5.4) for region A giving

$$\int_{\Omega_A} \psi_t^* (H - \varepsilon_t) \delta\psi \, d\Omega = \int_{\Omega_A} \psi_t^* (-\frac{\nabla^2}{2} + V - \varepsilon_t) \delta\psi_A \, d\Omega - \int_{\Omega_A} \delta\psi_A \frac{\nabla^2}{2} \psi_t^* \, d\Omega$$

$$+ \int_{\Omega_A} \psi_t^* (V - \varepsilon_t) \delta\psi_A \, d\Omega - \frac{1}{2} \int_{S_A} (\psi_t^* \nabla_n \delta\psi_A - \delta\psi_A \nabla_n \psi_t^*) dS \qquad (A5.6)$$

where S_A is the surface surrounding volume A. The first two terms on the R.H.S. cancel. A similar expression can be derived for integration over volume B.

Equation (A5.4) now becomes

$$\delta\varepsilon \int_{\Omega_{A+B}} \psi_t^* \psi_t d\Omega = -\frac{1}{2} \int_{S_A} (\psi_t^* \nabla_n \delta\psi_A - \delta\psi_A \nabla_n \psi_t^*) dS$$

$$- \frac{1}{2} \int_{S_B} (\psi_t^* \nabla_{n'} \delta\psi_B - \delta\psi_B \nabla_{n'} \psi_t^*) dS \qquad (A5.7)$$

where n and n' are the outward normals to the surfaces surrounding regions A and B respectively.

Now as the trial wave functions together with $\delta\psi_A$, and $\delta\psi_B$ satisfy the periodic boundary conditions (6.5) we see by reference to figure (6.5) that integrals over surfaces S_4, S_5 and S_6, S_7 vanish by cancellation of contributions from opposite points on the cell boundary where n or n' have opposite directions. Similar cancellation will occur for the parallel faces not shown in the figure. Equation (A5.7) then reduces to integrals over S_1, S_2 and S_3.

$$\delta\varepsilon \int_{\Omega_{A+B}} \psi_t^* \psi_t \, d\Omega = -\frac{1}{2} \int_{S_1+S_2} (\psi_t^* \nabla_n \delta\psi_A - \delta\psi_A \nabla_n \psi_t^*) dS$$

$$-\frac{1}{2} \int_{S_2+S_3} (\psi_t^* \nabla_{n'} \delta\psi_B - \delta\psi_B \nabla_{n'} \psi_t^*) dS \qquad \text{(A5.8)} .$$

These terms can be further simplified as the outward normal on S_2 in A is in the opposite direction to that on S_2 in B. In addition the periodic nature of the superlattice dictates that the wave functions on S_1 and S_3 are equal, however the outward normal on S_2 in A is in opposite direction to that on S_3 in B. Choosing as our positive direction the outward normal on S_2 in A we obtain

$$\delta\varepsilon \int_{\Omega_{A+B}} \psi_t^* \psi_t d\Omega = \frac{1}{2} \int_{S_2} [\psi_t^* (\nabla_n \delta\psi_B - \nabla_n \delta\psi_A) + (\delta\psi_A - \delta\psi_B) \nabla_n \psi_t^*] \, dS$$

$$-\frac{1}{2} \int_{S_1} [\psi_t^* (\nabla_n \delta\psi_B - \nabla_n \delta\psi_A) + (\delta\psi_A - \delta\psi_B) \nabla_n \psi_t^*] \, dS \qquad \text{(A5.9)}$$

If the trial wavefunctions in regions A and B were not independntly variable i.e. $\delta\psi_A = \delta\psi_B$ the R.H.S. of (A5.9) would vanish showing our original expression (A5.2) to be variational. However the problem is

then effectively reduced to the normal variational expression applicable to the wave function in a single material. In the present model with independently variable trial wavefunctions, first order variations of $\varepsilon(\delta\varepsilon)$ will only vanish if either terms on the R.H.S. of equation (A5.9) cancel or we add in terms to our original expression (A5.2) which cancel the above surface integrals. If these additional terms take the form given in equation (6.6) as

$$\frac{1}{4}\int_{S_2}\left[(\psi_B - \psi_A)(\nabla_n\psi_B^* + \nabla_n\psi_A^*) - (\psi_B^* + \psi_A^*)(\nabla_n\psi_B - \nabla_n\psi_A)\right] dS$$

$$-\frac{1}{4}\int_{S_1} \text{(same expression as above)}\ dS \qquad \text{(A5.10)}$$

substitution of conditions (A5.1) gives on ignoring terms of second order in small quantities:

$$\frac{1}{4}\int_{S_2}\left[2(\delta\psi_B - \delta\psi_A)\nabla_n\,\psi_t^* - 2\psi_t^*(\nabla_n\delta\psi_B - \nabla_n\delta\psi_A)\right]dS$$

$$-\frac{1}{4}\int_{S_1} \text{(same expression as above)}\ dS \qquad \text{(A5.11)}\ .$$

These terms clearly cancel the surface integrals in equation (A5.9) so causing $\delta\varepsilon$ to vanish. The disappearance of first order variations in energy thus satisfies the required condition that expression (6.6) be variational.

APPENDIX 6

Proof of Reality of Eigenvalues in Variational Expression (6.6)

We wish to prove that eigenvalue ε in the expression (A6.1) below is always real.

$$\varepsilon \int_{\Omega_{A+B}} \psi^* \psi \, d\Omega = \int_{\Omega_{A+B}} \psi^* H \psi \, d\Omega + \frac{1}{4} \int_{S_2} [(\psi_B - \psi_A)(\nabla_n \psi_B^* + \nabla_n \psi_A^*)$$

$$- (\psi_B^* + \psi_A^*)(\nabla_n \psi_B - \nabla_n \psi_A)] dS$$

$$- \frac{1}{4} \int_{S_1} (\text{same expression as above}) dS \qquad \text{(A6.1)} .$$

Rearranging terms in the integral over S_2 gives

$$\frac{1}{4} \int_{S_2} [(\psi_A^* \nabla_n \psi_A - \psi_A \nabla_n \psi_A^*) - (\psi_B^* \nabla_n \psi_B - \psi_B \nabla_n \psi_B^*)$$

$$+ (\psi_B^* \nabla_n \psi_A - \psi_A \nabla_n \psi_B^*) - (\psi_A^* \nabla_n \psi_B - \psi_B \nabla_n \psi_A^*)] dS \qquad \text{(A6.2)}$$

a similar expression is produced for the integration over S_1. Terms in the last two pairs of brackets appear in conjugate pairs and will give real values on integration. Applying Green's theorem to the Hamiltonian term in expression (A6.1) gives

$$\int_{\Omega_{A+B}} \psi^* \left(-\frac{\nabla^2}{2} + V\right)\psi \, d\Omega = \frac{1}{2}\int_{\Omega_{A+B}} (\nabla\psi^* \cdot \nabla\psi + \psi^* V\psi) d\Omega$$

$$- \frac{1}{2}\int_{S_A} \psi_A^* \nabla_n \psi_A \, dS - \frac{1}{2}\int_{S_B} \psi_B^* \nabla_n, \psi_B \, dS \qquad \text{(A6.3)} \; .$$

Applying the same arguments as used in Appendix 5 for cancellation of terms on opposing faces and choosing the normal on S_2 in A to be the positive direction expression (A6.3) reduces to

$$\int_{\Omega_{A+B}} \psi^* \left(-\frac{\nabla^2}{2} + V\right)\psi \, d\Omega = \frac{1}{2}\int_{\Omega_{A+B}} (\nabla\psi^* \cdot \nabla\psi + \psi^* V\psi) d\Omega$$

$$- \frac{1}{2}\int_{S_2} (\psi_A^* \nabla_n \psi_A - \psi_B^* \nabla_n \psi_B) dS - \frac{1}{2}\int_{S_1} (\psi_B^* \nabla_n \psi_B - \psi_A^* \nabla_n \psi_A) dS \qquad \text{(A6.4)} \; .$$

On substitution into (A6.2) all terms are now in conjugate pairs. The eigenvalue ε must therefore always be real.

APPENDIX 7

Evaluation of the Integral Terms from the Matching Conditions

We have from equation (6.12) the trial wavefunction in region B

$$\psi_B = \sum_j e^{i\underline{k}_{ll}\cdot\underline{r}_{ll}} u_j^B F_j^B + \sum_j \sum_{i\neq j} i \frac{(k_x P_{ij}^x + k_y P_{ij}^y)^B}{(E_j - E_i)^B} F_j^B u_i^B e^{i\underline{k}_{ll}\cdot\underline{r}_{ll}}$$

$$+ \sum_j \sum_{i\neq j} \left(\frac{P_{ij}^z}{E_j - E_i}\right)^B u_i^B \frac{\partial F_j^B}{\partial z} e^{i\underline{k}_{ll}\cdot\underline{r}_{ll}} \qquad \text{(A7.1)}$$

where the $\underline{r}$ and $\underline{z}$ dependence of u_j and F_j respectively have been omitted to simplify the notation. The term

$$\int_{\Omega_{cell}} (\psi_B^* \nabla\psi_A - \psi_A \nabla\psi_B^*) d\Omega \qquad \text{(A7.2)}$$

will be evaluated, all other terms in the matching conditions can then be derived from the resulting expression by suitable manipulation of labels A and B. Differentiating ψ_A with respect to z we obtain:

$$\frac{\partial\psi_A}{\partial z} = \sum_j e^{i\underline{k}_{ll}\cdot\underline{r}_{ll}} \left(u_j \frac{\partial F_j}{\partial z} + F_j \frac{\partial u_j}{\partial z}\right)^A$$

$$+ \sum_j \sum_i i \left(\frac{k_x P_{ij}^x + k_y P_{ij}^y}{E_j - E_i}\right)^A e^{i\underline{k}_{ll}\cdot\underline{r}_{ll}} \left(\frac{\partial F_j}{\partial z} u_i + F_j \frac{\partial u_i}{\partial z}\right)^A$$

$$+ \sum_j \sum_i \left(\frac{P_{ij}^z}{E_j - E_i}\right)^A e^{i\underline{k}_{ll}\cdot\underline{r}_{ll}} \left(\frac{\partial^2 F_j}{\partial z^2} u_i + \frac{\partial F_j}{\partial z} \frac{\partial u_i}{\partial z}\right)^A \qquad \text{(A7.3)}\ .$$

The term $\int \psi^*_B \nabla\psi_A \, d\Omega$ is now calculated neglecting all terms of

second order (i.e. those with two denominators), and noting that all integrals are taken over a lattice unit cell located at the interface

$$\int \psi_B^* \nabla \psi_A = \sum_{j\,j'} \int u_j^{B*} F_j^{B*} \left(u_{j'} \frac{\partial F_{j'}}{\partial z} + F_{j'} \frac{\partial u_{j'}}{\partial z} \right)^A d\Omega$$

$$+ \sum_{j\,j'\,i'} \int u_j^{B*} F_j^{B*} i \left(\frac{k_x P^x_{i'j'} + k_y P^y_{i'j'}}{E_{j'} - E_{i'}} \right)^A \left(\frac{\partial F_{j'}}{\partial z} u_{j'} + F_{j'} \frac{\partial u_{i'}}{\partial z} \right)^A d\Omega$$

$$+ \sum_{j\,j'\,i'} \int u_j^{B*} F_j^{B*} \left(\frac{P^z_{i'j'}}{E_{j'} - E_{i'}} \right)^A \left(\frac{\partial^2 F_{j'}}{\partial z^2} u_{i'} + \frac{\partial F_{j'}}{\partial z} \frac{\partial u_{i'}}{\partial z} \right)^A d\Omega$$

$$+ \sum_{j\,i\,j'} \int -i \left(\frac{k_x P^x_{ij} + k_y P^y_{ij}}{E_j - E_i} \right)^{B*} F_j^{B*} u_i^{B*} \left(u_{j'} \frac{\partial F_{j'}}{\partial z} + F_{j'} \frac{\partial u_{j'}}{\partial z} \right)^A d\Omega$$

$$+ \sum_{j\,i\,j'} \int \left(\frac{P^z_{ij}}{E_j - E_i} \right)^{B*} u_i^{B*} \frac{\partial F_j^{B*}}{\partial z} \left(u_{j'} \frac{\partial F_{j'}}{\partial z} + F_{j'} \frac{\partial u_{j'}}{\partial z} \right)^A d\Omega \qquad \text{(A7.4)}.$$

As the envelope functions change little over a lattice cell, they are taken to have their values at the relevant interface. The Bloch functions are normalised to the unit cells so:

$$\int u_j^* u_{j'} \, d\Omega = \delta_{jj'}$$

$$\int u_j^* u_{i'} \, d\Omega = 0$$

and also we define $P^z_{jj'}$ as

$$\int u_j^* \frac{\partial u_{j'}}{\partial z} = - P^z_{jj'} \qquad \text{(A7.5)}.$$

Then noting that $u_j^A = u_j^B$, which is an assumption of the model as described in Chapter 6, expression (A7.4) becomes

$$\int \psi_B^* \nabla\psi_A \, d\Omega = \sum_j \sum_{j'} \left(\delta_{jj'} F_j^{B*} \frac{\partial F_{j'}^A}{\partial z} - P_{jj'}^z F_j^{B*} F_{j'}^A \right)$$

$$- \sum_j \sum_{j'} \sum_{i'} i \left(\frac{k_x P_{i'j'}^x + k_y P_{i'j'}^y}{E_{j'} - E_{i'}} \right)^A P_{ji'}^z F_j^{B*} F_{j'}^A$$

$$- \sum_j \sum_{j'} \sum_{i'} \left(\frac{P_{i'j'}^z}{E_{j'} - E_{i'}} \right)^A P_{ji'} F_j^{B*} \frac{\partial F_{j'}^A}{\partial z}$$

$$+ \sum_j \sum_i \sum_{j'} i \left(\frac{k_x P_{ij}^x + P_{ij}^y k_y}{E_j - E_i} \right)^{B*} P_{ij'}^z F_j^{B*} F_{j'}^A$$

$$- \sum_j \sum_i \sum_{j'} \left(\frac{P^z}{E_j - E_i} \right)^{B*} P_{ij'}^z \frac{\partial F_j^{B*}}{\partial z} F_{j'}^A \qquad \text{(A7.6)} .$$

On subtracting the similar terms obtained from $\int \psi_A \nabla\psi_B^* \, d\Omega$ and using:

$$D_{jj'}^{\alpha\beta} = \frac{\delta_{jj'}\delta_{\alpha\beta}}{2} - \sum_i \frac{P_{ji}^\alpha P_{ij'}^\beta}{E_{j'} - E_i} \qquad \text{(A7.7)}$$

and

$$P_{jj'}^{z*} = - P_{j'j}^z$$

we obtain:

$$\int (\psi_B^* \nabla \psi_A - \psi_A \nabla \psi_B^*) d\Omega = 2 \sum_{jj'} [F_j^{B*} \frac{\partial F_{j'}^A}{\partial z} D_{jj'}^{Azz} - F_{j'}^A \frac{\partial F_j^{B*}}{\partial z} D_{jj'}^{Bzz}]$$

$$+ 2 \sum_{jj'} F_j^{B*} [ik_y (D_{jj'}^{Azy} + D_{jj'}^{Byz}) + ik_x (D_{jj'}^{Azx} + D_{jj'}^{Bxz}) - P_{jj'}^z] F_{j'}^Z \quad \text{(A7.8)} .$$

APPENDIX 8

Normalisation Factor for the Quantum Well Wavefunctions and Evaluation of Normalisation Integral (6.20)

This appendix serves to evaluate the normalisation integral of expression (6.20) and to determine the correct normalisation factor for the wavefunction ψ. Let D be the appropriate normalisation factor such that if:

$$\psi = D\left[\sum_j F_j(z)\, u_j\,(\underline{r})\, e^{i\underline{k}_{ll}\cdot\underline{r}_{ll}} + \sum_j \sum_i i\left(\frac{k\cdot P_{ij}}{E_j - E_i}\right) u_i\, F_j\, e^{i\underline{k}_{ll}\cdot\underline{r}_{ll}}\right] \qquad (A8.1)$$

$$\text{then} \int_{\Omega_A+\Omega_B} \psi^*\,\psi\, d\Omega = 1 \qquad (A8.2)$$

where the Bloch periodic parts of $u_j(\underline{r})$ of equation (A8.1) are taken to be normalised to the unit cell, and Ω_A and Ω_B are the volumes of materials A and B respectively, and superscripts A or B from the wavefunction expansion in the appropriate region are omitted.

Ignoring terms of second order in the energy denominators, expression (A8.2) gives:

$$\int_{\Omega_A+\Omega_B} \psi^*\,\psi\, d\Omega = D^*D \sum_j \sum_{j'} \int_{\Omega_A+\Omega_B} \left[F_j^*\, F_{j'}\, u_j^*\, u_{j'} - \sum_i i\left(\frac{k\cdot P_{ij}}{E_j - E_i}\right)^* F_j^*\, F_{j'}\, u_i^*\, u_j\right.$$

$$\left. + \sum_{i'} i\left(\frac{k\cdot P_{i'j'}}{E_{j'} - E_{i'}}\right) F_j^*\, F_{j'}\, u_j^*\, u_{i'}\right] d\Omega \qquad (A8.3)\ .$$

Now considering the first terms in the square brackets we use the lattice periodicity of the Bloch functions to express the product $u_j^* u_{j'}$ as a Fourier series expansion in terms of reciprocal lattice vectors

$$u_j^* u_{j'} = \sum_{\underline{g}} C_{\underline{g}} e^{i\underline{g}\cdot\underline{r}} \qquad \text{(A8.4)} .$$

Then

$$\int_{\Omega_A+\Omega_B} F_j^* F_{j'} u_j^* u_{j'} d\Omega = \int_{\Omega_A+\Omega_B} \sum_{\underline{g}} C_{\underline{g}} e^{i\underline{g}\cdot\underline{r}} F_j(z) F_{j'}(z) d\Omega \qquad \text{(A8.5)} .$$

Integrating over the plane of the layers gives

$$\int C_{\underline{g}} e^{i\underline{g}_{ll}\cdot\underline{r}_{ll}} e^{i\underline{g}_z\cdot\underline{z}} d\underline{r}_{ll} = A\, C_{\underline{g}} e^{i\underline{g}_z\cdot\underline{z}} \delta_{O,\underline{g}_{ll}} \qquad \text{(A8.6)}$$

(where A is the area of the planar interface), and hence

$$\int_{\Omega_A+\Omega_B} F_j^* F_{j'} u_j^* u_{j'} d\Omega = A \sum_{\underline{g}_z} C_{OO\underline{g}_z} \int_O^L e^{i\underline{g}_z\cdot\underline{z}} F_j(z) F_{j'}(z) dz . \qquad \text{(A8.7)} .$$

Equation (A8.7) contains the Fourier transform of $F_j F_{j'}$ for a discrete set of wavevectors $\underline{g}_z$. For quantum wells much wider than the lattice parameter only $\underline{g}_z = O$ gives a significant contribution. Thus

$$\int_{\Omega_A+\Omega_B} F_j^* F_{j'} u_j^* u_{j'} d\Omega = A\, C_{OOO} \int_O^L F_j F_{j'} dz \qquad \text{(A8.8)} .$$

Now multiplying (A8.4) by $e^{-i\underline{g}'\cdot\underline{r}}$ and integrating over a lattice unit cell gives

$$\int_{\Omega_{cell}} u_j^* \, u_{j'} \, e^{-i\underline{g}'\cdot\underline{r}} \, d\Omega = \sum_{\underline{g}} \int_{\Omega_{cell}} C_{\underline{g}} \, e^{i(\underline{g}-\underline{g}')\cdot\underline{r}} \, d\Omega$$

$$= \sum_{\underline{g}} C_{\underline{g}} \, \delta_{\underline{g},\underline{g}'} \, \Omega_{cell} = C_{\underline{g}'} \, \Omega_{cell} \qquad \text{(A8.9)} \; .$$

$$\text{Thus} \quad C_{OOO} = \frac{1}{\Omega_{cell}} \int_{\Omega_{cell}} u_j^* \, u_{j'} \, d\Omega \qquad \text{(A8.10)} \; .$$

Expression (A8.8) now becomes

$$\int_{\Omega_A+\Omega_B} F_j^* \, F_{j'} \, u_j \, u_{j'} \, d\Omega = \frac{A}{\Omega_{cell}} \int_{\Omega_{cell}} u^*_j \, u_{j'} \, d\Omega \int_0^L F_j^* \, F_{j'} \, dz$$

$$= \frac{A}{\Omega_{cell}} \, \delta_{jj'} \int_0^L F_j^* \, F_{j'} \, dz \qquad \text{(A8.11)} \; .$$

The same procedure can be followed for evaluation of the other terms in expression (A8.3). The kronecker delta term δ_{ij} arising from the overlap integral of the Bloch function periodic terms, then ensures all other terms vanish (as $i \neq j$).

Substituting equation (A8.11) in (A8.3) gives

$$\int_{\Omega_A+\Omega_B} \psi^* \, \psi \, d\Omega = \frac{D^*DA}{\Omega_{cell}} \sum_j \sum_{j'} \delta_{jj'} \int_0^L F_j^* \, F_{j'} \, dz$$

$$= \frac{D^*DA}{\Omega_{cell}} \sum_j \int_0^L F_j^* \, F_j \, dz \qquad \text{(A8.12)} \; .$$

This expression can now be substituted into equation (6.6) as the normalisation factor on the L.H.S. of the expression. It should be noted that the normalisation prefactors (D^2A/Ω_{cell}) can be omitted from equation (6.6) due to its appearance in every term of the expression.

If $N^{1/2}$ is the appropriate normalisation factor for the envelope functions such that

$$N \sum_j \int_0^L F_j^* F_j \, dz = 1 \qquad \text{(A8.13)}$$

Then $\frac{AD^2}{\Omega_{cell}} = N$

and $$\psi = \left\{\frac{N \Omega_{cell}}{A}\right\}^{1/2} \left[\sum_j F_j u_j e^{i\underline{k}_{ll} \cdot \underline{r}_{ll}} + \sum_j \sum_i i \left\{\frac{k \cdot P_{ij}}{E_j - E_i}\right\} u_i F_j e^{i\underline{k}_{ll} \cdot r_{ll}}\right] \qquad \text{(A8.14)} \; .$$

This normalised wavefunction is used in evaluation of the momentum matrix elements discussed in chapter 6.

APPENDIX 9

Derivation of Momentum Matrix Elements for Quantum Well States

An expression for the momentum matrix element of the transition from a spin split-off to a heavy hole sub-band is derived below. This expression can be applied to optical transitions between any sub-bands by appropriate manipulation of the subscripts H and S.

The wavefunctions in the form (6.12) for 'heavy hole' and 'spin split-off' sub-bands (normalised by the prescription (A8.14) must be substituted into the expression:

$$M = \int_{\Omega_A} \psi^*_{AH} \, |\underline{\varepsilon}\cdot\underline{p}| \, \psi_{AS} \, d\Omega + \int_{\Omega_B} \psi^*_{BH} \, |\underline{\varepsilon}\cdot\underline{p}| \, \psi_{BS} \, d\Omega \qquad \text{(A9.1)}$$

where

$$\psi_{AH} = \left\{\frac{N_H \Omega_{cell}}{A}\right\}^{1/2} \Big[\sum_j e^{i\underline{k}_{ll}\cdot\underline{r}_{ll}} F^A_{jH} u^A_j +$$

$$\sum_j \sum_i i \left\{\frac{k_{xH} p^x_{ij} + k_{yH} p^y_{ij}}{E_j - E_i}\right\}^A F_{jH} u^A_i e^{i\underline{k}_{llH}\cdot\underline{r}_{ll}}$$

$$\sum_j \sum_i \left\{\frac{p^z_{ij}}{E_j - E_i}\right\}^A u^A_i \frac{\partial F^A_{jH}}{\partial z} e^{i\underline{k}_{llH}\cdot\underline{r}_{ll}} \Big] \qquad \text{(A9.2)} \; .$$

Where the H subscript appearing on the envelope term F_j indicates that its expansion coefficients $a_{\ell j}$ are dependent on the particular state H being represented. A similar expression exists for ψ_{AS}.

Corresponding expressions also exist for the wavefunctions in material B, however as the wavefunction amplitude in this region is small, the transition matrix elements are also small and are therefore omitted from the calculation.

a) Radiation Polarised along the x-Direction

The choice of the in-plane x-direction for polarisation of laser light is appropriate to a TE mode of laser operations.

On using $\underline{\varepsilon}_x \cdot \underline{p} = -i \frac{\partial}{\partial x}$, dropping the A superscript, and ignoring terms of second order in energy denominator, substitution of (A9.2) (and the corresponding expression for the spin split-off sub-band) into (A9.1) gives:

$$M_x = -\int_{\Omega_A} i \frac{\Omega_{cell}}{A} N_H^{1/2} N_S^{1/2} \left[\sum_{j\,j'} F^*_{jH} u^*_j F_{j'S} \left(ik_{xS} u_{j'} + \frac{\partial u_{j'}}{\partial x} \right) \right.$$

$$+ \sum_{j\,j'\,i'} F^*_{jH} u^*_j F_{j'S}\, i \left(\frac{k_{xS} P^x_{i'j'} + k_{yS} P^y_{i'j'}}{E_{j'} - E_{i'}} \right) \left(ik_{xS} u_{i'} + \frac{\partial u_{i'}}{\partial x} \right)$$

$$+ \sum_{j\,j'\,i'} F^*_{jH} u^*_j \frac{\partial F_{j'S}}{\partial z} \left(\frac{P^z_{i'j'}}{E_{j'} - E_{i'}} \right) \left(i\, k_{xS} u_{i'} + \frac{\partial u_{i'}}{\partial x} \right)$$

$$- \sum_{j\,i\,j'} i \left(\frac{k_{xH} P^x_{ij} + k_{yH} P^y_{ij}}{E_j - E_i} \right)^* F^*_{jH} u^*_i F_{j'S} \left(i\, k_{xS} u_{j'} + \frac{\partial u_{j'}}{\partial x} \right)$$

$$\left. + \sum_{j\,i\,j'} \left(\frac{P^z_{ij}}{E_j - E_i} \right)^* u^*_i \frac{\partial F^*_{jH}}{\partial z} F_{j'S} \left(ik_{xS} u_{j'} + \frac{\partial u_{j'}}{\partial x} \right) \right] e^{i(\underline{k}_{llS} - \underline{k}_{llH}) \cdot \underline{r}_{ll}} \, d\Omega$$

(A9.3)

If we now choose a typical term in the above expression e.g. the second part of the first term and evaluate this as:

$$Y = -i \int_{\Omega_A} \frac{\Omega_{cell}}{A} (N_H N_S)^{1/2} \sum_j \sum_{j'} F^*_{jH} F_{j'S} u^*_j \frac{\partial u_{j'}}{\partial x} e^{i(\underline{k}_{llS} - \underline{k}_{llH}) \cdot \underline{r}_{ll}} d\Omega \tag{A9.4}$$

all other terms can be evaluated in a similar manner.

The Bloch functions have the periodicity of the lattice and can be expanded in a Fourier series in terms of reciprocal lattice vectors $\underline{g}$. Clearly $u^*_j \frac{\partial u_{j'}}{\partial x}$ is also lattice periodic hence we can write

$$u^*_j \frac{\partial u_{j'}}{\partial x} = \sum_{\underline{g}} C_{\underline{g}} (j,j') e^{i\underline{g} \cdot \underline{r}} \tag{A9.5}$$

multiplying by $e^{-i\underline{g}' \cdot \underline{r}}$ and integrating over a lattice unit cell gives

$$\int_{\Omega_{cell}} u^*_j \frac{\partial u_{j'}}{\partial x} e^{-i\underline{g}' \cdot \underline{r}} d\Omega = \sum_{\underline{g}} C_{\underline{g}} \int_{\Omega_{cell}} e^{i(\underline{g}-\underline{g}') \cdot \underline{r}} d\Omega$$

$$= C_{\underline{g}} \delta_{\underline{g},\underline{g}'} \Omega_{cell} \tag{A9.6}$$

$$\text{so} \quad C_{\underline{g}} = \frac{1}{\Omega_{cell}} \int_{\Omega_{cell}} u^*_j \frac{\partial u_{j'}}{\partial x} e^{-i\underline{g} \cdot \underline{r}} d\Omega \tag{A9.7}$$

Now substituting (A9.5) into (A9.4)

$$Y = -i \frac{\Omega_{cell}}{A} (N_H N_S)^{1/2} \int_{\Omega_A} \sum_j \sum_{j'} \sum_{\underline{g}} F^*_{jH} F_{j'S} C_{\underline{g}} e^{i\underline{g} \cdot \underline{r}} e^{i(\underline{k}_{llS} - \underline{k}_{llH}) \cdot \underline{r}_{ll}} d\underline{r}_{ll} dz \tag{A9.8}$$

Now following the prescription of Appendix 8 for the normalisation of the wave function we integrate over a layer plane (L.P). This gives

$$\sum_{\underline{g}} \int_{L.P} C_{\underline{g}}\, e^{i(\underline{k}_{llS}-\underline{k}_{llH}+\underline{g}_{ll})\cdot\underline{r}_{ll}}\, e^{i\underline{g}_z\cdot\underline{z}} d\underline{r}_{ll} = \sum_{\underline{g}} A\, C_{\underline{g}}\, \delta_{\underline{g}_{ll},\underline{k}_{llH}-\underline{k}_{llS}}\, e^{i\underline{g}_z\underline{z}} \quad (A9.9)\ .$$

As the values of $\underline{k}_{llS}$ and $\underline{k}_{llH}$ of physical interest are much smaller than the smallest, non-zero reciprocal lattice vector, then the only term contributing significantly to the sum of (A9.9) is that for which $\underline{g}_{ll} = 0$. Hence

$$\sum_{\underline{g}} A\, C_{\underline{g}}\, \delta_{\underline{g}_{ll},\underline{k}_{Hll}-\underline{k}_{Sll}}\, e^{i\underline{g}_z\underline{z}} \simeq \sum_{\underline{g}_z} A\, C_{0,0,\underline{g}_z}\, e^{i\underline{g}_z\underline{z}}\, \delta_{0,\underline{k}_{Hll}-\underline{k}_{Sll}} \quad (A9.10)$$

substitution in (A9.8) gives

$$Y = -i\,\Omega_{cell}\,(N_H N_S)^{1/2} \sum_{j}\sum_{j'}\sum_{g_z} \int_0^{L_A} C_{00\underline{g}_z}\, e^{i\underline{g}_z\underline{z}}\, \delta_{0,\underline{k}_{llH}-\underline{k}_{llS}}\, F^*_{jH}(z)\, F_{j'S}(z)\, dz \quad (A9.11)\ .$$

As with equation (A8.7) in appendix 8, only the $\underline{g}_z = 0$ term in (A9.11) makes a significant contribution to Y and therefore

$$Y \simeq -i\,\Omega_{cell}(N_H N_S)^{1/2} \sum_{j}\sum_{j'} \int_0^{L_A} C_{000}\, \delta_{0,\underline{k}_{llH}-\underline{k}_{llS}}\, F^*_{jH}(z)\, F_{j'S}(z)\, dz \quad (A9.12)\ .$$

From (A9.7)

$$C_{000} = \frac{1}{\Omega_{cell}} \int_{\Omega_{cell}} u^*_j \frac{\partial u_{j'}}{\partial x}\, d\Omega \quad (A9.13)$$

substitution into (A9.12) gives

$$Y = -i\ (N_H N_S)^{1/2}\ \delta_{O,\underline{k}_{llH}-\underline{k}_{llS}} \sum_{j}\sum_{j'} \int_{\Omega_{cell}} u_j^* \frac{\partial u_{j'}}{\partial x}\, d\Omega \int_{O}^{L_A} F_{jH}^* F_{j'S}\, dz \qquad (A9.14)$$

$$Y = i\ (N_H N_S)^{1/2}\ \delta_{O,\underline{k}_{llH}-\underline{k}_{llS}} \sum_{j}\sum_{j'} P^x_{jj'} \int_{O}^{L_A} F_{jH}^* F_{j'S}\, dz \qquad (A9.15)\ .$$

Evaluating the other terms from expression (A9.3) in a similar manner, and using the orthognality of the Bloch functions gives:

$$M_x = (N_H N_S)^{1/2}\ \delta_{O,\underline{k}_{llH}-\underline{k}_{llS}} \sum_{j}\sum_{j'} [\langle F_{jH}^* F_{j'S}\rangle [iP^x_{jj'} +$$

$$2k_x D^{xx}_{jj'} + k_y D^{xy}_{jj'} + k_y D^{yx}_{jj'},] -$$

$$\langle F_{jH}^* \frac{\partial F_{j'S}}{\partial z}\rangle\ i\ D^{xz}_{jj'} + \langle \frac{\partial F_{jH}^*}{\partial z} F_{j'S}\rangle\ i\ D^{zx}_{jj'},] \qquad (A9.16)$$

where $\langle F_{jH}^* F_{j'S}\rangle$ implies integration over the length L_A of region A, and use of the delta function $(\delta_{O,\underline{k}_{llH}-\underline{k}_{llS}})$ has been anticipated in order to drop the S and H subscripts on the wavevector $(\underline{k})$ terms.

The same expression (A9.16) can be used for both materials A and B with the appropriate choice of parameters.

Equation (A9.16) can be expressed as:

$$M_x = M_{Ax}\ \delta_{O,\underline{k}_{llH}-\underline{k}_{llS}}$$

and

$$|M_x|^2 = |M_{Ax}|^2\ \delta_{O,\underline{k}_{llH}-\underline{k}_{llS}} \qquad (A9.17)$$

which on using

$$\delta_{O,\underline{k}_{llH}-\underline{k}_{llS}} \equiv \frac{(2\pi)^2}{A}\,\delta(\underline{k}_{llS}-\underline{k}_{llH})$$

and anticipating a relevant integration gives

$$|M_x|^2 = |M_{Ax}|^2\,\frac{(2\pi)^2}{A}\,\delta(\underline{k}_{llS}-\underline{k}_{llH}) \qquad \text{(A9.18)}$$

where

$$M_{Ax} = (N_H N_S)^{1/2} \sum_j \sum_{j'} \left[\langle F^*_{jH} F_{j'S} \rangle \left[iP^x_{jj'} + 2k_x D^{xx}_{jj'} + k_y (D^{xy}_{jj'} + D^{yx}_{jj'}) \right] - \langle F^*_{jH} \frac{\partial F_{j'S}}{\partial z} \rangle iD^{xz}_{jj'} + \langle \frac{\partial F^*_{jH}}{\partial z} F_{j'S} \rangle iD^{zx}_{jj'} \right] \qquad \text{(A9.19)}$$

b) Radiation Polarised in the z-Direction

Radiation polarised in the superlattice z-direction corresponds to the TM mode of laser operations.

Following the same prescription as above we obtain:

$$M_z = (N_H N_S)^{1/2}\,\delta_{O,\underline{k}_{llH}-\underline{k}_{llS}} \sum_j \sum_{j'} \left[\langle F^*_{jH} F_{j'S} \rangle \left[i P^z_{jj'} + k_x (D^{zx}_{jj'} + D^{xz}_{jj'}) + k_y (D^{zy}_{jj'} + D^{yz}_{jj'}) \right] + \langle \frac{\partial F^*_{jH}}{\partial z} F_{j'S} \rangle i \left(D^{zz}_{jj'} - \frac{\delta_{jj'}}{2} \right) - \langle F^*_{jH} \frac{\partial F_{j'S}}{\partial z} \rangle i \left(D^{zz}_{jj'} + \frac{\delta_{jj'}}{2} \right) \right] \qquad \text{(A9.20)}$$

REFERENCES

Abram R.A., Childs G.N. and Saunderson P., 1984, J. Phys. C, 17, 6105.

Abram R.A., Rees G.J. and Wilson B.L.H., 1978, Adv. in Phys., 27, 799.

Adachi S., 1985, J. Appl. Phys., 58, R1.

Adams A.R., Asada M., Suematsu Y. and Arai S., 1980, Jpn. Jnl. Appl. Phys., 19, L621.

Alavi K. and Aggarwal R.L., 1979, J. Mg. and Mgc. Mat., 11, 136.

Altarelli M., 1983, Proc. 16th Int. Conf. Phys. Semi. - North Holland Publishing.

Altarelli M., Ekenberg U. and Fasolino A., 1985, Phys. Rev. B., 32, 5138.

Bardyszewski W., 1986, Solid State Comm., 57, 873.

Bastard G., 1981, Phys. Rev. B., 24, 5693.

Batey J., Wright S.L. and DiMaria D.J., 1985, J. Appl. Phys., 57, 484.

Berggren K.F. and Sernelius B.E., 1981, Phys. Rev. B., 24, 1971.

Brand S., 1984, Private communication.

Burnstein E., 1954, Phys. Rev. B., 93, 632.

Casey H.C. and Panish M.B., 1978, 'Heterostructure Lasers', Academic Press N. York. For other Casey references see end of list.

Chang Y.C. and Schulman J.N., 1985, Phys. Rev. B., 31, 2069.

Chelikowsky, J.R. and Cohen, M.H., 1976, Phys. Rev. B., 14, 556.

Chin R., Holonyak Jr.N., Vojak B.A., Hess K., Dupuis R.D. and Dapkus P.D., 1980, Appl. Phys. Lett., 32, 19.

Dutta N.K., Nelson R.J. and Barnes P.A., 1980, Electron. Lett. 16, 653.

Dutta N.K. and Nelson R.J., 1981, IEEE, Trans. Elec. Devices, 28, 1222.

Dutta N.K. and Nelson R.J., 1982, J. Appl. Phys., 53, 74.

Dutta N.K., 1983, J. Appl. Phys., 54, 1236.

Dingle R., Wiegmann W. and Henry C.H., 1974, Phys. Rev. Lett., 33, 827.

Dingle R., Gossard A.C. and Wiegmann W., 1975, Phys. Rev. Lett., 34, 1327.

Ettenberg M. and Kressel H., 1976, J. Appl. Phys., 47. 1538.

Fetter A.L. and Walecka J.D., 1971, 'Quantum Theory of Many Particle Systems', McGraw Hill.

Feynman R.P., 1949, Phys. Rev., 76, 749.

Gasiorowicz S., 1974, 'Quantum Physics', John Wiley & Sons.

Gradshteyn I.S. and Ryzhik I.M., 1980, 'Table of Integrals Series and Products', Academic Press.

Halperin B.I. and Lax M., 1966, Phys. Rev. B., 148, 722.

Hedin H. and Lundqvist B.I., 1969, Solid State Phys., 23, 1 (New York Acadmic Press).

Henry C.H., Logan R.A., Merritt F.R. and Luongo J.P., 1983, IEEE, J.Q. Elec., QE-19, 947.

Inkson J.C., 1976, J. Phys. C., 9, 1177.

Inkson J.C., 1984, 'Many Body Theory of Solids', New York-Plenum Press.

Kane, E.O., 1957, J. Phys. Chem. Sol., 1, 249.

Kronig, R. de L. and Penney W.G., 1931, Proc. Soc. London Ser. A., 130, 499.

Landolt and Börnstein, 1982, 'Numerical Data and Functional Relationships in Science and Technology, Vol. 17 - Semiconductors' - Springer-Verlag, Ed. K. Hellwege.

Löwdin P.O., J. Chem. Phys., 1951, 19, 1396.

Lundqvist B.I., 1967a, Phys. Kodens. Mater., 6, 193.

1967b, Phys. Kodens. Mater., 6, 206.

1968c, Phys. Kodens. Mater., 7, 117.

Luttinger J.M., 1956, Phys. Rev., 102, 1030.

Mahan G.D., 1981, 'Many Particle Physics', New York-Plenum Press.

Mattuck, R.D., 1976, 'A Guide to Feynman Diagrams in the Many Body Problem', McGraw-Hill.

Miller R.C., Gossard A.C., Kleinmann D.A. and Munteau O., 1984, Phys. Rev. B., 29, 3740.

Monaghan S., and Szydhlik P., 1986, Private Communication.

Moss T.S., 1954, Proc. Phys. Soc. B., 67, 775.

Mott N.F., 1974, 'Metal Insulator Transitions', Taylor and Francis.

Mott N.F. and Kaveh M., 1983, Phil. Mag. B., 47, 577.

Mozer A., Romanek K.M., Hildebrand O., Schmid W. and Pilkuhn M.H., 1983, IEEE, J.Q. Elec. QE-19, 913.

Nahory R.E., Pollack M.A. and De Winter J.C., 1979, Electron. Lett. 15, 695.

Rezek, E.A., Holonyak Jr.N. and Fuller B.K., 1980, J. Appl. Phys., 51, 2402.

Rice T.M., 1974, Il. Nuovo Cimento, 23, 226.

Saunders G.D. and Chang Y.C., 1985, Phys. Rev. B., 31, 6892.

Saunderson P., 1983, Ph.D. Thesis, Durham University.

Schiff L.I., 1955, 'Quantum Mechanics', McGraw Hill.

Schlosser H. and Marcus P.M., 1963, Phys. Rev. B., 131, 2529.

Schulman J.N. and Chang Y.C., 1985, Phys. Rev. B., 31, 2069.

Sernelius, B.E., 1986, Phys. Rev. B., 33, 8582.

Serre J. and Ghazali A., 1983, Phys. Rev. B., 28, 4704.

Sugimura A., 1981a, IEEE, J.Q. Elec., QE-17, 627.

1981b, Appl. Phys. Lett., 39, 21.

Sze S.M., 1981, 'Physics of Semiconductor Devices', New York, John Wiley and Sons.

Takeshima M., 1984a, Jpn. Jnl. Appl. Phys., 23, 428.

1984b, J. Appl. Phys., 56, 49.

1984c, J. Appl. Phys., 56, 691.

Tanaka S., Kobayashi H., Saito H. and Shionoya S., 1980, Jnl. Phys. Soc. Jpn., 49, 1051.

Vol'fson A.A. and Subashiev V.K., 1967, Soviet Phys. Semicond., 1, 327.

Wiley J.D., 1971, Phys. Rev. B., 4, 2485.

Wooten F., 1972, 'Optical Properties of Solids', Academic Press.

Yano M., Nishi H. and Takusagawa M., 1980, J. Appl. Phys., 51, 4022.

Yano M., Nishi H. and Takusagawa M., 1980, IEEE, J.Q. Elec. QE-16, 661.

Yano M., Imai H., Hori K.J. and Takusagawa M., 1981, IEEE, J.Q. Elec. QE-17, 619.

Ziman J.M., 1972, 'Theory of Solids', Cambridge University Press.

Casey H.C., and Stern F., 1976, J. Appl. Phys., 47, 631.

Casey H.C. Jnr., 1984, J. Appl. Phys., 56, 1959.